

# Lateral behavior of steel frames with discretely connected precast concrete infill panels

**Citation for published version (APA):**

Teeuwen, P. A. (2009). *Lateral behavior of steel frames with discretely connected precast concrete infill panels*. [Phd Thesis 1 (Research TU/e / Graduation TU/e), Built Environment]. Technische Universiteit Eindhoven. <https://doi.org/10.6100/IR656458>

**DOI:**

[10.6100/IR656458](https://doi.org/10.6100/IR656458)

**Document status and date:**

Published: 01/01/2009

**Document Version:**

Publisher's PDF, also known as Version of Record (includes final page, issue and volume numbers)

**Please check the document version of this publication:**

- A submitted manuscript is the version of the article upon submission and before peer-review. There can be important differences between the submitted version and the official published version of record. People interested in the research are advised to contact the author for the final version of the publication, or visit the DOI to the publisher's website.
- The final author version and the galley proof are versions of the publication after peer review.
- The final published version features the final layout of the paper including the volume, issue and page numbers.

[Link to publication](#)

**General rights**

Copyright and moral rights for the publications made accessible in the public portal are retained by the authors and/or other copyright owners and it is a condition of accessing publications that users recognise and abide by the legal requirements associated with these rights.

- Users may download and print one copy of any publication from the public portal for the purpose of private study or research.
- You may not further distribute the material or use it for any profit-making activity or commercial gain
- You may freely distribute the URL identifying the publication in the public portal.

If the publication is distributed under the terms of Article 25fa of the Dutch Copyright Act, indicated by the "Taverne" license above, please follow below link for the End User Agreement:

[www.tue.nl/taverne](http://www.tue.nl/taverne)

**Take down policy**

If you believe that this document breaches copyright please contact us at:

[openaccess@tue.nl](mailto:openaccess@tue.nl)

providing details and we will investigate your claim.

**LATERAL BEHAVIOR OF STEEL FRAMES  
WITH DISCRETELY CONNECTED  
PRECAST CONCRETE INFILL PANELS**

P.A. Teeuwen

Bouwstenen 139

ISBN 978-90-6814-622-6

NUR-code 955

© 2009 by P.A. Teeuwen

Cover design by A.W.M. van Gennip

Printed by Eindhoven University Press Facilities,  
Eindhoven University of Technology, The Netherlands

# **LATERAL BEHAVIOR OF STEEL FRAMES WITH DISCRETELY CONNECTED PRECAST CONCRETE INFILL PANELS**

PROEFSCHRIFT

ter verkrijging van de graad van doctor aan de Technische Universiteit Eindhoven,  
op gezag van de rector magnificus, prof.dr.ir. C.J. van Duijn,  
voor een commissie aangewezen door het College voor Promoties in het openbaar  
te verdedigen op donderdag 26 november 2009 om 16.00 uur

door

Paulus Andreas Teeuwen

geboren te Geldrop

Dit proefschrift is goedgekeurd door de promotoren:

prof.ir. C.S. Kleinman

en

prof.ir. H.H. Snijder

Copromotor:

dr.ir. H. Hofmeyer

Samenstelling van de promotiecommissie:

prof.ir. J. Westra	Technische Universiteit Eindhoven
prof.ir. C.S. Kleinman	Technische Universiteit Eindhoven
prof.ir. H.H. Snijder	Technische Universiteit Eindhoven
dr.ir. H. Hofmeyer	Technische Universiteit Eindhoven
prof.dr.ir. L. Taerwe	Universiteit Gent
prof.ir. F.S.K. Bijlaard	Technische Universiteit Delft
prof.ir. D.R.W. Martens	Technische Universiteit Eindhoven

## ACKNOWLEDGEMENTS

Successfully finishing this thesis has only been possible with the help from other persons whom I own some words of gratitude to for a diversity of reasons.

First of all, I wish to express my sincere gratitude to professor Cees Kleinman and professor Bert Snijder, for offering me the doctoral student position in this research project and for their supervision, encouragement, and generous support towards the completion of this thesis. Furthermore, my gratitude extends to Herm Hofmeyer for his scientific contribution and valuable guidance during the project.

Besides, I wish to thank the staff of the Pieter van Musschenbroek laboratory at Eindhoven University of Technology, especially Eric Wijen and Theo van de Loo, for their professional assistance before and during the experiments, yet also for the pleasant informal conversations during the breaks.

Furthermore, I would like to thank my (former) fellow doctoral students, for providing me support in various ways and for a good atmosphere at the office and at social events outside of work. I also would like to thank the student Jan-Pieter Kansen for his contribution to this thesis.

Finally, I wish to thank my parents and friends and especially my girlfriend Elke. Thank you for listening to me and encouraging me in difficult times. Without your patience and understanding, as well as your moral support, this thesis would not have been possible.

Paul Teeuwen

Eindhoven, September 2009

# SUMMARY

## **Lateral behavior of steel frames with discretely connected precast concrete infill panels**

As an alternative to the conventional structures for tall buildings, a hybrid lateral load resisting structure has been designed at Eindhoven University of Technology. It consists of discretely connected precast concrete panels with window openings in steel frames, and is a new application in infilled frames. Besides the structural advantages of hybrid construction, this structure offers an alternative construction method, improving the constructability of tall buildings. This will result in more economical and high quality buildings.

The infilled frame is a type of structure that has proven to be effective and efficient in bracing low-rise and medium-rise buildings to resist in-plane lateral loads. It acts by composite action between the infill and its surrounding frame. Structural interaction between the two components produces a composite structure with a complicated behavior due to the fact that the frame and the infill mutually affect each other. Since the early fifties extensive research has been done into the composite behavior of infilled frames with masonry and cast-in-place concrete infills without openings. However, the application of discretely connected concrete panels with openings as bracing elements in steel frame structures has not been performed yet and represents a new area of research in infilled frames.

The main objective of this investigation is to develop practical universally applicable design models for infilled steel frames with discretely connected precast concrete panels, allowing for an accurate prediction of the strength, stiffness and deformation capacity of this type of structure. In order to develop these design models, the structure has been subjected to experimental, numerical and analytical investigation.

First, full-scale tests on single-storey, single-bay infilled frame structures were carried out. Objectives of this experimental study were to observe the general behavior of the infilled frame in terms of stiffness, strength and failure modes. In addition, experiments were performed on components of the discrete panel-to-frame connection.

Subsequently, finite element models were developed and validated by simulating the experiments. For this purpose, finite element analyses taking non-linear material and structural behavior into account were performed. It has been shown that the finite element model developed for the overall infilled frame behavior can be used to predict the lateral load versus deflection relationship and the ultimate lateral load with good



accuracy. Accordingly, the validated finite element model has been used to carry out a parameter study to investigate various configurations of the infilled frame. Four parameters have been studied with respect to their influence on the structural response. These parameters are the frame member dimensions, the rotational stiffness of the frame joints, the infilled frame aspect ratio and the panel opening geometry.

From the simulated load-deformation curves, structural characteristics have been derived. These have served as a verification for the developed analytical models for the prediction of the lateral stiffness, the ultimate lateral load and deformation capacity of the structure under consideration. The analytical models are based on the concept of the equivalent diagonal strut, considering the structure as an equivalent braced frame system with a compression diagonal replacing the infill.

Finally, a practical method for designing steel frames with discretely connected precast concrete infill panels has been proposed. The aim of this method is to get a good prediction of the internal forces and the lateral deflection in the preliminary phase of the design, without the use of advanced computer simulations. The design method provides a useful guideline that a design engineer can follow, in order to design building structures consisting of steel frames with discretely connected precast concrete infill panels, resulting in a ductile structure, possessing both adequate strength and stiffness.

# SYMBOLS

Each symbol used in this thesis is explained where it is introduced. The list below gives an overview of the symbols that are frequently used in this thesis, subdivided according to the field of application they belong to.

## Symbols relevant for bolt-nut assemblies:

### Latin symbols:

$A_{Sb}$	: Shear area for bolt threads	[mm <sup>2</sup> ]
$A_{Sn}$	: Shear area for nut threads	[mm <sup>2</sup> ]
$A_b$	: Nominal area of the bolt shank	[mm <sup>2</sup> ]
$A_s$	: Tensile stress area of the bolt	[mm <sup>2</sup> ]
$C_1$	: Modification factor for nut dilation	[-]
$C_2$	: Modification factor for thread bending applied for the bolt	[-]
$C_3$	: Modification factor for thread bending applied for the nut	[-]
$D$	: Nominal diameter (of the nut)	[mm]
$D_1$	: Minor diameter of the nut	[mm]
$D_2$	: Pitch diameter of the nut	[mm]
$d_b$	: Nominal diameter of the bolt	[mm]
$d$	: Major diameter of the bolt	[mm]
$d_2$	: Pitch diameter of the bolt	[mm]
$d_3$	: Minor (root) diameter of the bolt	[mm]
$E_b$	: Young's modulus of the bolt material	[N/mm <sup>2</sup> ]
$F_B$	: Breaking load of the bolt	[N]
$F_S$	: Stripping load for bolt-nut assembly	[N]
$F_{Sb}$	: Stripping load for bolt threads	[N]
$F_{Sn}$	: Stripping load for nut threads	[N]
$f_{ub}$	: Tensile strength of the bolt material	[N/mm <sup>2</sup> ]
$f_{un}$	: Tensile strength of the nut material	[N/mm <sup>2</sup> ]
$f_{yb}$	: Yielding strength of the bolt material	[N/mm <sup>2</sup> ]
$f_{yn}$	: Yielding strength of the nut material	[N/mm <sup>2</sup> ]
$k_b$	: Stiffness of the bolt	[N/mm]
$L_s$	: Length of the bolt shank	[mm]
$L_{tg}$	: Length of the bolt thread included in the grip	[mm]
$m$	: Nut height	[mm]
$m^*$	: Effective nut height for stripping strength	[mm]
$p$	: Pitch of the thread	[mm]
$s$	: Width across the flats of nut	[mm]

**Symbols relevant for analytical models for semi-integral infilled frames**

Latin symbols:

$A$	: Cross-sectional area of a steel section	[mm <sup>2</sup> ]
$A_v$	: Shear area of a steel section	[mm <sup>2</sup> ]
$a$	: Height of the panel opening	[mm]
$b$	: Width of the panel opening	[mm]
$b$	: Width of a steel section	[mm]
$F_c$	: Strength of the panel-to-frame connection	[N]
$F_{ci}$	: Strength of component $i$ of the panel-to-frame connection	[N]
$F_h$	: Lateral load	[N]
$F_p$	: Strength of the infill panel	[N]
$F_{w,if}$	: Strength of the semi-integral infilled frame	[N]
$G_p$	: Dead weight of the infill panel	[N]
$g$	: Width of the gap between the panel and frame	[mm]
$H$	: Column height between centerlines of beams	[mm]
$h$	: Height of the infill panel	[mm]
$h$	: Height of a steel section	[mm]
$h'$	: Height of the panel's equivalent frame	[mm]
$I$	: Second moment of area	[mm <sup>4</sup> ]
$k_c$	: Stiffness of the panel-to-frame connection	[N/mm]
$k_{ci}$	: Stiffness of component $i$ of the panel-to-frame connection	[N/mm]
$k_{c,eff}$	: Effective stiffness of the panel-to-frame connection	[N/mm]
$k_{c,ini}$	: Initial stiffness of the panel-to-frame connection	[N/mm]
$k_{h,col}$	: Lateral stiffness resulting from column deformation	[N/mm]
$k_{h,f}$	: Lateral stiffness of the bare frame	[N/mm]
$k_{h,if}$	: Lateral stiffness of the semi-integral infilled frame	[N/mm]
$k_{h,p}$	: Lateral stiffness resulting from panel deformation	[N/mm]
$k_{h,\Sigma con}$	: Lateral stiffness resulting from connection deformations	[N/mm]
$k_p$	: Diagonal panel stiffness	[N/mm]
$L$	: Beam length between centerlines of column	[mm]
$L_{strut}$	: Length of the frame diagonal	[mm]
$l$	: Length of infill panel	[mm]
$l'$	: Length of the panel's equivalent frame	[mm]
$l_{strut}$	: Length of the panel diagonal	[mm]
$M_j$	: Resistance of the beam-to-column joint	[Nmm]
$r$	: Fillet radius	[mm]
$S_j$	: Rotational stiffness of the beam-to-column joint	[Nmm/rad]
$t_f$	: Thickness of the flange of a steel section	[mm]
$t_p$	: Thickness of the infill panel	[mm]
$t_w$	: Thickness of the web of a steel section	[mm]
$x$	: Distance of the bolts with respect to the column or beam	[mm]

## Symbols

---

### Greek symbols:

$\beta$	: Ratio of the total length to the flexible part of a beam	[-]
$\gamma$	: Ratio of the total length to the flexible part of a column	[-]
$\delta_n$	: Lateral deflection	[mm]
$\eta$	: Correction factor	[-]
$\mu$	: Factor accounting for the relative stiffness of the frame to the infill	[-]
$\varphi_f$	: Angle between the frame diagonal and the beam	[rad]
$\varphi_p$	: Angle between the panel diagonal and the beam	[rad]

### **Symbols relevant for materials**

### Latin symbols:

$E_c$	: Young's modulus of concrete	[N/mm <sup>2</sup> ]
$E_s$	: Young's modulus of steel	[N/mm <sup>2</sup> ]
$f_c$	: Compressive strength of concrete	[N/mm <sup>2</sup> ]
$f_{cd}$	: Design compressive strength of concrete	[N/mm <sup>2</sup> ]
$f_{ck}$	: Characteristic cylinder compressive strength of concrete	[N/mm <sup>2</sup> ]
$f_{cm}$	: Mean value of the compressive strength of concrete	[N/mm <sup>2</sup> ]
$f_{ct}$	: Tensile strength of concrete	[N/mm <sup>2</sup> ]
$f_{cu}$	: Stress limit for struts and nodes	[N/mm <sup>2</sup> ]
$f_u$	: Ultimate tensile strength of steel	[N/mm <sup>2</sup> ]
$f_y$	: Yield stress of steel	[N/mm <sup>2</sup> ]
$G_f$	: Fracture energy of concrete	[N/mm]
$G_s$	: Shear modulus of steel	[N/mm <sup>2</sup> ]
$k_{s,i}$	: Reduction factor for the strength of struts in strut-and-tie models	[-]
$k_{n,i}$	: Reduction factor for the strength of nodes in strut-and-tie models	[-]

### Greek symbols:

$\beta$	: Shear retention factor for concrete	[-]
$\gamma_c$	: Partial safety factor for concrete	[-]
$\gamma_s$	: Partial safety factor for steel	[-]
$\nu_c$	: Poisson's ratio of concrete	[-]
$\nu_s$	: Poisson's ratio of steel	[-]

# CONTENTS

<b>Chapter 1: INTRODUCTION .....</b>	<b>1</b>
1.1 <i>Infilled steel frames with precast concrete panels.....</i>	<i>1</i>
1.2 <i>Motivation and relevance .....</i>	<i>2</i>
1.3 <i>Problem statement and objectives .....</i>	<i>3</i>
1.4 <i>Research method .....</i>	<i>4</i>
1.5 <i>Thesis outline .....</i>	<i>5</i>
<b>Chapter 2: LITERATURE REVIEW .....</b>	<b>7</b>
2.1 <i>Infilled frames: State of the art.....</i>	<i>7</i>
2.1.1 <i>Analysis of infilled frames.....</i>	<i>8</i>
2.1.2 <i>Effect of openings .....</i>	<i>13</i>
2.1.3 <i>Infilled frames with precast concrete panels.....</i>	<i>17</i>
2.1.4 <i>Section conclusions.....</i>	<i>18</i>
2.2 <i>Structural bolts.....</i>	<i>19</i>
2.2.1 <i>Standard bolts: dimensions, grades and strengths.....</i>	<i>19</i>
2.2.2 <i>Strength considerations.....</i>	<i>19</i>
2.2.3 <i>Stiffness considerations .....</i>	<i>23</i>
2.3 <i>Strut-and-tie modeling of concrete.....</i>	<i>24</i>
2.3.1 <i>Historical overview of strut-and-tie modeling.....</i>	<i>26</i>
2.3.2 <i>Strength of struts and nodal zones .....</i>	<i>27</i>
<b>Chapter 3: CONCEPTUAL DESIGN .....</b>	<b>29</b>
3.1 <i>Discrete panel-to-frame connection .....</i>	<i>29</i>
3.2 <i>Mechanical model.....</i>	<i>33</i>
3.2.1 <i>Structural characteristics frame joints.....</i>	<i>34</i>
3.2.2 <i>Structural characteristics discrete panel-to-frame connections.....</i>	<i>34</i>
3.2.3 <i>Structural properties precast concrete panel with window opening .....</i>	<i>37</i>
3.3 <i>Chapter conclusions .....</i>	<i>38</i>
<b>Chapter 4: EXPERIMENTS .....</b>	<b>39</b>
4.1 <i>Component experiments.....</i>	<i>39</i>

4.1.1	Bolts in compression.....	39
4.1.2	Flanges in bending with web in compression .....	42
4.1.3	Plate in compression.....	44
4.1.4	Bolt with cap on plate in compression.....	47
4.2	<i>Full-scale experiments</i> .....	49
4.2.1	Test setup and test program.....	49
4.2.2	Experimental observations and results.....	55
4.3	<i>Chapter conclusions</i> .....	66
 <b>Chapter 5: FINITE ELEMENT MODELING .....</b>		<b>69</b>
5.1	<i>Component modeling</i> .....	69
5.1.1	Mesh and elements .....	70
5.1.2	Material properties.....	71
5.1.3	Boundary conditions and loading .....	72
5.1.4	Solution procedure .....	72
5.1.5	Validation of finite element model.....	73
5.2	<i>Full-scale modeling</i> .....	74
5.2.1	Mesh and elements .....	74
5.2.2	Material properties.....	75
5.2.3	Boundary conditions and loading .....	79
5.2.4	Solution procedure .....	79
5.2.5	Validation of finite element model.....	79
5.3	<i>Chapter conclusions</i> .....	84
 <b>Chapter 6: PARAMETER STUDIES.....</b>		<b>85</b>
6.1	<i>Component behavior</i> .....	85
6.1.1	Parameters considered.....	85
6.1.2	Material properties.....	86
6.1.3	Geometrical properties.....	86
6.1.4	Results.....	86
6.2	<i>Full-scale behavior</i> .....	90
6.2.1	Parameters considered.....	91
6.2.2	Material properties.....	94
6.2.3	Results parameter study.....	94
6.3	<i>Chapter conclusions</i> .....	97

<b>Chapter 7: ANALYTICAL MODELING .....</b>	<b>99</b>
7.1 <i>Lateral stiffness modeling</i> .....	99
7.1.1 Basic model.....	100
7.1.2 Advanced model .....	106
7.1.3 Lateral stiffness model.....	112
7.2 <i>Ultimate lateral load modeling</i> .....	112
7.2.1 Dead weight panel .....	113
7.2.2 Ultimate lateral load models .....	114
7.3 <i>Validation of analytical models</i> .....	115
7.4 <i>Chapter conclusions</i> .....	118
<b>Chapter 8: DESIGN RECOMMENDATIONS.....</b>	<b>119</b>
8.1 <i>Design method</i> .....	119
8.2 <i>Design example</i> .....	122
8.3 <i>Towards a completely integrated tall building system</i> .....	139
8.4 <i>Chapter conclusions</i> .....	142
<b>Chapter 9: CONCLUSIONS &amp; RECOMMENDATIONS .....</b>	<b>143</b>
9.1 <i>Conclusions</i> .....	143
9.2 <i>Recommendations for future research</i> .....	145
<b>REFERENCES .....</b>	<b>147</b>

**APPENDIXES**

**APPENDIX A.....155**

    A.1    *Resistance of H-section subject to transverse compression..... 155*

**APPENDIX B.....159**

    B.1    *Test specimens..... 159*

    B.2    *Measurement results ..... 165*

**APPENDIX C.....167**

    C.1    *Moment-rotation curves for rotational springs used in FE-analyses ..... 167*

    C.2    *Comparison of FE- and experimental results ..... 168*

        C.2.1    *Measured and simulated strains..... 168*

        C.2.2    *Experimental and simulated crack patterns ..... 169*

**APPENDIX D.....171**

    D.1    *Results parameter study on component..... 171*

    D.2    *Reinforcement configuration for panels used in parameter study ..... 174*

    D.3    *Results parameter study on infilled frame..... 179*

**APPENDIX E .....183**

    E.1    *Derivation of equations [7-21] to [7-24]..... 183*

    E.2    *Derivation of equations [7-27] to [7-31]..... 188*

    E.3    *M-N- $\kappa$ -diagrams used for equivalent frame members ..... 191*

**CURRICULUM VITAE .....195**





# Chapter 1: INTRODUCTION

## *Scope of the chapter*

*The subject of this thesis is the lateral behavior of steel frames with discretely connected precast concrete infill panels. In this first chapter, an introduction to this subject is provided. Thereupon, the motivation and relevance of this study are explained. Subsequently, the problem statement and objectives are defined and the adopted research method is presented. Finally, the outline of this thesis is given.*

## **1.1 Infilled steel frames with precast concrete panels**

In today's daily building practice, growing numbers of hybrid structures are being built. Hybrid construction combines the structural and architectural advantages of components made from different materials. Instead of competition between building materials which used to be the tendency, steel, timber, cast-in-situ or precast concrete, masonry and glass are more often joining forces using each material in its most effective way. These materials may work integrated or jointly. Hybrid construction is cost-effective as it combines the benefits to be derived from using components of different materials. Besides the structural advantages, benefits may be realized in the following areas: aesthetics, function, construction speed, safety and constructability. Consequently, hybrid structures result into substantial savings and higher quality buildings.

Taking the advantages of hybrid construction, a hybrid lateral load resisting structure has been designed at Eindhoven University of Technology, as an alternative for conventional structures for tall buildings. It consists of discretely connected precast concrete infill panels within steel frames, and is a new application in infilled frames. The infilled frame is a type of structure that has proven to be effective and efficient in bracing low-rise and medium-rise buildings to resist in-plane lateral loads. It acts by composite action between an infill and its confining frame. Structural interaction between the two components produces a composite structure with a complicated behavior as the infill and frame mutually affect each other.

Since the early fifties extensive investigations have been carried out into the composite behavior of framed structures with masonry and cast-in-place concrete infills. When connectors or strong bonding at the interfaces between the frame and the infill panel are absent, as for example with masonry infill, the structures are generally known as non-integral infilled frames (Figure 1-1a). When these structures are subjected to lateral loading, a large portion of the load is taken up by the infill panel at its loaded corner. The

provision of strong bonding or connectors at the interface enables the infill and frame to act compositely. These infilled frames are known as fully-integral infilled frames (Figure 1-1b). Part of the shearing load is transmitted from the frame to the infill panel through the connectors. A variety of methods have been developed for the design and analysis of non-integral and fully-integral infilled frames.

Discretely connected precast concrete infill panels may be able to provide similar improvements to frame structures as masonry and cast-in-place concrete infills. However, the application of discrete interface connections between the infill and frame results in completely different behavior from non-integral or fully integral infilled frames. Infilled frames with discrete connections between frame and panel are termed semi-integral infilled frames (Figure 1-1c), and represent a new area of research in infilled frames.

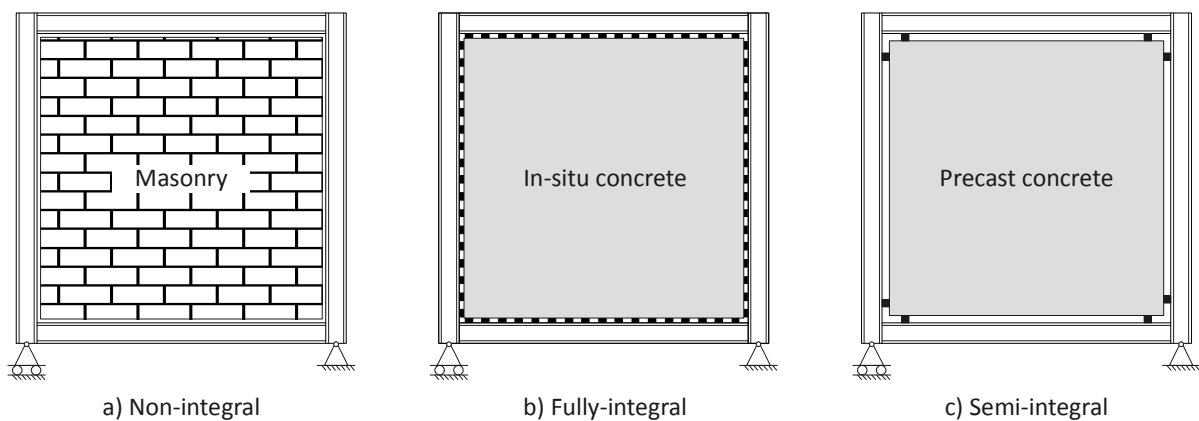


Figure 1-1: Classification of infilled frames

## 1.2 Motivation and relevance

Apart from the stiffening and strengthening effect of infills on frames as explained above, the concept of discretely connected precast concrete panels within steel frames offers the possibility to be developed into a so-called completely integrated tall building system. This involves entirely prefabricated elements arriving ready for installation on-site, supplied with insulation, windows, an outer skin of cladding and preinstalled installations for vertical transport within the building such as heating, ventilation, and air conditioning (HVAC), cable ducts, and water and sanitation systems. Such a building system may considerably improve the constructability of tall buildings as follows:

- The completely-integrated building system enables the assembly of tall buildings directly from a truck. The prefabricated elements can be scheduled to arrive “just in time” so they can be lifted directly from a truck into place with a minimum of manpower. Therefore, on-site building activities will in essence be restricted to

assembly, resulting in a rapid erection on-site, enabling faster construction times. Besides, this avoids the need for storage space on site and unnecessary handling.

- The completely-integrated tall building system provides the opportunity of simultaneously erecting (steel) structure and façade (elements). Consequently, a thermal, wind and waterproof story is provided immediately and does not require protection from weather. As a result, indoor construction activities can be initiated directly after a story has been erected, once more increasing the speed of construction.
- There are no formworks or scaffolding to build and no concrete pouring to be done on site. This means a smaller footprint, a cleaner, safer working environment and a reduction of construction noise.
- All structural elements are manufactured in factories in a favorable environment under strictly controlled conditions. As a result, high quality products can be produced every day, regardless of the weather. This is important in relation to strength, stiffness, durability and tolerances of the building elements. Consequently, high quality buildings can be achieved.
- The structure offers the attraction of ease of disassembling at the end-of-life of the building, providing the opportunity to reclaim all building components as whole elements. These could be transported and reinstalled in a comparable structure elsewhere, or be reused for other purposes.

In summary, having a completely-integrated tall building system, the composite structure will offer an alternative construction method, improving the constructability of tall buildings. This will result in high-quality buildings, provide economic benefit and reduce overall construction time, inconvenience, and the likelihood of claims.

### **1.3 Problem statement and objectives**

From the previous two sections, the conclusions are drawn that steel frames with discretely connected precast concrete infill panels are a potential alternative to conventional structures for tall buildings. Besides the structural advantages of hybrid construction, this structure offers the possibility to become part of a completely-integrated tall building system, improving the constructability of tall buildings and result in more economical and high quality buildings.

Although extensive research has been done into masonry and cast-in-place concrete infilled frames, little attention has been given to discretely connected precast concrete infill panels within steel frames. The investigation into the composite behavior of steel frames with discretely connected precast concrete infill panels represents a new area of research in infilled frames. Design rules are needed to facilitate application of this lateral load resisting structure for the construction of tall buildings.

The main objective of this investigation is to develop practical universally applicable design models for infilled steel frames with discretely connected precast concrete panels, allowing for an accurate prediction of the strength, stiffness and deformation capacity of this structure.

These design models will provide a first step in the design of semi-integral infilled frames, and will be suited to serve as a basis for developing design rules in standards, finally facilitating the application of this lateral load resisting structure.

#### **1.4 Research method**

First, design requirements are defined for the semi-integral infilled frame. Subsequently, a qualitative behavior analysis is performed to provide insight into the structure. A survey of applicable design methods for the analysis of (parts of) the structure is made and the shortcomings are determined. Accordingly, the research needs are established for further investigation. In order to achieve the main objective of this research, the finite element method can be used to study the infilled frame performance by varying different parameters. For this purpose, a validated finite element (FE) model is needed. Therefore, experimental data are needed as input for the FE-model and for validation of the FE-model as well. Therefore, full-scale tests on single-story single-bay infilled frames are carried out. Objectives of this full-scale experimental study are to observe the general behavior of an infilled frame in terms of stiffness, strength and failure modes. In addition, experiments are performed on components of the discrete panel-to-frame connection. The results of both experimental studies are used to develop and calibrate a FE-model that simulates the infilled frame behavior. Numerical analyses taking non-linear material and structural behavior into account are performed. The validated FE-model is used to carry out a parametric study. The parameters considered in the parametric study included those that are normally modified in the design process. On the basis of the results of the parametric study, analytical models enabling to predict the ultimate lateral load carrying capacity and lateral stiffness of the infilled frame are developed. Finally, a practical method for designing infilled steel frames with discretely connected precast concrete panels is developed. The flowchart in Figure 1-2 gives a schematic overview of the research method.

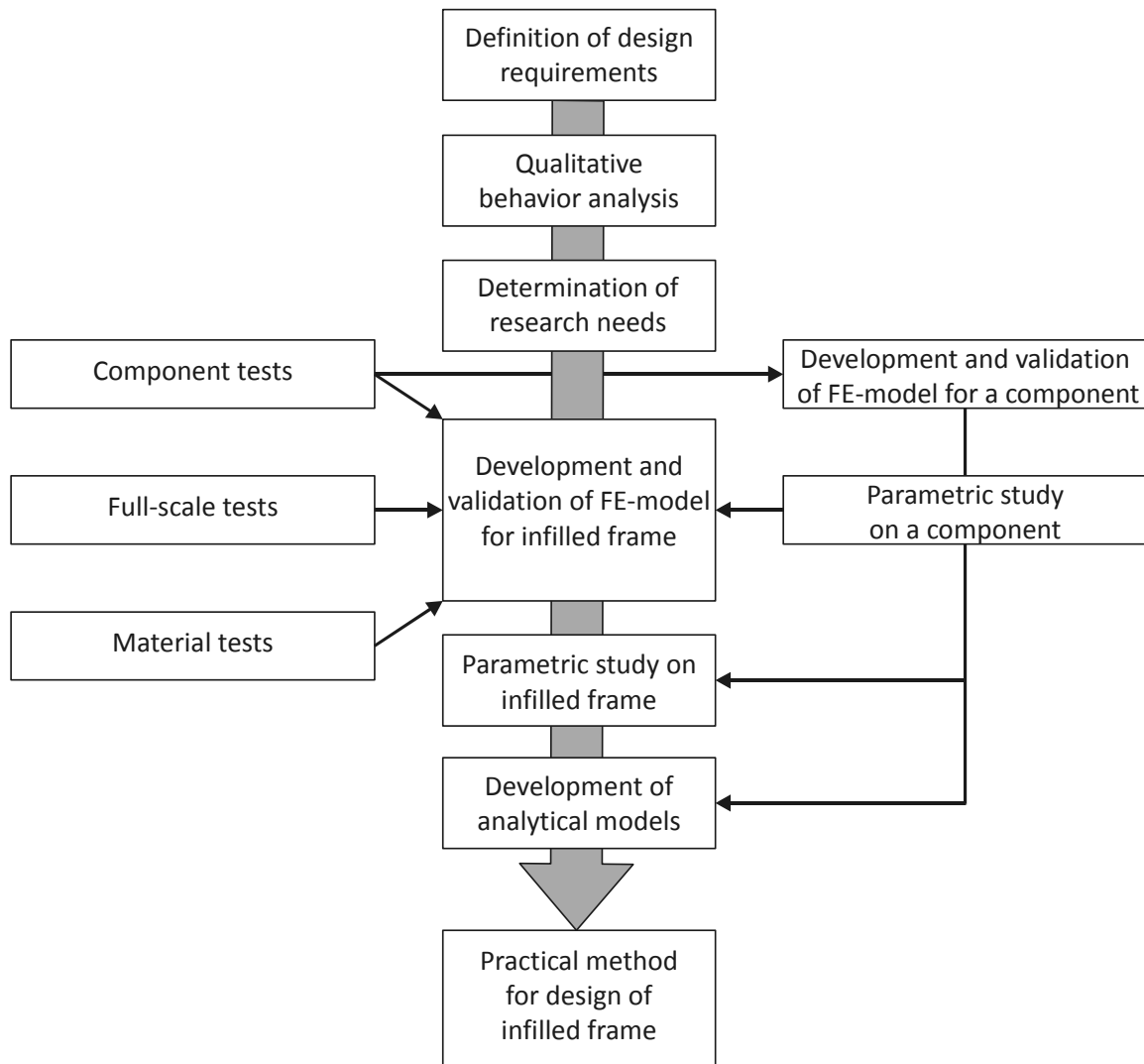


Figure 1-2: Flowchart of the research method

## 1.5 Thesis outline

This thesis is divided into 9 chapters. In the chapter at issue, the topic of research has been introduced and the motivation for the research has been explained. In chapter 2, a state-of-the-art review on infilled frames is presented. Besides, background material on structural bolts as well as strut-and-tie modeling of concrete is presented, as a thorough understanding of those is necessary for this research. In chapter 3, the conceptual design of an infilled steel frame with a discretely connected precast concrete panel is elucidated. A discrete panel-to-frame connection is introduced that enables steel frames and precast concrete panels to act compositely when subject to lateral loading. Subsequently, the behavior of the structure is qualitatively analyzed. Chapter 4 presents a detailed description of the experiments that were carried out, and discusses the results. Chapter 5 treats the finite element study that was conducted. A comparison between the experimental and numerical results is presented. In chapter 6 parameter studies are

described and discussed. The derivation of analytical models for predicting the ultimate lateral load carrying capacity and the lateral stiffness is outlined in chapter 7. In chapter 8, a method for designing infilled steel frames with discretely connected precast concrete panels will be presented. Besides, a worked out design example is provided to demonstrate the application of the design method. Finally, main conclusions and recommendations for further research are summarized in chapter 9.

# Chapter 2: LITERATURE REVIEW

## *Scope of the chapter*

*This chapter presents a literature review of the state-of-the-art of infilled frames (section 2.1). Furthermore, background material on structural bolts (section 2.2) as well as strut-and-tie modeling of concrete (section 2.3) is presented, as a thorough understanding of those is necessary for this research.*

## **2.1 Infilled frames: State-of-the-art**

The structural design of tall buildings is predominantly dictated by the requirements for stiffness and stability. A lateral load resisting system has to provide the building with sufficient strength and stiffness to resist lateral loads mainly caused by wind pressure or earthquakes. Traditionally, tall buildings were designed to make use of a single type of lateral load resisting system, initially simple moment resisting frames, braced frames and shear wall systems. The trend towards bigger and taller buildings created a demand for more efficient and innovative structural systems. One of these structures is the infilled frame, a lateral load resisting structure combining a frame with an infill acting as bracing within the frame. Gravity loads acting on the structure are supported by the frame structure only, while lateral loads are transferred to the foundation by composite action between the infill and its confining frame. Because of the stiffening and strengthening effect of infills on frames, the drift of the frame structure under lateral loading is considerably reduced.

Although the contribution of infills to the lateral stiffness and strength of frame structures has long been recognized, structural engineers have for a long time largely ignored their influence. Usually infill panels were considered as architectural, non-structural elements and designed according to criteria such as fire resistance and sound proofing. Main reasons were the lack of knowledge concerning the composite behavior of infilled frames and the lack of practical methods for predicting their stiffness and strength. However, ignoring the infills resulted in substantial inaccuracy in predicting the lateral stiffness which was not only conservative, but it could even critically cause certain elements in the lower parts of the structure to be overloaded (Stafford Smith, B., 1962).

It has been shown by many investigators that the contribution of infills to the lateral stiffness and strength of frames has great potential. However, due to the complexity of the interaction between infill and frame and the great number of influencing parameters, the structure is still poorly understood. There are no universally accepted design guidelines regarding infilled frames. Consequently, most of the current design codes do



not contain design guidelines for this type of structure. In the following section, a general review of the different analytical methods used for the analysis of infilled frames is presented. Thereafter, the effect of openings on infilled frame behavior and the application of precast concrete infill panels within frames are explicitly treated.

### 2.1.1 Analysis of infilled frames

Over the past few decades, several methods for the analysis of infilled frames have been proposed in the literature by various investigators. These methods can be divided into two groups, depending on the degree of refinement used to represent the structure. The first group consists of the macro models to which belong the simplified models that are based on a physical understanding of the structure. The second group involves the micro models including the finite element formulations, taking into account local effects in detail. Both types of methods will be discussed hereafter.

#### Macro models

The basic characteristic of the macro models is that they aim at predicting the overall stiffness and failure loads of infilled frames, without considering all possible failure modes of local failure. This group of models can be subdivided to their origin into the following three categories, based on:

- the concept of the equivalent diagonal strut
- the concept of the equivalent frame
- the theory of plasticity

#### *Equivalent diagonal strut analogy*

The simplest (and most developed) method for the analysis of non-integral infilled frames is based on the concept of the equivalent diagonal strut. This concept was initially proposed by Polyakov (1956) and later developed by other investigators. In this method, the infilled frame structure is modeled as an equivalent braced frame system with a compression diagonal replacing the infill (Figure 2-1).

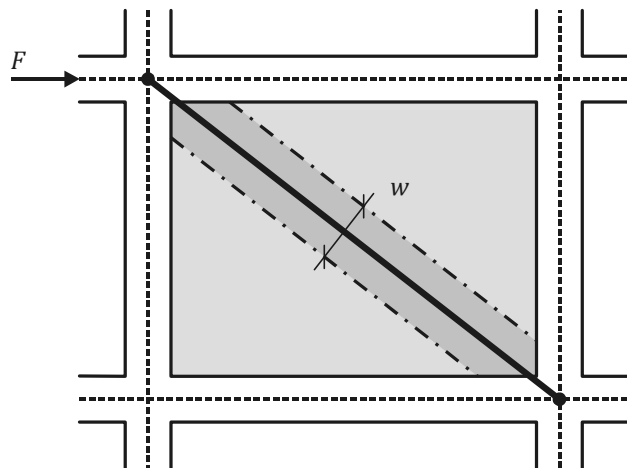


Figure 2-1: Equivalent diagonal strut analogy

This analogy was justified by observation of the phenomenon of slip and separation between the frame and infill except in the vicinity of the two compression corners at an

early stage of loading. The main challenge of this approach was to determine the width of the diagonal strut ( $w$ ).

Based on the investigation into single frames with brickwork and concrete infills, Holmes (1961) proposed to replace the infill by an equivalent pin-jointed diagonal strut having a width equal to one-third of the diagonal length. As the variation of structural parameters other than the diagonal length was ignored, the proposal was too simplistic. Stafford Smith (1966) started a series of tests with single square shaped steel frames with mortar infills. He found that the equivalent strut width increased with the increase of the relative stiffness of the frame to the infill, and related the width of the equivalent strut to the length of contact ( $\alpha$ ) between the frame and the infill using the following analytical equation:

$$\alpha = \frac{\pi}{2\lambda_h} \quad [2-1]$$

where  $\lambda_h$  is a non-dimensional parameter, similar to that used in beam on elastic foundation theory, expressing the relative stiffness of the infill to the frame as follows:

$$\lambda_h = \sqrt[4]{\frac{E_w t_w}{4E_f I_c h_w}} \quad [2-2]$$

in which  $E_w$  and  $t_w$  are the modulus of elasticity and thickness of the infill respectively;  $E_f I_c$  and  $h_w$  are the column rigidity and the height of the infill respectively. Having obtained the length of contact, a finite difference analysis gave the equivalent strut width in terms of the relative stiffness. Based on these results, different charts were proposed to calculate the equivalent width. For calculation of the ultimate strength in case of infill failure, the collapse load was calculated assuming it to be in equilibrium with the contact stresses.

An extension of the work to rectangular infilled frames was carried out by Stafford Smith (1967a; 1967b) and by Stafford Smith and Carter (1969). They found that the equivalent strut width was influenced by, besides the relative stiffness of the infill and the frame, the aspect ratio, the magnitude of the diagonal load on the infill and the stress-strain relationship of the infill material. A series of charts was produced to estimate the equivalent strut width as function of these properties.

Alternative proposals for the evaluation of the equivalent strut width have been suggested, e.g. by Mainstone (1971), Hendry (1981), Liauw and Kwan (1984b) and by Paulay and Priestley (1992). A modification of Mainstone's formula has currently been incorporated in provisions by the Federal Emergency Management Agency (FEMA 356,

2000). Alas, the diverse expressions for  $w$  result in a wide difference in effective widths for the equivalent diagonal strut. Consequently, none of them has been accepted in any design code. The common agreement, however, is that the width of the equivalent strut decreases when the parameter  $\lambda_h$  increases.

In the last decades it has become clear that one single strut is not sufficient to model the complex behavior of the infilled frame, as local effects resulting from the interaction between the infill and the surrounding frame are not reflected by connecting only the two loaded corners of the frame by a single strut. As a result, bending moments and shear forces in the frame members are not modeled realistically and the location of potential plastic hinges cannot be adequately predicted. More complex macro-models were then proposed by many researchers, all based on a number of diagonal struts. Figure 2-2 (a) to (e) show multiple strut models as reported in the state-of-the-art report on analytical modeling of infilled frames by Crisafulli et al. (2000). In spite of increasing complexity, the main advantage of these models is the ability to represent the actions in the frame more accurately.

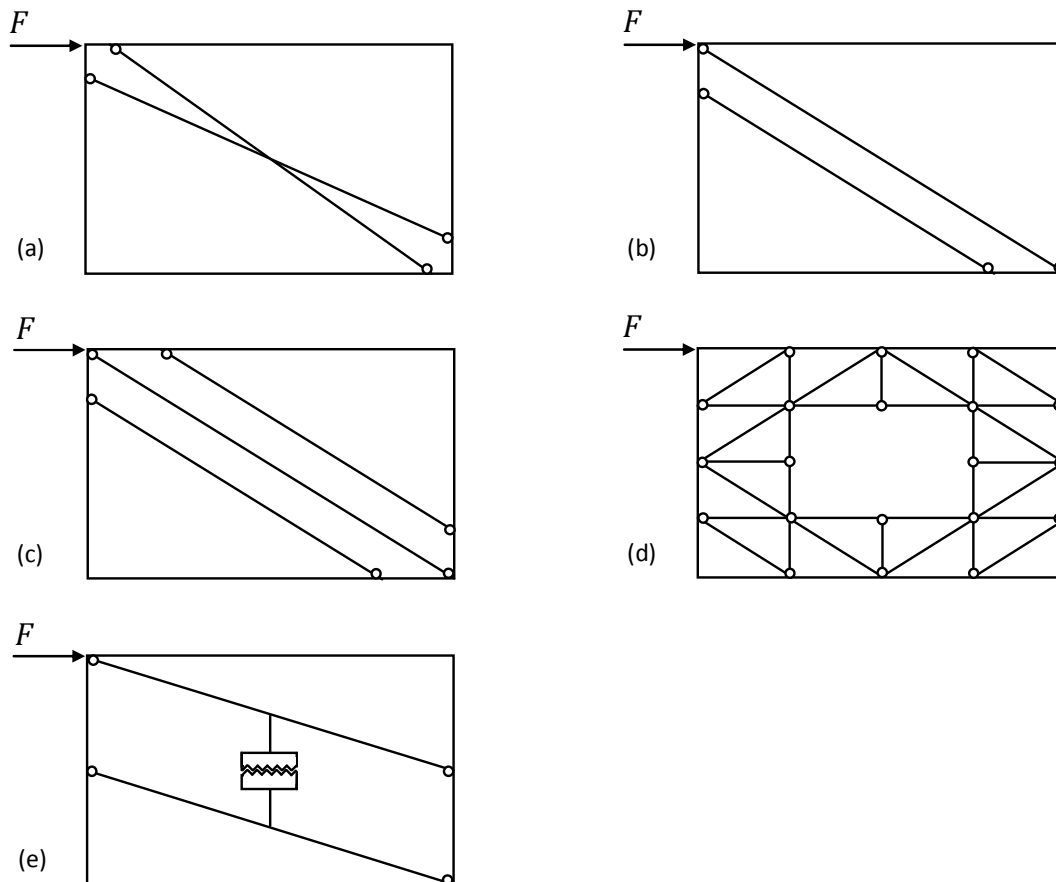


Figure 2-2: Modified diagonal strut models

#### *Equivalent frame analogy*

Liauw (1972) proposed the equivalent frame method for stiffness prediction of fully-integral infilled frames. This analysis method was based on the fact that the infill panel increases the frame's stiffness and strength by magnitudes which depend on the dimensions and the properties of the infill. Therefore, the actual frame was transformed into an equivalent frame with section properties of the columns and beams derived from composite T-sections. The dimensions of the equivalent frame were obtained from the centroidal axes of the actual infilled frame. Having transformed the actual structure into an equivalent frame, it was then possible to analyze the equivalent frame using standard structural analysis methods. The validity of the method was found to depend on the capacity of the shear connectors to sustain the composite action without allowing separation of the infill.

#### *Plastic analysis*

Since the diagonal strut concept was not suitable to predict the ultimate strength of infilled frames, plastic design principles were proposed to predict the collapse load of the structure.

Wood (1978) proposed a plasticity-based theory in which the stress redistribution at ultimate limit state and the importance of the bending strength of the frame were recognized. He assumed that plastic hinges developed at the corners of the bounding frame and that the infill panel was in a state of pure shear strain. Four different collapse modes were identified based on observations of full-scale as well as model tests. Liauw and Kwan conducted an extensive study on the behavior of infilled frames and developed a plasticity based method to deal with non-integral (Liauw, T. C. et al., 1983) and integral infilled frames (Liauw, T. C. et al., 1984b). In this method, stress redistribution due to the development of cracks and crushing of the infill towards collapse, and of the shear strength at the infill/frame interface provided by the shear connectors were taken into account. This study of single-bay infilled frames was later extended by Liauw and Lo (1988) and by Kwan et al. (1990) to multi-bay infilled frames. They performed experiments using small-scale models having up to two bays and four stories.

Extending the plasticity based methods used by Wood and Liauw and Kwan, which assumed failure by collapse mechanisms due to development of plastic hinges in the frames, Saneinejad and Hobbs (1995) observed that concentrated stresses preceded the formation of collapse mechanisms. They proposed a strut model that is based on the development of plasticity in the infill at the loaded corners. Collapse loads determined by the method of Saneinejad and Hobbs were consistently closer to experimental values than those according to earlier methods.

Micro models

The development of finite element methods offered some relief to the shortcomings pointed out in the previous paragraphs. The first approach to analyze infilled frames by linear finite element analysis was suggested by Mallick and Severn (1967). They introduced an iterative technique taking into account separation and slip at the structural interface. Plane stress rectangular elements were used to model the infill while standard beam elements were used for the frame. However, as a consequence of the assumption that the interaction forces between the frame and the infill along their interface consisted of normal forces only, the axial deformation of the columns was neglected in their formulation. The effect of slip and interface friction was considered by introducing shear forces along the length of contact. The contact problem was solved by initially assuming that infill and frame nodes have the same displacement. Having determined the load along the periphery of the infill, tensile forces were located in the model. Subsequently the corresponding nodes of the frame and infill were released which allowed them to displace independently in the next iteration. This procedure was repeated until a prescribed convergence criteria was achieved.

Barua and Mallick (1977) and Mallick and Garg (1971) refined this method by taking into account the axial deformation of the frame. Several single-story single-bay rectangular infilled frames were analyzed and the results were in good agreement with experimental results for height to span ratios smaller than two.

The distribution of elastic stress was studied by Riddington and Stafford Smith (1977), by introducing short stiff linking members as interface elements. Separation between the frame and infill was indicated by the presence of tensile force in the link. Linking members loaded in tension were removed and subsequently the structure was re-analyzed. Also non-friction slip at the frame-to-infill boundary was taken into account by introducing pin-connected links. On the basis of this study, Stafford Smith and Riddington (1978) presented equations suitable for practical design. The applications of these equations in infill frame design have been illustrated by Stafford Smith and Coull (1991).

King and Pandey (1978) presented an improvement to the above technique. They used friction elements at the interface whereby the material properties were adjusted according to idealized elasto-plastic friction-slip characteristics based on shear box tests. However, the relief of friction due to the reduction of normal stress or the separation at the interface had not been considered.

During the period prior to 1980, the finite element analyses were confined to elastic analysis. Liauw and Kwan (Liauw, T. C. et al., 1982) proposed the use of nonlinear finite element analysis to deal with the whole range of problems in infilled frames. Three

different types of elements were used to study infilled frame behavior. Simple bar elements capable of simulating both separation and slip were used to model the infill-to-frame interface. The infill panel was modeled by triangular plane stress elements while standard prismatic bending elements were used for the frame. Nonlinearities of the material and the structural interface were taken into account. Also, the initial lack of fit at the interface was considered. The nonlinear behavior of concrete infills in steel frames without shear connectors (Liauw, T. C. et al., 1984a) and with shear connectors (Kwan, K. H. et al., 1984) was experimentally and numerically studied. These researchers found that for non-integral infilled frames nonlinearity arose mainly from crushing of the loaded corners of the infill and thereupon yielding of the frame and that the effects on the stiffness degradation were significant. For fully-integral infilled frames, nonlinearity arose mainly from cracking and crushing of the infill material, yielding of the infill-frame connection and formation of plastic hinges in the frame. The provision of shear connectors considerably reduced the stress concentrations in the compression corners of the infills as well as the magnitudes of frame shear and moment at the joints. The nonlinear finite element method showed good agreement with experimental results for both lateral stiffness and ultimate strength.

From that time on, the finite element method has been extensively used as a research instrument in both static and dynamic analyses of infilled frames, e.g. (Afefy, H. M. et al., 2002; Asteris, P. G., 2008; Dawe, J. L. et al., 2001; Ghosh, A. K. et al., 2002; Moghaddam, H. A. et al., 2006; Ng'andu, B. M., 2006; Puglisi, M. et al., 2009).

#### **2.1.2 Effect of openings**

Infills are often provided with openings to accommodate doors and windows. Their location and size may have significant effect on the stiffness and load carrying capacity of the composite structure. Depending on their location, openings can interrupt the development of a main compression strut in the infill. Although many investigations have been carried out on solid infilled frames, the available literature on infilled frames with openings is relatively limited.

The effect of openings on the behavior of infilled frames was experimentally investigated by Benjamin and Williams (1958). They conducted a series of experiments on infills with central window openings, with dimensions proportional to the infill dimensions by a ratio of one third, and measured a 50% reduction of the ultimate strength.

As reported by Mallick and Garg (1971), Coull tested in 1966 a few infilled frames having central openings with and without reinforcement around the openings. He observed that these openings reduced the stiffness and strength of infilled frames by about 60 - 70% and by 45% respectively as compared with a solid infill panel. The effect of nominal

reinforcement around the openings was negligible considering first cracking load and strength. The failures occurred due to crushing of one of the loaded corners of the infill panel. Considerable cracking of the infill panels had occurred before failure.

Mallick and Garg (1971) investigated the effect of possible positions of openings on the behavior of infilled frames. Their objectives were to study the relative merits and demerits of different opening positions and to recommend suitable opening positions for doors and windows. Non-integral infilled frames as well as fully-integral infilled frames were considered. Square openings at the corners were used having sides of one-quarter of the side dimension of the infill panel. The sides of central openings were one-fifth of the panel side. The experimental results were compared with theoretical predictions obtained by using a finite element approach. They observed that the composite action between the frame and the infill panel was adversely affected as the opening position was moved towards the compression diagonal. If an opening was provided at either end of the loaded diagonal of a non-integral infilled frame, its lateral strength was reduced by about 75% and its stiffness by 85-90% compared to that of a similar infilled frame with a solid infill panel. For fully-integral infilled frames, the presence of an opening on either end of the loaded diagonal reduces its stiffness by 60-70% (Figure 2-3).

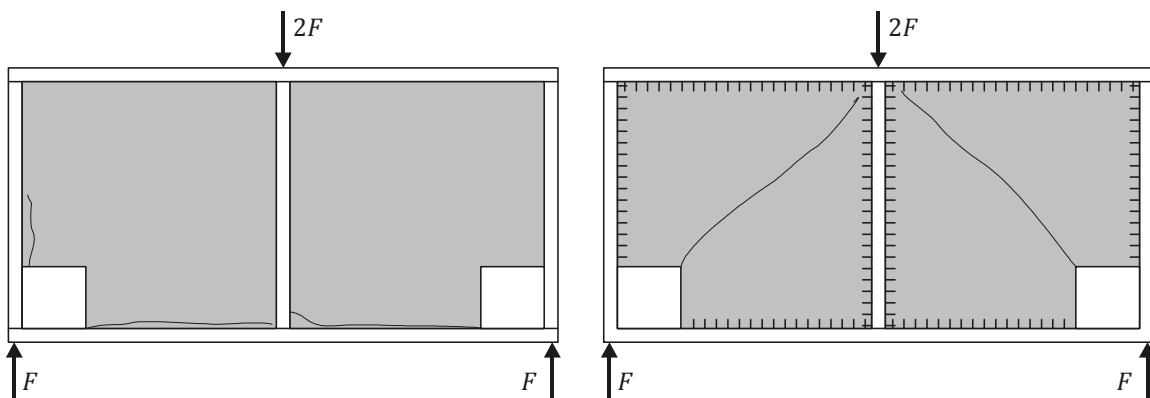


Figure 2-3: Crack patterns for non-integral (left) and fully-integral (right) infilled frame having an opening at the end of the diagonals

For both types of frames, the loss of strength and stiffness due to a central opening was about 25-50% as compared to that of similar frames without openings (Figure 2-4).

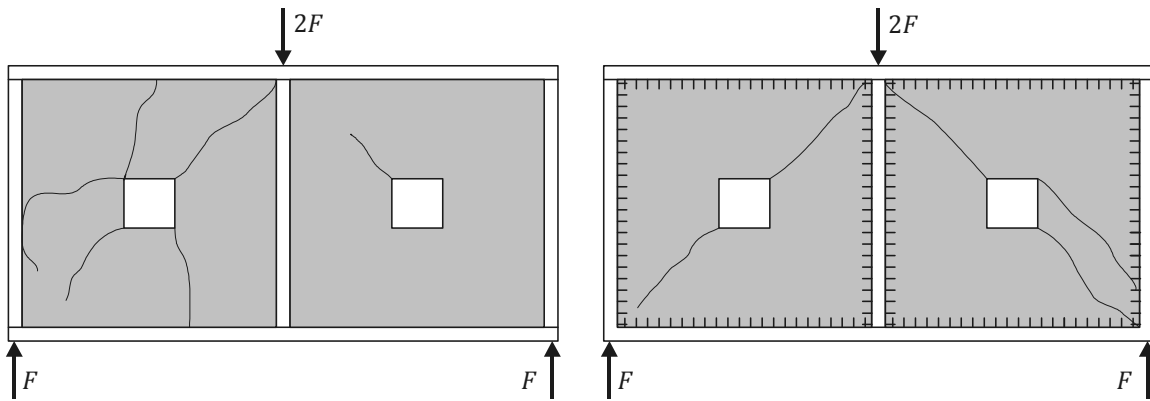


Figure 2-4: Crack patterns for non-integral (left) and fully-integral (right) infilled frame having a central opening

About the position of openings they concluded that door openings could be best located in the centre of the lower half of the panel. Window openings could be best located in the mid-height region of the left or right half of the panel, as near to the vertical edge of the panel as possible.

Liau (1972) pointed out that when treating an infilled frame with an opening, the concept of replacing the infill by an equivalent diagonal strut is inappropriate. He proposed an approximate method of analysis using the equivalent frame method. Experimental results on the stiffness of two elastic models having various sizes of openings in the infill were compared with analytical results. The comparison showed good agreement when the opening was more than 50% of the full infill area. The method was on the conservative side when the opening was less than 50% of the full infill area.

The behavior of multi-story infilled frames, consisting of four-story steel frames with reinforced concrete infills with or without door openings was investigated by Liau and Lee (1977). Non-integral infilled frames as well as fully-integral infilled frames were considered. They approached the diagonal strut analogy with the use of the strain energy method to establish the sectional area of the equivalent diagonal strut. The method enabled the predictions of stiffness and strength of infilled frames with or without opening in the infill panel. They observed that the structural behavior of a non-integral infilled frame changed when doorways in the infills were crossing the compression diagonal, producing bending and shearing in the walls and the beams of the infill panel. The stiffness and strength was drastically reduced. In fully-integral infilled frames the provision of openings in the infills did not change the basic behavior of the structure and the reductions in stiffness and strength were relatively moderate. With the exception of the strength prediction, good agreements between experimental and analytical results were obtained in terms of mode of failure and stiffness.



Dawe and Seah (1989) studied the effect of openings in masonry infills in steel frames. They found that the inclusion of steel reinforcement around the opening increased the initial stiffness, but did not increase the ultimate strength. Furthermore, they found that openings located away from the diagonal strut resulted in a slightly higher ultimate load than for openings located nearer to the diagonal. Therefore, and while the lateral load is normally applied in both directions, they concluded that the best location to accommodate door openings is the center of the wall.

Asteris (2003) studied the influence of infill panel openings on the behavior of brickwork infilled plane frames. A detailed parametric study was carried out using as parameters the position and the percentage of the masonry infill panel opening for the case of single-story single-bay infilled frames. He found that an increase in the opening percentage led to a decrease on the lateral stiffness of infilled frames, reaching 87% for a bare frame (100% opening). For openings exceeding 50%, the stiffness factor remained practically constant. Furthermore, it was shown that the overall action between the frame and the infill is adversely affected as the opening position is moved towards the compression diagonal.

The non-linear in-plane behavior of masonry-infilled steel frames with openings was numerically investigated by Mohebkhah et al. (2008). A finite element model was used to investigate the effect of door opening positions on the lateral stiffness, the ductility and the collapse load of such frames. It was found that the model could be used to predict the collapse load and joint cracking patterns and to explore the possible failure modes of masonry-infilled steel frames with a given location for openings and relative area. Results from the numerical modeling and previous experimental studies found in literature were compared which indicated a good correlation. A further analysis was performed to investigate the effect of door frame confinement on the lateral capacity of a specimen with a central opening. The analysis showed that, by adding a conventional door frame, the lateral load capacity of the infilled frame specimen increased up to 28%.

Mondal and Jain (2008) performed an investigation into the lateral stiffness of masonry infilled reinforced concrete frames with central openings. They proposed a reduction factor for the effective width of a diagonal strut over that of the solid infill to calculate its initial stiffness when a central window opening is present. Experimental results available from published literature were supplemented by finite element analyses. They concluded that the effect of an opening on the initial lateral stiffness of infilled frames should be neglected if the area of opening was less than 5% of the area of the infill panel, meaning that the frame should be analyzed as a solid infilled frame. They also pointed out that the effect of an infill on the initial lateral stiffness of infilled frames may be ignored if the area of opening exceeds 40% of the area of the infill panel, which means that the frame should be analyzed as a bare frame.

### 2.1.3 Infilled frames with precast concrete panels

With the rise of the precast concrete industry, a new area of research in infilled frames was created. A precast infill panel system for strengthening of existing concrete frame buildings was first investigated by Frosch. The objectives were to develop an infill system that eliminated the application of interface dowels, the application of extensive concrete formwork and the pouring of large volumes cast-in-place concrete. In the system, several precast concrete panel elements were used to assemble an infill wall. The panels were provided with shear keys along the side to allow for force transfer, and were connected to one another through the use of reinforced cast-in-place closure strips. Connection to the existing frame was realized by the application of steel pipes (shear lugs) which eliminated the need for interface dowels. Connection tests (Frosch, R. J., 1999a; Frosch, R. J., 1999b) as well as large scale tests (Frosch, R. J., 1996) were carried out to verify the performance of connection details and to study the overall system behavior. Design and detailing guidelines for the precast infill wall system were developed to provide engineers with a method for proportioning the various elements of the precast infill wall system.

At Eindhoven University of Technology a research program on infilled steel frames with discretely connected precast concrete infill panels (semi-integral infilled frames) was initiated, aiming at development of design rules for this composite structure. In a numerical study (Tang, R. B. et al., 2003) the influence of discrete interface connections on the structural behavior of a square steel frame with a precast concrete infill panel subject to lateral load was investigated. This study was limited to linear elastic analysis. Ten different patterns of discrete interface connections were numerically investigated for which the number and the locations of the connections were varied. It was observed that interface connections on beams were more efficient than on columns, and that the lateral stiffness of the structure improved when connections were located closer to the frame joints. It could be observed that the contribution of discretely connected panels to the performance of steel frames was significant and they concluded that semi-integral infilled frames might achieve similar improvements in structural performance as fully-integral infilled frames.

In subsequent experimental research (Hoenderkamp, J. C. D. et al., 2005; Hoenderkamp, J. C. D. et al., 2007) tests on individual panel-to-frame connections were performed. This connection consisted of steel plates precast in pockets at the edge of the panel and was designed for a failure mechanism consisting of bearing failure in the bolt holes in order to avoid brittle failure. The connection was assumed to act as a hinge, and able to transfer normal and shear forces. As a result, the infill panel was loaded in both compression and tension. Thereupon, a full-scale experiment was performed on a single-story single-bay infilled frame. However, the infilled frame did not fail by the anticipated failure mechanism as the structure failed by anchor pull-out.

Simultaneously, a second type of discrete panel-to-frame connection was developed at Eindhoven University of Technology. This connection consisted of structural bolts on the column and beam of the frame, confining the precast concrete infill panel within the frame. The connections were located in the panel corners, and assumed to transfer compressive forces only. Therefore, the effect of the infill panel was more similar to the action of a diagonal strut bracing the frame. Full-scale experiments were performed on a single-story single-bay infilled frame. The structural system acted as was expected. However the discrete interface connection appeared to be too weak. The flanges of the steel frame deformed plastically under the compression produced by the bolts. In a subsequent study, the capacity of the connection was increased by situating backing plates on the flanges either with or without diaphragms between the flanges. Also, the effect of a window opening in the infill panel was experimentally investigated (Teeuwen, P. A. et al., 2006). It was found that, even provided with window openings, the contribution of precast concrete infill panels to the performance of steel frames was substantial. However, this time plastic deformation occurred at the, in the panel corners installed, steel angles, under the compression produced by the bolts.

#### **2.1.4 Section conclusions**

The presented state-of-the-art review on infilled frames shows that extensive investigations have been done into the structural behavior of infilled frames with masonry and cast-in-place concrete infills. Several analytical models have been developed to describe the composite infilled frame behavior. However, so far none of them has been accepted in the current design codes.

Although a lot of the investigations were conducted on infilled frames with solid infills, few studies have been conducted on infilled frames with openings. Those studies that were carried out are mainly restricted to masonry infills. It has been demonstrated that the presence of an opening in the infill substantially alters the performance of infilled frames. Furthermore, recommendations have been made for suitable opening positions within an infill.

The application of precast concrete infill panels created a new area of research in infilled frames. It has been shown that discretely connected precast concrete panels in steel frames might achieve good structural performance. Even with window opening, the contribution of the infill to the frame has shown to be significant. However, more research is needed to investigate the interaction between the panel and frame through discrete interface connections, and to develop analytical methods for the design of this type of infilled frame.

## 2.2 Structural bolts

In this section the background of standard hexagonal bolts and nuts is presented. The dimensions, grades and strengths of the structural bolts are discussed. Subsequently, a survey of current considerations for predicting the strength and stiffness of bolts subject to tensile loading is presented.

### 2.2.1 Standard bolts: dimensions, grades and strengths

There are many systems for specifying the dimensions of bolts. In large parts of the world the ISO metric screw thread has replaced the much older systems. Metric screws are specified by the ISO 261 and ISO 262 standards. A metric ISO screw thread is designated by the letter M followed by two numbers, both expressed in millimeters and separated by the multiplication sign “x” (e.g. M24x3.0). The ‘M’ indicates that the bolt is metric. The following number is the nominal diameter in millimeters. The last number gives the pitch of the thread. Threads other than the ISO metric threads commonly used are Unified Thread Standard, (UTS), which is still in common use in the United States and Canada, British Standard Whitworth (BSW) and British Association screw threads (BA). However, these will not be discussed further in this work.

High-strength bolts usually have a hexagonal head with an ISO strength rating stamped on the head. This indication exists of two numbers separated by a decimal point. The number before the point is the guaranteed minimal tensile ultimate strength ( $f_{ub}$ ) in  $\text{N/mm}^2$  divided by 100. The number after the point is 10 times the ratio of the tensile yielding strength or 0.2% proof strength ( $f_{yb}$ ) to the tensile ultimate strength. For example, a property class 4.6 bolt has a nominal (minimum) tensile ultimate strength of  $400 \text{ N/mm}^2$ , and a tensile yield strength of 0.6 times tensile ultimate strength or  $0.6 \times 400 = 240 \text{ N/mm}^2$ . Most commonly used bolts are 4.6, 8.8, 10.9 and 12.9 bolts.

For nuts, a minimal tensile strength is not directly prescribed. The indication of the grade for steel nuts exists of one number that matches the first number of the bolt with the highest grade that enables the nut to be loaded up till a certain proof stress without stripping of the threads in the nut. The proof strength of a standard nut is generally greater than the proof strength of the bolt with which it is supposed to be used. Designers prefer bolt failure to nut failure because a failure of the bolt is more obvious.

### 2.2.2 Strength considerations

Tensile loading is the most fundamental mode of loading bolts. Failure of a bolt under axial tensile loading generally occurs in one of three modes: 1) tension failure through the shank or threaded section of the bolt, 2) stripping of the bolt threads, or 3) stripping of the nut threads.

Structural bolts are designed so that tension failure of the bolt will occur before stripping of the threads. A general-purpose bolt breaks in tension through the threads, as if it were breaking through an equivalent solid shank with a diameter between that of the pitch and minor diameters. The area of this equivalent shank is called the tensile stress area of the bolt ( $A_s$ ), which can be calculated with the following empirical equation:

$$A_s = \frac{\pi}{4} (d_b - 0.9382p)^2 \quad [2-3]$$

Where:

$d_b$  = nominal diameter of the bolt [mm]

$p$  = pitch of the thread [mm]

The breaking load ( $F_B$ ) of a bolt is related to its tensile stress area as follows:

$$F_B = f_{ub} A_s \quad [2-4]$$

Thread stripping is a shear failure which occurs either by stripping of the threads of the bolt or by stripping of the threads of the nut, depending on their relative strengths. If the nut threads are stronger than the bolt threads, thread failure occurs by stripping of the thread of the bolt at a diameter established by the minor diameter of the thread of the bolt. If the bolt threads are stronger than the nut threads however, thread failure will occur by stripping of the thread of the nut at a diameter established by the major diameter of the thread of the bolt.

To prevent thread stripping failure, bolt-nut assemblies are designed based on Alexander's theory (Alexander, E. M., 1977), a calculation method in which the minimum nut height and the proof load are calculated from the geometrical conditions of a bolt-nut assembly and the mechanical properties of their materials. According to this theory it is possible to calculate the bolt stripping strength ( $F_{sb}$ ) and the nut stripping strength ( $F_{sn}$ ) with the following equations:

$$F_{sb} = \frac{f_{yb}}{\sqrt{3}} A_{sb} C_1 C_2 \quad [2-5]$$

$$F_{sn} = \frac{f_{yn}}{\sqrt{3}} A_{sn} C_1 C_3$$

With:

$$A_{sb} = \frac{\pi m^* D_1}{p} \left[ \frac{p}{2} + \frac{1}{\sqrt{3}} (d_2 - D_1) \right]$$

$$A_{sn} = \frac{\pi m^* d}{p} \left[ \frac{p}{2} + \frac{1}{\sqrt{3}} (d - D_2) \right]$$

Where:

$A_{sb}$  = bolt thread shear area [mm<sup>2</sup>]

$A_{sn}$  = nut thread shear area [mm<sup>2</sup>]

$m^*$  = effective nut height for stripping [mm] (for standard nuts  $m^* = 0.75D$ )

$D_1$  = minor diameter of the nut thread [mm]

$D_2$  = pitch diameter of the nut thread [mm]

$d$  = major diameter of the bolt thread [mm]

$d_2$  = pitch diameter of the bolt thread [mm]

$p$  = pitch of the thread [mm]

In the equations above, three strength reduction factors are used ( $C_1$  to  $C_3$ ). The first factor ( $C_1$ ) is a modification factor for nut dilation. Due to the 30° flank angle of standard threads, axial loads generate a wedging action, producing dilation (radial displacement) of the internally threaded part which reduces the shear stress supporting area. An internally threaded part with thinner walls allows more dilation. This explains the strength advantage of heavy nuts over regular nuts. The dilation strength reduction factor ( $C_1$ ) is calculated as follows (see Figure 2-5 for definition of  $s$  and  $D$ ):

$$C_1 = -\left(\frac{s}{D}\right)^2 + 3.8\left(\frac{s}{D}\right) - 2.61 \quad [2-6]$$

This equation is valid for values of  $s/D$  between 1.4 and 1.9 (Figure 2-6). No advantage is given for values of  $s/D$  greater than 1.9.

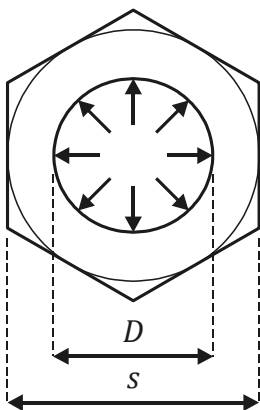


Figure 2-5: Nut dilation

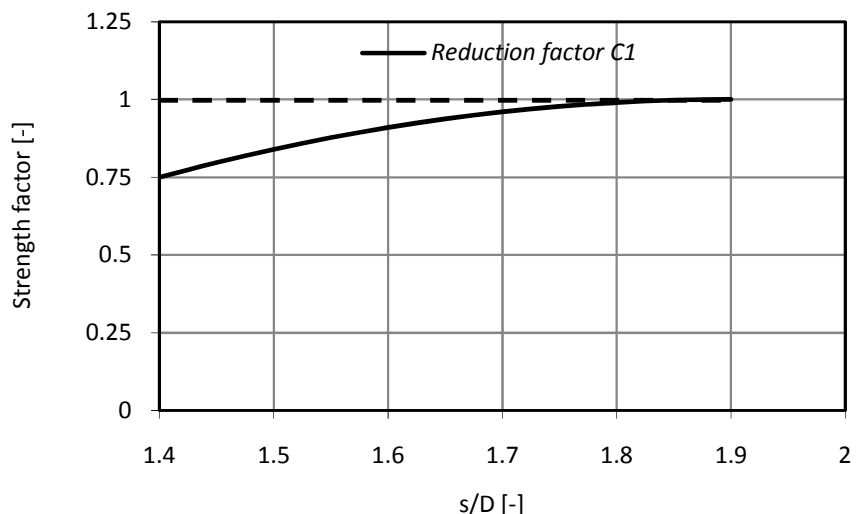


Figure 2-6: Dilation strength reduction factor  $C_1$

Strength reduction factors  $C_2$  and  $C_3$  account for bending of the bolt and nut threads, respectively. As described before, the relative strength always determines which member will bend. If there is a too big difference between the two materials, the weaker of the

two threads will deflect under the relatively stiff action of the other. This creates a form of thread disengagement that again reduces the shear stress supporting area. As the engaged threads bend, there is less effective thread shear area. Also, the bent thread has a decreased flank angle, creating more dilation. The strength ratio  $R_s$  is defined as follows:

$$R_s = \frac{f_{un}A_{Sn}}{f_{ub}A_{Sb}} \quad [2-7]$$

Depending of the value of  $R_s$ , the strength reduction factors  $C_2$  and  $C_3$  can be determined with the following empirical equations:

$$C_2 = 5.594 - 13.682R_s + 14.107R_s^2 - 6.057R_s^3 + 0.9353R_s^4 \quad (\text{for } 1 < R_s < 2.2) \quad [2-8]$$

$$C_2 = 0.897 \quad (\text{for } R_s \leq 1)$$

$$C_3 = 0.728 + 1.769R_s - 2.896R_s^2 + 1.296R_s^3 \quad (\text{for } 0.4 < R_s < 1) \quad [2-9]$$

$$C_3 = 0.897 \quad (\text{for } R_s \geq 1)$$

Figure 2-7 graphically shows the relationship between the reduction factors ( $C_2$  and  $C_3$ ), and the strength ratio  $R_s$ .

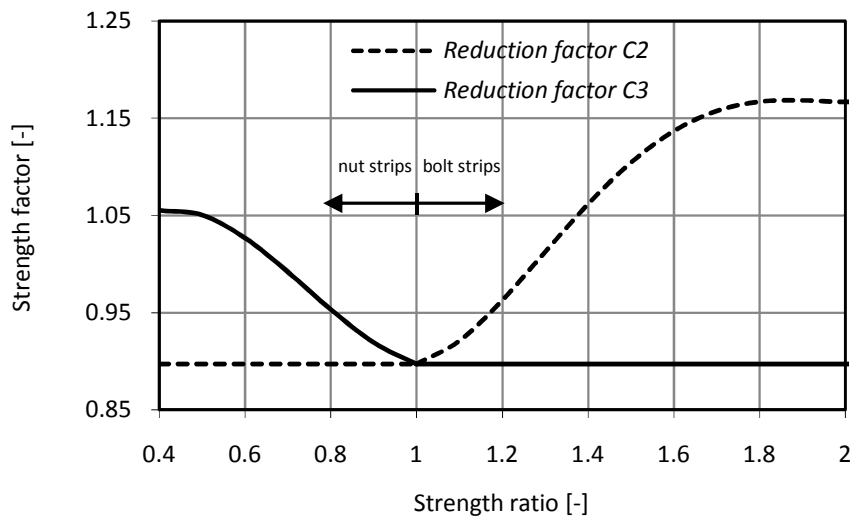


Figure 2-7: Strength reduction factors  $C_2$  and  $C_3$  for thread bending

Several other factors as coefficient of friction, dynamic friction, corrosion and temperature can also modify the strength. However, these are out of the scope of this research, and will therefore not be considered.

### 2.2.3 Stiffness considerations

The process of determining the bolt (elastic) stiffness is based on basic applied mechanics. When an axial load is applied to the ends of a straight cylindrical rod, it stretches. The stiffness of an axially loaded member can be expressed by the following equation:

$$k = \frac{EA}{L} \quad [2-10]$$

However, the preceding equation is applicable only to parts with a uniform cross-section. Bolts typically have significant changes in geometry. The cross-sectional area of the bolt's shank ( $A_b$ ) is larger than that of its threaded portion ( $A_s$ ). This difference in area can be represented by considering a component spring with different stiffnesses in series. Accordingly, the bolt stiffness ( $k_b$ ) is given by the following equation:

$$k_b = \left[ \frac{L_s}{EA_b} + \frac{L_{tg}}{EA_s} \right]^{-1} \quad [2-11]$$

The bolt shank length ( $L_s$ ) and the bolt threaded length included in the grip ( $L_{tg}$ ) should include a part of the head and nut thickness respectively, to allow for local deformations. Recommendations for the value of the factor  $\xi$  in equation [2-12] range from 0.3 to 0.6.

$$k_b = \left[ \frac{\xi d_b}{EA_b} + \frac{L_s}{EA_b} + \frac{L_{tg}}{EA_s} + \frac{\xi d_b}{EA_s} \right]^{-1} \quad [2-12]$$

Eurocode 3 EN 1993-1-8 (2005), which deals with connection design in detail, defines the stiffness for a single bolt-row (2 bolts) as follows:

$$k_b = 1.6 \left[ \frac{L_b}{EA_s} \right]^{-1} \quad [2-13]$$

where  $L_b$  is the bolt elongation length, taken as equal to the grip length plus half the sum of the height of the bolt head and the height of the nut.

Swanson and Leon (2001) investigated the elastic-plastic behavior of bolted T-stub connection components. Based on observations on T-stub component tests and individual bolt tests, the bolt stiffness model represented in Table 2-1 was developed, incorporating a variable bolt stiffness that captures the changing behavior of the bolts as a function of the loads that they are subjected to. The bolt stiffness model is made up of four linear segments. The first segment models the bolt before its pretension is overcome. Until the pretension is overcome, the bolts are assumed to be infinitely rigid. The second segment models the bolt during the linear-elastic portion of its response, according to equation [2-11]. The third segment models the bolt after initial yielding has started. A limit of 85%



of the tensile capacity is used to identify the onset of yielding. The fourth segment models the bolt after it has reached a plastic state.

Table 2-1: Bolt stiffness model

Segment	Bolt load	Bolt stiffness
1	$0 \leq F < F_{B;0}$	$k_{b;1} = 1000 k_b$
2	$F_{B;0} \leq F < 0.85F_B$	$k_{b;2} = k_b$
3	$0.85F_B \leq F < 0.90F_B$	$k_{b;3} = 0.10k_b$
4	$0.90F_B \leq F < F_B$	$k_{b;4} = 0.02k_{bb}$

### 2.3 Strut-and-tie modeling of concrete

For the design of structural concrete components, it is common practice to subdivide a structure into two different kinds of regions. The first ones are the B-regions, where B stands for beam or Bernoulli. For B-regions the Bernoulli hypothesis of a cross-section remaining plane after bending is satisfied. Therefore, the design of a B-region is well understood and the entire flexural and shear behavior can be predicted by relatively simple calculations using conventional beam theory and parallel chord truss analogy respectively. The second types of regions are D-regions, where D stands for disturbed or discontinuity. The D-regions, in contrast, are those parts of a structure where the above standard methods do not apply. D-regions include parts near abrupt changes in geometry (geometrical discontinuities) or concentrated forces (statical discontinuities). Based on St. Venant's principle, the extent of a D-region spans about one section depth of the region on either side of the discontinuity. Familiar types of these regions are joints, corners, corbels, openings and deep beams. An example of the division between B-regions and D-regions in a beam with concentrated load and opening is shown in Figure 2-8.

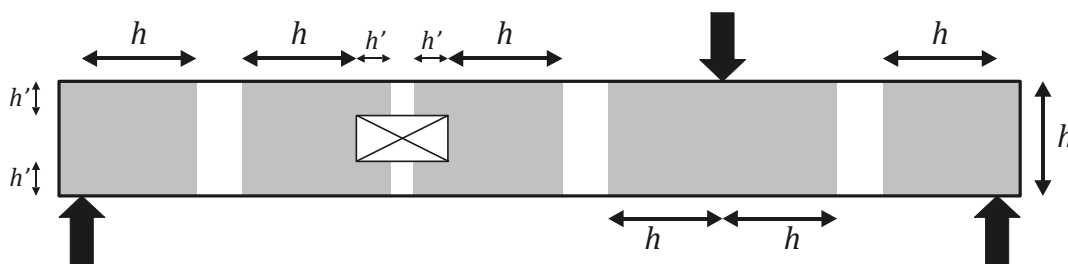


Figure 2-8: B-regions (white) and D-regions (grey) of a beam with concentrated load and opening

The Strut-and-Tie Method (STM) forms an analysis and design methodology for all types of D-regions in structural concrete. In this method, internal stresses are assumed to be transferred through a truss mechanism. The tensile ties and compressive struts serve as truss members connected by nodes. Struts are the compression members of a strut-and-tie model and represent concrete stress fields whose principal compressive stresses are predominantly along the centerline of the strut. The geometry of a strut varies widely and

depends on the force path that each individual strut is intended to model. To cover all cases of compression fields, the idealized shape of concrete stress fields surrounding a strut can be prismatic, fan-shaped or bottle-shaped (Figure 2-9) (Schlaich, J. et al., 1991). The most basic type of strut is prismatic, having a uniform cross-section over the length of the strut. The fan-shaped stress field is an idealization of a stress field with negligible curvature. As a result, it does not develop additional transverse stresses besides the transverse stresses resulting from the Poisson effect. The bottle shaped stress field, on the other hand, accounts for considerable transverse stresses, being compression in the bottle neck and tension further away. It is therefore necessary to reinforce the stress field in the transverse direction.

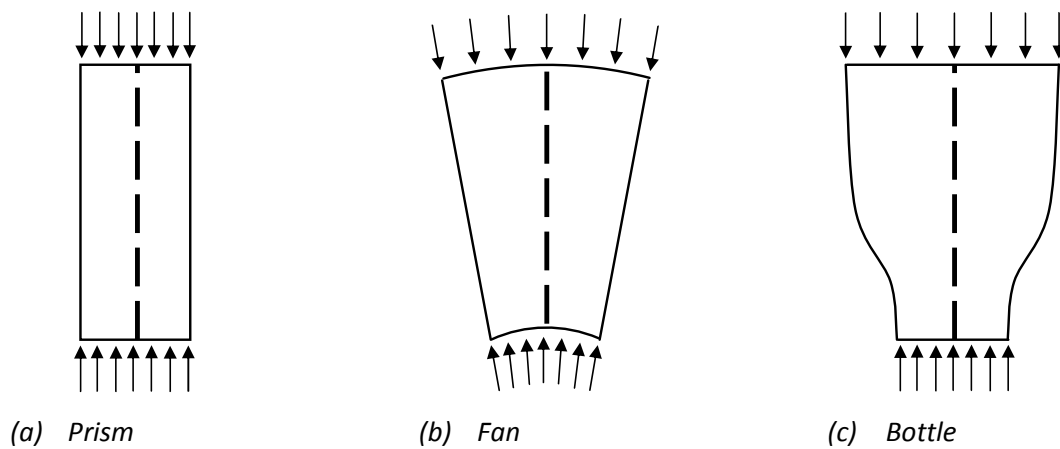


Figure 2-9: Basic type of struts: (a) prismatic, (b) fan-shaped, (c) bottle-shaped

Ties are the tension members of a strut-and-tie model and mostly represent reinforcing steel or occasionally concrete stress fields with principal tension predominant in the tie direction. Its cross-section results from the tie force in the ultimate limit state and the design yield strength of the steel.

Nodes are, analogous to joints in a truss, the places where forces are transferred between struts, ties and exterior loads. As a result, these regions are subject to a multi-axial state of stress. Nodes are classified by the types of forces being connected. Figure 2-10 shows basic types of nodes in a 2-D member, where C is used to denote compression and T is used to denote tension (Schlaich, J. et al., 1987).

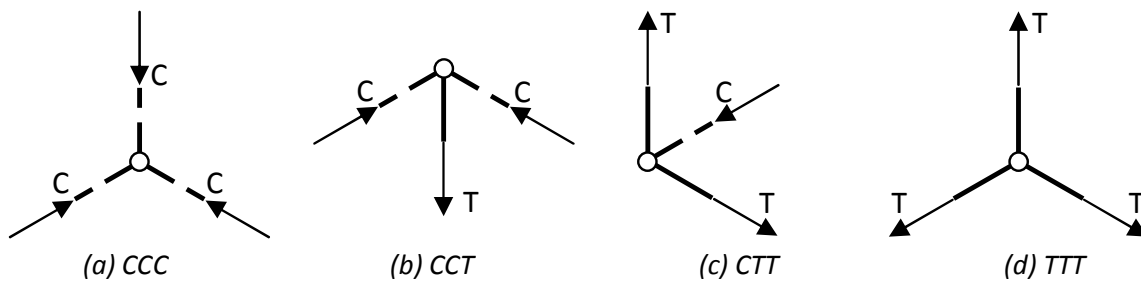


Figure 2-10: Classification of nodes

To allow safe transfer of strut and tie forces through nodal zones, the concrete stress levels in nodes may not exceed the concrete limiting strength in the nodal zone. The strength of concrete in nodal zones depends on a number of factors, including confinement provided by compressive reactions or by transverse reinforcement, the effect of strain discontinuities within the nodal zones and the splitting stresses resulting from intersecting tension ties (Yun, Y. M. et al., 1996). Considerable research has been conducted in an effort to determine the limiting strength of concrete in nodal zones. An extensive literature study regarding the approaches for evaluating the limits of nodal zone strengths is presented in a publication of Yun (2006).

The strut-and-tie model accounts for the distribution of both flexure and shear. It is based on the lower-bound theory of limit analysis which implies that there is no unique strut-and-tie model for a given problem. In other words, more than one admissible strut-and-tie model may be developed for each load case as long as the selected truss is in equilibrium with the boundary forces and the stresses in the struts, ties, and nodes do not exceed allowable limit stresses. The lower-bound theorem guarantees that the capacity obtained from all statically admissible stress fields is lower than or equal to the actual collapse load. Although the STM is also applicable to B-regions, the STM is not preferred to the conventional beam theory for the design for flexure and the parallel chord truss analogy for the design for shear. An example of a strut-and-tie model for a deep beam is shown in Figure 2-11.

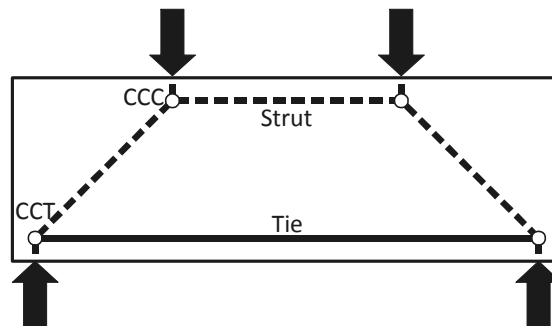


Figure 2-11: Example of strut-and-tie model for deep beam

### 2.3.1 Historical overview of strut-and-tie modeling

The idea of the strut-and-tie method came from the truss analogy method introduced independently by Ritter (1899) and Mörsh (1908), who at the beginning of the 20<sup>th</sup> century investigated the resultants of the internal stresses by means of truss models. The model was used to idealize the flow of force in a cracked concrete beam. The application of plasticity based design procedures to the design of structural discontinuities provided the opportunity to follow the forces through a structure.

Drucker (1961) proposed the application of stress fields to reinforced concrete beam design, based on the concept of the lower bound theorem of limit analysis. Schlaich started in 1979 to work on strut-and-tie models for disturbed regions (D-regions) in concrete structures to explain the structural behavior in these regions. He further developed the strut-and-tie concept and summarized the knowledge on strut-and-tie models in a landmark paper (Schlaich, J. et al., 1987). Schlaich and Schäfer (1991) developed strut and tie models by utilizing stress trajectories from finite element analysis. Directions of struts and ties were taken in accordance with the directions of principal compressive and tensile stresses determined with the finite element analysis. Approaches for determination of the effective stress levels of concrete struts and for verifying the bearing capacity of nodal zones in strut-and-tie models were proposed by Yun and Ramirez (1996). The effective stress levels of the concrete struts were determined by implementing the principal stress ratios of finite element analysis corresponding to the strut regions of the strut-and-tie model. This method was extended with a nonlinear strut-and-tie model approach (Yun, Y. M., 2000). Muttoni et al. (1997) developed the method with stress fields, closely related to the strut-and-tie method, using limit state analysis to structural concrete. They pointed out that the limit state theory of perfect plasticity provides a consistent scientific basis, from which simple and, above all, clear models may be derived to determine the static strength of reinforced concrete structures. Liang (2002) developed a performance-based strut-and-tie modeling procedure for reinforced concrete. His optimization procedure consists of eliminating the lowest stressed portions from the structural concrete member to find the actual load path. It is proposed that minimizing the strain energy is equivalent to maximizing the overall stiffness of a structure and that the strut-and-tie system should be based on system performance (overall stiffness) instead of component performance (compression struts and tension ties). Most of the studies are mainly focused on two dimensional structures. In the work of Leu (2006), a strut-and-tie design methodology is proposed for three dimensional reinforced concrete structures.

### **2.3.2 Strength of struts and nodal zones**

Although extensive research has been performed in an effort to determine the limiting strength of concrete struts and nodal zones, substantial differences exist between the results. These differences mainly originate from uncertainties associated with defining the characteristics of an idealized truss within a continuum of structural concrete. For European practice, recommendations for design by the STM can be found in the FIP recommendation (FIP Commission 3 on Practical Design, 1999). Provisions for the STM have been incorporated in Eurocode 2 (EN 1992-1-1, 2004). These will be applied in this study and are for that reason presented here:

Stress limits according to Eurocode 2 EN 1992

The stress limit  $f_{cu}$  for struts should be obtained from:

$$f_{cu} = k_s f_{cd} \quad [2-14]$$

With:

$$f_{cd} = f_{ck} / \gamma_c \quad [2-15]$$

Where:

$f_{cd}$  = design compressive strength of concrete

$f_{ck}$  = characteristic cylinder compressive strength of concrete

$\gamma_c$  = partial safety factor for concrete

$k_s = 1.0$  for struts in uni-axial compression or with transverse compression

$k_s = 0.6 (1 - f_{ck}/250)$  for struts with transverse tension

The concrete compressive stresses in the nodal zone boundaries are limited as follows:

$$f_{cu} = k_n \left( 1 - \frac{f_{ck}}{250} \right) f_{cd} \quad [2-16]$$

Where:

$k_n = 1.00$  for CCC nodes

$k_n = 0.85$  for CCT nodes

$k_n = 0.75$  for CTT nodes

$k_n = 3.00$  for CCC nodes in a three axial state of stress.

For more detailed information considering the strut-and-tie approach, reference is made to an extensive state-of-the-art report by the ASCE-ACI Committee 445 on Shear and Torsion (ASCE-ACI Committee 445, 1998).

## Chapter 3: CONCEPTUAL DESIGN

### *Scope of the chapter*

*In this chapter, two existing discrete panel-to-frame connections are evaluated on their practical and structural performance. Based on this evaluation, one discrete panel-to-frame connection is selected for application in this research project. Next, a mechanical system is presented, representing the structural behavior of a semi-integral infilled frame constructed with the selected connection. Considering the mechanical system, a survey of applicable design methods is made and the shortcomings are listed. Thereupon the research needs are established for further investigation.*

### **3.1 Discrete panel-to-frame connection**

Essential parts of the semi-integral infilled frame are the discrete interface connections between the precast concrete panel and the steel frame. Considering that all interaction between the panel and the frame occurs through these connections, they may significantly influence the overall infilled frame behavior and thus largely determine its structural characteristics.

To obtain a building system which restricts on-site building activities principally to assembly works, well-designed discrete panel-to-frame connections are required. Besides enabling panel and frame to act compositely when laterally loaded, the connections must contribute to the improvement of the constructability. Therefore, the following additional requirements were defined for the panel-to-frame connections:

- The connections must enable a fast erection on site.
- The connections should allow the assembly to be performed with a minimum of manpower.
- The connections must enable adoption of manufacturing and site erection tolerances.
- The connections and their reinforcement detailing may not adversely influence economic manufacturing of the precast panels and their transport.
- The connections must allow inspection and adjustment in a simple way.
- The connections must allow to be designed to govern the strength of the structure, providing a safe and controllable failure mechanism for the structure.

Although most requirements are quite straight forward and familiar in (precast) construction, the last point may need some more clarification.

The infilled frame structure is meant to be designed such, that the strength of the structure will be governed by the panel-to-frame connections. For that purpose, a safe failure mechanism is necessary which can be aimed for in advance. Consequently, good ductility should be achieved.

In section 2.1.3 it was mentioned that two different types of discrete panel-to-frame connections have been developed at Eindhoven University of Technology. These two connection types show completely different structural behavior characteristics, which also results in dissimilar overall infilled frame behavior. The first type (Type I) consists of two steel plates which are connected together (Figure 3-1a). One plate is welded to a single U-shaped reinforcing bar that acts as an anchor bolt. This plate is precast at mid-section in a pocket at the edge of the panel. The second plate is welded to the steel beam. The two plates are connected together with two bolts, leaving a small gap between panel and frame along the complete panel circumference. The connection is assumed to act as a hinge, enabling the transfer of normal and shear force between panel and frame. As a result, the infill panel is loaded in both compression and tension, similarly to X-bracing in a trussed frame. The connections are designed for a failure mechanism consisting of bearing failure in the bolt holes of the steel plates.

The second connection type (Type II) is realized by structural bolts on the column and beam in every corner of the steel frame (Figure 3-1b). The precast concrete infill panel is confined within the steel frame by these bolts, leaving a small gap between panel and frame along the complete panel circumference. To introduce forces into the panel, steel angles are cast in the concrete at every corner of the panel. The connections are located in the panel corners, and are unable to transfer tensile forces. Therefore, only the bolts in the compression corners are active in a laterally loaded system. Consequently, the infill panel has to act as a diagonal under compression what makes the effect of the infill panel similar to the action of a diagonal compression strut bracing the frame. The connections are designed for a bolt failure mechanism, aiming at bolt shear through the nut.

For this study, one connection type is selected for further investigation. In order to make a well-founded decision, both connection types are judged on their practical and structural performance. First of all, the properties of both connection types are tested against the requirements concerning the manufacturing and construction process that were defined in the previous paragraphs. A survey of this is provided in Table 3-1. As demonstrated by the table, both connections meet the requirements to a reasonably high degree. Although some of the requirements are satisfied by both types on the same level, connection Type II shows important advantages in the assembly procedure and the adoption of tolerances which is expected to considerably increase the speed of construction. Therefore, based on the requirements concerning construction, connection Type II is preferred to Type I.

CONCEPTUAL DESIGN

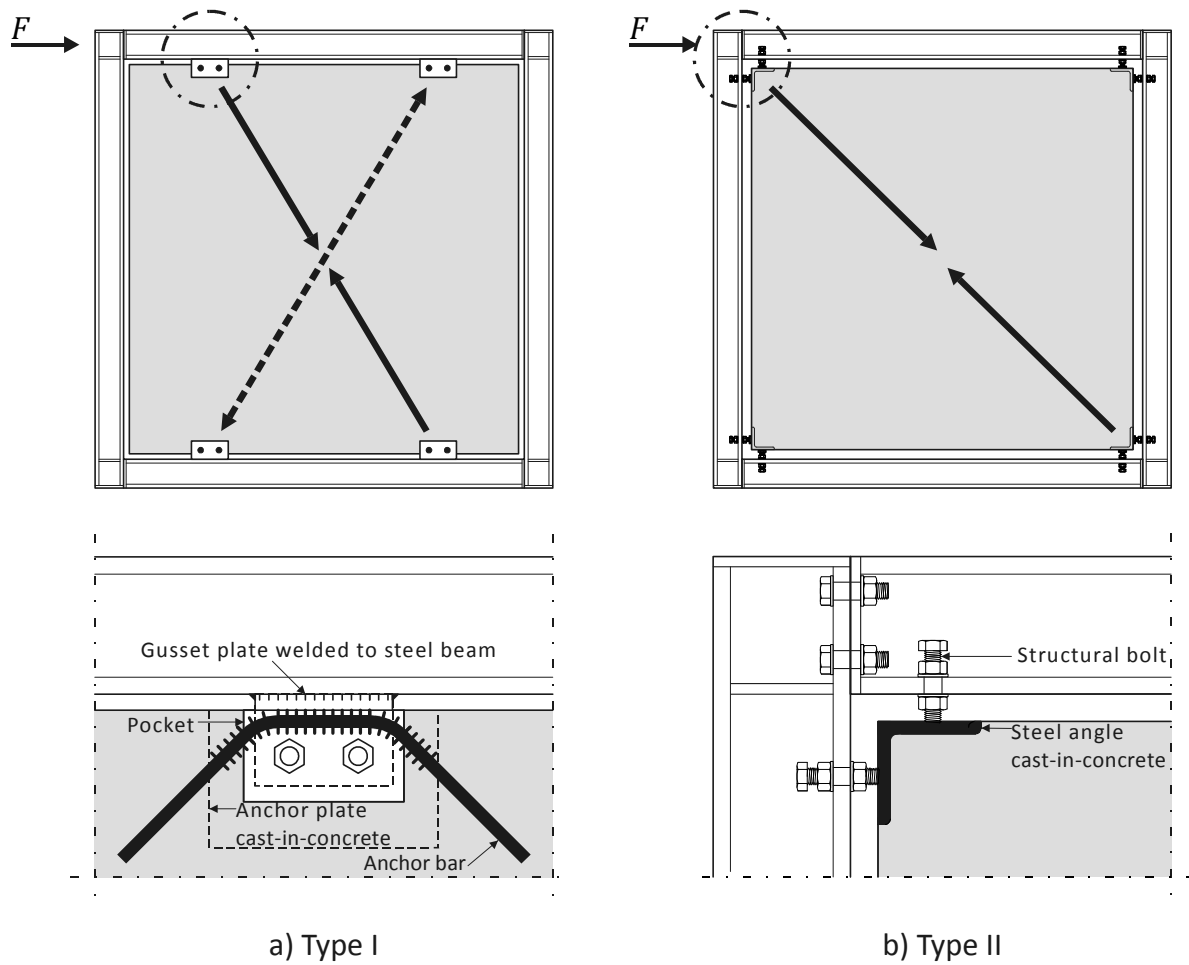


Figure 3-1: discrete panel-to-frame connections

Table 3-1: Properties discrete panel-to-frame connection concerning manufacturing and construction

Requirement	Type I	Type II
<b>Fast erection on site</b>	- Dry connection; functions immediately after assembly	- Dry connection; functions immediately after assembly
<b>Assembly procedure</b>	- Panel needs to be lifted into exact position by crane - Panel needs temporary strutting until the top beam is installed - Tightening 8 bolts	- Bolts enable exact positioning of the panels in both horizontal and vertical direction by setting the bolts - Panel can be fixed directly by the bolts on the columns - Tightening 16 bolts;
<b>Adoption of tolerances</b>	- Tolerances can be adopted only if bolt holes are reamed on site	- Tolerances can be adopted in both horizontal and vertical direction by adjusting bolts
<b>Manufacturing and transport</b>	- No special mould needed - Connections can be used to lift the panel	- No special mould needed - Lifting equipment required
<b>Inspection and adjustment</b>	- Possible	- Possible
<b>Desired failure mode governing the strength</b>	- Bearing failure mechanism in the bolt holes of the steel plates	- Bolt failure mechanism, aiming at bolt shear through nut



Secondly, the structural performance of both connection types and the consequences for the overall infilled frame behavior are evaluated. Therefore, stiffness and strength (including failure) properties of both structural systems are compared:

- Stiffness properties

As pointed out by Tang et al. (Tang, R. B. et al., 2003) the lateral stiffness of a semi-integral infilled frame improves when the connections are located closer to the frame joints. Connection Type I requires a substantial anchoring length of the welded anchor bar, which demands a considerable length away from the panel corners. Connection Type II, on the other hand, can be located close to the frame joints, resulting in a higher stiffness. Besides, no large bending moments are introduced in the members of the steel frame by the action of the panel. Consequently, for Type II the infilled frame behavior shows more resemblance to the extensively investigated and well-known non-integral infilled frame, which already has proven to be effective and efficient in bracing multi-story buildings.

- Strength properties

Concrete shows good structural performance under compression but behaves significantly worse in tension. Therefore, tensile forces applied to a concrete element must usually be carried back into the reinforcement. Particularly close to edges, the transfer of high tensile forces might even become critical, and result in concrete edge breakout failure. This failure mode is often observed for connections installed at less than critical edge distance under either tension or shear loading. For this failure mode not the connection but the concrete fails, which was also the case for the full-scale experiment using connection Type I (Hoenderkamp, J. C. D. et al., 2005). The application of connections in concrete close to edges, subject to large tensile forces might provide a limited capacity accompanied by brittle failure behavior.

For connection Type II the anticipated failure mode is a bolt failure mechanism consisting of bolt shear through the nut. In case of a bolt failure, the bolts can rather easily be replaced while the steel structure and the concrete panel remain undamaged. Although yielding of the steel angle under the axial compression of the bolts was observed during the previous full-scale experiment with connection Type II (Teeuwen, P. A. et al., 2006), it worked out that this could be prevented by making relative simple adjustments to the connection.

In summary, also from structural point of view, connection Type II is preferred to Type I. Consequently, connection Type II is selected to be further developed, and applied for this study.

### 3.2 Mechanical model

A mechanical model is proposed for the semi-integral infilled frame with connection Type II (Figure 3-2). The model is based on the concept of the equivalent diagonal strut, in which the global action of the panel is represented by a translational spring having stiffness  $k_p$  and strength  $F_p$ . Frame members are represented by beam elements. The frame joints are represented by rigid offsets to take the depth of the columns and beams into account, and a rotational spring with stiffness  $S_j$  and resistance  $M_j$ . The discrete panel-to-frame connections are represented by translational springs having stiffness  $k_c$  and strength  $F_c$ .

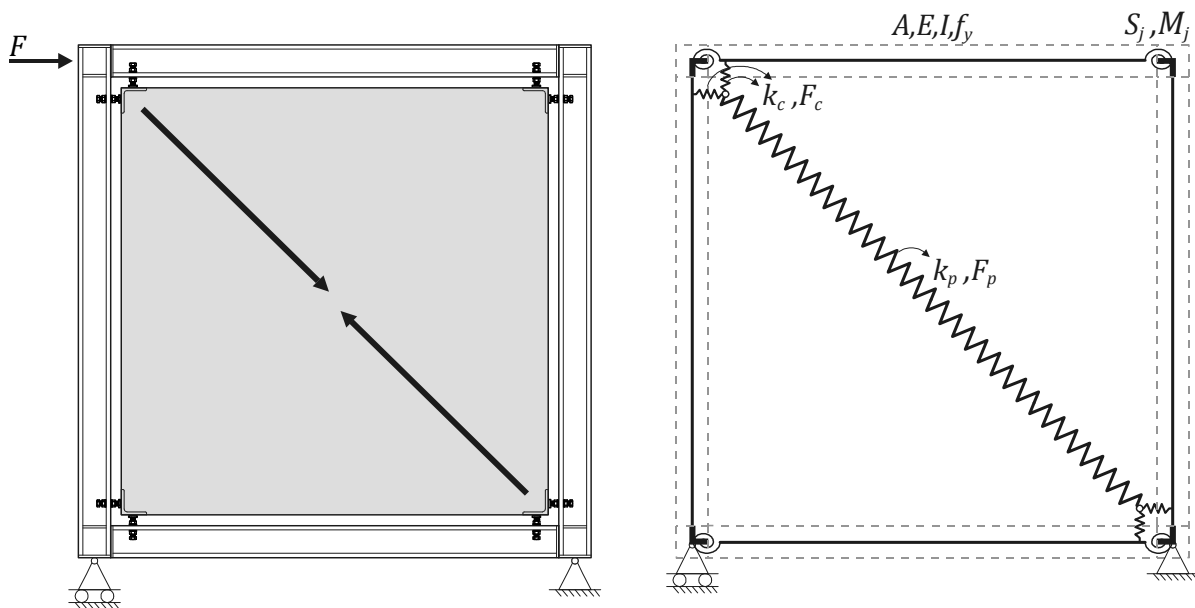


Figure 3-2: Semi-integral infilled frame with connection type II (left) and mechanical model (right)

The proposed model enables analyzing a building structure consisting of semi-integral infilled frames by standard structural analysis methods. Input for the model are geometrical and material properties of the frame members and the characteristics of the three types of springs representing the frame joints, the discrete panel-to-frame connections and the infill panel respectively.

The frame members can be designed for stiffness and strength (including stability) according to existing standards as for example Eurocode 3 EN 1993-1-1 (2005). However, to obtain the distribution of forces and moments in the structure, the structural properties of the three types of springs must be known. These should be determined and designed as well, e.g. by design rules. Nevertheless, current design rules might not be adequate to predict the springs' structural characteristics, or actually they do not exist. In the next sections, the shortcomings are determined and the research needs, in order to allow determination of all input for the mechanical model, are established.

### 3.2.1 Structural characteristics frame joints

For many years, extensive research on bolted and welded beam-to-column joints has been carried out. For example, in the Netherlands research was conducted e.g. by Witteveen et al. (1982) and by Stark and Bijlaard (1988). Design rules to determine the structural behavior of joints in building frames in terms of strength, stiffness and deformation capacity have been incorporated in e.g. Eurocode 3 EN 1993-1-8. Hence, the (initial) rotational stiffness ( $S_j$ ) and the resistance ( $M_j$ ) of the frame joints can be predicted by existing design rules and, therefore, require no further investigation.

### 3.2.2 Structural characteristics discrete panel-to-frame connections

The discrete panel-to-frame connection can be partitioned into basic components, analogously to the component method in Eurocode 3 EN 1993-1-8 for the design of joints. The basic idea of this method is to consider a joint as an assembly of individual simple components. Consequently, the structural characteristics of the connection depend on the properties of its basic components. The method allows accommodating different joint typologies under the same basic principles.

The identified basic panel-to-frame connection components include a web in compression, flanges in bending, bolts in compression and a plate in compression. These components act in series. Consequently, the overall connection behavior can be represented by considering the component springs shown in Figure 3-3. The connection stiffness ( $k_c$ ) can be determined from the stiffnesses of its basic components, each represented by its elastic stiffness coefficient ( $k_{ci}$ ). The connection strength ( $F_c$ ) is dictated by the resistance of its critical basic component which, according to design requirements, is preferred to be the component 'bolts in compression' ( $F_{c3}$ ). Therefore, the strength of the other three components must exceed the strength of the bolt component, where in this particular case strength is defined as the onset of yielding. In other words, no plastic deformation is allowed in the other three components at the moment of bolt failure.

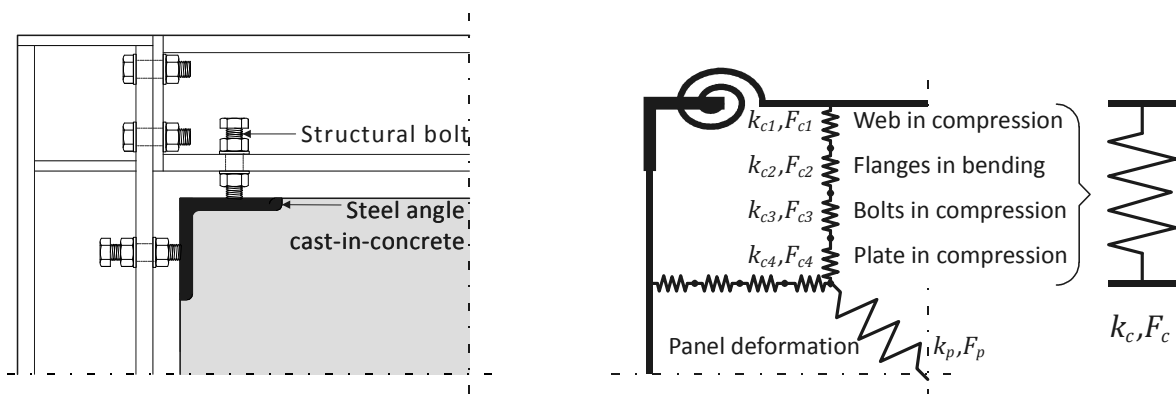


Figure 3-3: Discrete panel-to-frame connection Type II and mechanical model

For the serial component spring of the panel-to-frame connection, the following equations with respect to the stiffness ( $k_c$ ) and strength ( $F_c$ ) hold:

$$k_c = \left[ \frac{1}{k_{c1}} + \frac{1}{k_{c2}} + \frac{1}{k_{c3}} + \frac{1}{k_{c4}} \right]^{-1} \quad [3-1]$$

$$F_c = \min[F_{c1}, F_{c2}, F_{c3}, F_{c4}] \quad [3-2]$$

### Flanges in bending

The flange bending component in the panel-to-frame connection shows similarity to flanges in bending at the tension side of columns in bolted beam-to-column connections. Yet, here the flanges are subjected to transverse tension instead of compression. Analytical models for the determination of the flange capacity were developed by Zoetemeijer (1974). The results of this work suggest that an equivalent T-stub with an effective length ( $l_{eff}$ ) can be used to model the tension region of the column flange (Figure 3-4). To define the effective length, the complex pattern of yield lines that occurs around the bolt(s) is converted into a simple equivalent T-stub. Subsequently, simplified equations based on simple bending theory are used for calculating the strength and elastic stiffness of the T-stub assembly. However, the full elastic-plastic response is not covered.

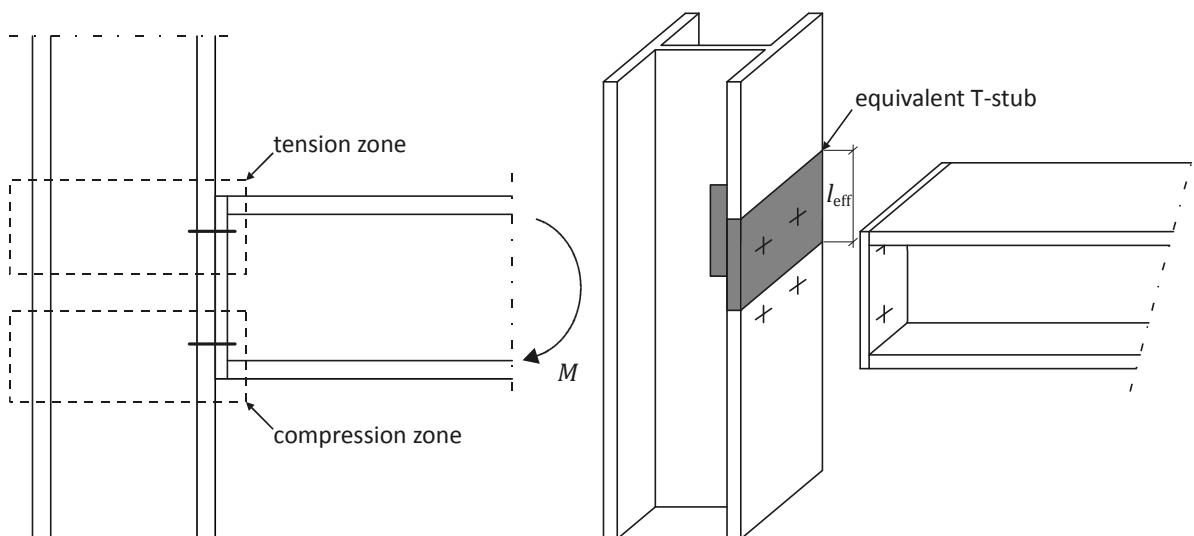


Figure 3-4: Tension and compression zone in bolted end plate connection (left) and equivalent T-stub representation of the tension zone (right)

In these models a prying action is assumed to develop at the end of the flange. Prying is a phenomenon in which additional tensile forces are induced in the bolts due to deformation of the connection near the bolt. The prying action is implicit in the expression for the calculation of the effective length. However, due to absence of this prying action, these expressions might be inaccurate for the prediction of the structural characteristics of the flange bending component in the panel-to-frame connection. Therefore, a

numerical parametric study will be performed to find the full elastic-plastic behavior of H-flanges in bending (section 6.1). In this study, the effect of the position of the bolt with respect to the end plate on the structural response will be investigated for several types of H-sections. In order to validate the FE-model (section 5.1), component experiments will be carried out (section 4.1.2).

#### Web in compression

A web subject to transverse compression applied directly through the flange may fail in one of the following three ways. The most likely form of failure is web crushing. In this case, the local stresses developed in the web exceed the yield strength of the steel. For slender webs, it is possible that failure occurs by buckling of the web or by some form of local instability known as web crippling. Eurocode 3 EN 1993-1-5 (2006) covers each of the three failure modes (buckling, crippling, crushing) for fabricated or rolled beam sections.

However, when the load is applied indirectly via bending of the flanges to the web, web crushing, web crippling and web buckling are not likely to occur while flange yielding governs the strength. A calculation to demonstrate this, based on the regulations by Eurocode 3 EN 1993-1-5, is provided in Appendix A. Accordingly, only the stiffness of the web in compression is of interest. Therefore, the web stiffness will be considered as well in the numerical parametric study concerning the component flange bending (section 6.1).

#### Bolts in compression

As compressive loading is a less conventional mode of loading bolts, design rules for bolts subject to compressive loading are lacking. As pointed out in section 2.2.2, bolts and nuts are designed so that tension failure of the bolt occurs before stripping of the threads. However, when subject to compressive loading, other failure behavior might govern the strength of a bolt-nut assembly. To provide insight into the behavior of bolts subject to compressive loading, experiments will be carried out (section 4.1.1). Besides, the application of Alexander's theory to bolts subject to compressive loading will be validated.

#### Plate in compression

When compressing a bolt to a steel plate, the stress state under the bolt is not a simple uni-axial state of stress but a more complex tri-axial state of stress. Although no plastic deformation is desired in this component before bolt failure takes place, yielding of the steel angle under the compression produced by the bolts was observed during previous full-scale experiments. Therefore improvements have to be made to the connection. Experiments will be carried out to provide insight into the behavior of steel plates subject to compression produced by bolts (section 4.1.3). Based on the findings, the connection will be improved. Then, the modified component will be subject to experimental investigation in order to determine its structural characteristics (section 4.1.4).

**3.2.3 Structural properties precast concrete panel with window opening**

As the infilled frame structure is developed to be applied in a building’s facade, window openings in the panels are inevitable. In this study, central panel openings are considered. From a practical and structural point of view this is the best location to accommodate window openings (Dawe, J. L. et al., 1989). By application of connection Type II the infill panel has to act as a diagonal strut in compression. However, a central panel opening will interrupt the development of a main compression strut.

The load distribution in a panel with central window opening can be obtained by developing a strut-and-tie model. As the development of a main compression strut is interrupted, the load is transferred around the opening. This results in tensile forces in the outer edge of the panel which have to be resisted by appropriate reinforcement. Figure 3-5a shows the positions of the concrete struts and tensile ties as well as two other concrete struts, which are necessary to maintain equilibrium. The adopted strut-and-tie model can be considered as two knee frames, pin connected to each other in the loaded corners. These corners are, according to the adopted strut-and-tie model, unable to support bending forces. Therefore, this stress field will cause considerable deformations, concentrated in open cracks. In order to avoid these considerable concentrated deformations, additional reinforcement is required around the inner edge of the panel to support tensile forces there. This results in the strut-and-tie model shown in Figure 3-5b.

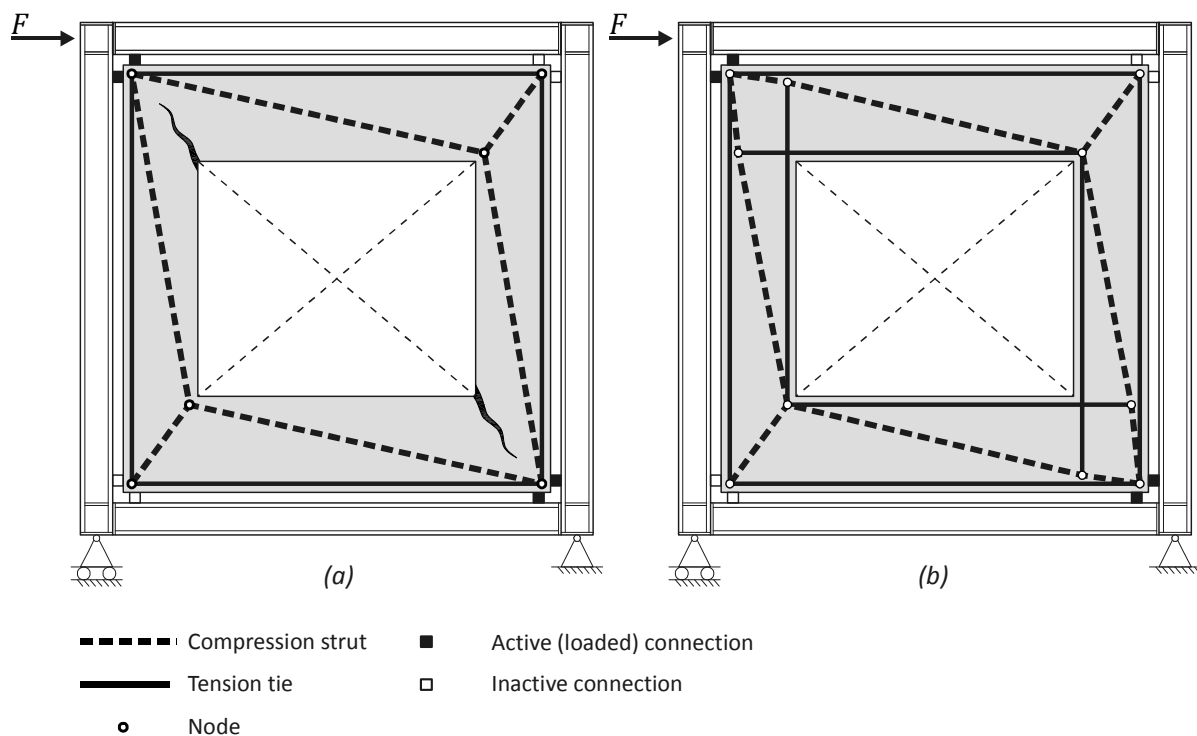


Figure 3-5: Development of STM for laterally loaded infilled frame with central panel opening

This strut-and-tie model can be applied to determine the required amount of reinforcement, to provide the demanded strength ( $F_p$ ) of infill panels with window openings. However, a simple method to establish the panel stiffness ( $k_p$ ) does not exist yet. Therefore, in order to come to design models for the determination of the panel stiffness, the size and vertical position of the panel opening will be experimentally investigated (section 4.2). This allows the development of a finite element model (section 5.2) to be used in parameter studies (section 6.2). Based on the results of these studies, a simple model to find the equivalent panel stiffness, as a function of parameters, as opening position, geometry and the reinforcement, will be developed.

### 3.3 Chapter conclusions

In this chapter, a discrete panel-to-frame connection was selected for further study. This connection comprises structural bolts on the column and beam in every corner of the steel frame, confining the precast concrete panel within the steel frame. Thereupon, a mechanical model was proposed for the semi-integral infilled frame with the preferred panel-to-frame connection. This model enables analyzing a building structure consisting of semi-integral infilled frames by standard structural analysis methods. Input for the model are geometrical and material properties of the frame structure and the structural characteristics of springs representing the frame joints, panel-to-frame connections and the infill panel respectively. Research will be carried out in order to enable determination of all required structural characteristics by design methods. A survey of the available and required design methods is provided in Table 3-2.

Table 3-2: Design methods for elements in mechanical model

	Strength		Stiffness	
	Symbol	Method	Symbol	Method
<b>Frame:</b>				
Members	$N, V, M$	EN 1993-1-1	$A, E, I$	Applied mechanics
Joints	$M_j$	EN 1993-1-8	$S_j$	EN 1993-1-8
<b>Panel-to-frame connection:</b>				
	$F_c$	Component method:	$k_c$	Component method:
Web in compression	$F_{c1}$	Excluded	$k_{c1}$	To be defined
Flanges in bending	$F_{c2}$	To be defined	$k_{c2}$	To be defined
Bolts in compression	$F_{c3}$	Theory §2.2.3 to be validated	$k_{c3}$	Theory §2.2.3
Plate in compression	$F_{c4}$	To be defined	$k_{c4}$	To be defined
<b>Panel:</b>				
	$F_p$	STM	$k_p$	To be defined

# Chapter 4: EXPERIMENTS

## ***Scope of the chapter***

*This chapter presents the experimental part of this study. Section 4.1 treats the experiments that were performed to study the behavior of the four basic components of the panel-to-frame connection described in chapter 3. The various test programs carried out and test setups applied are described, and the test results are presented and discussed. Thereupon, an elaborated description of the full-scale experimental study for studying the composite characteristics of the semi-integral infilled frame is provided in section 4.2. The test setup, measurements and procedures used are explained and the test results are presented and evaluated. The concluding section 4.3 summarizes the most important findings.*

## **4.1 Component experiments**

In the previous chapter, a mechanical model was presented for the semi-integral infilled frame. In this model, the discrete panel-to-frame connection is partitioned into four basic components. The identified components include ‘web in compression’, ‘flanges in bending’, ‘bolts in compression’ and ‘plate in compression’. This section presents various experiments that are carried out in order to study the structural behavior of these components. The results will be used to validate a finite element model (section 5.1) and to calibrate springs that represent the discrete panel-to-frame connection in finite element models for full-size laterally loaded semi-integral infilled frames (section 5.2).

### **4.1.1 Bolts in compression**

First of all, experiments are carried out to study the desired failure mechanism for the semi-integral infilled frame, being a bolt failure consisting of bolt shear through the nut. Therefore, high-strength bolt-nut assemblies are tested in compression. The results are used as well to validate the applicability of Alexander’s theory (Alexander, E. M., 1977) for strength prediction of bolt-nut assemblies in compression.

#### **Test setup and test program**

High-strength M24 bolt-nut assemblies are tested by compressive loading in a compression test setup (Figure 4-1). The load is applied under controlled displacement conditions. For this purpose the loading plate is controlled at 0.10 mm/min. Deformations are measured with three linear variable differential transformers (LVDTs) equally divided around the circumference of the shank of the bolt. Based on these three measurements, the average deformation in the middle of the bolt can be derived. Additionally, it can be shown whether, besides to normal force, the bolt is subject to bending moment. The LVDT



measuring distance applied is 50 mm. For the fastening of the LVDTs to the bolt, a fixing medium is designed.

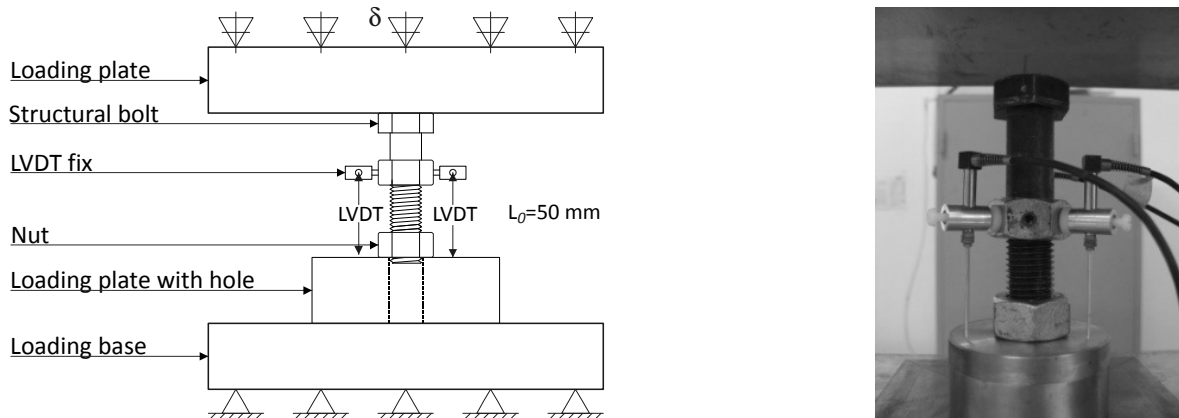


Figure 4-1: Overview of test setup for component 'bolts in compression'

Regular bolt-nut combinations (RC), being nuts with a grade indication that matches the first number of the bolts with which they are used, as well as unusual combinations (UC) are tested in compression. The latter combinations are also dealt with in order to possibly find failure mechanisms with a large deformation capacity. A survey of the test program is provided in Table 4-1. All tests are carried out twice, indicated with the character A or B respectively at the end of the test code.

Table 4-1: Test program for component 'bolts in compression'

Combination	Bolt grade	Nut grade
M24-RC1.A; M24-RC1.B	8.8	8
M24-UC1.A; M24-UC1.B	8.8	10
M24-RC2.A; M24-RC2.B	10.9	10
M24-UC2.A; M24-UC2.B	10.9	8

Tensile tests are performed on test coupons made out of bolts from the same series as used for the tests, to determine the actual material properties of the bolts. Table 4-2 gives the yield stress ( $f_{yb}$ ) (equivalent to the 0.2 proof stress for the 10.9 bolts) and the ultimate tensile stress ( $f_{ub}$ ) of the bolts applied.

Table 4-2: Bolt material properties

Test coupon	$f_{yb}$ [N/mm <sup>2</sup> ]	$f_{ub}$ [N/mm <sup>2</sup> ]
8.8M24 bolt	571	768
10.9M24 bolt	1028	1112

It is noticeable that the strength properties of the 8.8M24 bolt are lower than its nominal properties ( $f_{yb} = 640 \text{ N/mm}^2$  and  $f_{ub} = 800 \text{ N/mm}^2$ ).

Experimental observations and results

Figure 4-2 presents the load-deformation diagrams of the M24 bolt-nut assemblies subject to compressive loading. The deformation shown is the calculated average deformation in the centre of the bolt. Furthermore, the analytical yield ( $F_{Sy}$ ) and ultimate stripping strength levels ( $F_{Su}$ ) according to Alexander's theory are presented in the graphs.

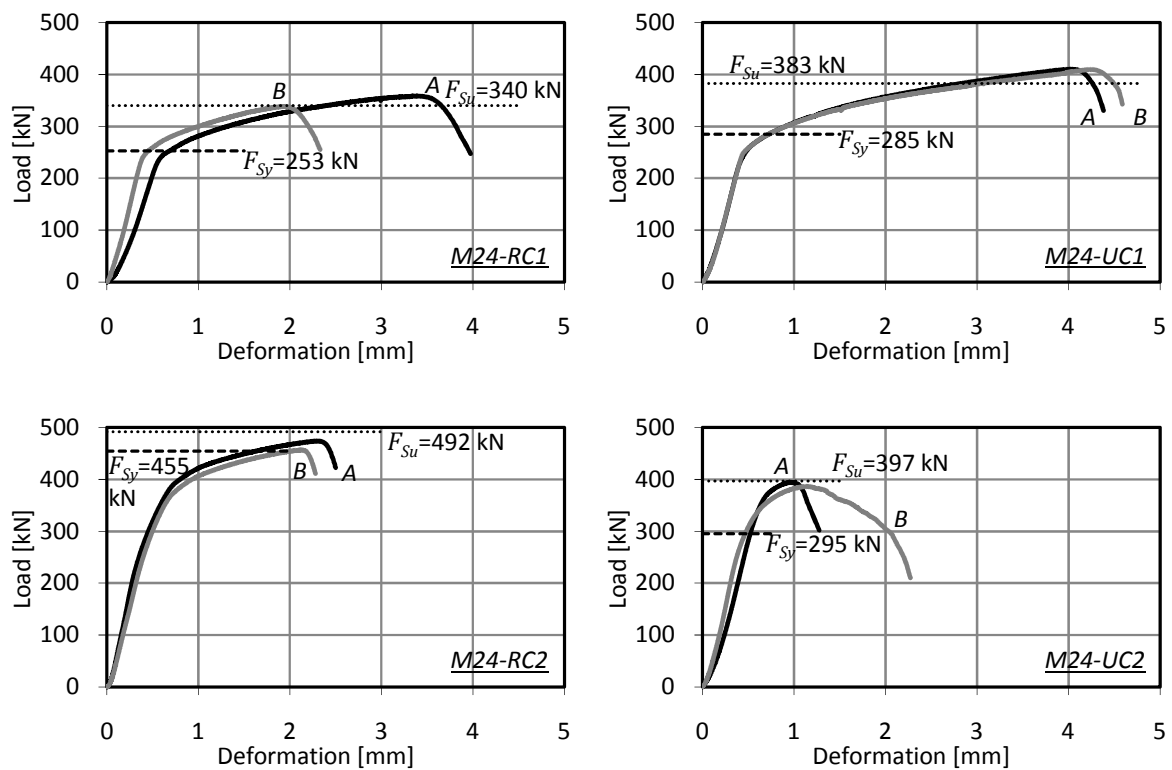


Figure 4-2: Load-deformation response of bolt-nut assemblies subject to compressive loading

The observed failure mode for all bolt-nut assemblies is stripping of the threads of the bolt (Figure 4-3). In addition, for test series UC1, longitudinal and transverse plastic deformation of the threaded part of the bolt above the nut is also visible after the tests (Figure 4-3b). For test series UC2, the threads of the nut have deformed plastically, although no stripping occurred (Figure 4-3c). Considering deformation capacity, it is shown that the regular bolt-nut combinations possess almost an even deformation capacity. The application of bolts of lower grades than the nuts results in more ductility (UC1). On the other hand, the combination of bolts with higher grades than the nuts provides less ductility (UC2). Therefore, the use of the latter combination is not to be recommended.

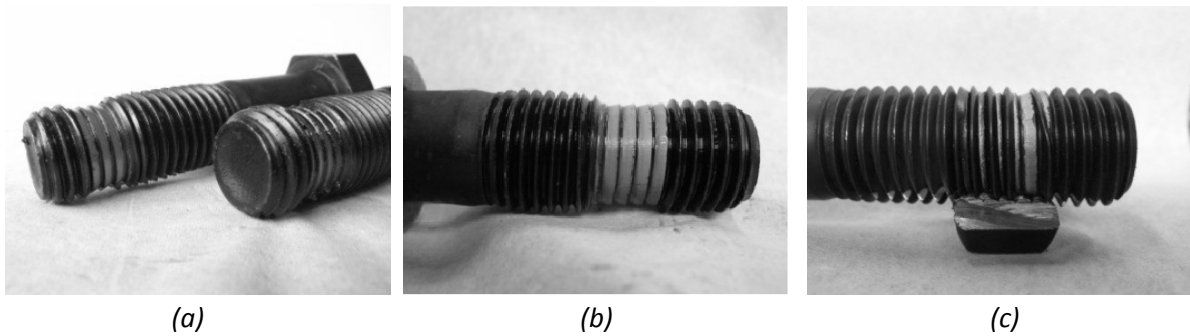


Figure 4-3: Bolt thread stripping failure with some yielding of the threaded part (b) or the nut (c)

#### Discussion of test results

The average experimentally found failure loads are presented in Table 4-3 together with the bolt yield strength ( $F_{By}$ ), the tensile strength ( $F_{Bu}$ ) and the ultimate stripping strength ( $F_{Su}$ ) according to Alexander's theory. In the last column, a comparison is made between the analytically determined stripping strength and the experimental strength.

Table 4-3: Survey of experimental and analytical results

Combination	Tensile strength $F_{By}$ [kN] $F_{Bu}$ [kN]		Stripping strength $F_{Su}$ [kN]	Experimental strength [kN]	Comparison
<b>M24-RC1</b>	202	271	340	349	-3%
<b>M24-UC1</b>	202	271	383	410	-6%
<b>M24-RC2</b>	363	393	492	465	+6%
<b>M24-UC2</b>	363	393	397	391	+2%

The results show that, unlike bolts subject to tensile loading, bolts subject to compressive loading fail by thread stripping failure and not by axial failure of the bolt, although some yielding of the bolt takes place. Good agreement is shown between the experimentally found ultimate strengths and the ultimate strength predictions according to Alexander's theory. Therefore, this theory can be applied for prediction of the stripping strength of bolt-nut assemblies subject to compressive loading.

#### **4.1.2 Flanges in bending with web in compression**

A test program is carried out to study the component 'flanges in bending' in combination with the component 'web in compression'. The main objective of the test results is to validate the finite element model used for studying these two components (section 5.1).

#### Test setup and test program

HE200B sections with welded end plates are subject to transverse compressive loading, introduced by 10.9M24 bolts on the flanges, in a compression test setup. The load is applied under controlled displacement conditions. For this purpose the loading plate is controlled at 0.10 mm/min in the elastic range and at 0.20 mm/min in the plastic range. LVDTs are used to measure displacements under the bolts and under the end of the

outside of the flanges. 3 strain gauges with lengths of 10 mm, equally divided around the shank of the bolt, are used to measure strains at the bolt surface. These measurements allow determination of the load distribution over the two bolts. Figure 4-4 gives an overview of the test setup. The geometry of the test specimen is shown in Figure 4-5. Two identical tests are performed.

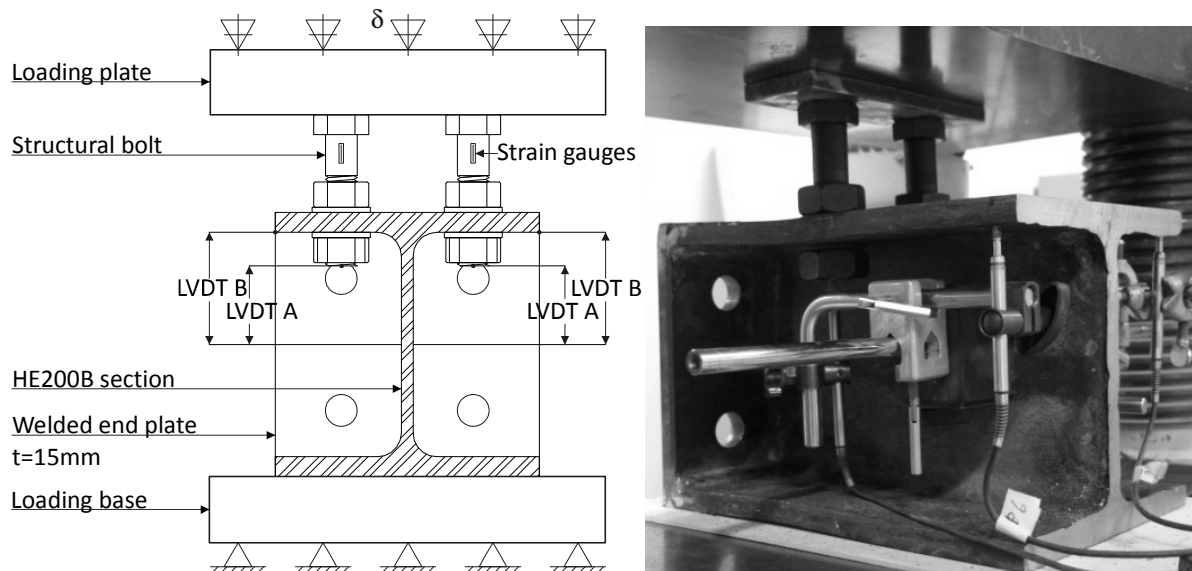


Figure 4-4: Overview of test setup for component 'flanges in bending with web in compression'

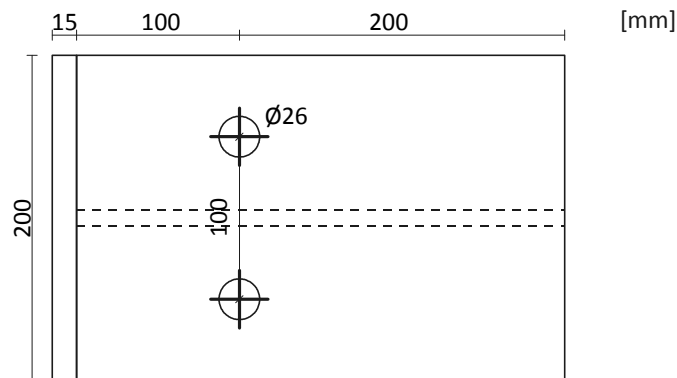


Figure 4-5: Geometry test specimen

The steel of the HE200B section is grade S355. To determine the actual material properties, tensile tests are performed on test coupons taken from the flanges and web of the section. Table 4-4 gives the yield stress ( $f_y$ ) and the ultimate tensile stress ( $f_u$ ).

Table 4-4: Material properties HE200B sections

Test coupon taken from:	$f_y$ [N/mm <sup>2</sup> ]	$f_u$ [N/mm <sup>2</sup> ]
Web	423	519
Flange	356	465

### Experimental observations and results

Figure 4-6 presents the load-displacement diagrams of the two tests with HE200B sections subject to transverse compression. The shown displacement is the maximum measured under the two bolts (LVDTs A) and plotted against the load in the bolt. The load-deformation curve can be approximated by a linear elastic branch followed by a nearly unlimited second plastic branch. The plastic behavior results from yielding of the flanges, and represents a ductile failure mechanism. At the end of the branches, the tests were stopped.

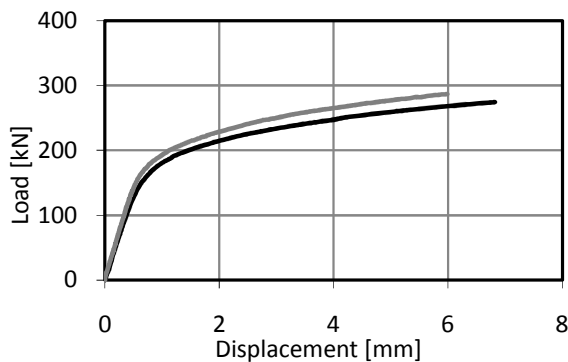


Figure 4-6: Load-deformation response of HE200B sections in compression (left) en picture of deformed flange (right)

### Discussion of test results

Good agreement is shown between the measurement results of the two tests. Furthermore, geometrical and material properties of the specimens applied are determined. Therefore, the test results are suited for validating a finite element model.

#### **4.1.3 Plate in compression**

As yielding of the steel angle under the compression produced by the bolts was observed during the previous full-scale experiment with connection Type II (Teeuwen, P. A. et al., 2006), a test program is carried out to study the failure behavior of steel plates loaded in compression by bolts. The test results serve as a basis to improve the connection, by eliminating yielding.

### Test setup and test program

10.9M24 bolts (length 120 mm) on steel plates of grade S235 or S690 respectively are tested in a compression test setup. The load is applied under controlled displacement conditions. For this purpose the loading plate is displaced at 0.10 mm/min. Three LVDTs equally divided around the bolt are used to measure the deformation of the bolt and the steel plate. For safety reasons, the bolt is guided without friction through a fixed steel plate, in order to prevent unexpected shooting away. The test setup and instrumentation are schematically shown in Figure 4-7.

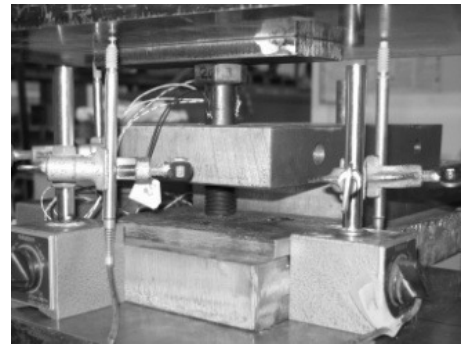
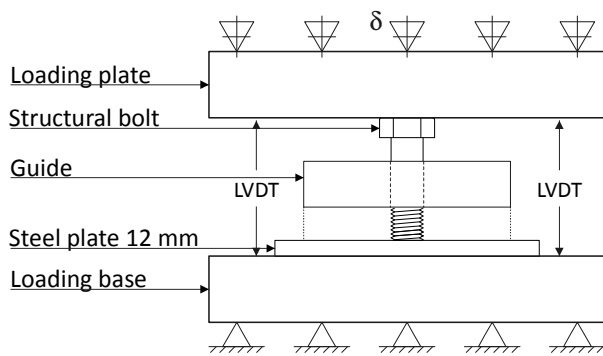


Figure 4-7: Overview of test setup for component 'plate in compression'

Two series of tests are performed. For the first test series, bolts were used having an originally slightly hollow bottom. Therefore, a second test series is performed with bolts having a flattened bottom in order to get an even contact area with the plate. For this purpose, the bolts were processed by milling. All tests are carried out twice. A survey of the test program is provided in Table 4-5. The characters A and B in the test code refer to the first or second test respectively.

Table 4-5: Test program for component 'plate in compression'

Type	Steel grade plate	Bottom bolt
S235_1.A; S235_1.B	S235	Normal
S235_2.A; S235_2.B	S235	Flat by milling
S690_1.A; S690_1.B	S690	Normal
S690_2.A; S690_2.B	S690	Flat by milling

To establish the actual material properties, tensile tests are performed on test coupons taken from of the steel plates. Table 4-6 gives the yield stress ( $f_{yp}$ ) and the ultimate tensile strength ( $f_{up}$ ). The state of stress under the bolt is a complex tri-axial state of stress. Hence, for simplification, the uni-axial yield strength of the steel plate under the bolt area ( $S_{yp}$ ) according to equation 4.1 and the yield strength of the bolt ( $S_{yb}$ ) (equation 4.2) are provided in the table. The bolt material properties can be found in Table 4-2.

$$S_{yp} = A_{br} f_{yp} \quad [4-1]$$

$$S_{yb} = A_s f_{yb} \quad [4-2]$$

Where:

$A_{br}$  = Root area of the bolt [ $\text{mm}^2$ ]

$A_s$  = Tensile stress area of bolt [ $\text{mm}^2$ ]

$f_{yp}$  = Yield stress of steel plate [ $\text{N}/\text{mm}^2$ ]

$f_{up}$  = Ultimate tensile stress of steel plate [ $\text{N}/\text{mm}^2$ ]

Table 4-6: Material properties and strengths

Test coupon	$f_{yp}$ [N/mm <sup>2</sup> ]	$f_{up}$ [N/mm <sup>2</sup> ]	$S_{yp}$ [kN]	$S_{yb}$ [kN]
S235	318	419	103	363
S690	837	872	271	363

#### *Experimental observations and results*

Figure 4-8 presents the load-deformation response of the compression tests on bolts on steel plates. The presented deformation is the calculated average deformation in the centre of the bolt. All tests are stopped around 400 kN. It is shown that the flattening of the bottom of the bolt (2A, 2B) results in a shorter settling stage and a higher stiffness. Considering the tests with flattened bottoms, the diagram of the test on steel plate S235 shows a curved behavior. Plastic deformation of the steel plate (Figure 4-9) occurs at an early stage of loading. No plastic deformation is visual at the bolt.

The diagram of the test on steel plate S690 can, after a settling stage, be approached reasonably accurately with bi-linear behavior. Plastic deformation hardly occurred at the steel plate (Figure 4-9) but it did at the bolt. The onset of yielding occurs around 350 kN, corresponding to the yield strength of the bolt ( $S_{yb}$ ) which is substantially greater than the uni-axial yield strength of the steel plate under the bolt area ( $S_{yp} = 271$  kN).

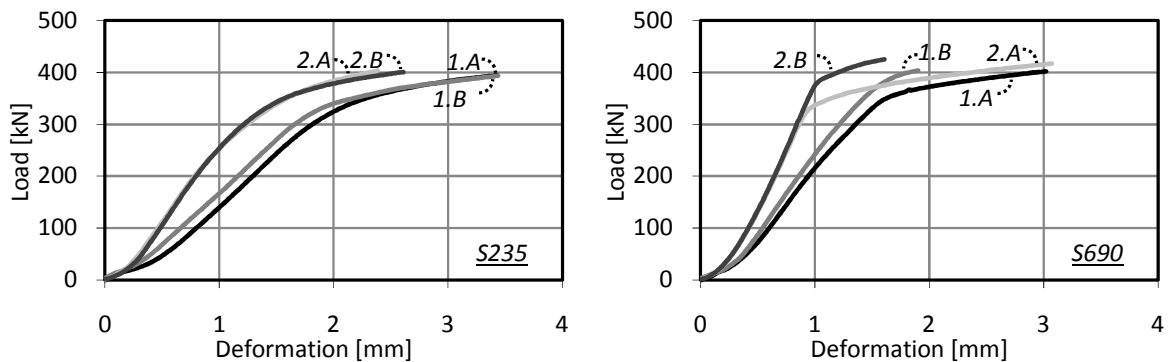
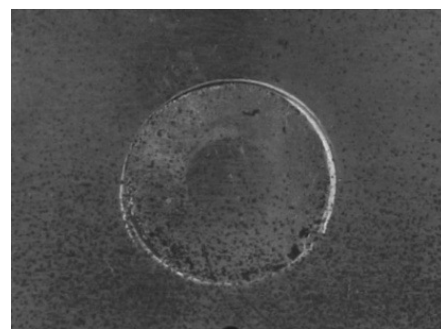


Figure 4-8: Load-deformation response of compression tests on bolts on steel plates



S235



S690

Figure 4-9: Imprints of bolts in steel plates

Discussion of test results

It is shown by the experiments that application of high-strength steel plates under the bolts results in a considerable reduction of plastic plate deformation. Due to confinement of the plate material under the bolt, a tri-axial state of stress occurs resulting in an increase of the plate strength. As a consequence, bolt yielding governs the strength. Based on these observations, it is decided to modify the original discrete panel-to-frame connection (Figure 3-1, Type II) as follows.

High-strength steel plates made of 34CrNiMo6 (nominal material properties  $f_y = 800 \text{ N/mm}^2$  and  $f_u = 1000\text{-}1200 \text{ N/mm}^2$ ) are introduced under the bolts. From practical point of view, the plates are provided with a hole to allow fixing them under the bolt by acting as a cap (Figure 4-10). The caps allow dispersion of the applied load through their depth. Assuming a minimum dispersion at a 1:1 gradient within a cap with a thickness of 10 mm, for a M24 bolt the contact area increases by a factor  $\pi \cdot 22^2 / \pi \cdot 12^2 = 3.4$ . As a consequence, stresses in the steel angle are considerably reduced.

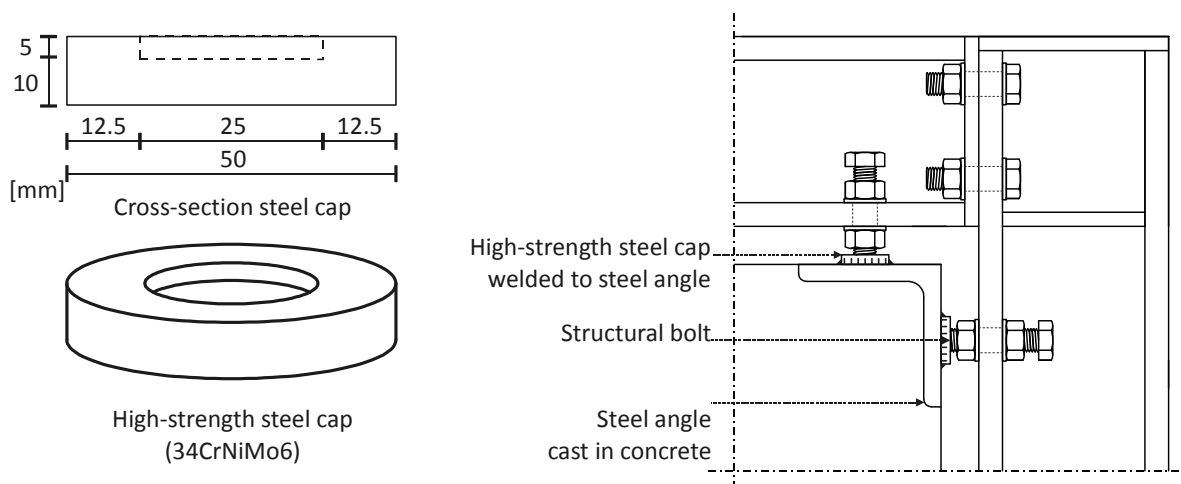


Figure 4-10: Improved discrete panel-to-frame connection

To obtain the structural characteristics of the modified component, experiments are carried out which are described in the next section.

#### 4.1.4 Bolt with cap on plate in compression

As the steel cap is loaded by a bolt that enters partly the hole in the cap, it is impracticable to measure deformations of the cap and plate only. Therefore, the load deformation characteristics of the modified component 'plates in compression' are obtained in combination with the component 'bolt in compression'. The load is applied under controlled displacement conditions. For this purpose the loading plate is displaced at 0.10 mm/min. Three LVDTs equally divided around the bolt are used to measure the deformation of the bolt, cap and plate. The length of the bolt-nut assembly including the



cap and plate is 65 mm, corresponding dimensions in the specimens for the full-scale tests. Two identical tests are performed. The aim of this test is to calibrate the springs that represent the discrete panel-to-frame connection in finite element models for full-size laterally loaded semi-integral infilled frames.

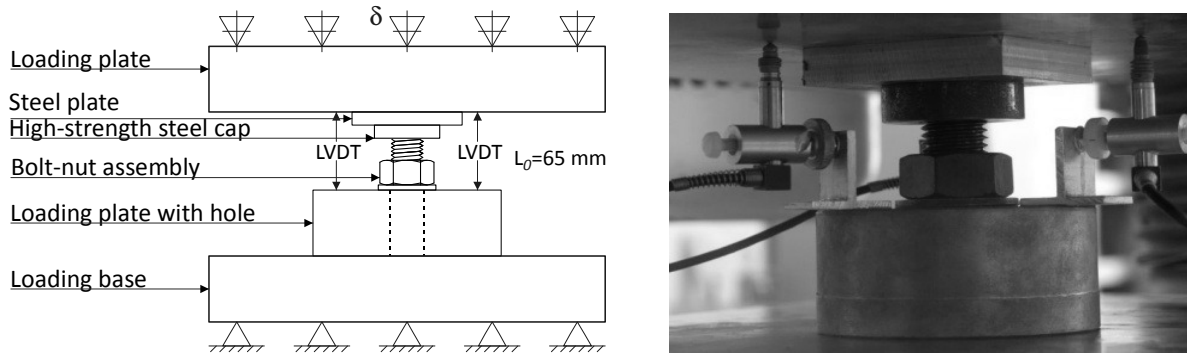


Figure 4-11: Overview of test setup for modified component plates in compression

#### Experimental observations and results

Figure 4-12 presents the load-deformation diagrams of the two compression tests. The deformation shown is the calculated average deformation in the centre of the bolt. Except for the settling-in stage, good correlation is shown between the measurement results. After the test, no plastic deformation is visual at the cap or plate.

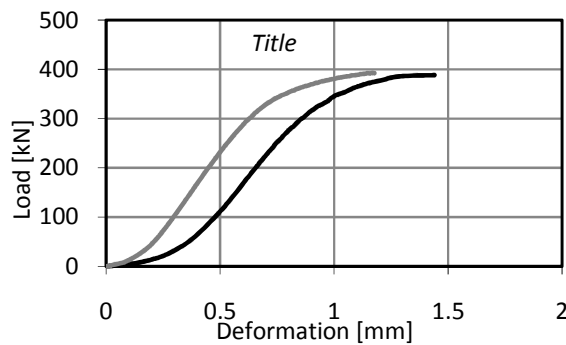


Figure 4-12: Load-deformation response of compression test on bolt with cap on plate

#### Discussion of test results

The modified component shows no plastic plate deformation, while the failure mechanism consists of bolt shear through the nut. Therefore, it is considered an adequate modification to the connection. Furthermore, the results of the two tests demonstrate a good correlation and allow determination of stiffness and strength characteristics for the components 'plates in compression' and 'bolt in compression'. Consequently, the results are suited for calibrating springs representing the considered panel-to-frame connection components in finite element models for full-size laterally loaded semi-integral infilled frames.

## 4.2 Full-scale experiments

In order to provide insight into the composite behavior between steel frames and discretely connected precast concrete infill panels provided with window openings, full-scale experiments on single-story single-bay infilled frame structures have been conducted. The main objective of the full-scale experiments is to observe the general behavior of the structure in terms of stiffness, strength and ductility. At the same time, the influence of the chosen parameter, being the size and position of the window opening, is investigated. The results of these experiments are used to validate a finite element model for full-size laterally loaded semi-integral infilled frames (section 5.2).

### 4.2.1 Test setup and test program

#### *Test rig*

A specifically designed test rig has been used to perform the full scale tests on the infilled frame structures (Figure 4-13a). This test rig is composed of two rigid triangular frames, constructed of HE300B members. These two triangular frames are transversely linked through rigid steel members at their corners. A specimen can be positioned between the two triangular frames and is supported on two different supports. At the side of the jack, the lower corner of the specimen is fixed in the vertical direction to the test rig by four steel M30 rods (Support A, Figure 4-13c). This support is intended to act as a roller support with a restrained displacement in vertical direction only. At the opposite lower corner, the specimen is supported in a heavy steel block which restrains the specimen from both horizontal and vertical displacement (Support B, Figure 4-13d). This support is supposed to act as a pin support. A specimen can be loaded laterally by a hydraulic jack that is coupled to the top corner of the triangular frames by stiff steel plates, acting at the height of the top beam centre (Figure 4-13b). This jack has a stroke of 200 mm and a capacity of 2 MN.

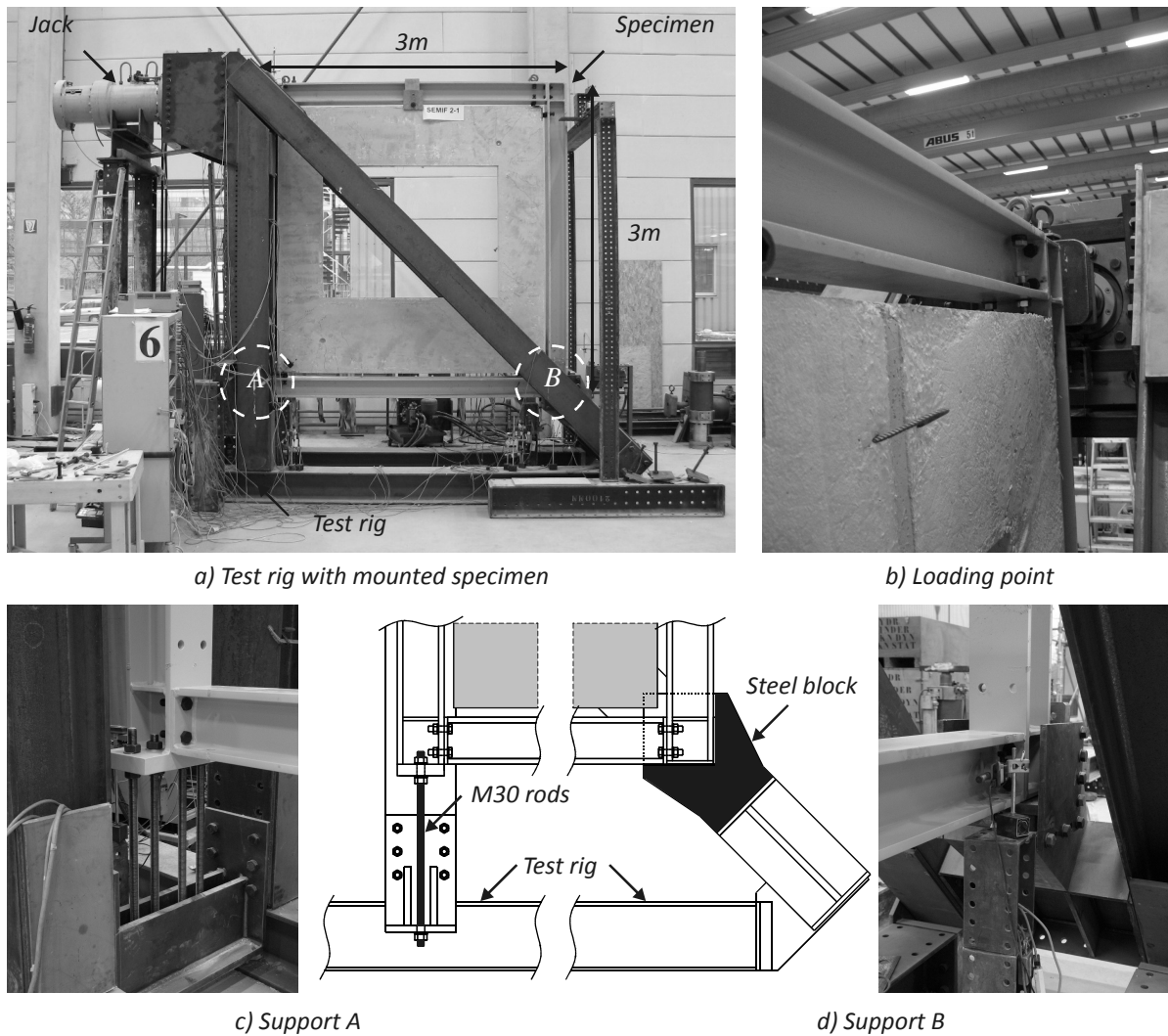


Figure 4-13: Test rig with mounted specimen

### Measurements

The behavior of a specimen under lateral loading is recorded as follows (a scheme of the arrangement of the instrumentation is shown in Figure 4-14):

The global position of the specimen in relation to the ground is measured with LVDTs and digital clock gauges (DCGs) at the four corners of both frame ( $\Delta_1$  to  $\Delta_8$ ) and panel ( $\Delta_9$  to  $\Delta_{16}$ ). The LVDTs and DCGs were fixed to independent, stand alone, measuring frames.

Deformations of the panel are measured across both diagonals ( $\delta_{13}$  to  $\delta_{14}$ ) with Cable-Extension Position Transducers (PTs). To find the strain distribution in the precast concrete panel, strain gauge rosettes (gauge lengths 60 mm) are placed on specific locations (Rosettes A to K) on one side of the panel. These locations are situated in the centre of the compression struts, and on nodes between these struts (see strut-and-tie model provided in Figure 3-5). Since due to cracking of concrete in tension zones rosettes will be damaged

and become unable to provide measurements, 6 LVDTs ( $\delta_a$  to  $\delta_f$ ) are used in these zones. Deformations are measured over a distance of 300 mm, in order to determine the average strain and initiation of cracks in these zones.

Deformations of the discrete interface connections are measured at one side of the specimens. To this end, LVDTs are coupled at bolt height between the panel and the outer flanges, measuring the deformation of the entire connection ( $\delta_1$  to  $\delta_8$ ). Four LVDTs are applied to measure the displacement of the discrete connection bolts in the loaded corners with respect to the opposite flange ( $\delta_9$  to  $\delta_{12}$ ). With these LVDTs the anticipated bolt failure behavior can be recorded. During the tests, the lateral deflection  $\Delta_2$  and the lateral load  $F$  are monitored. Newly initiated cracks and crack propagation are marked on the specimens and failure mechanisms are observed.

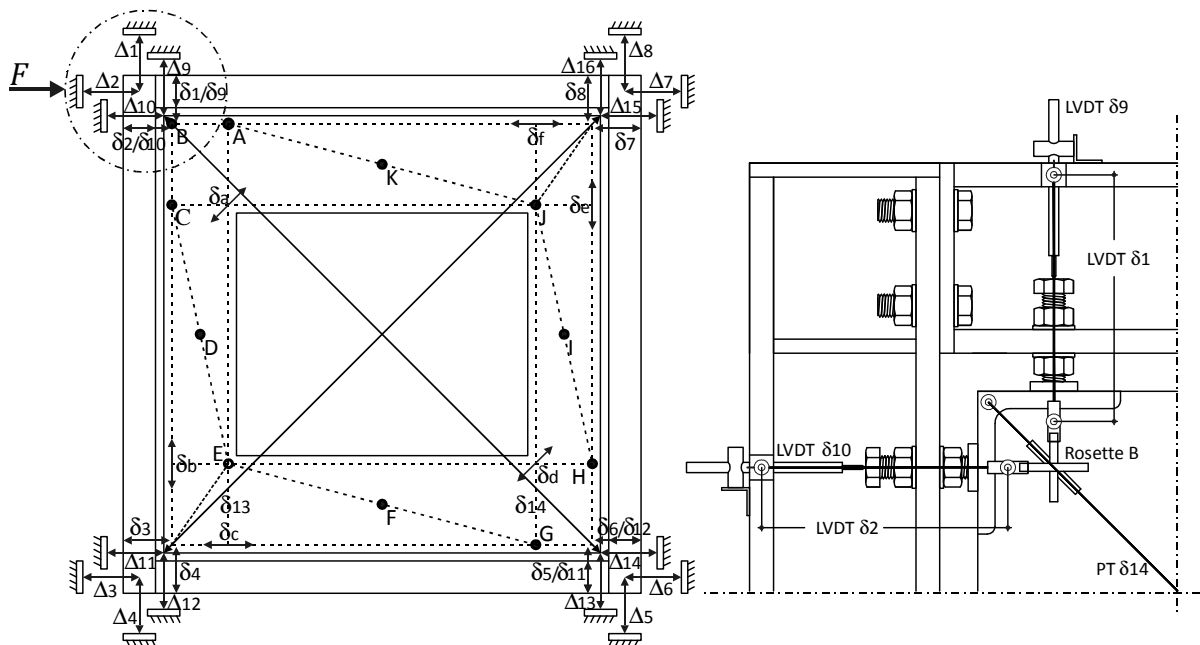


Figure 4-14: Measurement scheme (left) and detailed view of measurements surrounding the connection (right)

In Table 4-7 the applied instrumentation is presented with its specifications including the range and resolution. The specified resolution is the actual resolution of the instrumentation that could be achieved using the operating measurement system, and not the resolution for the individual instrument specified by the producer.

Table 4-7: Specification of applied instrumentation

Instrument	Model	Range [mm]	Resolution [mm]
LVDTs $\Delta_1, \Delta_8$	HBM W20 TK	+/- 20	0.01
LVDT $\Delta_2$	HBM W50TS	+/- 50	0.01
LVDT $\Delta_7$	Celesco PT1A	+/- 50	0.05
LVDT $\Delta_9$	HBM W10TK	+/- 10	0.01
DCGs $\Delta_3, \Delta_4, \Delta_{11}, \Delta_{12}, \Delta_{13}, \Delta_{14}$	Mitutoyo IDF150	50	0.003
DCG $\Delta_5$	Mitutoyo IDU 1025	25	0.01
DCG $\Delta_6$	Mitutoyo IDC112B	10	0.001
PTs $\Delta_{10} + \Delta_{15}$	Celesco PT1 series	+/- 50	0.05
LVDT $\Delta_{16}$	HBM W10TK	+/- 10	0.01
LVDTs $\delta_1, \delta_4, \delta_5, \delta_8$	HBM W20	+/- 20	0.01
LVDTs $\delta_2, \delta_3, \delta_6, \delta_7$	HBM W10K	+/- 10	0.01
LVDTs $\delta_9 + \delta_{11}$	Solartron AX/5/S	+/- 5	0.001
LVDTs $\delta_{10} + \delta_{12}$	SM3	+/- 1.5	0.001
PTs $\delta_{13} + \delta_{14}$	Celesco PT1A	+/- 25	0.025
LVDTs $\delta_a$ to $\delta_f$	SM3	+/- 1.5	0.001
Strain Gauge A to K	PLR-60-11	2 %	1 $\mu\text{m/m}$

### Test specimens

The single-story, single-bay, 3 by 3 m infilled frame structure subject to lateral loading consists of a simply connected steel frame, constructed of HE180M sections in S235 for columns and beams. The discrete panel-to-frame connections, designed for a ‘bolt failure’ mechanism, are constructed with 8.8 bolts with grade 8 nuts. To investigate the effect of the size and position of the window opening in the infill panel on the infilled frame behavior, five different panel geometries are tested. The geometrical properties are provided in Table 4-8. Each panel is tested twice, resulting in a total number of 10 full-scale tests. As no failure of the frame is expected, only two identical steel frames are used for the entire test program. The five precast reinforced concrete panels ( $l \times h \times t = 2700 \times 2700 \times 200 \text{ mm}^3$ ) are alternately discretely connected to one of the steel frames.

Table 4-8: Test program full-scale tests

Designation	Height window opening [mm]	Opening % [%]	Vertical position x/y [-]
FS-1A; FS-1B	1050	25.9	1.20
FS-2A; FS-2B	1350	33.3	1.25
FS-3A; FS-3B	1500	37.0	1.00
FS-4A; FS-4B	1650	40.7	1.330
FS-5A; FS-5B	1800	44.4	1.00

The design of the main bending reinforcement is performed using the strut-and-tie method, outlined in section 2.3. The “standard method” of the shear design procedure that can be found in Eurocode 2 EN 1992-1-1 is used to design the members of the

concrete panel to resist shear. Based on the results of these methods, the panels are all reinforced to support a lateral load of 550 kN, which equals the tensile strength of two 8.8 bolts, with longitudinal reinforcement  $\varnothing 25$  and stirrup reinforcement  $\varnothing 8$  with a concrete cover of 15 mm. Steel angles (150×150×15) in S235 are cast in every corner of the panel. Wedge reinforcement is provided in the corners to prevent concrete tensile splitting there. All applied reinforcement is FeB500. The specimens are illustrated in Figure 4-15. More detailed drawings of the panel reinforcement are provided in Appendix B.1.

The panels are cast in a precast-concrete factory. A self-compacting concrete is applied of concrete grade C45/55. The concrete mixture comprises aggregates (sand (0 - 6 mm) and gravel (4 - 16 mm)), limestone meal, Portland cement CEM I 52,5 R (which develops a high early strength that is needed for a one-day casting cycle), super plasticizer, and water (water-cement ratio = 0.45).

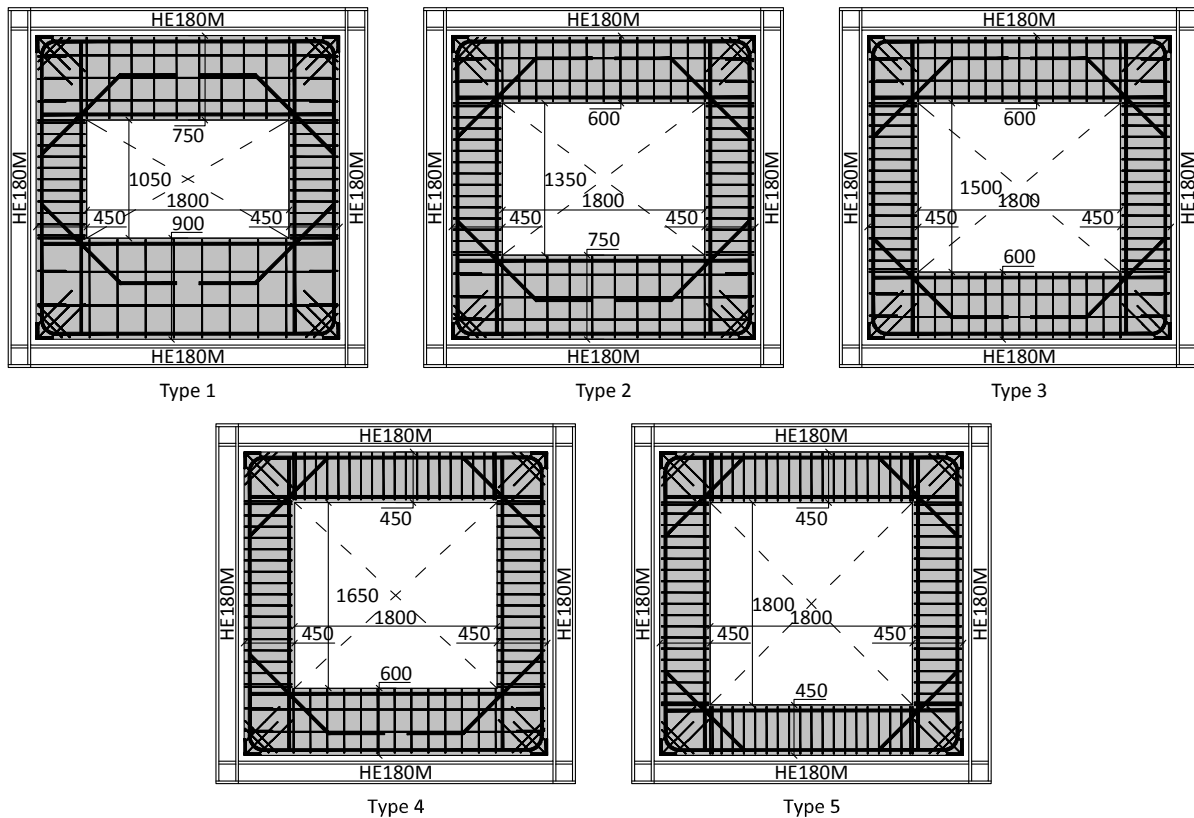


Figure 4-15: Geometric properties and reinforcement configurations of specimens

Standard material tests are performed on the day of testing, to find the actual cylinder compressive strength  $f_c$  (according to NEN-EN 12390-3:2009), the tensile strength  $f_{ct}$  (according to NEN-EN 12390-6:2000) and the Young's modulus  $E_c$  (according to ISO/DIS 1920-10:2009). The results of the material tests, which are mean values of two tests, are presented in Table 4-9.

Table 4-9: Material properties concrete

Panel type	$f_c$ [N/mm <sup>2</sup> ]	$f_{ct}$ [N/mm <sup>2</sup> ]	$E_c$ [N/mm <sup>2</sup> ]
1	62.2	3.9	3.54E+04
2	64.4	3.9	3.67E+04
3	70.6	4.2	3.66E+04
4	75.6	4.4	3.70E+04
5	66.0	3.9	3.72E+04

### Testing procedures

In order to quantify the contribution of an infill panel to the stiffness of its confining frame structure, the stiffness of the bare frame structure (without the infill) has to be known. For that reason, the bare frame is tested each time before mounting the precast concrete infill panel within the frame. Therefore, first the beams and columns are assembled. The bolts in the beam-to-column connections are torque controlled tightened up to a specified torque of 400 Nm, to obtain identical initial stiffnesses of the bare frames for all tests as best possible. Other conditions that might influence the coefficient of friction and so the torque as e.g. surface conditions, corrosion and temperature, are supposed to remain unchanged as each time the same series of bolts are used within identical climatic circumstances. The test procedure of the bare frames involves a preload up to 20 kN to close up initial gaps and contact tolerances between the specimen and the test rig. After the unloading, the bare frames are loaded again up to a load of 60 kN. This load is chosen such, that deformations of the frame are in the elastic range and therefore do not influence the infilled frame behavior.

After the bare frame is tested, it is fixed to the, from practical point of view, horizontally positioned panel. Then, the discrete connection bolts are placed and tightened up to a specified torque of 275 Nm, once again to provide identical boundary conditions as best possible for all tests. Since the infilled-frames are assembled in a horizontal position, the dead weight does not influence the initial prestress levels in the bolts. After erecting the infilled frame structure and thereupon installing the measurement instrumentation, it is positioned in the test rig. The testing procedure of the infilled frames involves a preload of 50 kN (and unloading), for reasons stated earlier. Next, the infilled frames are loaded up to failure. For both bare frame and infilled frame, the load is applied under controlled displacement conditions. For this purpose the stroke of the jack is controlled at 1 mm/min. At this rate, the duration of the tests with the infilled frames is about 1 hour.

As mentioned before, all panels are tested a second time. To this end, the panel is turned around its vertical axis of symmetry and replaced in the confining frame. By doing this, the tension zones where cracks have developed during the first test with the panel become compression zones during the second test, causing the cracks to close. The possible effect of the initially present cracks on the global structural behavior is investigated by making

measurements on the panels. Again, the bare frame structure is tested before the panel is mounted.

Finally, after the last infilled frame test is carried out, one bare frame is loaded up to failure in order to provide additionally insight into the non-linear behavior of the bare frame.

#### 4.2.2 Experimental observations and results

This chapter presents the results of the full-scale experiments. First, the overall load-deflection behavior is discussed. Next, the local panel behavior and the local connection behavior are considered. The most relevant results describing the major characteristics are presented in this chapter. A survey of the measurement results is provided in Appendix B.2.

##### Overall behavior

Figure 4-16 presents the lateral load-deflection response of the most severely deflected bare frame. The graph shows the actual deflection of the specimen, which means that a correction has been made for rigid body displacements and rotations. These occur as a result of deformations of the test rig and sliding of the specimen in its supports, and have to be deducted from the total measured deflection to obtain the actual deflection of the specimen only. In order to determine the actual lateral deflection of a specimen, the displacement measured at the loaded upper corner of the specimen ( $\Delta_2$ ) is reduced by the displacements due to rigid body translation and rotation measured at the specimen corners by LVDTs  $\Delta_4$ ,  $\Delta_5$  and  $\Delta_6$  (for the measurement scheme, see Figure 4-14).

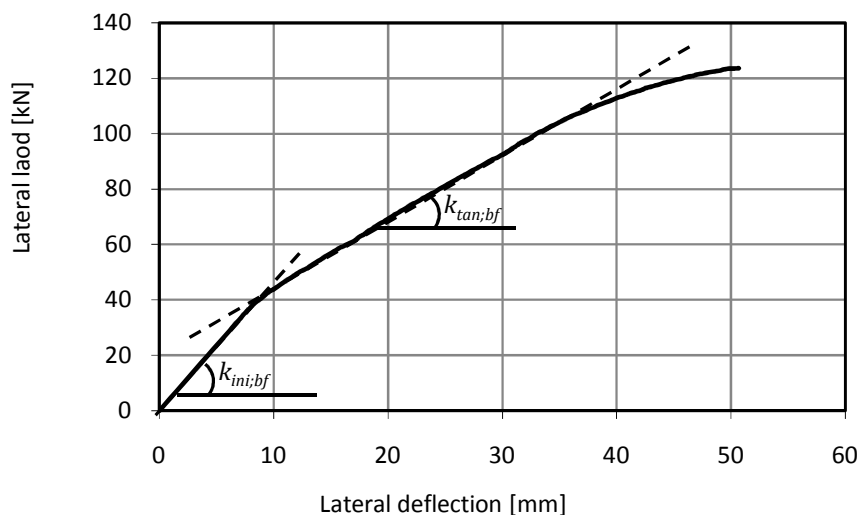


Figure 4-16: Load-deflection response bare frame



Up to a lateral deflection of 35 mm, the response can be reasonably accurately approximated by a graph consisting of two linear branches with an initial ( $k_{ini;bf}$ ) and tangent stiffness ( $k_{tan;bf}$ ). Thereafter, the stiffness decreases due to plastic deformations occurring in the beam-to-column connection. Values for  $k_{ini;bf}$  and  $k_{tan;bf}$  are around 5.1 and 2.5 kN/mm respectively. Actual bare frame stiffnesses for each bare frame test are shown in Table 4-10. On the basis of these results, the rotational spring stiffnesses of the beam-to-column connections can be determined, which will be used for the calibration of the finite element models.

In Figure 4-17 the load-deflection response of the 10 tested infilled frames and the bare frame considered above is shown. The second number in the test code refers to the first or second test respectively with the same panel.

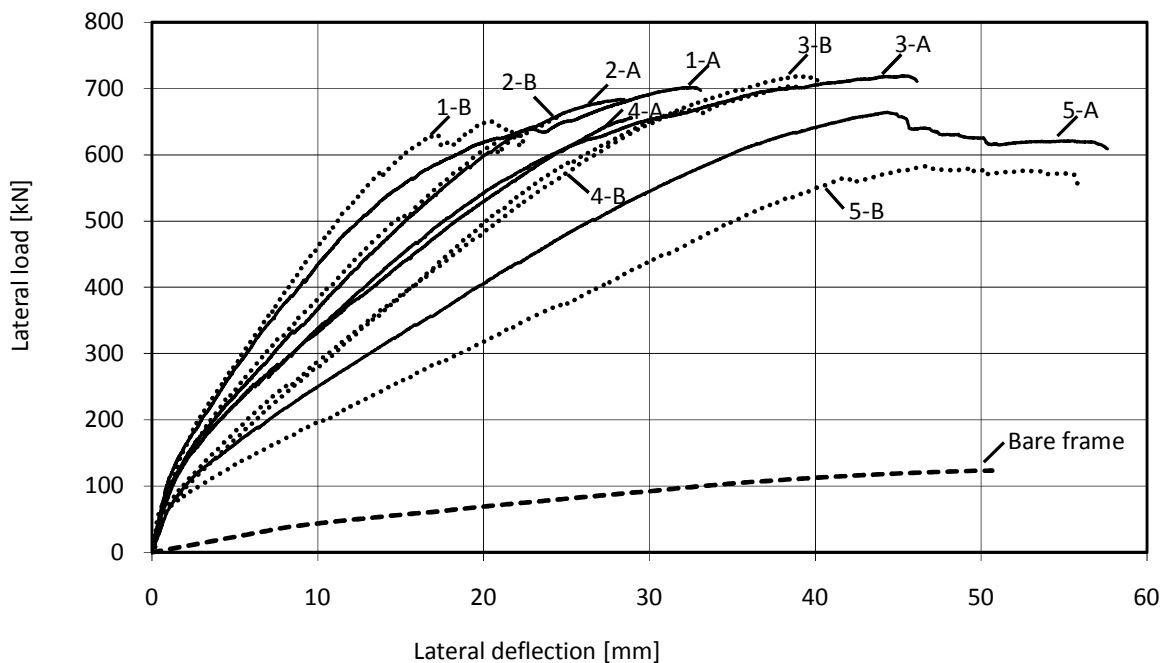


Figure 4-17: Load-deflection response of infilled frames

The typical infilled frame behavior is characterized by a relatively high initial stiffness, resulting from the tightening and thus prestressing of the discrete panel-to-frame connection in combination with uncracked panel behavior. Prestressing in this case restrains the tension corners of the panel. This initially results in a force system in the panel, comparable to the effect of two compression diagonals (Figure 4-18, left). Next, the lateral stiffness decreases due to the initiation of cracks, and the loss of contact between the panel and frame in the tension corners which results in a force system in the panel comparable to the effect of both a compression and tension diagonal (Figure 4-18, right).

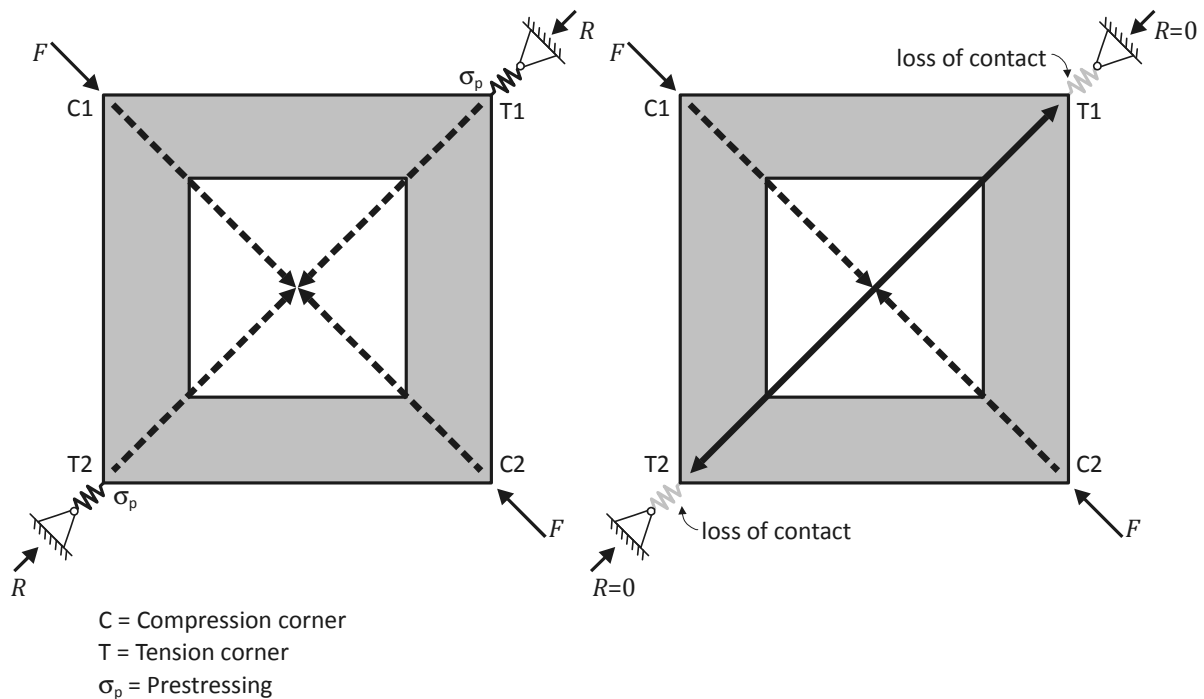


Figure 4-18: Initial force system in panel with restraints in tension corners (left) and after loss of contact between the panel and frame in the tension corners (right)

The behavior then can be considered linear up to around 500 kN, followed by a non-linear branch and finally failure. For test numbers 1-A to 4-B, failure of the infilled frame structures occurred by shearing of the panel-to-frame connection bolts through the nuts by stripping of the threads of the bolts (Figure 4-19).

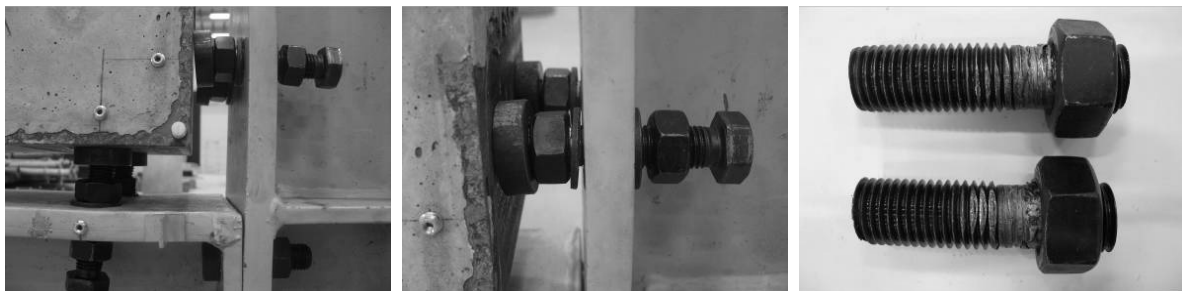


Figure 4-19: 'Bolt shear through nut' failure

Although the differences between the normal force levels in the bolts are only marginal, the bolts on the lower beam should fail first since these bolts support the largest part of the panel's dead weight. However, the observed specific location of the failed bolts differs for all tests (Table 4-10). This might be explained by the scatter in the material properties of the bolts or by the presence of less or more friction between the bolt shaft and the nut. For test numbers 2-B and 4-A rather brittle failure behavior was observed while for the remaining tests a small decrease of the load was observed after the ultimate load is reached, preceding the final failure point. All failure modes were accompanied by a loud

bang and at the same time a drop in load. After this load drop, it could be observed that the structure is still able to support some lateral load, since the load started to increase again. However, at that moment it was decided to end the test as the structure is considered to be failed.

For test 5-A failure occurred at the two tension corners of the panel with concrete spalling and reinforcement yielding (Figure 4-20). As no obvious load drop was observed, it was decided to end the test after a lateral deflection was measured of 60 mm which is 1/50 times the height of the structure. At this moment the structure was still able to support a lateral load of 600 kN. Due to the substantial damage to the panel, a second test was not possible without making repairs. Therefore, test 5-B was carried out using a repaired panel. In order to repair the panel, loose pieces of concrete were removed from the panel. Thereafter, the remaining holes were filled up with non-shrinking mortar. As a result of this repair, both the stiffness and ultimate strength of the structure decreased substantially. Once more, the structure failed at the tension corners of the panel which, by loading the panel in its other direction, are the opposite ones of the previous test.

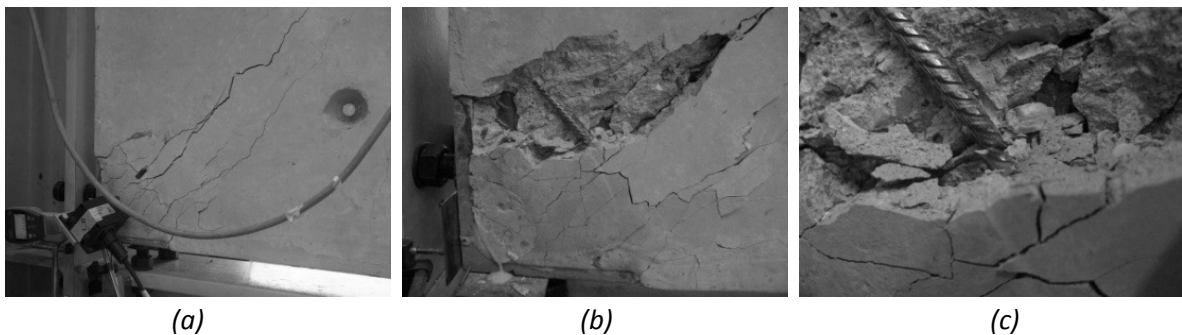


Figure 4-20: Failure panel corner (a) with concrete spalling (b) and wedge reinforcement yielding (c)

Based on the load-deflection graphs, the stiffness and strength of all tested infilled frame structures can be quantified (Table 4-10). Terms used to describe the infilled frame behavior are the ultimate strength ( $F_{u,if}$ ), being the maximum load level reached, the secant stiffnesses ( $k_{sec;1,if}$  and  $k_{sec;2,if}$ ) and the tangent stiffness ( $k_{tan,if}$ ) (Figure 4-21). The secant stiffness  $k_{sec;2,if}$  is determined by taking the ultimate load  $F_{u,if}$  with corresponding deflection. For secant stiffness  $k_{sec;1,if}$  the load corresponding to a lateral deflection of  $\delta_h = 10$  mm is taken, which is 1/300 of the height of the structure. The value 1/300 of the height of the structure is the recommended serviceability limit state for the lateral deflection of a story in a multi-story building according to Eurocode 3 ENV 1993-1-1 (1992). The tangent stiffness is also determined at the lateral deflection of 10 mm, by calculating a linear regression over the range of  $10 \text{ mm} \pm 1 \text{ mm}$ . Finally, a comparison is made between the tangent stiffness of the infilled frame and its bare frame by means of a stiffness factor  $\chi = k_{tan,if}/k_{tan,bf}$ .

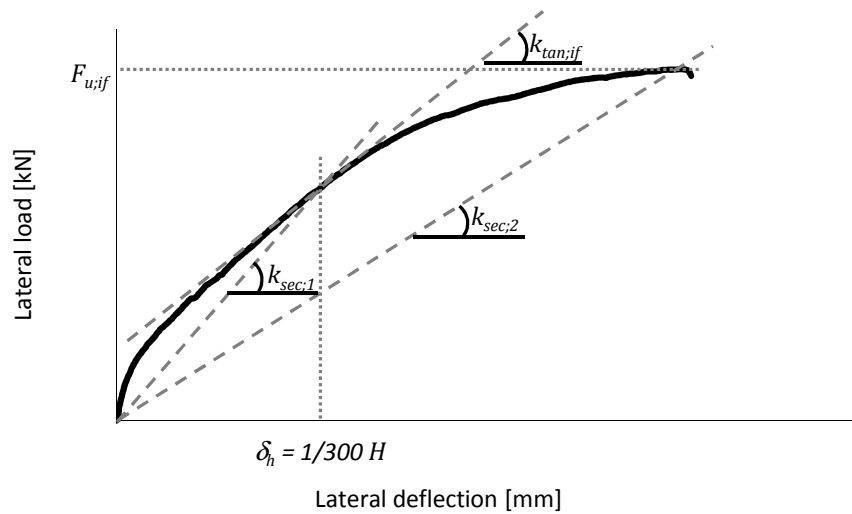


Figure 4-21: Illustration of terms for consideration of infilled frame behavior

Table 4-10: Test results infilled frames

Test No.	Frame stiffness		Infilled frame stiffness			$\chi$	Strength $F_{u;if}$ [kN]	Failure location*
	$k_{ini,bf}$	$k_{tan,bf}$	$k_{sec,1;if}$	$k_{sec,2;if}$	$k_{tan;if}$			
FS-1A	5.1	2.5	43.5	21.5	29.8	11.9	701	C1-C
FS-1B	5.2	2.4	46.1	31.7	32.0	13.3	650	C2-B
FS-2A	5.4	2.4	36.9	24.2	27.6	11.5	684	C1-C
FS-2B	5.4	2.8	38.2	26.8	25.3	9.0	658	C2-B
FS-3A	5.8	2.1	33.9	15.9	22.6	10.8	719	C2-C
FS-3B	4.7	2.4	28.0	18.4	19.3	8.0	719	C2-C
FS-4A	4.6	2.4	33.2	18.4	20.3	8.5	656	C1-C
FS-4B	4.9	2.6	28.7	18.5	20.7	8.0	704	C2-C
FS-5A	5.2	2.5	25.1	15.0	16.1	6.4	664	(Panel)
FS-5B	4.8	2.6	20.1	12.5	10.3	4.0	583	(Panel)

\*See Figure 4-18 for locations C1 and C2. -C and -B refer to the panel-to-column and panel-to-beam connection respectively.

The results in Table 4-10 show that the observed lateral stiffness of the infilled frames ranges between 4.0 and 13.3 times the bare frame stiffness, depending on the size of the window opening. Besides, all specimen types are able to support a lateral load of 583 kN or more. As mentioned before, for four panel geometries (type 1 to 4), the discrete connections were governing the strength of the structure as aimed at by design while for the test with the largest opening (type 5) the infill panel failed first.

#### Panel behavior

Figure 4-22 shows the load-deformation response of the infill panels, measured over the compression and tension diagonal of the panels respectively (Figure 4-14:  $\delta_{13}$  and  $\delta_{14}$ ). As mentioned before, for test 5-A and 5-B the ultimate strength of the panel is exceeded which is also shown in the graphs by the comparatively large (plastic) deformations. For all

other tests, the ultimate strength of the panels is not reached which is shown by the reasonably straight path at the top of the graphs, implying that some strength and deformation capacity are left. Furthermore, the graphs indicate a decrease of panel stiffness resulting from reusing the panels for the second test.

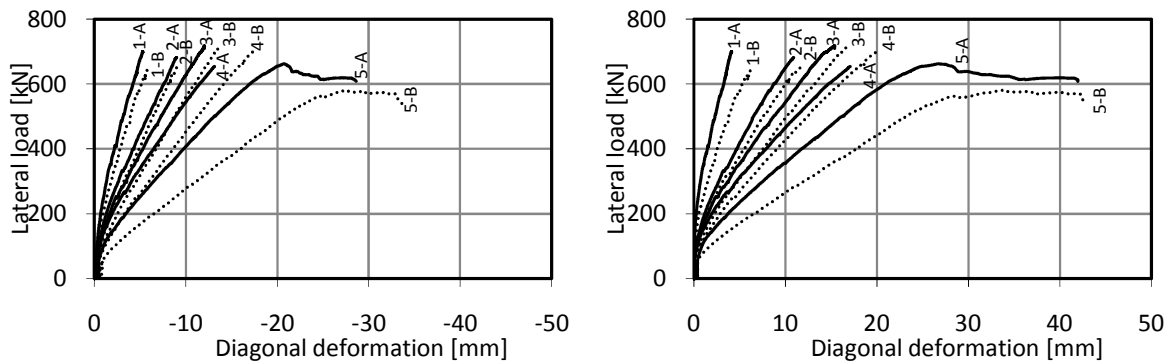


Figure 4-22: Deformation panels measured over the compression (left) and tension (right) diagonal

#### Principal Strains/Stresses

During each test 12 rectangular rosettes have been used to measure the strains on the concrete panel. Given the measurements of 3 independent strains from the 3 gauges in a rectangular rosette, it is possible to calculate the principal strains and their orientation with respect to the rosette. For a rosette with gauges labeled a, b and c as shown in Figure 4-23, the principal strains  $\varepsilon_1$  and  $\varepsilon_2$  and the principal direction  $\theta$  can be calculated with equations 4-3 and 4-4 respectively (Sharpe, W. N. J., 2008).

$$\varepsilon_{1,2} = \frac{\varepsilon_a + \varepsilon_c}{2} \pm \frac{1}{\sqrt{2}} \sqrt{(\varepsilon_a - \varepsilon_b)^2 + (\varepsilon_b - \varepsilon_c)^2} \quad [4-3]$$

$$\theta = \frac{1}{2} \tan^{-1} \left( \frac{\varepsilon_a - 2\varepsilon_b + \varepsilon_c}{\varepsilon_a - \varepsilon_c} \right) \quad [4-4]$$

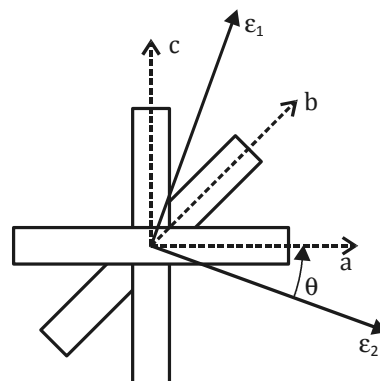
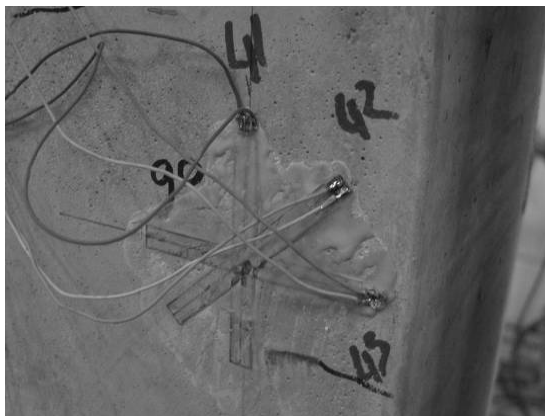


Figure 4-23: Rectangular rosette gauge orientation

For the following discussion, the principal strains are represented as Mohr's circles. Each Mohr's circle is drawn with its centre coinciding with the centre of the rosette. The arrow and its length represent the direction and the magnitude of the minor principal strain ( $\epsilon_2$ ). The direction of the major principal strain ( $\epsilon_1$ ) is perpendicular to minor principal strain, and its magnitude can be read from the Mohr's circle, being the distance to the y-axis. Examples of some possible configurations to illustrate this, are given in Figure 4-24.

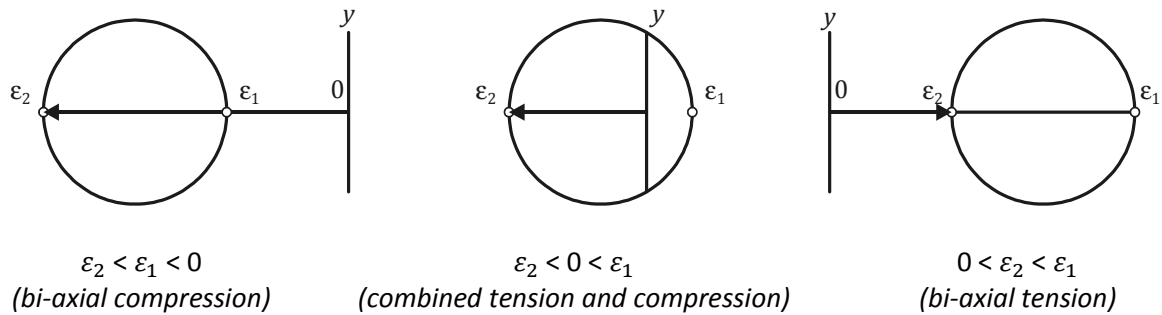


Figure 4-24: Some possible Mohr's circle configurations

Figure 4-25 and Figure 4-26 give the principal strain distribution for test 1-A, 3-A, and 5-A at identical load levels ( $F = 250$  kN and  $F = 500$  kN). If a cross is shown in the figure, the rosette is damaged by cracks entering the compression zone, and therefore the corresponding measurements are unusable. It can be seen that the qualitative strain distribution for all panels is fairly the same. Obviously, the panel with the largest window opening and thus the smallest concrete cross-sections shows the highest strains which can also be seen in the figure.

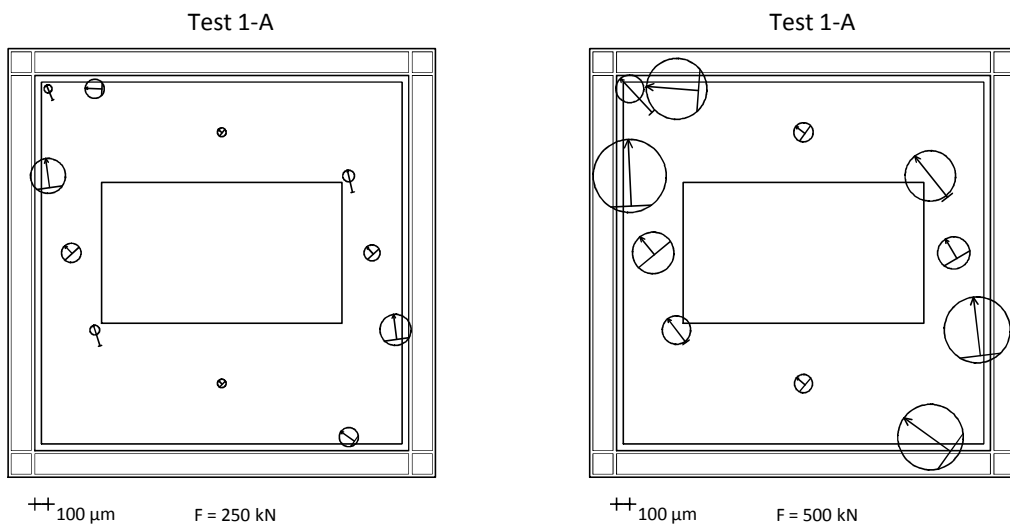


Figure 4-25: Principal strains represented as Mohr's circles for test 1-A

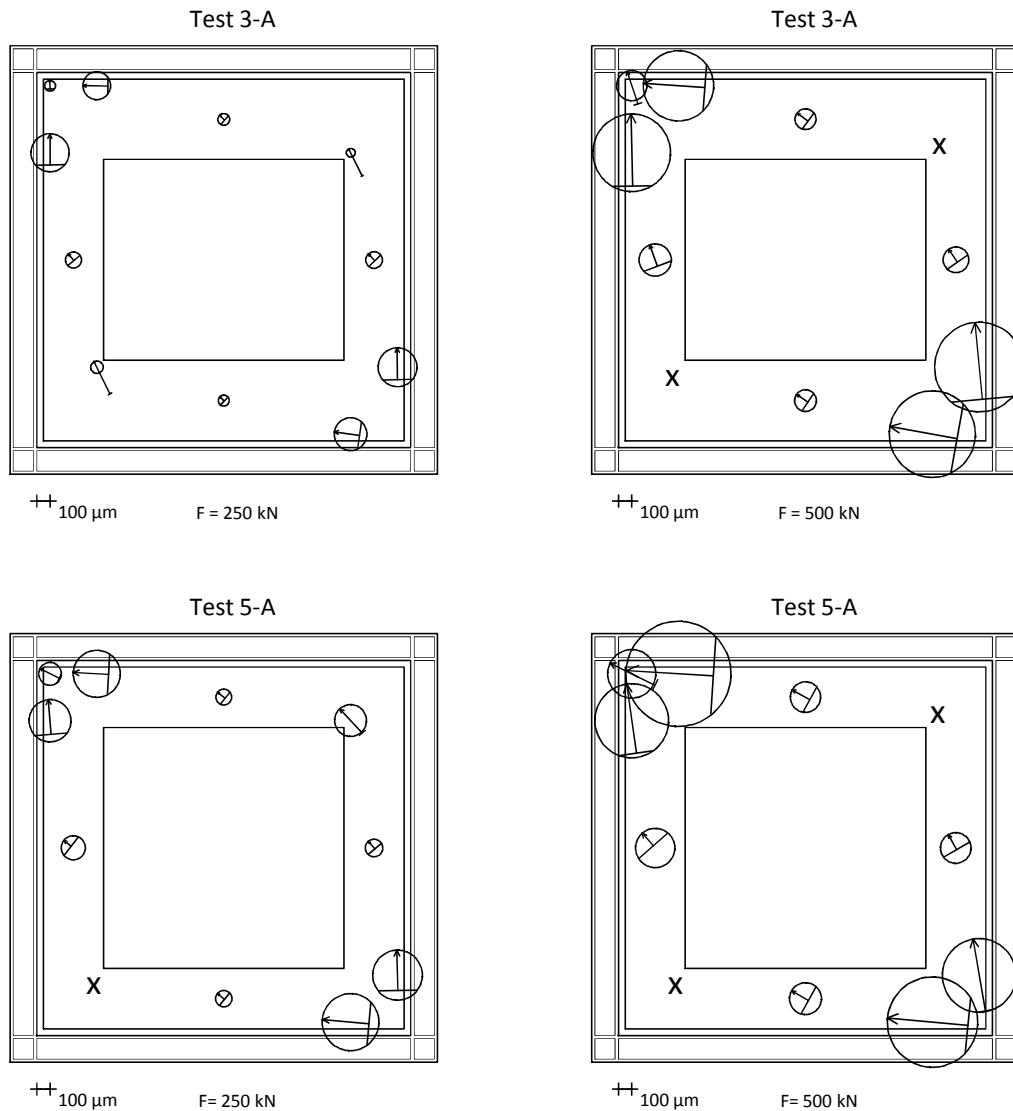


Figure 4-26: Principal strains represented as Mohr's circles for tests 3-A and 5-A

The principal strain distribution shows that high principal strains are measured near the window corners (rosette E and J) and in the proximity of the loaded corners of the panel (rosette A, C, G and H). It is shown that the regions near the loaded corner (rosette B) and near the window corners (rosette E and J) are loaded in bi-axial compression. Other regions are loaded in combined tension and compression (rosettes A, C, D, F, G, H, I, K). To determine the state of stress at the rosette, stress-strain relations must be used to express the stress components in terms of strain components. For linear elastic behavior, Hooke's law for the biaxial stress state can be expressed as follows (Timoshenko, S. P. et al., 1970):

$$\sigma_1 = \frac{E_c}{(1 - \nu^2)} (\varepsilon_1 + \nu \varepsilon_2)$$

$$\sigma_2 = \frac{E_c}{(1 - \nu^2)} (\varepsilon_2 + \nu \varepsilon_1)$$

[4-5]

Values for the Young's modulus  $E_c$  are obtained from standard material tests, and are provided in Table 4-9. The Poisson's ratio is taken as  $\nu_c = 0.2$ , according to Eurocode 2 EN 1992-1-1. In Table 4-11 to Table 4-13, the measured maximum compressive and tensile principal stresses are presented and the location of measurement at load levels  $F = 250$  kN (Table 4-11),  $F = 500$  kN (Table 4-12) and at ultimate load  $F = F_u$  (Table 4-13).

Table 4-11 : Maximum Principal stresses at  $F = 250$  kN.

	Maximum compressive principal stress $\sigma_2$ with corresponding values $\sigma_1$ and $\theta$				Maximum tensile principal stress $\sigma_1$ with corresponding values $\sigma_2$ and $\theta$			
	$\sigma_1$ [N/mm <sup>2</sup> ]	$\sigma_2$ [N/mm <sup>2</sup> ]	$\theta$ [rad]	Rosette	$\sigma_1$ [N/mm <sup>2</sup> ]	$\sigma_2$ [N/mm <sup>2</sup> ]	$\theta$ [rad]	Rosette
<b>1-A</b>	-0.11	<b>-7.79</b>	-1.44	C	<b>1.80</b>	-2.46	-0.83	D
<b>2-A</b>	0.37	<b>-10.64</b>	-1.54	H	<b>1.11</b>	-2.04	-0.81	I
<b>3-A</b>	-8.72	<b>-11.57</b>	-1.11	E	<b>1.53</b>	-2.22	-0.81	I
<b>4-A</b>	-12.87	<b>-28.09</b>	-1.45	E	<b>2.30</b>	-3.95	-0.88	D
<b>5-A*</b>	0.24	<b>-12.90</b>	-0.09	G	<b>3.74</b>	-1.83	-0.66	D

\*Rosette E damaged

Table 4-12: Maximum Principal stresses at  $F = 500$  kN

	Maximum compressive principal stress $\sigma_2$ with corresponding values $\sigma_1$ and $\theta$				Maximum tensile principal stress $\sigma_1$ with corresponding values $\sigma_2$ and $\theta$			
	$\sigma_1$ [N/mm <sup>2</sup> ]	$\sigma_2$ [N/mm <sup>2</sup> ]	$\theta$ [rad]	Rosette	$\sigma_1$ [N/mm <sup>2</sup> ]	$\sigma_2$ [N/mm <sup>2</sup> ]	$\theta$ [rad]	Rosette
<b>1-A</b>	-1.94	<b>-18.02</b>	-1.52	C	<b>3.87</b>	-5.34	-0.89	D
<b>2-A**</b>	-3.40	<b>-22.81</b>	-1.50	C	<b>0.99</b>	-4.17	-1.02	I
<b>3-A**</b>	-0.78	<b>-21.19</b>	-1.48	H	<b>1.95</b>	-3.89	-0.96	I
<b>4-A*</b>	1.35	<b>-34.75</b>	-0.84	J	<b>3.70</b>	-9.63	-1.00	D
<b>5-A**</b>	0.03	<b>-24.30</b>	-0.07	A	<b>5.48</b>	-3.61	-0.85	D

\*Rosette E damaged, \*\*Rosettes E and J damaged

Table 4-13: Maximum principal stress at  $F = F_u$

	Maximum compressive principal stress $\sigma_2$ with corresponding values $\sigma_1$ and $\theta$				Maximum tensile principal stress $\sigma_1$ with corresponding values $\sigma_2$ and $\theta$			
	$\sigma_1$ [N/mm <sup>2</sup> ]	$\sigma_2$ [N/mm <sup>2</sup> ]	$\theta$ [rad]	Rosette	$\sigma_1$ [N/mm <sup>2</sup> ]	$\sigma_2$ [N/mm <sup>2</sup> ]	$\theta$ [rad]	Rosette
<b>1-A</b>	-1.73	<b>-27.05</b>	-0.64	G	<b>4.21</b>	-7.92	-0.93	D
<b>2-A***</b>	-5.70	<b>-32.27</b>	-1.43	C	<b>1.12</b>	-5.57	-0.51	K
<b>3-A**</b>	-3.74	<b>-33.68</b>	-1.44	H	<b>1.83</b>	-8.41	-1.14	D
<b>4-A**</b>	-3.31	<b>-30.52</b>	-1.42	H	<b>2.90</b>	-6.39	-0.53	K
<b>5-A***</b>	0.77	<b>-34.72</b>	-0.10	A	<b>5.21</b>	-5.70	-0.90	D

\*\*Rosettes E and J damaged, \*\*\*Rosettes E, J and H damaged



In particular the two window corners (rosette E and J) are subject to large principal stresses. Initially this area is subject to bi-axial compression. At higher lateral loads, these two rosettes become unable to provide measurements due to crack formation through the rosettes. It is shown by the table that the maximum tensile principal stresses are measured at rosette D and I, which are located in the middle of the panel “columns”, having the smallest cross-section. However, it must be mentioned that no rosettes are located in the actual tension zones of the panel, since they would be damaged there immediately. To evaluate more thoroughly stresses and local deformations of the concrete panels, the experiments will be supplemented by finite element analyses. The measured principal strains and stresses will be used to validate the finite element model.

Finally, a comparison is made between the principal strain distribution found during the first and second test respectively with the same infill panel. Figure 4-27 shows for panel 1 the principal strain distribution found in the two tests at a lateral load  $F = 500$  kN. It can be observed that for most measured locations, the strains are higher during the panel’s second test. This phenomenon is shown for all panels (Appendix B), and may be attributed to changes in the stiffness of the aggregate and cement matrix due to cracks closing again.

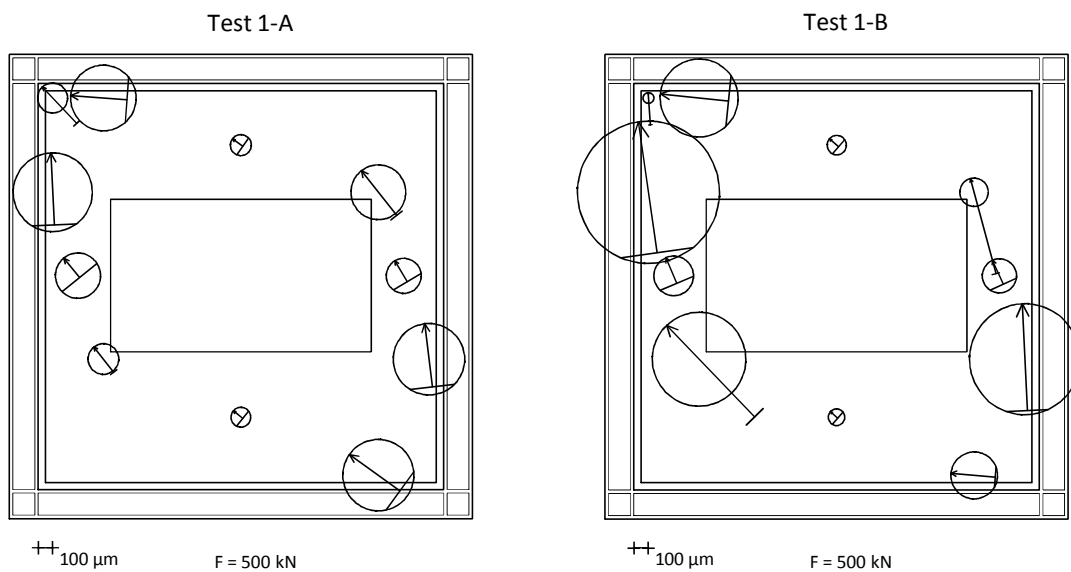
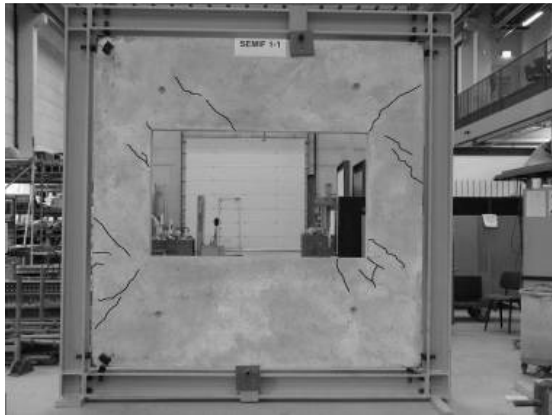


Figure 4-27: Principal strain distribution for panel 1 at first (left) and second test (right)

### Cracks

During the tests, attention was paid to observe the formation of cracks in the infill panel. If a crack was observed, it was marked on the panel and the end of the crack was marked with the corresponding load at that moment. It must be mentioned that this method does not provide information about the exact moment of crack initiation, but it informs about the crack configuration at a certain moment during the test. In Figure 4-28 the final crack patterns of all panels after their first test are shown. It can be seen that the crack patterns

are qualitatively identical, but that the crack intensity increases when the window opening becomes larger. The first crack is always observed near the lower tensile loaded window corner at a lateral load of around 90 kN (test 5-A) to 150 kN (test 1-A).



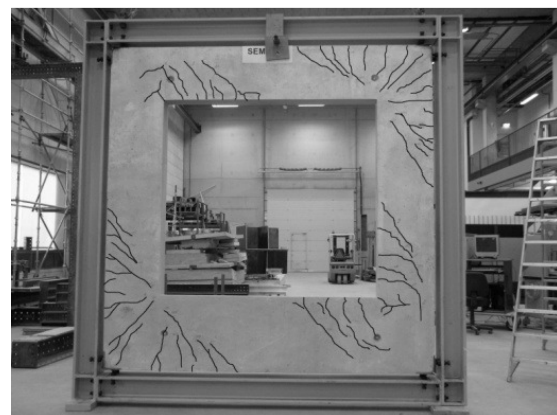
*Test 1-A*



*Test 2-A*



*Test 3-A*



*Test 4-A*



*Test 5-A*

*Figure 4-28: Final crack patterns*

Discrete panel-to-frame connection behavior

Considering the discrete panel-to-frame connection behavior, the results of two (arbitrary) tests are discussed. Figure 4-29 shows for test 4-A and 4-B the load-deformation behavior of the discrete interface connection, measured between the head of the discrete connection bolts and their opposite flanges (Figure 4-14:  $\delta_9$  to  $\delta_{12}$ ). This displacement comprises deformation due to flange bending together with shear deformation of the bolt through the nut, including the anticipated bolt failure. The elastic behavior of both graphs is quite comparable. However, a large difference is shown for the plastic and failure behavior. The cross in the graphs indicates the moment of failure of bolt shear through the nut. It is shown that the location of failure for the two tests is not the same ( $\delta_{10}$  and  $\delta_{12}$  respectively). Furthermore, the graphs of test 4-A show a much more brittle failure behavior than the graphs of test 4-B. This explains the rather sudden failure behavior that was observed in the overall load-deflection behavior.

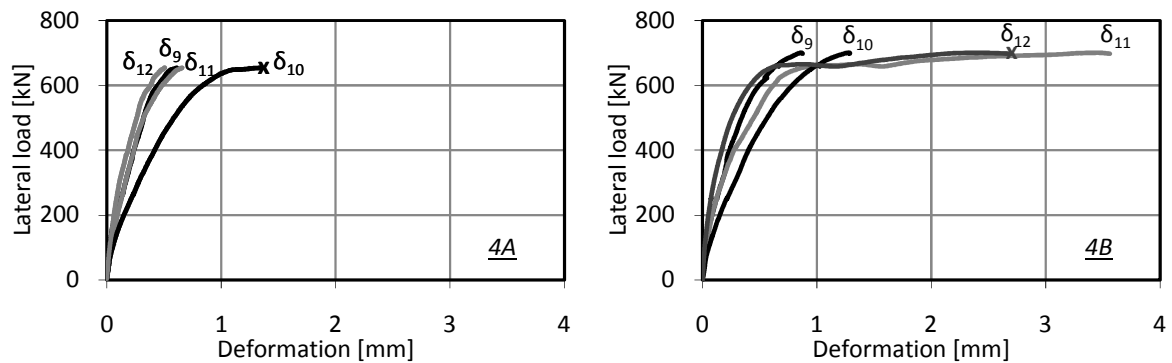


Figure 4-29: Load-deformation behavior panel-to-frame connection tests 4A (left) and 4B (right)

### 4.3 Chapter conclusions

An experimental study consisting of various test programs was carried out to provide insight into the structural behavior of the four identified components of the discrete panel-to-frame connection. The results of these tests are used for calibration and/or validation of finite element models presented in the next chapter. Notable conclusions regarding this study are:

- Unlike bolts subject to tensile loading, bolts subject to compressive loading fail by thread stripping failure and not by yielding of the bolt. The use of bolts with lower grades than the nuts results in more ductile behavior while for the bolt combined with nuts with lower strength less ductility occurs. Applicability of Alexander's theory for bolt-nut assemblies subject to compression has successfully been validated.
- Based on the observation that the application of high-strength steel plates under the compression bolts results in a considerable reduction of plastic plate

deformation while bolt yielding governs the strengths, an improvement is made for the component 'plate in compression' by adding high-strength steel caps between the bolts and the steel angle.

- HE200B sections have been subject to transverse compression introduced via bolts on the flanges. The test results allow validating a finite element model for studying the components 'flanges in bending' and 'web in compression'.

Thereupon, a full-scale test program was carried out for studying infilled frame behavior of semi-integral infilled frames provided with window openings. The test program consisted of ten full-scale tests on single-story, single-bay, 3 by 3 m infilled frame structures with five different opening geometries. The following conclusions are drawn with regard to the structural behavior of the tested infilled frame structures:

- The typical infilled frame behavior is characterized by a relatively high initial stiffness, resulting from a force system in the panel comparable to the effect of two compression diagonals. Next, the lateral stiffness decreases due to the initiation of cracks, and the loss of contact between the panel and frame in the tension corners, providing a force system in the panel comparable to the effect of both a compression and tension diagonal. The behavior then can be considered linear up to around 500 kN, followed by a non-linear branch and finally failure.
- For eight tests, failure of the infilled frame structures occurred by the preferred panel-to-frame connection failure, consisting of shearing of the bolts through the nuts by stripping of the threads of the bolts. Some of these bolt failures were rather sudden and brittle. The specific location of failure differed for all tests. After failure of the bolts, the structure was still able to support the lateral load. Failure of the bolts does not result in failure of the structure, as force transmission is redirected to the loaded corners of the frame by contact pressure between frame and panel. Therefore, the rather brittle bolt failure behavior can be considered as an acceptable failure mechanism. For the tests with the largest window opening, the infill panel governed the strength of the structure. It failed at the two tension corners of the panel by concrete spalling and reinforcement yielding.
- The discretely connected precast concrete infill panels with window openings significantly improved the performance of the steel frames. The observed tangent stiffnesses range between 4 and 13 times the bare frame stiffness.



# Chapter 5: FINITE ELEMENT MODELING

## *Scope of the chapter*

*This chapter presents finite element models developed for studying the structural behavior of the components 'flanges in bending with web in compression' (section 5.1) and the behavior of semi-integral infilled frames with window openings (section 5.2). An elaborated description of the design of the models is provided. Subsequently, in order to check the validity of the finite element models, they are compared with the component experiment for 'flanges in bending with web in compression' or the full-scale experiments respectively. At the end of this chapter (section 5.3), conclusions regarding the simulations of these experiments are given.*

## **5.1 Component modeling**

A finite element model is developed for simulating the component experiment 'flanges in bending with web in compression' (section 4.1.2). For this purpose, the finite element program ANSYS, release 11.0 (ANSYS Inc., 2007) is used. The validated finite element model is developed to be used in a parameter study in order to find the strength and stiffness characteristics of other H-sections (having different dimensions) subject to transverse compression introduced indirectly through the flanges.

The choice of the FE-method depends on the problem to be analyzed. To find the plastic resistance, material non-linear behavior has to be taken into account. Therefore, the tests are simulated performing physical nonlinear analyses, using material properties obtained from tensile tests on test coupons taken from the same member as the specimens are made from.

In chapter 3 it was demonstrated, based on regulations by Eurocode 3 EN 1993-1-5, that applying a transverse load indirectly via bending of the flanges to the web, the strength is governed by flange yielding and not by a web failure mechanism. Accordingly, the FE-model is to be developed for simulating flange yielding mechanisms only. As a consequence, geometrical imperfections and residual stresses can be ignored as these are not to influence the plastic resistance for flange yielding mechanisms. Because the flanges are not sensitive to buckling, and the displacements are relative small and thus the resulting stiffness changes are insignificant, geometrical linear analyses are performed.

To obtain a reliable finite element model, the geometry (Figure 5-1a) (the section height ( $h$ ), section width ( $b$ ), web thickness ( $t_w$ ) and flange thickness ( $t_f$ )) is modeled accurately as measured. A description of the finite element model is provided in the next paragraph.

### 5.1.1 Mesh and elements

The cross-section of wide flange beams can be divided into different areas: the top and bottom flange, the web and the fillets (Figure 5-1a). To model the cross-section, two different element types can be used: shell and solid elements. Shell elements generally require less input than solid elements, reducing the calculation time. However, using these elements, the exact geometry cannot be modeled as the fillets are ignored while the web and flange slightly overlap.

As the contribution of the fillets is expected to be of substantial influence on the results, solid elements instead of shell elements are used to model the H-section. The FE-model consists of 8-node (SOLID 45) and 20-node (SOLID 95) structural solids. SOLID 95 is a higher order version of SOLID 45 which can tolerate irregular shapes without much loss of accuracy.

Half a section is modeled by taking advantage of symmetry (Figure 5-1a). Besides, to reduce the number of elements, degrees of freedom and so the calculation time, only the upper half of the section is modeled, because it was experimentally observed that deformations are largely localized in the upper flange. Moreover, deformations of the lower half are marginal in comparison with deformations of the upper half, due to dispersion of the applied load through the depth of the section (Figure 5-1b).

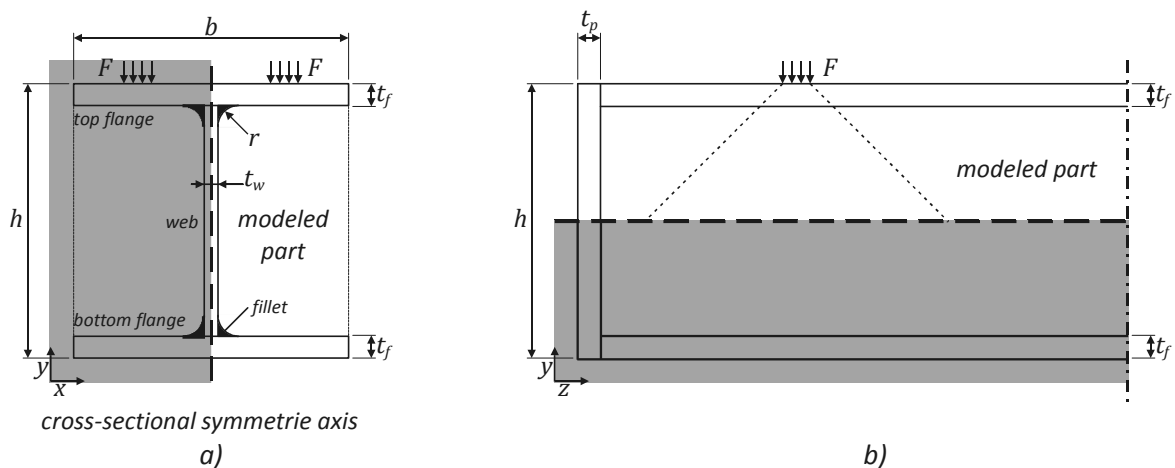


Figure 5-1: Model design

Figure 5-2a illustrates the finite element model. Four elements (SOLID 45) through the thickness are applied to model the flange and the web (Figure 5-2c). This is generally the recommended minimum number to correctly describe the shear stress due to Saint Venant-torsion (la Poutré, D. B., 2005). For the parts of the flange near the bolt hole, a fine mesh is used as large stress gradients are expected at this location. Parts further away have a courser mesh. A detailed view of the mesh surrounding the bolt hole (SOLID 95) is presented in Figure 5-2b.

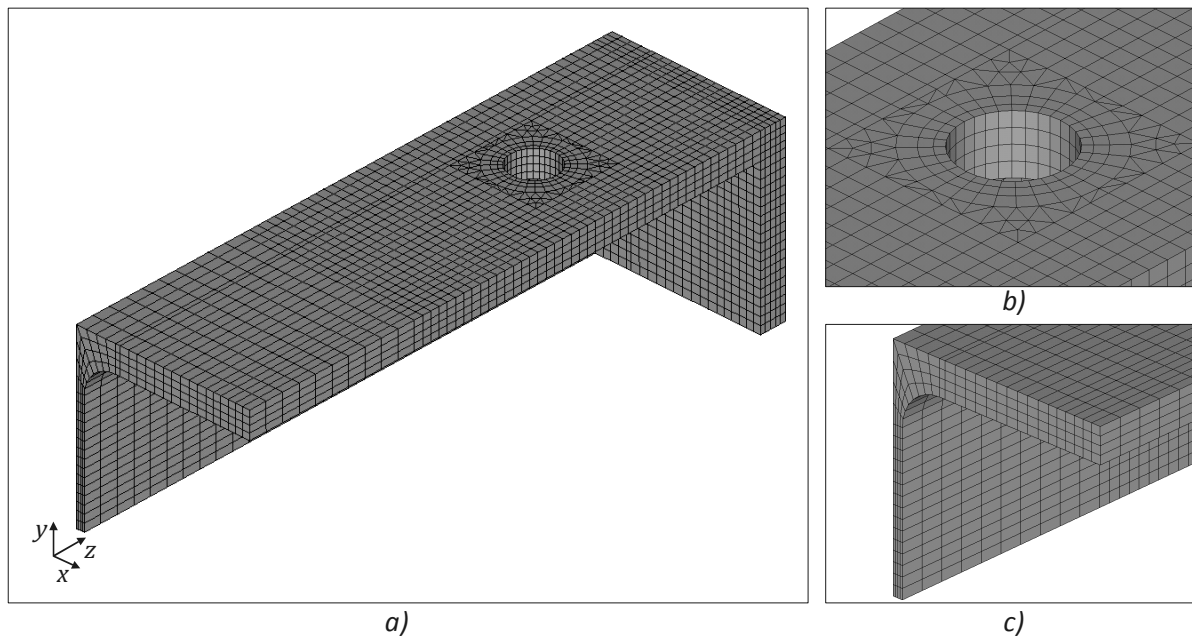


Figure 5-2: Finite element model

### 5.1.2 Material properties

Tensile tests on coupons, taken from the flanges and the web of the same HE200B section as the specimens were made from, were performed to determine the actual material properties of the test specimens (Table 4-4). As a substantial difference is shown between the material properties of the flange and the web, it was decided to use the material properties with the lowest strength, being those of the flanges, for the entire model. This is a conservative assumption which is not likely to influence the results, as the experiments showed that flange failure governed the strength with no yielding of the web.

Since the finite element program uses true stresses and true strains, and not engineering stresses and strains as measured, a conversion has to be carried out according to equations [5-1] and [5-2] (ANSYS Inc., 2007). The measured and true stress-strain relationships of a representative tensile test on a coupon taken from the flange are presented in Figure 5-3. Note that for small-strain response, true strain and engineering strain are essentially identical.

$$\sigma_r = \sigma_e(1 + \varepsilon_r) \quad [5-1]$$

$$\varepsilon_r = \ln(1 + \varepsilon_e) \quad [5-2]$$

Where:

$\sigma_r$  = true stress [N/mm<sup>2</sup>]

$\sigma_e$  = engineering stress [N/mm<sup>2</sup>]

$\varepsilon_r$  = true strain [mm/mm]

$\varepsilon_e$  = engineering strain [mm/mm]



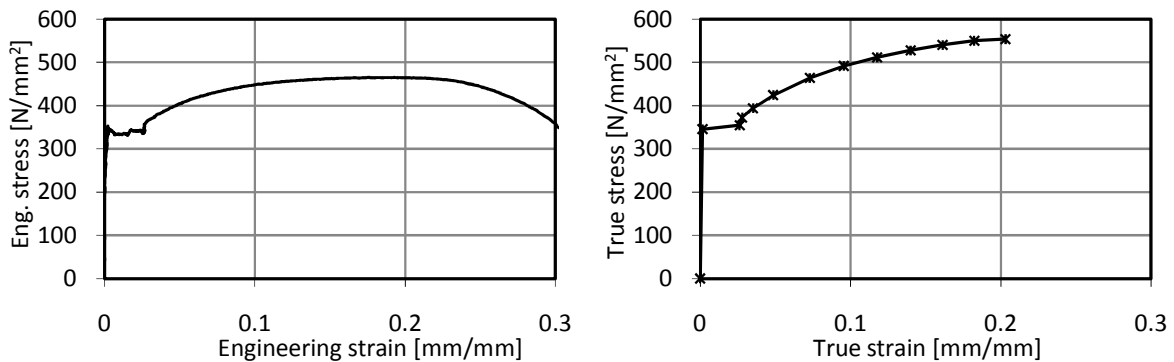


Figure 5-3: Engineering stress-strain relationship (left) and true stress-strain relationship (right)

### 5.1.3 Boundary conditions and loading

Several boundary conditions are applied to the finite element model (Figure 5-4). The bottom of the model is fixed along the  $y$ -axis,  $u_y = 0$ . For nodes at the cross-sectional symmetry axis, symmetry boundary conditions are applied, thus  $u_x = \varphi_y = \varphi_z = 0$ , where  $u_i$  is the displacement in  $i$ -direction and  $\varphi_i$  is the rotation around the  $i$ -axis. In order to find the actual behavior, two extreme types of load applications are applied alternately to the model (Figure 5-4). The first one (LA-1) models the load applied to the flange by a bolt as a pressure uniformly distributed over the area of the washer. This loading condition allows free bending of the flange without a clamping moment of the bolt to the flange occurring. The second load application (LA-2) models a prescribed displacement over the area of the washer along the  $y$ -axis. This means that the area of the washer remains entirely horizontal, representing a full clamping moment of the bolt at the top surface.

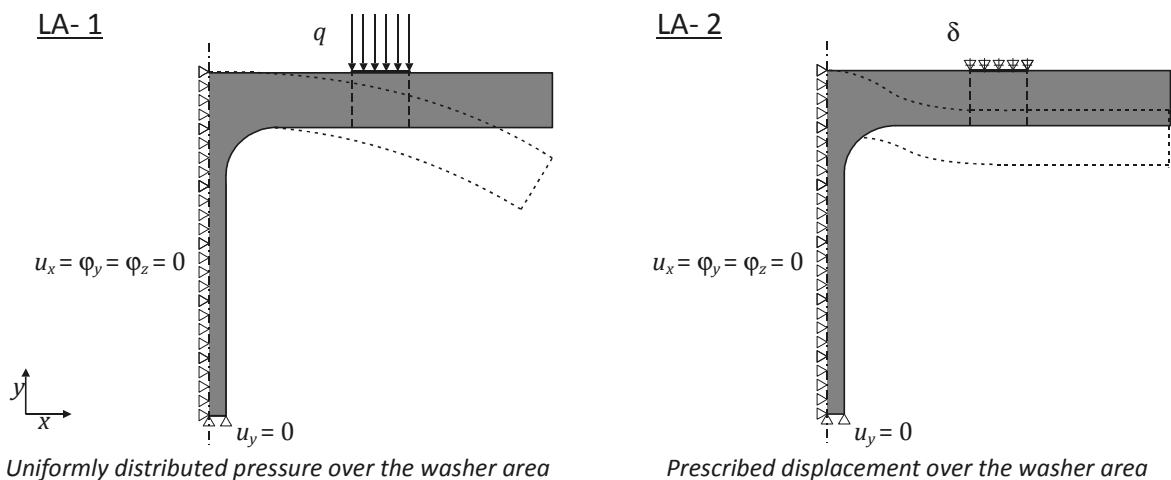


Figure 5-4: Boundary conditions, load applications and schematic deformation

### 5.1.4 Solution procedure

The analyses of the models LA-1 and LA-2 are carried out force controlled and displacement controlled respectively. For both analyses, the full Newton-Raphson

procedure, in which the stiffness matrix is updated at every equilibrium iteration, is applied to find the solution.

### 5.1.5 Validation of finite element model

Figure 5-5 shows the experimentally found load-deformation response together with the numerical simulations. Both simulations show good agreement in the elastic range and provide an accurate, approximately identical prediction of the linear elastic stiffness. The finite element model with the load applied as a prescribed displacement (LA-2) shows a slight overestimation the strength. The finite element model with the load applied as a pressure uniformly distributed over the diameter of the washer (LA-1), on the other hand, provides an accurate prediction of the onset of yielding. However, the model gives a conservative prediction of the plastic stiffness. The real behavior seems to be in between the two simulations. Seeing that the experimental branches tend to fit the graph representing the full clamping moment by increasing deformation, it seems that the influence of the clamping moment by the bolt to the flange increases with increasing flange deformation.

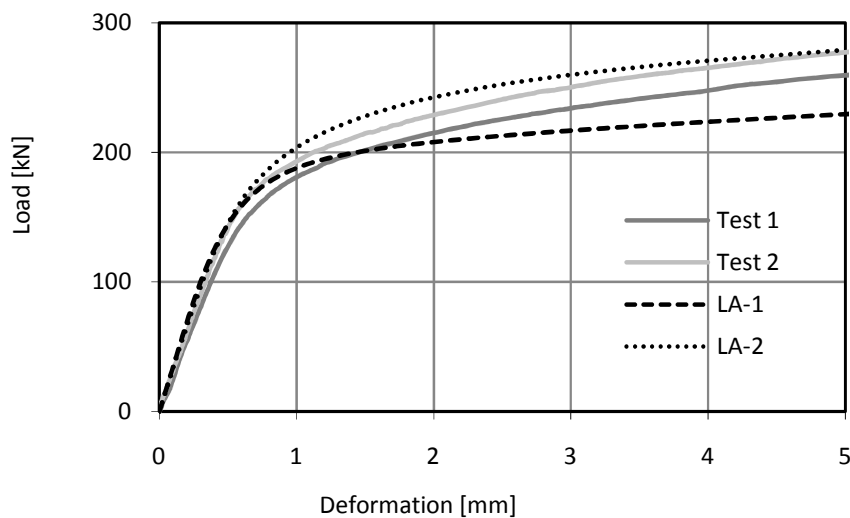


Figure 5-5: Experimental and simulated load-deformation response

Nevertheless, the finite element model with the load applied as a pressure uniformly distributed over the diameter of the washer (LA-1) provides a safe prediction of the real behavior. Besides, the plastic stiffness is of minor importance for design purposes, taking into account that the desired failure mode of the connection is a bolt failure mechanism, allowing no plastic deformation in the other components. Therefore the finite element model (LA-1) is suited to study the response of the components 'flanges in bending' and 'web in compression' for other HE-sections in a parameter study (chapter 6.1), and thus to find the elastic stiffness and strength.

## 5.2 Full-scale modeling

For studying the behavior of the semi-integral infilled frame with window opening, the full-scale experiments are supplemented by finite element analyses. The finite element program used is DIANA, release 9.2 (DIANA, 2007). The aim of the finite element research is to develop and validate a finite element model that simulates the experimental infilled frame behavior, taking into account non-linear material characteristics and geometrical non-linearity. The validated finite element model can then be used to carry out parameter studies to investigate other configurations of the semi-integral infilled frame.

Figure 5-6 illustrates the two-dimensional finite element model that has been developed for simulating the full-scale experiments. The model can be divided into the following three groups: panel, frame and discrete panel-to-frame connections. For each group, the applied element types and material properties are discussed below.

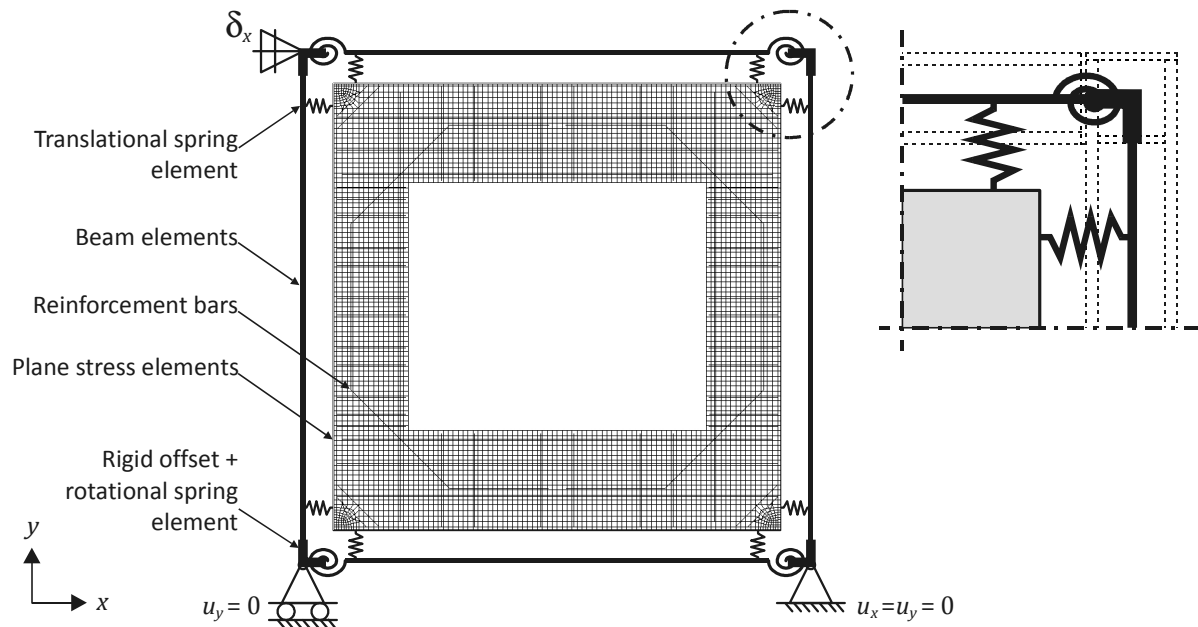


Figure 5-6: Finite element model with corner detail (specimen type 3)

### 5.2.1 Mesh and elements

#### Panel

The concrete panel is modeled with eight-node isoparametric plane stress elements (type CQ16M) with a thickness of 200 mm. The longitudinal reinforcement and stirrups are modeled with reinforcement bars, embedded in the plane stress elements. The technique of embedding allows the lines of the reinforcement to deviate from the lines of the mesh. The embedded reinforcements do not have degrees of freedom of their own. The reinforcement strains are computed from the displacement field of the plane stress elements, implying a perfect bond between the reinforcement and the surrounding concrete (DIANA, 2007).

Frame

The three-node, two-dimensional class-III beam element (type CL9BE) is used to model the frame members. This element is based on the Mindlin–Reissner theory which takes shear deformation into account. This theory assumes that the cross-sections remain planar but not necessarily perpendicular to the deformed beam axis, contrary to the Bernoulli beam theory which does not take shear deformation into account, assuming cross-sections to remain planar as well as normal to the deformed beam-axis. The sectional properties of the beam elements correspond to the sections used experimentally (HE180M). The beam-to-column connection is modeled with a rigid offset to take the column and beam depth into account, and a two-node rotational spring element (type SP2RO), representing the stiffness of this connection.

Discrete panel-to-frame connection

The discrete panel-to-frame connections are represented by two-node translational spring elements (type SP2TR), and are only able to support axial compressive forces. An initial force in the springs is applied in order to represent the pretensioning resulting from the torque controlled tightening of the bolts.

**5.2.2 Material properties**Panel

Prior to cracking, concrete can be modeled sufficiently accurately as isotropic, linear elastic (de Borst, R., 2002). The initial Young's modulus ( $E_c$ ) is determined by performing standard material tests on concrete prisms. The Poisson's ratio of concrete under uni-axial compressive stress ranges from 0.15 to 0.22, with a representative value of 0.19 or 0.20 (ASCE Task Committee on Concrete and Masonry Structure, 1982). For this study, a Poisson's ratio is adopted of  $\nu_c = 0.2$ . To find the actual tensile strength ( $f_{ct}$ ) and compressive strength ( $f_c$ ), standard material tests are performed with concrete 150 mm cubes. A survey of the applied material properties is provided in Table 5-1.

In addition, a non-linear concrete material model is used that combines the Drucker-Prager plasticity model for the compressive regime with a smeared cracking model for the tensile regime. For the behaviour of the concrete in compression the Drucker-Prager yield surface limits the elastic state of stress (Figure 5-7). The DIANA software evaluates the yield surface using the current state of stress, the angle of internal friction ( $\phi$ ) and the cohesion ( $c$ ). According to a recommendation by the DIANA software manual (DIANA, 2007), the angle of internal friction of the concrete is approximated to be  $\phi = 10^\circ$ . The cohesion ( $c$ ) can then be calculated as follows:

$$c = f_c \frac{(1 - \sin \phi)}{2 \cos \phi} \quad [5-3]$$

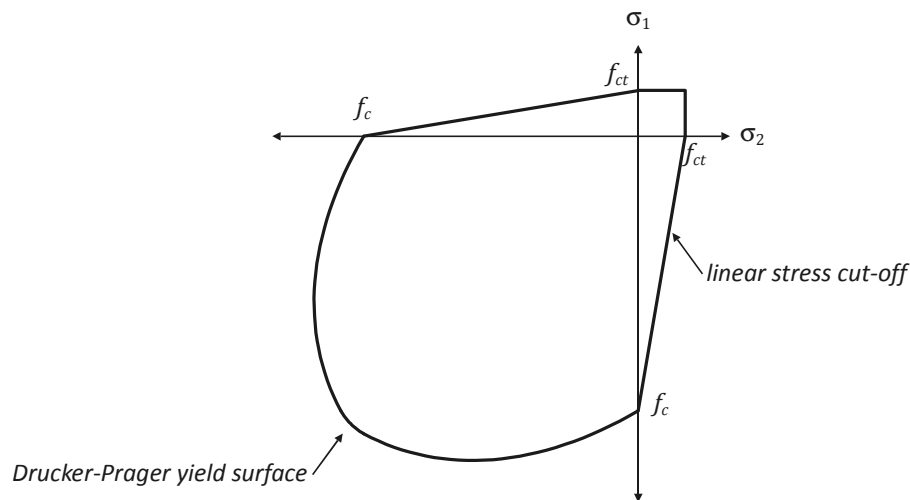


Figure 5-7: Failure surface in two dimensional principal stress space

For the smeared crack approach, a multi-directional fixed crack model is applied, in which typically the direction of the normal to the crack is fixed upon initiation of the crack. A linear stress cut-off criterion is applied (Figure 5-7), which means that a crack arises if the major principal tensile stress exceeds the minimum of  $f_{ct}$  and  $f_{ct}(1 + \sigma_{lateral}/f_c)$ , with  $\sigma_{lateral}$  being the lateral principal stress. Besides, a linear tension softening based on the fracture energy of concrete ( $G_f$ ) is adopted according to the CEB-FIP Model Code (Comité Euro-International du Béton, 1993) (Figure 5-8a). The area under the tension-softening curve gives the fracture energy. The fracture energy of concrete is the energy required to propagate a tensile crack of unit area, and is released in an element if the tensile strength is exceeded. Subsequently, the deformations localize in the element. With this approach the results obtained are objective with regard to mesh refinement.

The fracture energy is related to the compressive strength and the maximum aggregate size, and has been estimated from equation [5-4] (Comité Euro-International du Béton, 1993).

$$G_f = G_{f0}(f_{cm}/f_{cm0})^{0.7} \quad [5-4]$$

With:

$$f_{cm} = f_{ck} + \Delta f \quad [5-5]$$

Where:

$G_{f0}$  = Base value of fracture energy depending on the maximum aggregate size  $d_{max}$ . For this study,  $d_{max} = 16$  mm, resulting in  $G_{f0} = 0.030$  Nmm/mm<sup>2</sup>

$f_{cm}$  = Mean value of compressive strength [N/mm<sup>2</sup>]

$f_{cm0} = 10$  N/mm<sup>2</sup>

$f_{ck}$  = Characteristic compressive strength

$\Delta f = 8$  N/mm<sup>2</sup>

Subsequently, the found fracture energy has been adapted proportionally to the ratio between the nominal strength according to Eurocode 2 and the measured tensile strength (for  $G_f$ , see Table 5-1).

Due to cracking of concrete, the shear stiffness is reduced, generally known as shear retention. A constant shear retention factor  $\beta = 0.2$  is used which is a commonly adopted value (de Borst, R., 2002). When the cracked concrete is unloaded in tension, the secant modulus is used to evaluate the stiffness (Figure 5-8a). For unloading of concrete in compression, the elastic stiffness is adopted for stiffness calculations (Figure 5-8b).

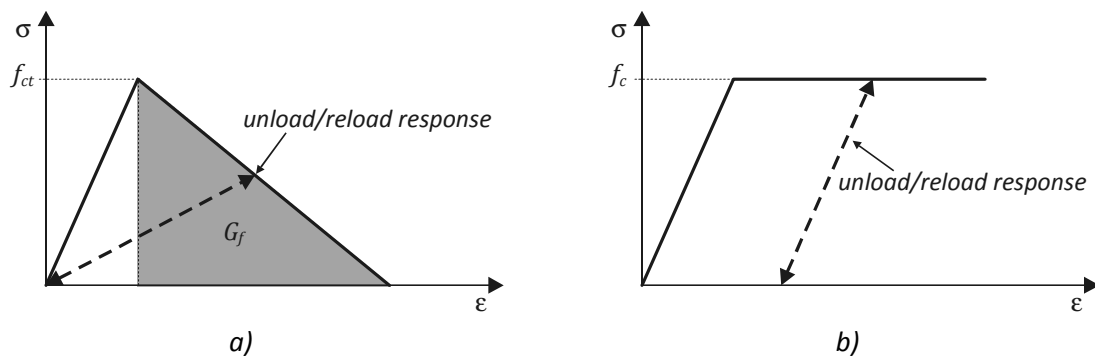


Figure 5-8: Material modeling of concrete in tension (a) and compression (b)

Table 5-1: Material properties concrete

Panel type	$E_c$ [N/mm <sup>2</sup> ]	Measured $f_c$ [N/mm <sup>2</sup> ]	$f_{ct}$ [N/mm <sup>2</sup> ]	Calculated $G_f$ [Nmm/mm <sup>2</sup> ]
1	3.54E+04	62.2	3.9	0.097
2	3.67E+04	64.4	3.9	0.099
3	3.66E+04	70.6	4.2	0.104
4	3.70E+04	75.6	4.4	0.109
5	3.72E+04	66.0	3.9	0.097

For the embedded reinforcement bars, a Young's modulus of  $E_s = 2.0E+05$  N/mm<sup>2</sup> is taken. The stress-strain curve of the reinforcement bars is assumed to be elastic-perfectly plastic, with yielding according to the Von Mises criterion, with a yield stress equal to  $f_y = 560$  N/mm<sup>2</sup>.

Frame

For the frame, steel having the elastic material properties for the Young's modulus  $E_s = 2.1E+05$  N/mm<sup>2</sup> and the Poisson's ratio  $\nu_s = 0.3$  is used, in combination with Von Mises plasticity ( $f_y = 235$  N/mm<sup>2</sup>). The rotational springs representing the beam-to-column connections are calibrated on the load-deflection curves of the full-scale tests with the bare frames by means of simulating these tests by varying rotational spring characteristics. The moment-rotation curve for the rotational springs for specimen type 3 is shown in Figure 5-9. The curves used for all other simulations are provided in Appendix C.1.

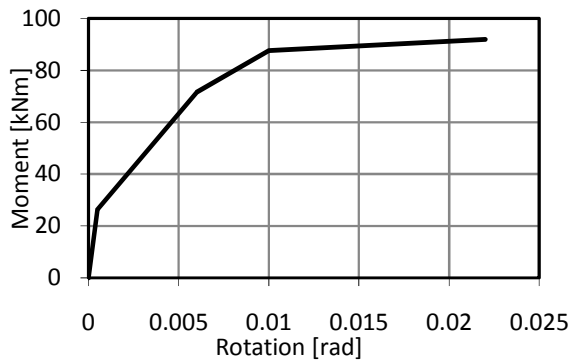


Figure 5-9: Moment-rotation response for rotational springs for specimen type 3

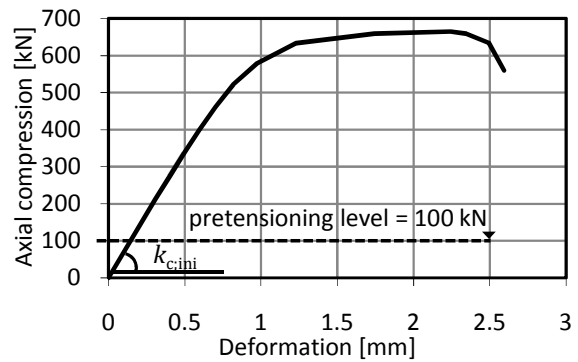


Figure 5-10: Load-deformation response for translational springs for all specimen types

Discrete panel-to-frame connection

The discrete panel-to-frame connections are modeled with non-linear translational spring elements, with no tension capacity. Input is the stiffness diagram presented in Figure 5-10. The initial connection stiffness ( $k_{c,ini}$ ) is composed of the structural characteristics obtained from the component experiment ‘bolt with cap on plate in compression’ (Figure 5-11) in combination with results from a finite element simulation using the FE-model presented in section 5.1 for the HE180M section experimentally used (Figure 5-12).

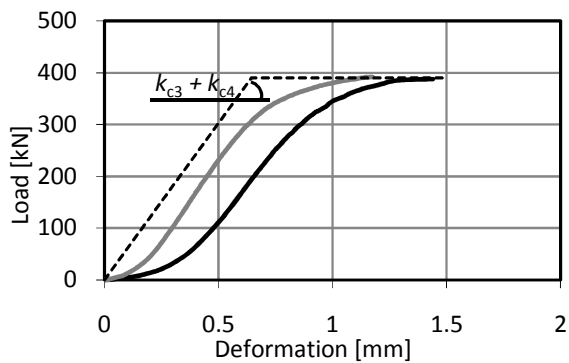


Figure 5-11: Load-deformation response of compression tests on bolt with cap on plate, with bilinear approximation

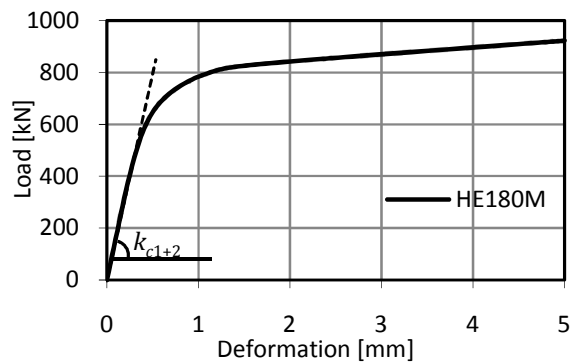


Figure 5-12: Load-deformation response for HE180M section subject to transverse load introduced indirectly through the flanges

Combining the found linear elastic stiffnesses gives the initial connection stiffness ( $k_{c,ini}$ ) of the discrete panel-to-frame connection as follows :

$$k_{c,ini} = \left[ \frac{1}{k_{c1+2}} + \frac{1}{2k_{c3+4}} \right]^{-1} \quad [5-6]$$

The factor 2 in the equation accounts for two bolts found in one panel-to-frame connection.

Subsequently, the non-linear branch of the compression test on the bolts applied for the discrete panel-to-frame connection (Figure 4-2: M24-RC1.B) is superposed on this initial connection stiffness ( $k_{c,ini}$ ). Combined, this gives the load-deformation response presented in Figure 5-10, to be used for each translation spring for all specimen types.

### 5.2.3 Boundary conditions and loading

Support conditions matching the test-setup are used (Figure 5-6). The loads applied to the finite element model include initial prestressing of the translational springs, representing the tightening of the panel-to-frame connection (load case 1), the dead weight (load case 2), and horizontal loading at the left upper corner up to failure (load case 3). In the finite element analyses, the prestressing load from the bolts (100 kN) is simulated with initial stresses and applied to the infilled frame first. After the structure has become in an equilibrium condition, the dead weight is applied to the infilled frame. This order of loading is correct, since the bare frame was fixed to the horizontally positioned panel. Therefore, the dead weight initially did not influence the prestressing forces in the bolts. Finally, the lateral load is applied to the left upper corner of the infilled frame.

### 5.2.4 Solution procedure

A displacement controlled procedure is applied to impose the load up to failure, using the regular Newton-Raphson iteration procedure to find the solution. A phased analysis that comprises two calculation phases is conducted, to enable determining the effect of the prestressing and erecting of the specimen. Between the two phases, the finite element model changes by addition of a constraint in the left upper corner, which is needed to apply the prescribed lateral displacement to the model. The results from the first phase are automatically used as initial values in the second phase.

### 5.2.5 Validation of finite element model

Validation of the finite element model is accomplished by comparing the following experimental and numerical results: the global load-deflection behavior, the ultimate load with corresponding failure mode, the local panel and connection deformations and the final crack patterns. The results for specimen type 3 have been selected for a more detailed discussion. Results for the other specimen types can be found in Appendix C.2.

To explicitly treat the structural behavior of the infilled frame at the different stages of loading, the deformed shapes of specimen 3 are shown (Figure 5-13), presenting the deformation after the prestress load from the bolts and the dead weight only are applied to the model ( $\delta_h = 0$ ) (left) and at ultimate deflection  $\delta_h = \delta_u$  (right). As a result of the tightening of the bolts, the infill panel is slightly uniformly-prestressed in the steel frame. The magnitude of the prestress loads is initially equal in all springs. After the dead load is applied to the model, the beam springs at the bottom of the model (T2-B and C2-B) are



further loaded while the upper beam springs (T1-B and C1-B) are slightly unloaded. Thereafter, the horizontal load is applied to the model resulting in gradually unloading of the springs in the unloaded corners of the infilled frame (T1-B, T1-C, T2-B and T2-C). Although the translational springs in the unloaded corners are still in contact with the panel at ultimate deflection, they are unstressed since they are unable to support axial tensile forces. This is correct, as loss of contact between infill panel and frame in the tension corners was visually observed during the tests. Figure 5-14 gives the progress of the load in the springs versus the time.

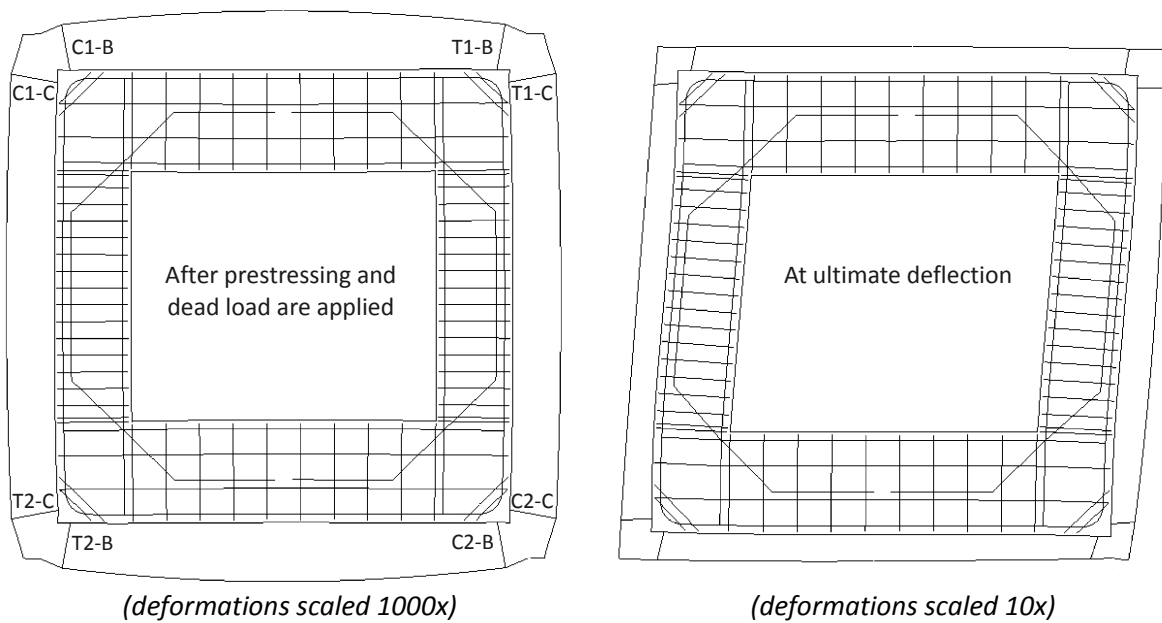


Figure 5-13: Deformed finite element model of specimen type 3

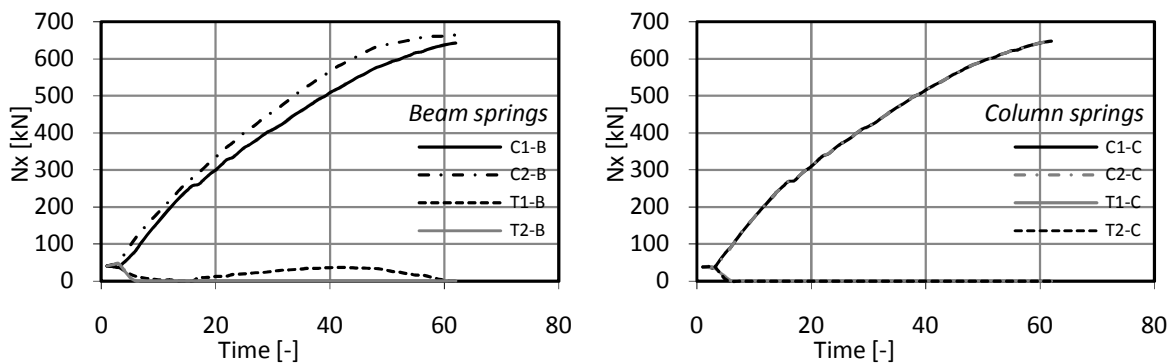


Figure 5-14: Axial load in translational springs versus time

From these figures it can be observed that under lateral load, the infill panel tends to act as a diagonal strut bracing the steel frame. However, due to the presence of the opening in the panel, direct support from the load to the support by a strut under compression is impossible. Therefore the load is transferred around the opening to the support by inclined normal forces, giving double curvature bending of the panel members, which is confirmed by the deformed shape of the C2 panel (Figure 5-13, right).

The simulated and experimental global responses (test numbers n-A) of all specimens are presented with dashed and solid lines respectively in Figure 5-15. Comparison shows that the load-deflection behavior obtained from the finite element analysis is quite similar to the experimental results for each test. The initial higher stiffness is present, followed by the approximately linear branch and finally failure. The simulated failure modes of specimens 1 to 4 are connection failure, which are identical to the experimental failure. However, contrary to the experimentally found locations of failure (for locations, see Table 4-10), the specific failure locations for all simulations are identical, being the vertical translational spring in the right lower corner (Figure 5-13: C2-B). Theoretically this is correct, since this translational spring is, besides the lateral load, also loaded with a major part of the dead weight of the infill panel. However, there is only a slight difference with the magnitude of the axial forces in the other loaded springs at ultimate load ( $\pm 2.5\%$ , see Figure 5-14), and other phenomena such as the exact magnitude of the prestress load and the level of friction in the connections may also contribute to the experimental location of failure. Therefore, the experimentally found failure locations in some tests can differ from the simulated ones.

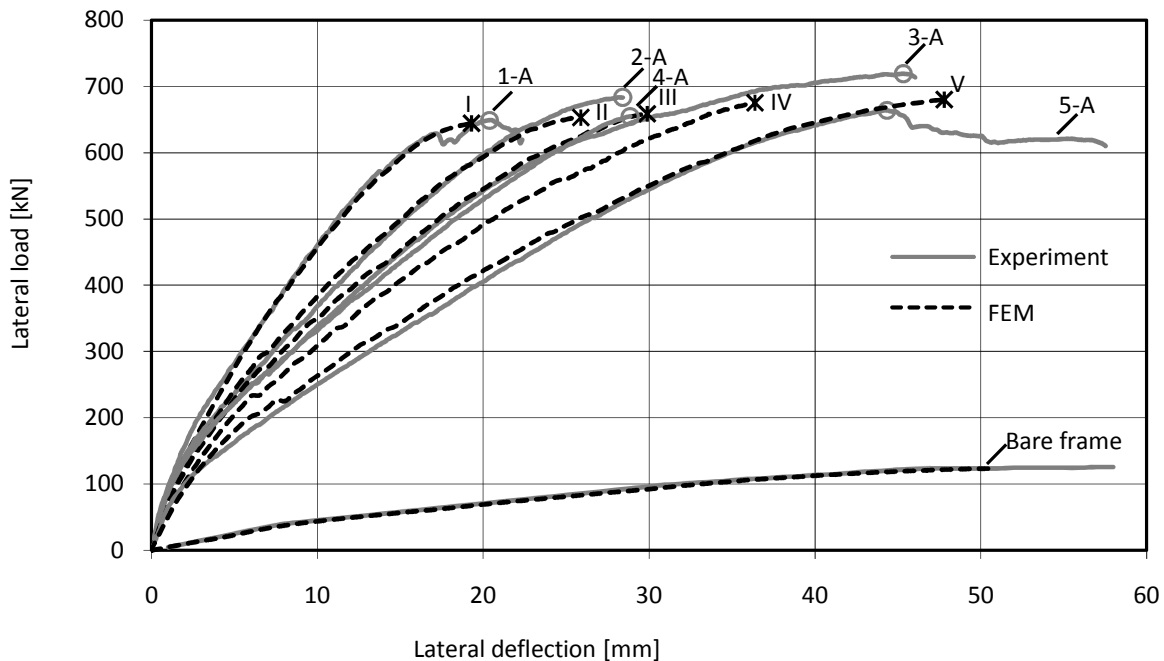


Figure 5-15: Experimental and simulated load-deflection response of infilled frame

For tests 5A and 5B, the infill panel failed first in the experiments, with considerable deformations concentrated in open cracks and yielding of the wedge reinforcement. Although the finite element simulation indicates panel failure with yielding of the wedge reinforcement (Figure 5-17), the smeared crack model is not appropriate to adequately describe the post-peak behavior. To obtain a more accurate post-peak prediction, the

concrete model could be supplied with discrete cracks. In this combined approach, the smeared crack model is used to model the distributed cracking and concrete crushing, while interface elements are inserted between the continuum elements along the potential crack path, where major cracking can be expected based on the experimental observations. However, panel failure will be prevented in the design, since the panel-to-frame connection will be designed to govern the strength of the structure. Therefore, the smeared crack approach is satisfactory for design purposes as meant in this thesis.

Besides the global behavior, also the accuracy of the simulated local behavior of the infill panel is investigated. Six LVDTs (Figure 4-14:  $\delta_a$  to  $\delta_f$ ) were positioned on the concrete panel surface, measuring local deformations over a distance of 300 mm in order to determine average strains and crack initiation in the tension zones of the panel. For each LVDT measurement, a comparison is made between the experiment and the simulation. In Figure 5-16 the measured and simulated average strains for test 3 are presented (LVDTs  $\delta_c$ ,  $\delta_d$  and  $\delta_e$ ). It is shown that the finite element model qualitatively represents the strains on the surface of the concrete panel reasonably accurate. The discrepancies between the experimental and simulated strains, in particular present in the early stage of loading, can be explained by the fact that the FE-model is based on the principle of smeared cracks while the measurement, in contrary, incorporates discrete cracking. As a result, the differences fade out during loading, increasing the discrete crack intensity, as shown by the figure. Also for the other simulations (Appendix C.2.1), sufficient agreement is shown between the measured and simulated local panel deformations. Therefore, also by this check, the finite element model may be considered to be validated.

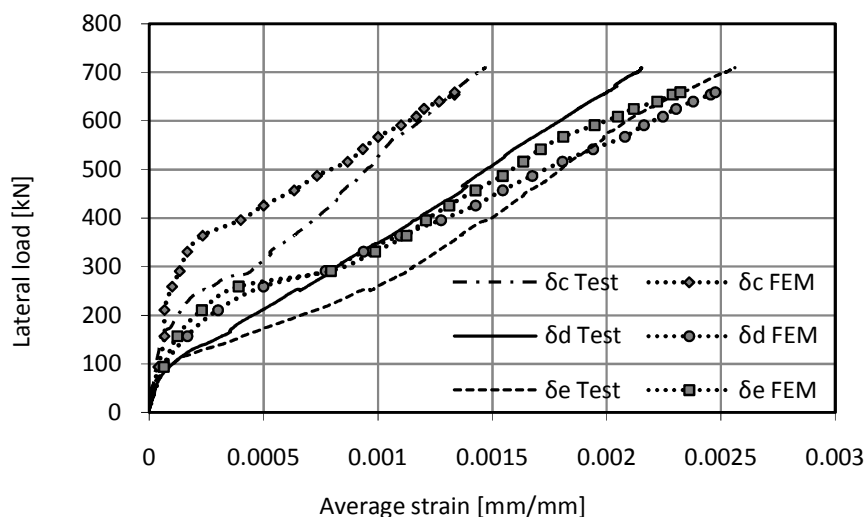


Figure 5-16: Measured and simulated strains for specimen type 3

To provide a better understanding of the stress distribution in the infill panel, the deformed shape of the panel of specimen 3, together with a contour plot of the major

principal stresses at ultimate load is shown in Figure 5-18. The figure shows that the two window corners loaded in compression are subjected to large compressive stresses. Concrete crushing is indicated in the elements surrounding these window corners when considering the Von Mises plastic strains. This phenomenon is shown in all simulated tests. Confirmed by the fact that in none of the simulations the crushed area expands to other elements than the ones directly surrounding the window corner, the high plastic strains may be attributed to the geometrical discontinuity (right angle) that is present at the window corners.

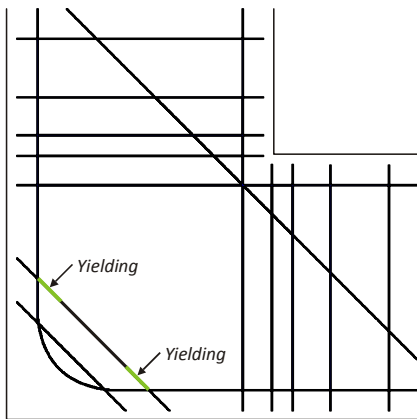


Figure 5-17: Yielding wedge reinforcement (specimen type 5)

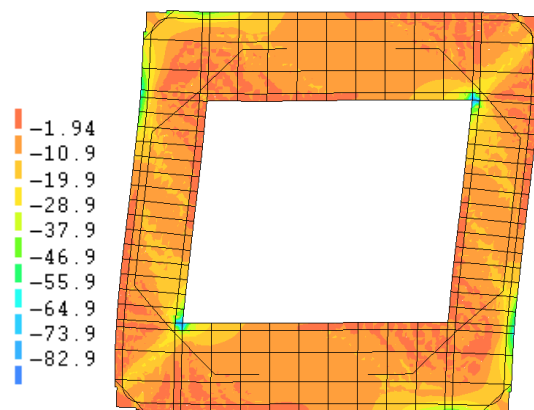


Figure 5-18: Deformed panel with minor (compressive) principal stresses in  $\text{N/mm}^2$  (specimen type 3)

Figure 5-19 shows for specimen type 3 the smeared crack pattern of the concrete panel at ultimate load, together with the experimentally found crack pattern (see Appendix C.2.2 for the crack patterns of the other specimen types). Considering the experimental crack patterns it can be noticed that the patterns are qualitatively identical while the crack intensity increases when the window opening becomes larger. Comparing the experimental crack patterns with the simulated ones, good qualitative agreement between the numerical crack patterns and the experimental crack patterns is observed.

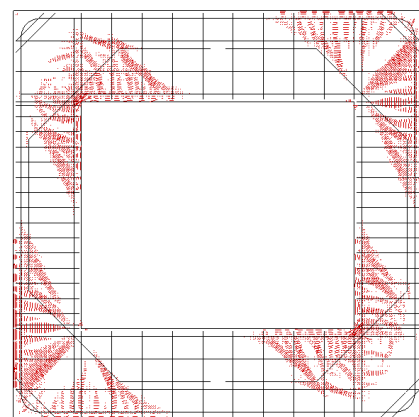


Figure 5-19: Experimental (left) and simulated (right) crack patterns (specimen type 3)

The comparisons presented above between experimental results and numerical predictions of the semi-integral infilled frame indicate that the finite element model used in this study is adequate, and that the corresponding results are reliable. The finite element investigation will, therefore, be further extended to investigate other configurations of semi-integral infilled frames in a parametric study that serves as verification for the development of design models.

### **5.3 Chapter conclusions**

A finite element model has been developed for studying the combined components 'flanges in bending' and 'web in compression'. Two types of load applications were applied alternately to the finite element model. The model with the load applied to the flange by a bolt as pressure uniformly distributed over the area of the washer (LA1) is able to predict the linear elastic stiffness and the onset of yielding. The model provides a conservative prediction of the plastic behavior. Because the plastic stiffness is of minor importance for design purposes of this structure, the model is appropriate to carry out parameter studies in order to find the response of other HE-sections subject to transverse compression introduced through the flanges (chapter 6.1).

Finite element models have been developed, simulating the response of the tested semi-integral infilled frames with window openings. The simulations were performed taking into account non-linear material properties based on tests and geometrical non-linearity. The models have been validated with the full-scale test results. A comparison between the full-scale experiments and simulations shows that the finite element models are able to predict the lateral load versus deflection relationship of the semi-integral infilled frame, and the ultimate lateral load for all failure mechanisms. Therefore, it is concluded that the finite element model is well suited for studying the infilled frame performance by varying different parameters (chapter 6.2).

# Chapter 6: PARAMETER STUDIES

## Scope of the chapter

This chapter deals with parameter studies that were performed in this research. Section 6.1 discusses the parameter study carried out in order to investigate the structural behavior of the combined component ‘flanges in bending with web in compression’ by varying different parameters. The considered parameters are described and the results are discussed. Subsequently, a parameter study performed to investigate various configurations of the semi-integral infilled frame is presented in section 6.2. A description of the varied parameters is provided and the influence of the parameters is discussed in detail. In the last section 6.3, the most important conclusions regarding the parameter studies are summarized.

## 6.1 Component behavior

Section 5.1 discussed a finite element model developed for simulating the component experiment ‘flanges in bending with web in compression’. This validated finite element model is now used to carry out a parameter study. The aim of this study is to find the structural characteristics of European rolled HEA- and HEB-sections subject to transverse compression, related to parameters dominating the response.

### 6.1.1 Parameters considered

The primary parameter that dominates the structural response is the position of the bolts on the flanges (Figure 6-1). To achieve relatively high strength and stiffness, the bolt distance to the web is taken as small as possible, considering requirements for minimal pitch and end distances. A distance of  $\frac{1}{2}b$  between the bolts showed to be a practical dimension that meets these requirements. Accordingly, the investigated parameter is the distance of the bolt with respect to the front of the end plate ( $x$ ). The thickness of the endplate ( $t_p$ ) is kept equal to the flange thickness ( $t_f$ ) of the section considered.

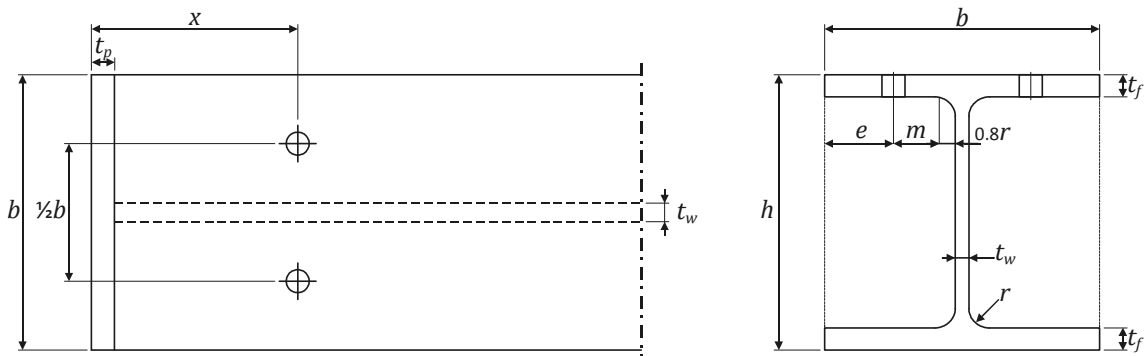


Figure 6-1: Illustration of investigated geometrical parameter  $x$  (left) and sectional properties (right)

The distance  $x$  is related to the section width  $b$  by the non-dimensional parameter  $\zeta$  as follows:

$$\zeta = x / b \quad [6-1]$$

Numerical simulations are carried out for  $\zeta = \frac{1}{4}, \frac{3}{8}, \frac{1}{2}$  and  $\frac{5}{8}$ . Further increase of the factor  $\zeta$  does not significantly influence the behavior as will be demonstrated in the next paragraphs. The sections considered are European rolled HEA- and HEB-sections with heights ranging from 200 to 400 mm, as these heights are most common in the area of application of infilled frames.

### 6.1.2 Material properties

Steel having the elastic material properties for the Young's modulus  $E_s = 2.1E+05 \text{ N/mm}^2$  and the Poisson's ratio  $\nu_s = 0.3$  is adopted. The stress-strain curve is assumed to be elastic-perfectly plastic, with yielding according to the Von Mises criterion. Analyses are performed for steel grades S235 and S355 having yield strengths  $f_y = 235$  and  $f_y = 355 \text{ N/mm}^2$  respectively.

### 6.1.3 Geometrical properties

The nominal geometrical properties of the modeled sections are in accordance with Euronorm 53-62, which defines the dimensions for European wide flange beams. The geometrical parameters used to model the H-sections are the section height ( $h$ ), the section width ( $b$ ), the web thickness ( $t_w$ ), the flange thickness ( $t_f$ ) and the fillet radius ( $r$ ) (Figure 6-1).

### 6.1.4 Results

Figure 6-2 presents the typical load-deformation response for HE300A and HE300B sections in S355, subject to transverse compression for  $\zeta = \frac{1}{4}, \frac{3}{8}, \frac{1}{2}$  and  $\frac{5}{8}$  respectively. The applied geometrical properties of the considered sections are given in Table 6-1. The load-deformation response of the other sections in S355 can be found in Appendix D.1.

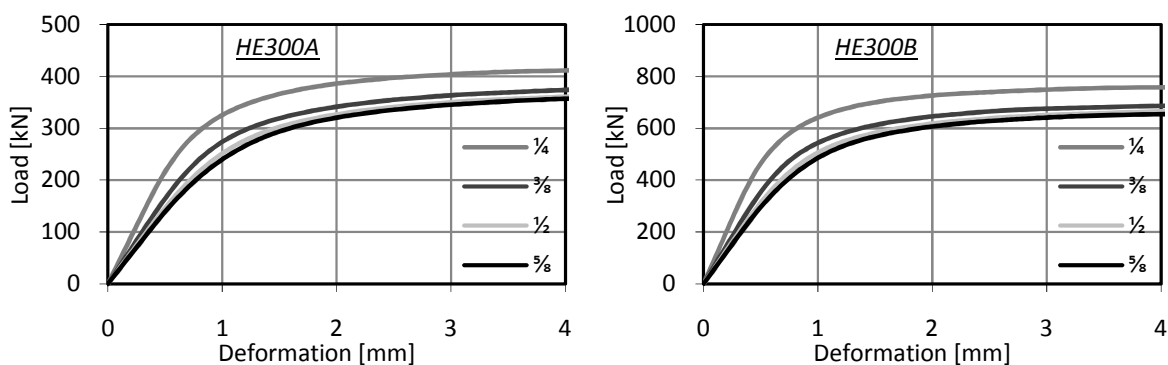


Figure 6-2: Load-deformation response of HE300A (left) and HE300B (right) sections in S355, subject to transverse compression for  $\zeta = \frac{1}{4}, \frac{3}{8}, \frac{1}{2}$  and  $\frac{5}{8}$

## PARAMETER STUDIES

Table 6-1: Nominal values of geometrical properties of European rolled H300A and H300B sections

	HE300A	HE300B
$h$ [mm]	290	300
$b$ [mm]	300	300
$t_w$ [mm]	8.5	11
$t_f$ [mm]	14	19
$r$ [mm]	27	27

It is shown that the load-deformation characteristics for both sections are qualitatively identical. Nevertheless, the stiffness and strength of the HE300B section are approximately twice as large as those of the HE300A section, which is to be attributed principally to the differences between the flange and web thicknesses. Furthermore, it can be seen that for both sections the variation between the response for  $\zeta = \frac{1}{2}$  and  $\frac{5}{8}$  is very small. This means that for a distance from the bolt to the end plate  $x > \frac{5}{8}b$ , the contribution of the end plate can be considered negligible.

Based on the obtained load-deformation curves, the structural characteristics are derived. For this purpose, several methods are available. An overview of approaches given in literature can be found in a publication of Steenhuis et al. (Steenhuis, C. M. et al., 2002), which deals with the derivation of the strength, stiffness and rotation capacity of steel and composite joints. In this publication, five different approaches are discussed. In all approaches, the elastic stiffness is simply taken as the initial stiffness. Yet, for determination of the strength, different approaches are applied. In two of the approaches, the strength is determined by drawing a line through the part of the test curve with the post limit stiffness. Subsequently, the strength is taken at the intersection with the vertical axis or with the line of the initial stiffness respectively. In a different approach, the strength is chosen as 0.9 times the ultimate strength. Finally, two approaches are discussed which are based on a secant stiffness, taken as one third of the initial stiffness. Accordingly, the intersection of the secant stiffness with the test curve defines the strength.

However, the approaches discussed above are not suited for this study. Drawing a line through the post-limit stiffness of the curve seems to result in a rather arbitrarily strength (Figure 6-3:  $F_{u1}$ ), as there is no obvious linear post limit stiffness. Furthermore, an ultimate strength is not found in the simulated curves. Finally, taking the secant stiffness as one third of the initial stiffness, and then taking the intersection with the test curve gives extensive plastic deformation (Figure 6-3:  $F_{u2}$ ). This latter approach will not be selected as the design of the semi-integral infilled frame is based on bolt failure and no plastic deformation of other components, as defined in section 3.2.2.



Another approach, to be found in the former Dutch code (TGB-staal, 1972), consists of a deformation criterion. According to this criterion, the load that gives a deformation of 1/50 times the span (where for cantilevers twice the span is taken) can be considered as the ultimate strength. However, this approach gives considerable plastic deformation as well (Figure 6-3:  $F_{u3}$ ).

Therefore, a new approach is defined here with an allowed plastic deformation as deformation criterion. Because allowing no plastic deformation at all results in a very conservative model strength, a rather arbitrary value of  $\delta_{pl} = 1/100m$  is defined as the allowed plastic deformation (for  $m$ , see Figure 6-1). Subsequently, the model strength is determined by drawing a line with the linear elastic stiffness through a deformation of  $\delta_{pl}$ , where the linear elastic stiffness of the combined component ( $k_{c_{1+2}}$ ) is simply taken as the initial stiffness ( $k_{c;ini}$ ). The design strength of the combined component ( $F_{c_{1+2}}$ ) is then taken at the intersection with the simulated curve (Figure 6-4).

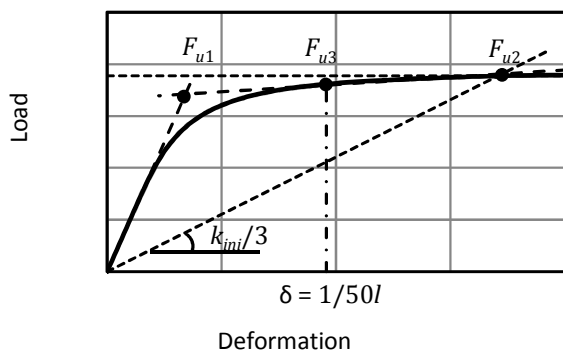


Figure 6-3: Derivation of  $F_u$  according to existing approaches

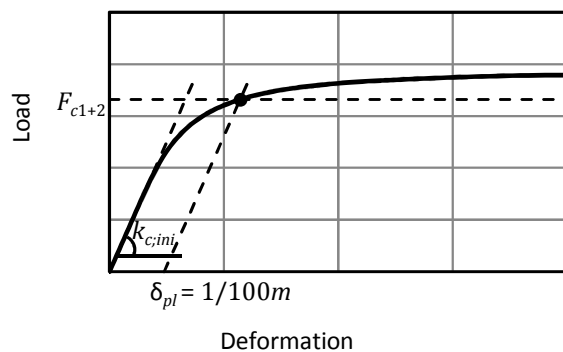


Figure 6-4: Defined approach for derivation of  $F_{c_{1+2}}$  for this thesis

An overview of the derived strength and stiffness characteristics for steel S355 is provided in Table 6-2 and in Table 6-3 for European rolled HEA and HEB-sections respectively.

Table 6-2: Characteristics for European rolled HEA-sections in S355 subject to transverse compression

Section type	$\zeta = 1/4$		$\zeta = 3/8$		$\zeta = 1/2$		$\zeta = 5/8$	
	$k_{c_{1+2}}$ [N/mm]	$F_{c_{1+2}}$ [N]	$k_{c_{1+2}}$ [N/mm]	$F_{c_{1+2}}$ [N]	$k_{c_{1+2}}$ [N/mm]	$F_{c_{1+2}}$ [N]	$k_{c_{1+2}}$ [N/mm]	$F_{c_{1+2}}$ [N]
HE200A	4.39E+5	2.07E+5	3.09E+5	1.78E+5	2.69E+5	1.68E+5	2.53E+5	1.64E+5
HE220A	4.40E+5	2.38E+5	3.13E+5	2.06E+5	2.73E+5	1.95E+5	2.57E+5	1.90E+5
HE240A	4.69E+5	2.77E+5	3.39E+5	2.43E+5	2.98E+5	2.32E+5	2.81E+5	2.26E+5
HE260A	4.46E+5	2.94E+5	3.28E+5	2.61E+5	2.90E+5	2.50E+5	2.75E+5	2.44E+5
HE280A	4.14E+5	3.07E+5	3.06E+5	2.73E+5	2.71E+5	2.62E+5	2.56E+5	2.56E+5
HE300A	4.46E+5	3.52E+5	3.32E+5	3.15E+5	2.95E+5	3.03E+5	2.80E+5	2.97E+5
HE320A	5.81E+5	4.35E+5	4.30E+5	3.88E+5	3.80E+5	3.74E+5	3.61E+5	3.67E+5
HE340A	6.83E+5	4.96E+5	5.03E+5	4.42E+5	4.44E+5	4.25E+5	4.20E+5	4.17E+5
HE360A	7.94E+5	5.61E+5	5.81E+5	4.99E+5	5.12E+5	4.80E+5	4.84E+5	4.71E+5
HE400A	9.78E+5	6.64E+5	7.12E+5	5.89E+5	6.25E+5	5.66E+5	5.90E+5	5.57E+5

Table 6-3: Characteristics for European rolled HEB-sections in S355 subject to transverse compression

Section type	$\zeta = \frac{1}{4}$		$\zeta = \frac{3}{8}$		$\zeta = \frac{1}{2}$		$\zeta = \frac{5}{8}$	
	$k_{c_{1+2}}$ [N/mm]	$F_{c_{1+2}}$ [N]	$k_{c_{1+2}}$ [N/mm]	$F_{c_{1+2}}$ [N]	$k_{c_{1+2}}$ [N/mm]	$F_{c_{1+2}}$ [N]	$k_{c_{1+2}}$ [N/mm]	$F_{c_{1+2}}$ [N]
HE200B	12.63E+5	4.79E+5	8.58E+5	4.04E+5	7.36E+5	3.81E+5	6.89E+5	3.72E+5
HE220B	11.84E+5	5.18E+5	8.16E+5	4.43E+5	7.03E+5	4.19E+5	6.59E+5	4.10E+5
HE240B	12.15E+5	5.81E+5	8.38E+5	4.99E+5	7.21E+5	4.72E+5	6.75E+5	4.61E+5
HE260B	11.19E+5	6.00E+5	7.86E+5	5.21E+5	6.81E+5	4.96E+5	6.40E+5	4.86E+5
HE280B	10.19E+5	6.19E+5	7.22E+5	5.40E+5	6.27E+5	5.14E+5	5.89E+5	5.03E+5
HE300B	10.01E+5	6.63E+5	7.29E+5	5.89E+5	6.42E+5	5.67E+5	6.08E+5	5.57E+5
HE320B	12.06E+5	7.71E+5	8.72E+5	6.85E+5	7.65E+5	6.59E+5	7.23E+5	6.48E+5
HE340B	13.53E+5	8.45E+5	9.74E+5	7.51E+5	8.52E+5	7.22E+5	8.04E+5	7.11E+5
HE360B	15.08E+5	9.20E+5	10.81E+5	8.19E+5	9.43E+5	7.88E+5	8.88E+5	7.77E+5
HE400B	17.55E+5	10.27E+5	12.54E+5	9.24E+5	10.88E+5	8.90E+5	10.23E+5	8.78E+5

Figure 6-5 presents the load-deformation response for HE300A and 300B sections in S235 and S355 respectively, for  $\zeta = \frac{1}{2}$ . It is shown that the initial stiffness is identical for both steel grades. Nevertheless, the strength of the sections in S355 is considerably larger.

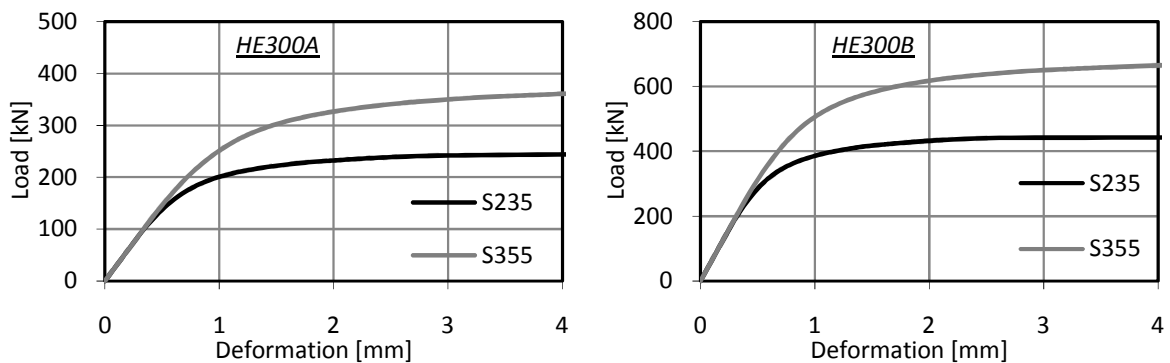
Figure 6-5: Load-deformation response of HE300A and HE300B sections in S235 and S355 ( $\zeta = \frac{1}{2}$ )

Table 6-4 gives the strength of HE300A and HE300B sections in S235 and S355 respectively and the ratio between them. To guarantee this factor to be valid for all other sections as well, two more analyses were performed for the most extreme sections considered in S235, which are HE200A and HE400B ( $\zeta = \frac{1}{2}$ ) (the graphs can be found in Appendix D.1).

Table 6-4: Model strength of HEA and HEB sections in S235 and S355 respectively

HEA	S235	S355	Ratio	HEB	S235	S355	Ratio
200; $\zeta = \frac{1}{2}$	118	168	0.70	300; $\zeta = \frac{1}{4}$	460	663	0.69
300; $\zeta = \frac{1}{4}$	245	352	0.70	300; $\zeta = \frac{3}{8}$	410	589	0.70
300; $\zeta = \frac{3}{8}$	220	315	0.70	300; $\zeta = \frac{1}{2}$	394	567	0.69
300; $\zeta = \frac{1}{2}$	212	303	0.70	300; $\zeta = \frac{5}{8}$	389	557	0.70
300; $\zeta = \frac{5}{8}$	209	297	0.70	400; $\zeta = \frac{1}{2}$	617	890	0.69

It is shown that there exists a constant ratio of 0.7 between the strengths of the considered sections in S235 and S355. Accordingly, the design strength of the other sections in S235 can be found by multiplying the strength of the section in S355 with a

## PARAMETER STUDIES

factor equal to 0.7. An overview of the derived characteristics ( $k_{c_{1+2}}$  and  $F_{c_{1+2}}$ ) for steel in S235 is provided in Table 6-5 and Table 6-6.

Table 6-5: Characteristics for European rolled HEA-sections in S235 subject to transverse compression

Section type	$\zeta = \frac{1}{4}$		$\zeta = \frac{3}{8}$		$\zeta = \frac{1}{2}$		$\zeta = \frac{5}{8}$	
	$k_{c_{1+2}}$ [N/mm]	$F_{c_{1+2}}$ [N]	$k_{c_{1+2}}$ [N/mm]	$F_{c_{1+2}}$ [N]	$k_{c_{1+2}}$ [N/mm]	$F_{c_{1+2}}$ [N]	$k_{c_{1+2}}$ [N/mm]	$F_{c_{1+2}}$ [N]
HE200A	4.39E+5	1.45E+05	3.09E+5	1.25E+05	2.69E+5	1.18E+05	2.53E+5	1.15E+05
HE220A	4.40E+5	1.67E+05	3.13E+5	1.44E+05	2.73E+5	1.37E+05	2.57E+5	1.33E+05
HE240A	4.69E+5	1.94E+05	3.39E+5	1.70E+05	2.98E+5	1.62E+05	2.81E+5	1.58E+05
HE260A	4.46E+5	2.06E+05	3.28E+5	1.83E+05	2.90E+5	1.75E+05	2.75E+5	1.71E+05
HE280A	4.14E+5	2.15E+05	3.06E+5	1.91E+05	2.71E+5	1.83E+05	2.56E+5	1.79E+05
HE300A	4.46E+5	2.46E+05	3.32E+5	2.21E+05	2.95E+5	2.12E+05	2.80E+5	2.08E+05
HE320A	5.81E+5	3.05E+05	4.30E+5	2.72E+05	3.80E+5	2.62E+05	3.61E+5	2.57E+05
HE340A	6.83E+5	3.47E+05	5.03E+5	3.09E+05	4.44E+5	2.98E+05	4.20E+5	2.92E+05
HE360A	7.94E+5	3.93E+05	5.81E+5	3.49E+05	5.12E+5	3.36E+05	4.84E+5	3.30E+05
HE400A	9.78E+5	4.65E+05	7.12E+5	4.12E+05	6.25E+5	3.96E+05	5.90E+5	3.90E+05

Table 6-6: Characteristics for European rolled HEB-sections in S235 subject to transverse compression

Section type	$\zeta = \frac{1}{4}$		$\zeta = \frac{3}{8}$		$\zeta = \frac{1}{2}$		$\zeta = \frac{5}{8}$	
	$k_{c_{1+2}}$ [N/mm]	$F_{c_{1+2}}$ [N]	$k_{c_{1+2}}$ [N/mm]	$F_{c_{1+2}}$ [N]	$k_{c_{1+2}}$ [N/mm]	$F_{c_{1+2}}$ [N]	$k_{c_{1+2}}$ [N/mm]	$F_{c_{1+2}}$ [N]
HE200B	12.63E+5	3.35E+05	8.58E+5	2.83E+05	7.36E+5	2.67E+05	6.89E+5	2.60E+05
HE220B	11.84E+5	3.63E+05	8.16E+5	3.10E+05	7.03E+5	2.93E+05	6.59E+5	2.87E+05
HE240B	12.15E+5	4.07E+05	8.38E+5	3.49E+05	7.21E+5	3.30E+05	6.75E+5	3.23E+05
HE260B	11.19E+5	4.20E+05	7.86E+5	3.65E+05	6.81E+5	3.47E+05	6.40E+5	3.40E+05
HE280B	10.19E+5	4.33E+05	7.22E+5	3.78E+05	6.27E+5	3.60E+05	5.89E+5	3.52E+05
HE300B	10.01E+5	4.64E+05	7.29E+5	4.12E+05	6.42E+5	3.97E+05	6.08E+5	3.90E+05
HE320B	12.06E+5	5.40E+05	8.72E+5	4.80E+05	7.65E+5	4.61E+05	7.23E+5	4.54E+05
HE340B	13.53E+5	5.92E+05	9.74E+5	5.26E+05	8.52E+5	5.05E+05	8.04E+5	4.98E+05
HE360B	15.08E+5	6.44E+05	10.81E+5	5.73E+05	9.43E+5	5.52E+05	8.88E+5	5.44E+05
HE400B	17.55E+5	7.19E+05	12.54E+5	6.47E+05	10.88E+5	6.23E+05	10.23E+5	6.15E+05

The strength of a flange ( $F_{c_{1+2}}$ ) is influenced by axial stresses ( $\sigma_{com;Ed}$ ) in the member resulting from axial force or bending moment. Therefore, a reduction of the strength because of possible local buckling has to be contemplated. According to e.g. ENV 1993-1-1 Annex J, the possible reduction of the moment resistance of the column flange should be allowed for when the maximum longitudinal compressive stress  $\sigma_{com;Ed}$  exceeds 180 N/mm<sup>2</sup> by multiplying the flange strength by a reduction factor  $k_{fc}$  (Zoetemeijer, 1975):

$$k_{fc} = \frac{2f_{y;fc} - 180 - \sigma_{com;Ed}}{2f_{y;fc} - 360} \quad [6-2]$$

Generally, the reduction factor  $k_{fc}$  is 1.0 and no reduction is necessary. It can therefore be omitted in preliminary calculations.

The derived flange characteristics are to be used to find the overall panel-to-frame connection stiffness and strength (chapter 7).

## 6.2 Full-scale behavior

In the previous chapter (section 5.2), a finite element model was presented, developed in order to supplement the full-scale experimental behavior of the semi-integral infilled frames. This validated finite element model is now used to perform a parameter study. The aim of this study is to investigate other configurations of the semi-integral infilled frame in order to further improve the understanding of the structural response of this composite structure. Besides, a wide range of results is provided, serving as verification for the development of design models.

### 6.2.1 Parameters considered

The parameters investigated are the frame member dimensions, the rotational stiffness of the frame joints, the infilled frame aspect ratio and the panel opening geometry including reinforcement layout. Each parameter is described below.

#### *Frame member dimensions*

The test specimens consisted of frame members HE180M only. This frame is applied in the parameter study as well and is denoted as ‘weak frame’. In addition, a more practical frame is studied, consisting of HE400B columns and HE320A beams (denoted as ‘strong frame’). This frame has been chosen based on practical considerations for the design of ten to twenty-story high commercial buildings. In practice, the increased section height of the frame members reduces the space between the columns and beams, requiring a smaller panel. However, in order to evaluate the effect of the frame members only, the height and width of the panel are kept constant for each aspect ratio in the parameter study. The geometrical properties for the frame members used are provided in Table 6-7.

By changing the frame members, the characteristics of the panel-to-frame connection change as well. Figure 6-6 shows the load deformation response of the panel-to-frame connections for the sections applied. The graphs were composed in the same way as described in section 5.2.2, having the linear elastic stiffness for the combined component ‘flanges in bending with web in compression’ obtained from Table 6-2 or Table 6-3.

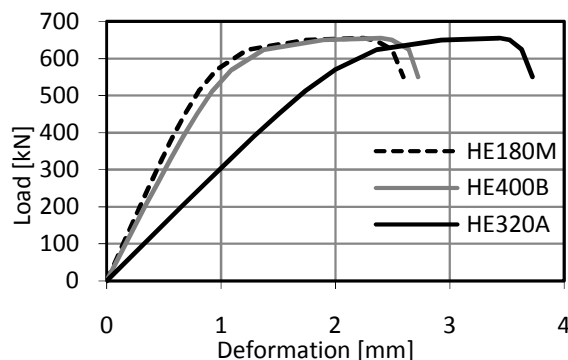


Figure 6-6: Load-deformation characteristics of panel-to-frame connections

Rotational stiffness of frame joints

For the simulation of the full-scale tests, the frame joints have been calibrated with experimental results obtained from testing the bare frame. In the parameter study, the initial joint stiffness ( $S_{j,ini}$ ) is estimated using a simplified design equation for the prediction of the initial rotational stiffness of a flexible joint (Steenhuis, C. M. et al., 1994) based on Eurocode 3 EN 1993-1-8:

$$S_{j,ini} = \frac{Ez^2t_f}{k_x} \quad [6-3]$$

Where:

$E$  = Young's modulus [N/mm<sup>2</sup>]

$z$  = lever arm, which in this particular case, equals the distance from the centre of the compression flange to the bolt row in tension [mm]

$t_f$  = column flange thickness [mm]

$k_x$  = coefficient dependent on the layout of the joint (in case of a bolted end-plate connection,  $k_x = 11.5$ )

Values of the joint stiffnesses applied are given in Table 6-7. In addition to the flexible connections, hinged connections are studied ( $S_{j,ini} = 0$ ).

Table 6-7: Geometrical properties of frame members used in parameter study

Property	Weak frame	Strong frame
Moment of inertia of column $I_{column}$	7.38E+7 mm <sup>4</sup>	5.59E+8 mm <sup>4</sup>
Moment of inertia of beam $I_{beam}$	7.38E+7 mm <sup>4</sup>	2.18E+8 mm <sup>4</sup>
Area of column $A_{column}$	1.11E+4 mm <sup>2</sup>	1.92E+4 mm <sup>2</sup>
Area of beam $A_{beam}$	1.11E+4 mm <sup>2</sup>	1.18E+4 mm <sup>2</sup>
Rotational stiffness of frame joints $S_{j,ini}$	8.29+9 or 0 Nmm/rad	19.1+9 or 0 Nmm/rad

Infilled frame aspect ratio

The infilled frame aspect ratio is defined as  $\alpha = H/L$ , where  $H$  and  $L$  are the height and length of the infilled frame respectively. The specimens tested experimentally have dimensions  $L \times H = 3.0 \text{ m} \times 3.0 \text{ m}$ , equal to an aspect ratio of  $\alpha = 1$ . In this parameter study, three more aspect ratios are studied which are  $\alpha = \frac{1}{2}$ ,  $\alpha = \frac{2}{3}$  and  $\alpha = 1\frac{1}{2}$ . The height of the infilled frame is kept constant, equal to 3.0 m. Consequently, the infilled frames considered are sized  $L \times H = 6.0 \text{ m} \times 3.0 \text{ m}$ ,  $4.5 \text{ m} \times 3.0 \text{ m}$ ,  $3.0 \text{ m} \times 3.0 \text{ m}$  and  $2.0 \text{ m} \times 3.0 \text{ m}$  respectively (Figure 6-7).

Panel opening geometry

The five panel opening geometries investigated experimentally are considered in the parameter study as well. Consequently, each aspect ratio includes five panel opening geometries (henceforward referred to as panel type). The dimensions of the window openings result from keeping the heights of the panel members (indicated with  $x$ ,  $y$  and  $z$  in Figure 6-7) constant. The applied dimensions for  $x$ ,  $y$  and  $z$  are given in Table 6-8. The thickness of the panels is kept constant ( $t_w = 200$  mm). The reinforcement is determined in accordance with the panel opening geometry using the strut-and-tie model presented in Figure 3-5 (see Appendix D.2 for the panel geometries with corresponding reinforcement configurations).

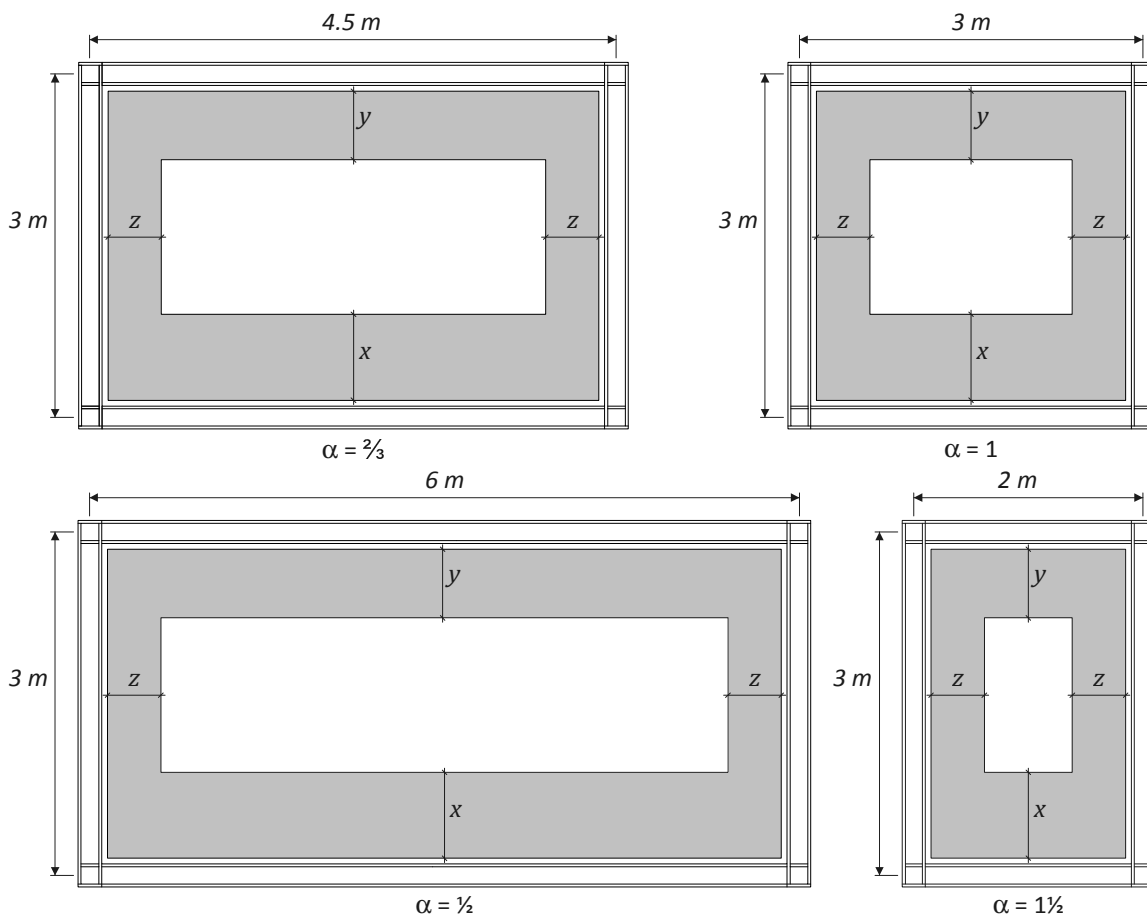


Figure 6-7: Investigated aspect ratios and transformed panel opening geometry

Table 6-8: Applied dimensions for  $x$ ,  $y$  and  $z$

Panel type	$x$ [mm]	$y$ [mm]	$z$ [mm]
1	900	750	450
2	750	600	450
3	600	600	450
4	600	450	450
5	450	450	450

Overview

Table 6-9 gives an overview of the analyses performed in the parameter study with the parameters investigated. In total, 64 analyses are carried out including 8 bare frame analyses, 40 analyses with infilled frames having flexible frame joints and 16 analyses with infilled frames having pinned frame joints.

Table 6-9: Survey of analyses performed in parameter study with investigated parameters

Analysis No.	Frame members	Frame joints	Panel geometry	Aspect ratio
1 – 4	Weak	Flexible	No panel (bare frame)	½, ⅔, 1, 1½
5 – 24	Weak	Flexible	Type 1 to 5	½, ⅔, 1, 1½
25 – 32	Weak	Pinned	Type 1 and 5	½, ⅔, 1, 1½
33 – 36	Strong	Flexible	No panel (bare frame)	½, ⅔, 1, 1½
37 – 56	Strong	Flexible	Type 1 to 5	½, ⅔, 1, 1½
57 – 64	Strong	Pinned	Type 1 and 5	½, ⅔, 1, 1½

**6.2.2 Material properties**

In the parameter study, concrete of grade C50/C60 and reinforcement steel with nominal material properties according to Eurocode 2 EN 1992-1-1 are assumed for the infill panel. The applied concrete and reinforcement properties are shown in Table 6-10.

Table 6-10: Material properties used for infill panel

Property	Value	Property	Value
$E_c$	3.7E+04 N/mm <sup>2</sup>	$G_f$	0.105 Nmm/mm <sup>2</sup>
$\nu$	0.2	$\beta$	0.2
$f_{ct}$	4.1 N/mm <sup>2</sup>	$E_s$	2.0E+05 N/mm <sup>2</sup>
$f_c$	50 N/mm <sup>2</sup>	$f_y$	560 N/mm <sup>2</sup>

For the steel frame, elastic-perfectly plastic behavior is assumed, having the elastic material properties Young's modulus  $E_s = 2.1E+05$  N/mm<sup>2</sup> and Poisson's ratio  $\nu_s = 0.3$  in combination with Von Mises plasticity with yield strength  $f_y = 355$  N/mm<sup>2</sup>.

**6.2.3 Results parameter study**

The load-deflection response of all simulations can be found in Appendix D.3. From these curves, the ultimate load ( $F_u$ ), the initial stiffness ( $k_{ini}$ ) and the secant stiffness ( $k_{sec;2}$ ) are derived, where the secant stiffness is determined by taking the ultimate load with the corresponding deflection. An overview of the results is given in Table D-1 and Table D-2 for the weak and strong frame respectively. The findings for each parameter considered are qualitatively discussed in the next paragraphs.

Influence of frame member dimensions

The load-deflection response of two infilled frames constructed with a weak frame (grey line) and strong frame (black line) respectively are shown in Figure 6-8 ( $\alpha = 1$ , panel type 3). The dashed line in the matching color shows the bare frame behavior of the corresponding infilled frame.

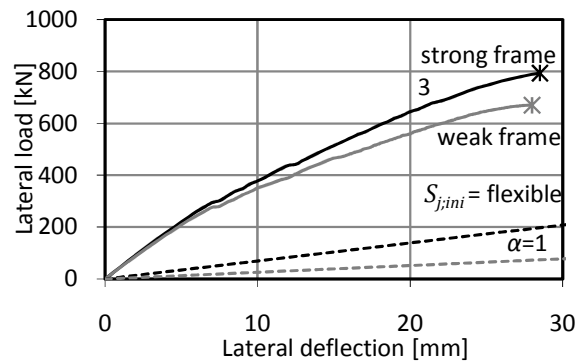


Figure 6-8: Load-deflection response of (infilled) frames with weak and strong frame respectively

It is shown that, despite the considerably higher bare frame stiffness of the strong frame, the difference in the initial infilled frame stiffness is low. Furthermore, a comparable ductility is achieved. However, applying the strong frame, the ultimate strength of the infilled frame considerably increases. This is also the case for the other aspect ratios and panel types (see Appendix D.3 for results).

By changing the frame members, the characteristics of the panel-to-frame connections change as well. The influence of these connections is demonstrated by considering infilled frames having pinned frame joints. The load-deflection response of two infilled frames with panel type 1 and type 5, having a weak (grey line) and strong (black line) frame respectively are shown in Figure 6-9, for  $\alpha = \frac{2}{3}$  and for  $\alpha = 1\frac{1}{2}$ . Despite the fact that both bare frame stiffnesses are zero, the strong frame gives for  $\alpha = \frac{2}{3}$  a higher infilled frame stiffness. However, for  $\alpha = 1\frac{1}{2}$ , the structure with the weaker HE180M frame acts stiffer. This is to be attributed to the stiffness of the panel-to-frame connection and demonstrates that the infilled frame exhibits complex behavior.



## PARAMETER STUDIES

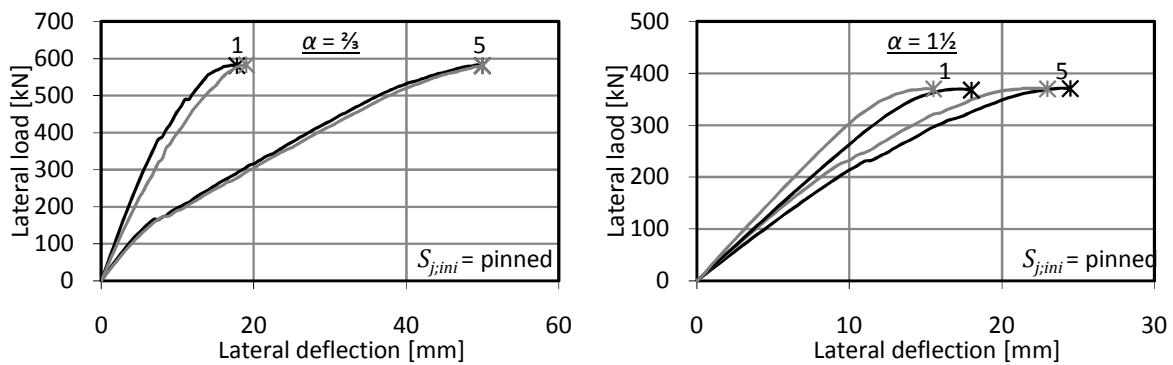


Figure 6-9: Load-deflection response for infilled frames with pinned frame joints

### Influence of rotational stiffness of frame joints

Figure 6-10 shows for weak and strong frames the load-deflection response of two infilled frames with small window openings (panel type 1, black lines) and large window openings (panel type 5, grey lines), having flexible (solid lines) and pinned frame joints (dashed lines) respectively ( $\alpha = 1$ ). It is shown that the application of pinned joints results in a lower ultimate strength compared to the infilled frame with flexible frame joints. Moreover, for a frame with pinned joints, the relative stiffness of the frame to the panel has no influence on the ultimate strength. This is demonstrated by the ultimate loads of the pinned infilled frames, which are approximately identical (nearly 600 kN), independently of the applied panel (type 1 or 5) of frame (weak or strong).

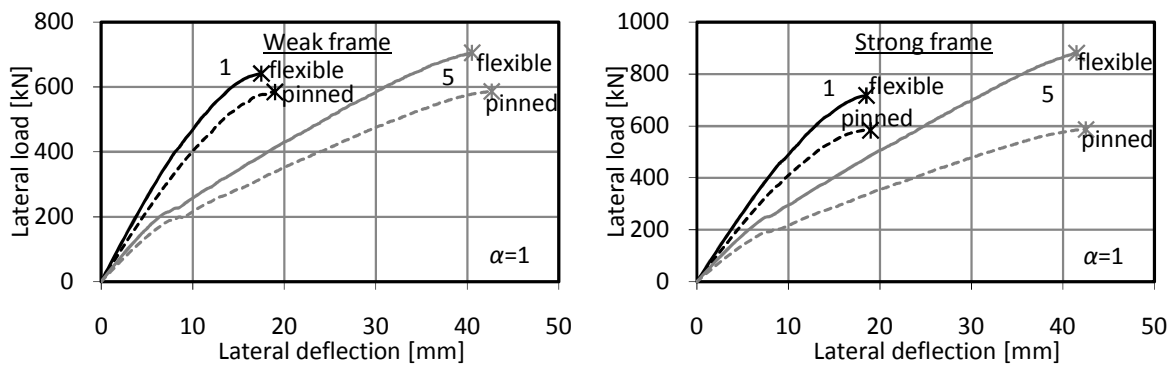


Figure 6-10: Load-deflection response of infilled frames with flexible and pinned frame joints ( $\alpha = 1$ )

### Influence of the aspect ratio

The results presented in Tables D-1 and D-2 of Appendix D.3 demonstrate that the aspect ratio influences the location of connection failure. For  $\alpha = \frac{1}{2}$  and  $\frac{2}{3}$ , failure occurred at the column connection at the upper loaded corner of the infilled frame (Figure 5-13, C1-C). For  $\alpha = 1$  and  $1\frac{1}{2}$ , the beam connection at the lower loaded corner of the infilled frame failed (Figure 5-13, C2-B).

Influence of the panel opening geometry

The effects of the size and position of the window opening has experimentally been investigated (section 4.2). The tests showed that a decrease of the relative stiffness of the infill to the frame results in a decrease of the lateral stiffness. The results of the parameter study are presented in Figure 6-11, showing the load-deflection response for infilled frames with panel type 1 to 5, having a weak and strong frame respectively. The results show in addition to the decrease of stiffness an increase of the ultimate strength. This effect is more evident considering the strong frame.

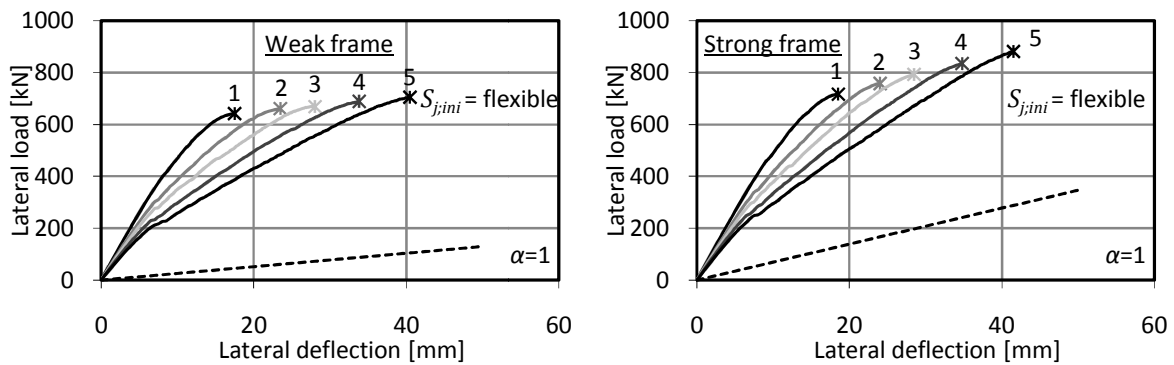


Figure 6-11: Load-deflection response of infilled frames with varied panel opening geometries

Figure 6-12 graphically demonstrates that the increase of strength can be attributed to the contribution of the bare frame. The shaded part under the bare frame curve exactly fits between the ultimate strengths defined by the infilled frames with pinned frame joints and the infilled frames with the flexible connections.

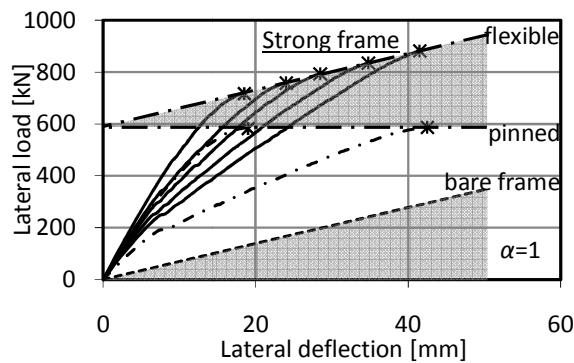


Figure 6-12: Illustration of increase of strength attributed to bare frame

The results of this study serve as verification for the development of analytical models, to be presented in the next chapter.

### 6.3 Chapter conclusions

A first parameter study was carried out to find the strength and stiffness characteristics of European rolled HEA- and HEB-sections with heights ranging from 200 to 400 mm, subject to transverse compression introduced indirectly through the flanges. The parameters considered were the distance of the bolt with respect to the end plate and the section type. Based on the obtained load-deformation graphs, the linear elastic stiffness and design strength were derived. These are to be used to find the overall panel-to-frame connection stiffness and strength (chapter 7).

A second parameter study was performed to investigate various configurations of the semi-integral infilled frame. Four parameters have been studied with respect to their influence on the structural response. These parameters are the frame member dimensions, the rotational stiffness of the frame joints, the infilled frame aspect ratio and the panel opening geometry. The major findings are summarized below:

- For infilled frames with flexible joints, an increase of the relative stiffness of the frame to the infill results in an increase of the ultimate strength and secant stiffness.
- For infilled frames with flexible joints, an increase of the window opening and thus a decrease of the relative stiffness of the infill to the frame results in a decrease of the secant stiffness and in an increase of the ultimate strength and deformation capacity.
- For infilled frames with pinned frame joints, the ultimate strength is independent of the relative stiffness of the infill to the frame.
- The aspect ratio of the infilled frame defines the location of connection failure.

From the simulated load-deformation curves, characteristics were derived which serve as a verification for the development of analytical models for the prediction of the lateral stiffness, the ultimate lateral load and deformation capacity of the semi-integral infilled frame (chapter 7).

# Chapter 7: ANALYTICAL MODELING

## Scope of the chapter

This chapter discusses analytical models to predict the lateral stiffness (section 7.1) and the ultimate lateral load (section 7.2) of the semi-integral infilled frame with a window opening. In these models, the strength of the structure is supposed to be governed by the panel-to-frame connections. A description of the development of these models is given. Subsequently, the analytical models are compared with the results obtained from the parameter study discussed in the previous chapter, in order to check their validity (section 7.3). The concluding section 7.4 summarizes the most important results.

## 7.1 Lateral stiffness modeling

In chapter 3, the mechanical model shown in Figure 7-1a was proposed for the semi-integral infilled frame. However, for a good understanding, a basic representation of this model (Figure 7-1b) is used first to approach the semi-integral infilled frame analytically. Afterwards, the analytical model for the basic model will be extended, allowing the application for the (originally proposed) advanced model as well.

In the basic model, the strut is pin-connected directly to the frame corners, neglecting the (rigid) offset. Furthermore, the translational springs representing the panel-to-frame connections are situated at one end of the strut between the strut and the frame, using one equivalent spring in horizontal and vertical direction respectively. Accordingly, the spring stiffnesses of the equivalent springs equal  $\frac{1}{2}k_{c,column}$  and  $\frac{1}{2}k_{c,beam}$  respectively.

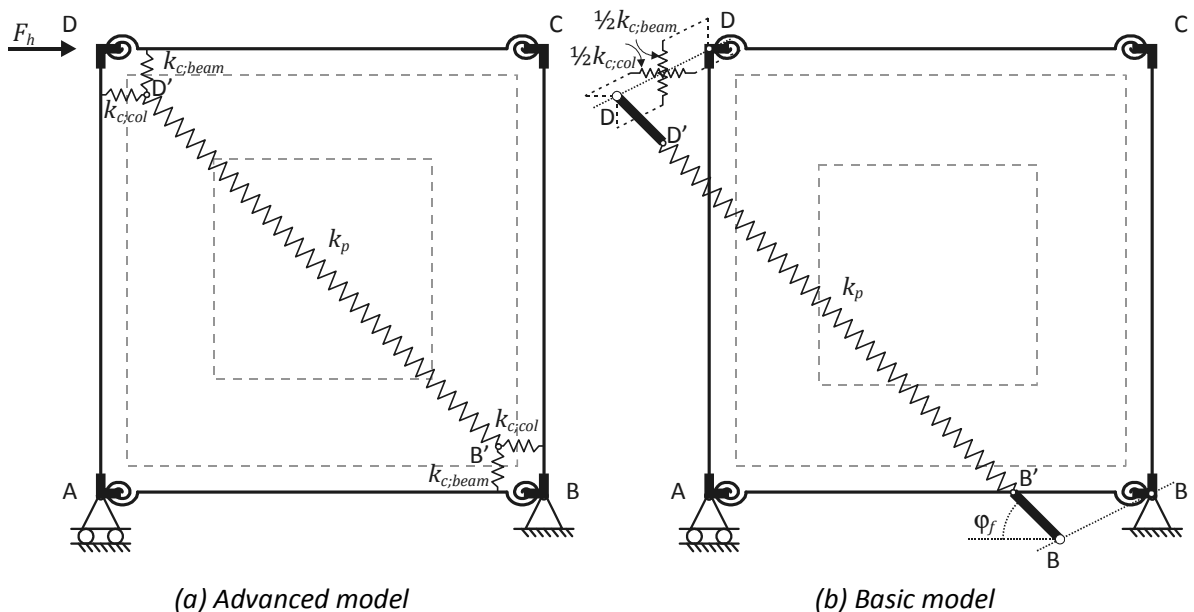


Figure 7-1: Mechanical models for the semi-integral infilled frame with a window opening

### 7.1.1 Basic model

The basic model (Figure 7-1b) is a statically indeterminate system; stiffness and strength depend on the relative stiffness between the diagonal strut including its connections to the frame and the surrounding frame. The load versus deflection response of this model can be represented by the spring system shown in Figure 7-2. The spring system represents the lateral load-displacement response between node D (loaded node) and node B (fixed node) of the infilled frame (Figure 7-1b). The spring system consists of a spring representing the bare frame stiffness ( $k_{h,f}$ ) which acts in parallel with three serial springs (the bracing system), representing a stiffness resulting from the panel deformation ( $k_{h,p}$ ), a stiffness resulting from the deformations of the panel-to-frame connections ( $k_{h,\Sigma con}$ ) and a stiffness resulting from frame column lengthening ( $k_{h,col}$ ). The latter is a result from the action of the infill panel on the frame, giving additionally to a compression force in the panel diagonal, a tensile force in the loaded frame column, and thus has to be considered a component of the bracing system as well.

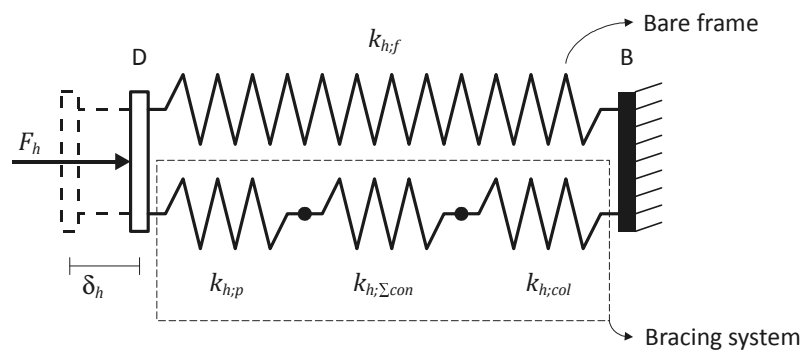


Figure 7-2: Spring system representing lateral load-deflection response of basic model

Accordingly, the following equation holds for the spring system and thus for the lateral stiffness the semi-integral infilled frame ( $k_{h,if}$ ):

$$k_{h,if} = \frac{F_h}{\delta_h} = k_{h,f} + \left[ \frac{1}{k_{h,p}} + \frac{1}{k_{h,\Sigma con}} + \frac{1}{k_{h,col}} \right]^{-1} \quad [7-1]$$

In the following sections, equations for the four stiffness terms are derived.

#### Stiffness of the bare frame

To find the bare frame stiffness, the braced frame from Figure 7-1b is considered having an infinitely small strut, thus  $k_p = 0$  (Figure 7-3). In this case, the load is supported by the bare frame only. The structural behavior is analyzed elastically, allowing the use of the principle of superposition. Consequently, the structure may be analyzed for separate load cases and the individual components of stress, strain and displacements are additive.

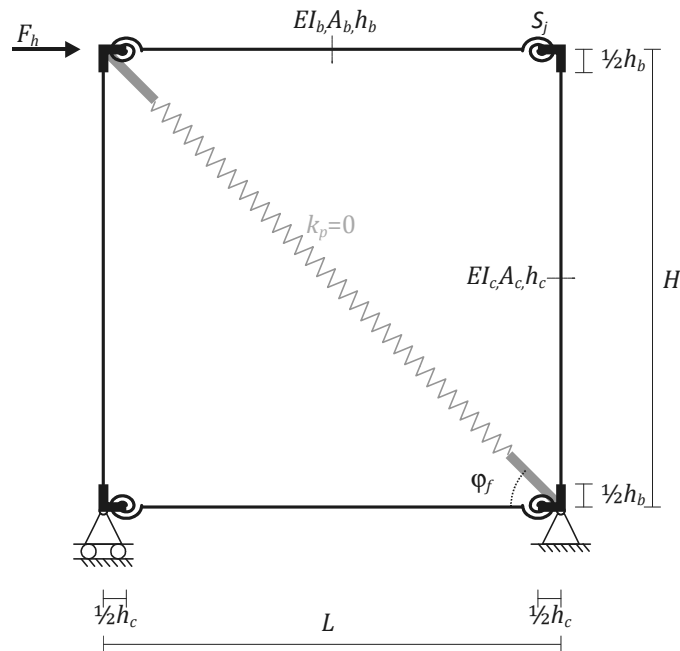


Figure 7-3: Basic model having an infinitely small strut, thus  $k_p = 0$

Figure 7-4 gives the diagrams of forces for the laterally loaded bare frame:

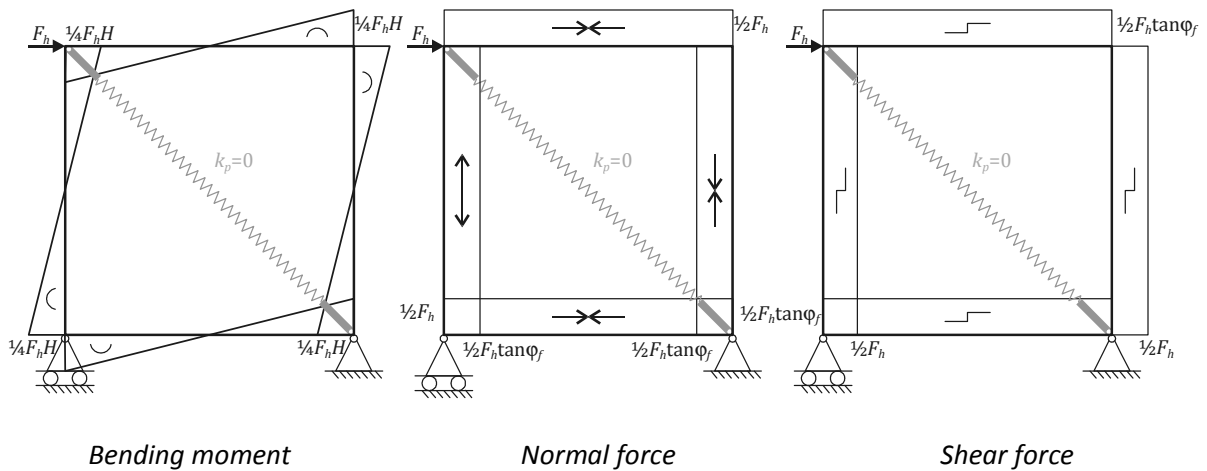


Figure 7-4: Diagrams of forces for laterally loaded bare frame

The total deflection at the top of the frame consists of a deflection due to bending of the columns, beams and rotation in the beam-to-column connections ( $\delta_{h1;f}$ ), a deflection due to the axial deformation of the columns and beams ( $\delta_{h2;f}$ ) and a deflection due to the shear deformation of the columns and beams ( $\delta_{h3;f}$ ).

For convenience, two factors ( $\beta_f$  and  $\gamma_f$ ) are introduced to express the contribution of the rigid ends of the beams and columns as follows:

$$\beta_f = \frac{L}{L - h_c} \quad [7-2]$$

$$\gamma_f = \frac{H}{H - h_b} \quad [7-3]$$

where  $L$  and  $H$  are the length and height of the frame respectively, and  $h_c$  and  $h_b$  the section height of the column and beam.

The elastic deflection of the bare frame due to bending of the frame members ( $\delta_{h1,f}$ ) is equal to the sum of the deflection caused by double curvature bending of the beams (first term in equation [7-4]), double curvature bending of the columns (second term in equation) and rotation of the flexible beam-to-column connections (third term in equation):

$$\delta_{h1,f} = \frac{F_h L H^2}{24 E \beta_f^3 I_b} + \frac{F_h H^3}{24 E \gamma_f^3 I_c} + \frac{F_h H^2}{4 \beta_f^2 S_j} \quad [7-4]$$

The elastic deflection of the bare frame due to axial deformations ( $\delta_{h2,f}$ ) is equal to the sum of the axial deformation of the beams (first term in equation [7-5]), plus the horizontal component resulting from the (vertical) axial deformation of the columns (second term in equation).

$$\delta_{h2,f} = \frac{F_h L}{2 E \beta_f A_b} + \frac{F_h H \tan \varphi_f}{2 E \gamma_f A_c} \tan \varphi_f \quad [7-5]$$

The elastic deflection of the bare frame due to shear deformations ( $\delta_{h3,f}$ ) is equal to the sum of the shear deformation of the columns (first term in equation [7-6]), plus the horizontal component resulting from the shear deformation of the beams (second term in equation).

$$\delta_{h3,f} = \frac{F_h H}{2 G \gamma_f A_{v;c}} + \frac{F_h H \tan \varphi_f}{2 G \beta_f A_{v;b}} \quad [7-6]$$

where  $A_v$  is the shear area of the cross-section, for rolled wide flange beams to be derived according to the following equation (Eurocode 3 EN 1993-1-1):

$$A_v = A - 2 b t_f + (t_w + 2 r) t_f \quad [7-7]$$

Having obtained the deflections due to bending moment, normal force and shear force, the stiffness of the bare frame ( $k_{h,f}$ ) can be found by dividing the lateral load  $F_h$  by the sum of the deflections:

$$k_{h,f} = \frac{F_h}{\sum \delta_{hi,f}} \quad [7-8]$$

Stiffness of the bracing system

To find the stiffness of the bracing system, the braced frame from Figure 7-1b is considered having pinned frame joints, thus  $S_j = 0$ . In this case, the load is supported by axial compression in the strut and axial tension in the loaded column only (Figure 7-5). Other frame members remain unloaded. Stiffness terms are derived for the three components of the bracing system. Again, the structural behavior is analyzed elastically, allowing the use of the principle of superposition.

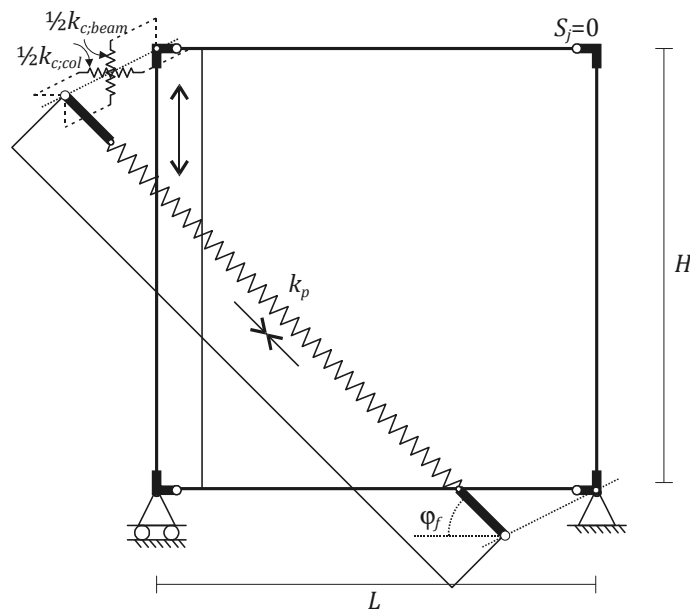


Figure 7-5: Normal force diagram for basic model having pinned frame joints, thus  $S_j = 0$

Strut

First, the stiffness resulting from strut deformation is derived. Assuming an axial force in the strut equal to  $N_{x;strut}$ , the lateral deflection due to deformation of the strut equals:

$$\delta_{h;strut} = \frac{N_{x;strut}}{k_p} \frac{1}{\cos \varphi_f} \quad [7-9]$$

Accordingly, the stiffness resulting from strut deformation ( $k_{h;p}$ ) is given by:

$$k_{h;p} = \frac{F_h}{\delta_{h;strut}} = \frac{F_h k_p \cos \varphi_f}{N_{x;strut}} \quad [7-10]$$

Panel-to-frame connections

Next, the stiffness resulting from deformations of the panel-to-frame connections are derived. Assuming an axial load in the panel-to-column and the panel-to-beam connections equal to  $N_{x;c,col}$  and  $N_{x;c,beam}$  respectively, the lateral deflection due to connection deformations equals:



$$\delta_{h;\Sigma con} = \frac{N_{x;c;col}}{\frac{1}{2}k_{c;col}} + \frac{N_{x;c;beam}}{\frac{1}{2}k_{c;beam}} \tan \varphi_f \quad [7-11]$$

Accordingly, the stiffness resulting from connection deformations ( $k_{h;\Sigma con}$ ) is given by:

$$k_{h;\Sigma con} = \frac{F_h}{\delta_{h;\Sigma con}} = \frac{F_h}{\left( \frac{2N_{x;c;col}}{k_{c;col}} + \frac{2N_{x;c;beam}}{k_{c;beam}} \tan \varphi_f \right)} \quad [7-12]$$

#### Column

Finally, the stiffness resulting from column deformation is derived. Assuming a tensile force in the column equal to  $N_{x;col}$ , the lateral deflection due to column deformation equals:

$$\delta_{h;col} = \frac{N_{x;col}H}{EA_c} \tan \varphi_f \quad [7-13]$$

Consequently, the stiffness resulting from column deformation ( $k_{h;col}$ ) equals:

$$k_{h;col} = \frac{F_h}{\delta_{h;col}} = \frac{F_h EA_c}{N_{x;col}H \tan \varphi_f} \quad [7-14]$$

Having obtained the stiffness coefficients  $k_{h;f}$ ,  $k_{h;p}$ ,  $k_{h;\Sigma con}$  and  $k_{h;col}$ , equation 7-1 gives the overall stiffness of the semi-integral infilled frame, represented by the basic model. Though, the diagonal panel stiffness  $k_p$  is still unknown. A method to derive the diagonal panel stiffness is presented in the following paragraph.

#### Derivation diagonal panel stiffness

In order to find the diagonal panel stiffness ( $k_p$ ), the panel is modelled as an equivalent frame having dimensions  $h'$  by  $l'$  and sectional properties  $EI_{col}$ ,  $EI_{b;top}$  and  $EI_{b;bottom}$  (Figure 7-6). Rigid arms are used to model the depth of the columns and beams.

Because the dimensions of the equivalent frame deviate from the original panel, the action and reaction forces are displaced. Consequently, the equivalent frame should additionally to the lateral load  $P_h$  be loaded by two bending moments  $M_1$  and  $M_2$  as well. However, these will be compensated for by a correction factor, presented in the next paragraphs.

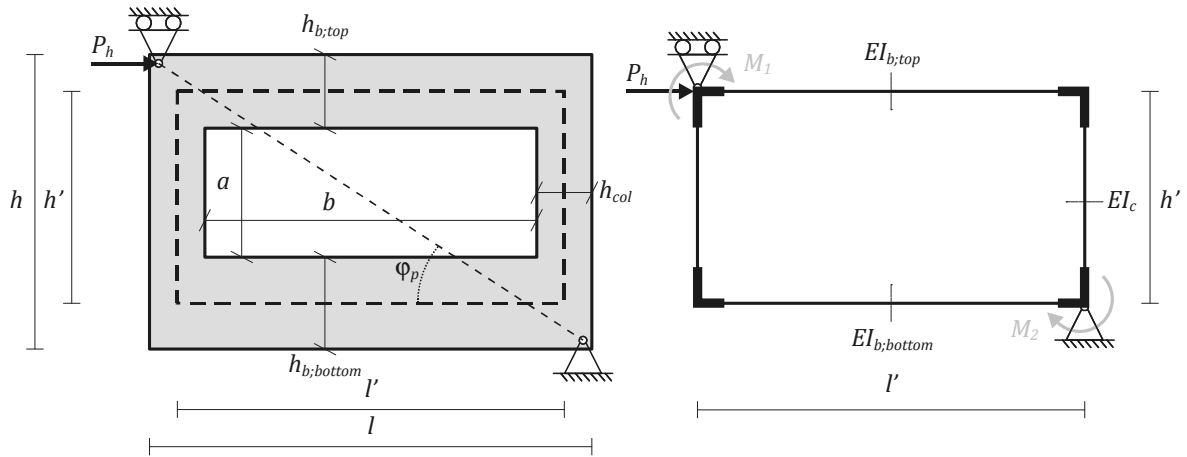


Figure 7-6: Infill panel with equivalent frame representation

Likewise for the bare frame, two factors ( $\beta_p$  and  $\gamma_p$ ) are defined to express the contribution by the rigid ends of the beams and columns:

$$\beta_p = \frac{l'}{b} \quad [7-15]$$

$$\gamma_p = \frac{h'}{a} \quad [7-16]$$

The lateral stiffness of the equivalent frame is determined considering deformations due to bending of the frame members only. The deflection of the equivalent frame due to lateral load  $P_h$  is equal to the sum of the horizontal displacements caused by double curvature bending of the top beam (first term in equation [7-17]), double curvature bending of the bottom beam (second term in equation) and double curvature bending of the columns (third term in equation):

$$\begin{aligned} \delta_{h,p} &= \frac{P_h l' h'^2}{48 \beta_p^3 EI_{b;top}} + \frac{P_h l' h'^2}{48 \beta_p^3 EI_{b;bottom}} + \frac{P_h h'^3}{24 \gamma_p^3 EI_{col}} \quad [7-17] \\ &= \frac{P_h h'^2 (\gamma_p^3 EI_{col} \beta_p^3 EI_{b;bottom} l' + \gamma_p^3 EI_{col} \beta_p^3 EI_{b;top} l' + 2 \beta_p^3 EI_{b;bottom} \beta_p^3 EI_{b;top} h')}{48 \beta_p^3 EI_{b;top} \beta_p^3 EI_{b;bottom} \gamma_p^3 EI_{col}} \end{aligned}$$

Since the equivalent frame (beam model) offers a poor representation for the in-plane loaded plate structure (continuum), and additionally because the bending moments  $M_1$  and  $M_2$  and shear and axial deformations were not taken into account, a correction factor  $\eta$  is introduced. This factor can be determined by making linear elastic finite element calculations of a plate structure and its equivalent frame as previously defined. Subsequently, the correction factor  $\eta$  equals the quotient of the found lateral deflections as follows:

$$\eta = \frac{\delta_{h;FEM}}{\delta_{h;p}} \quad [7-18]$$

Table 7-1 gives the correction factor  $\eta$  for the panels considered in the parameter study.

Table 7-1: Correction factor  $\eta$  for panels considered in parameter study

Panel type	$\alpha = \frac{1}{2}$	$\alpha = \frac{2}{3}$	$\alpha = 1$	$\alpha = 1\frac{1}{2}$
1	2.42	2.78	3.71	5.95
2	1.92	2.24	2.63	3.72
3	1.75	1.92	2.32	3.12
4	1.58	1.62	2.03	2.67
5	1.45	1.57	1.84	2.36

Although considering the panel as an equivalent frame is not very accurate, making the correction factor  $\eta$  necessary, this approach provides the opportunity to take the effect of cracked concrete into account by using a reduced Young's modulus in equation [7-17]. NEN 6720, Table 15 for example gives equations for the reduced Young's modulus taking the effect of cracks, the amount of reinforcement, the concrete compressive strength and normal force into account. Instead, an effective flexural rigidity ( $EI$ ) might be derived from  $M-N-\kappa$ -diagrams. The value of the correction factor  $\eta$  remains unaltered for the cracked situation. Accordingly, an initial ( $k_{p;ini}$ ) and secant diagonal panel stiffness ( $k_{p;sec}$ ) can be determined.

Having found the lateral deflection  $\delta_{h;p}$  and the correction factor  $\eta$ , the deformation of the diagonal is given by the following equation:

$$\delta_{diagonal} = \delta_{h;p} \cos \varphi_p \eta \quad [7-19]$$

Accordingly, the diagonal panel stiffness ( $k_p$ ) is given by:

$$k_p = \frac{N_{x,strut}}{\delta_{diagonal}} = \frac{P_h / \cos \varphi_p}{\delta_{h;p} \cos \varphi_p \eta} \quad [7-20]$$

$$= \frac{48\beta_p^3 EI_{b;top} \beta_p^3 EI_{b;bottom} \gamma_p^3 EI_{col}}{h'^2 (\gamma_p^3 EI_{col} \beta_p^3 EI_{b;bottom} l' + \gamma_p^3 EI_{col} \beta_p^3 EI_{b;top} l' + 2\beta_p^3 EI_{b;bottom} \beta_p^3 EI_{b;top} h')} \eta \cos^2 \varphi_p$$

### 7.1.2 Advanced model

In this section, the originally proposed advanced model is considered. This model is approached analytically likewise the basic model with the spring system shown in Figure 7-2. However, as a result of the offset of the connection between the strut and the frame, there is a different system of forces resulting in additional shear and bending deformation of the frame members. These have to be incorporated in the analytical equations.

Furthermore, because the nodes of the panel-to-frame connections and the strut do not coincide with the frame corners, for which the spring system from Figure 7-2 is valid, the effect of the local deformations of the panel-to-frame connections and the infill panel on the global deflection of the infilled frame has to be taken into account.

System of forces

The advanced model presented in Figure 7-7 is considered, having pinned frame joints, thus  $S_j = 0$

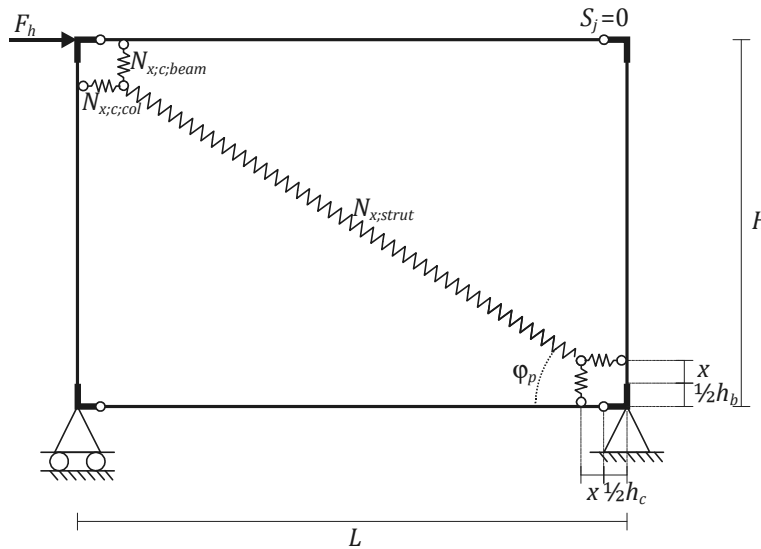


Figure 7-7: Advanced model having pinned frame joints, thus  $S_j = 0$

Figure 7-8 schematically shows the diagram of normal forces for the model:

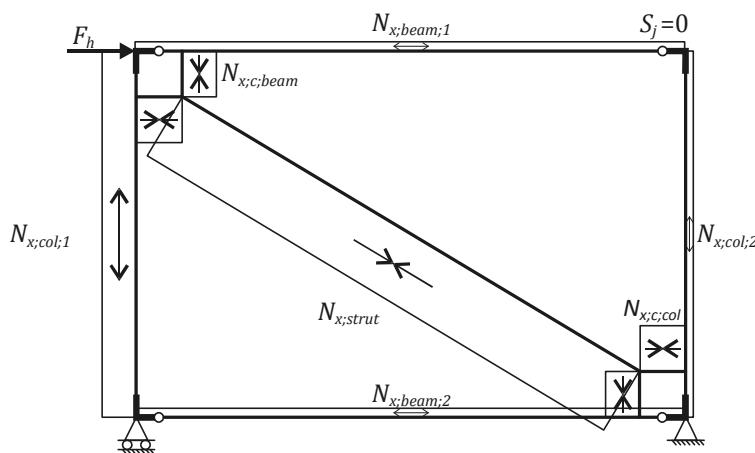


Figure 7-8: Diagram of normal forces for advanced model having pinned frame joints

It can be shown that the normal forces in the panel-to-column ( $N_{x;c;col}$ ) and panel-to-beam connections ( $N_{x;c;beam}$ ) are equal to (for a derivation, see Appendix E.1):

$$N_{x;c;col} = \frac{F_h H}{(H - h_b - 2x)\beta_f} \quad [7-21]$$

$$N_{x;c;beam} = N_{x;c;col} \tan \varphi_p = \frac{F_h \tan \varphi_p H}{(H - h_b - 2x)\beta_f} \quad [7-22]$$

Accordingly, the normal force in the strut ( $N_{x;strut}$ ) is given by:

$$N_{x;strut} = \frac{N_{x;c;col}}{\cos \varphi_p} = \frac{F_h H}{(H - h_b - 2x)\beta_f \cos \varphi_p} \quad [7-23]$$

The axial force in the loaded column ( $N_{x;col;1}$ ) equals (for a derivation, see Appendix E):

$$N_{x;col;1} = N_{x;c;beam} \left( \frac{L - h_c - x}{L - h_c} \right) = \frac{(L - h_c - x) F_h H \tan \varphi_p}{(L - h_c)(H - h_b - 2x)\beta_f} \quad [7-24]$$

Due to the offset of the panel-to-frame connection with respect to the frame corners, bending and shear deformations take place in the frame members. Therefore, an effective panel-to-frame connection spring stiffness ( $k_{c;eff}$ ) is derived, which includes stiffness coefficients for shear ( $k_{c;V}$ ) and bending deformation ( $k_{c;M}$ ) in addition to the initial spring stiffness ( $k_{c;ini}$ ) as follows:

$$\frac{1}{k_{c;eff}} = \frac{1}{k_{c;ini}} + \frac{1}{k_{c;V}} + \frac{1}{k_{c;M}} \quad [7-25]$$

Where:

$k_{c;ini}$  = Initial connection stiffness

$k_{c;V}$  = Stiffness resulting from shear deformation

$k_{c;M}$  = Stiffness resulting from bending deformation

The initial connection stiffness  $k_{c;ini}$ , is given by the following equation:

$$k_{c;ini} = \left[ \frac{1}{k_{c_{1+2}}} + \frac{1}{2k_{c_{3+4}}} \right]^{-1} \quad [7-26]$$

Where:

$k_{c_{1+2}}$  = Stiffness coefficient for flanges with web in compression

$k_{c_{3+4}}$  = Stiffness coefficient for bolt with cap in compression

The effective panel-to-frame connection spring stiffness is to be used afterwards in equation [7-35].

To derive the stiffness coefficients for shear and bending deformation, the shear force and bending moment diagrams for a beam and column member as schematically shown in Figure 7-9 are considered.

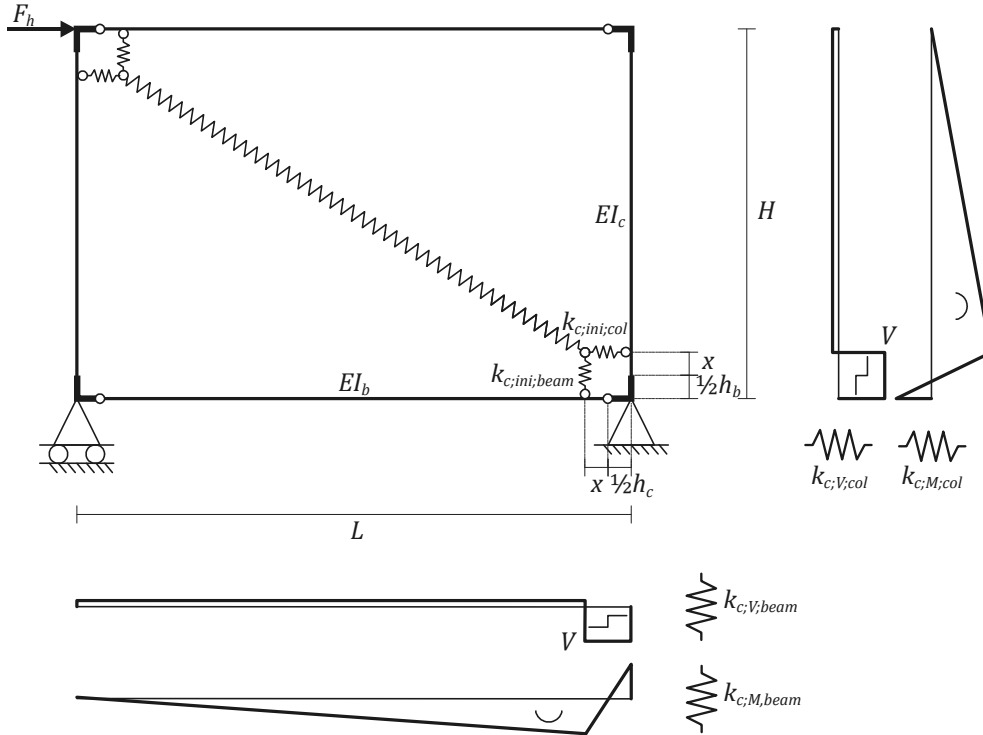


Figure 7-9: Stiffness coefficients for discrete interface connection

The stiffness coefficient resulting from shear deformation for the panel-to-beam connection is given by (for derivation, see Appendix E.2):

$$k_{c;V;beam} = \frac{GA_{v;b}(L - h_c)}{(L - h_c - x)x} \quad [7-27]$$

The stiffness coefficient resulting from shear deformation for the panel-to-column connection is given by (for derivation, see Appendix E.2):

$$k_{c;V;col} = \frac{GA_{v;c}(H - h_b)}{(H - h_b - x)x} \quad [7-28]$$

The stiffness coefficient resulting from bending deformation for the panel-to-beam connection is given by (for derivation, see Appendix E.2):

for  $S_j=0$

$$k_{c;M;beam} = \frac{3EI_b(L - h_c)}{(L - h_c - x)^2 x^2} \quad [7-29]$$

for  $S_j \neq 0$

$$k_{c;M;beam} = \infty \quad [7-30]$$

For  $S_j \neq 0$ , deformations due to bending moment showed to be negligible (considering magnitudes for  $x$  which are in the application of the infilled frame). Consequently, the stiffness coefficient for bending is taken  $k_{c;M} = \infty$ .

The stiffness coefficient resulting from bending deformation for the panel-to-column connection is given by (for derivation, see Appendix E.2):

for  $S_j=0$

$$k_{c;M;col} = \frac{3EI_c(H - h_b)}{(H - h_b - x)^2 x^2} \quad [7-31]$$

for  $S_j \neq 0$

$$k_{c;M;col} = \infty \quad [7-32]$$

Extending equations for the basic model to allow application for the advanced model

The spring system from Figure 7-2 represents the load-displacement response between node D and node B of the basic model (see Figure 7-1a). In the advanced model, the nodes between the panel-to-frame connections and the strut (nodes D' and B', see Figure 7-1b) do not coincide with the frame corners (nodes D and B, see Figure 7-1b). As a consequence, to allow the application of the spring system for the advanced model, the effect of (local) displacements between node D' and B' on (global) displacements between node D and B has to be taken into account.

This is done, assuming a linear relation between the local and global displacements, by multiplying the local displacements by  $(L_{strut}/l_{strut})$ , where  $L_{strut}$  is the (diagonal) length between node D and B, and  $l_{strut}$  the (diagonal) length between nodes D' and B'.

Accordingly, equation [7-10] for the stiffness resulting from strut deformation ( $k_{h;p}$ ) for the basic model is extended to the following equation for the advanced model:

$$k_{h;p} = \frac{F_h k_p \cos \varphi_f}{N_{x;strut} \left( \frac{L_{strut}}{l_{strut}} \right)} \quad [7-33]$$

Substitution of  $N_{x;strut}$  given by equation [7-23], gives the following equation:

$$k_{h;p} = \frac{k_p \cos \varphi_f \cos \varphi_p l_{strut} (H - h_b - 2x) \beta_f}{HL_{strut}} \quad [7-34]$$

Equation [7-12] for the stiffness resulting from connection deformations ( $k_{h;\Sigma con}$ ) according to the basic model is extended to the following equation for the advanced model as follows:

$$k_{h;\Sigma con} = \frac{F_h}{\left(\frac{L_{strut}}{l_{strut}}\right) \left(\frac{2N_{x,c,col}}{k_{c,eff,col}} + \frac{2N_{x,c,beam}}{k_{c,eff,beam}} \tan \varphi_f\right)} \quad [7-35]$$

Where  $N_{x,c,col}$  and  $N_{x,c,beam}$  are given by equation [7-21] and [7-22] respectively. Substitution gives the following equation:

$$k_{h;\Sigma con} = \frac{k_{c,eff,beam} k_{c,eff,col} l_{strut} (H - h_b - 2x) \beta_f}{2HL_{strut} (k_{c,eff,beam} + k_{c,eff,col} \tan \varphi_p \tan \varphi_f)} \quad [7-36]$$

The equation for the stiffness resulting from column deformation ( $k_{h,col}$ ) according to the basic model is suited for the advanced model as well. Consequently, the stiffness resulting from strut deformation is given by equation [7-14], where  $N_{x;column}$  is given by equation [7-24]. Substitution gives the following equation:

$$k_{h,col} = \frac{EA_c (L - h_c) (H - h_b - 2x) \beta_f}{H^2 \tan \varphi_p \tan \varphi_f (L - h_c - x)} \quad [7-37]$$



### 7.1.3 Lateral stiffness model

In this section, the analytical model for the lateral stiffness in accordance with the advanced mechanical model is recapitulated.

The lateral stiffness of the semi-integral infilled frame with a window opening can be determined according to the following equation:

$$k_{h;if} = k_{h;f} + \left[ \frac{1}{k_{h;p}} + \frac{1}{k_{h;\Sigma con}} + \frac{1}{k_{h;col}} \right]^{-1} \quad [7-38]$$

Where:

$$k_{h;f} = \left[ \frac{LH^2}{24E\beta_f^3 I_b} + \frac{H^3}{24E\gamma_f^3 I_c} + \frac{H^2}{4\beta_f^2 S_j} + \frac{L}{2E\beta_f A_b} + \frac{H \tan^2 \varphi_f}{2E\gamma_f A_c} + \frac{H}{2G\gamma_f A_{v;c}} + \frac{H \tan \varphi_f}{2G\beta_f A_{v;b}} \right]^{-1} \quad [7-39]$$

$$k_{h;p} = \frac{k_p \cos \varphi_f \cos \varphi_p l_{strut} (H - h_b - 2x) \beta_f}{HL_{strut}} \quad [7-40]$$

$$k_{h;\Sigma con} = \frac{k_{c;eff;beam} k_{c;eff;col} l_{strut} (H - h_b - 2x) \beta_f}{2HL_{strut} (k_{c;eff;beam} + k_{c;eff;col} \tan \varphi_p \tan \varphi_f)} \quad [7-41]$$

$$k_{h;col} = \frac{EA_c (L - h_c) (H - h_b - 2x) \beta_f}{H^2 \tan \varphi_p \tan \varphi_f (L - h_c - x)} \quad [7-42]$$

In section 7.3, a comparison will be made between the results obtained from this analytical model and the results obtained from finite element analyses performed in the parameter study.

## 7.2 Ultimate lateral load modeling

This section discusses the development of analytical models for prediction of the ultimate lateral load of the semi-integral infilled frame. In these models, the strength of the structure is supposed to be governed by the panel-to-frame connections. For that purpose, the infill panel should be designed with the strut-and-tie method (chapter 2) to fulfill the demanded strength.

**7.2.1 Dead weight panel**

Since the infill panel is supported by the panel-to-frame connections, the panel’s dead weight influences the lateral load carrying capacity of the semi-integral infilled frame. Initially, the panel’s dead weight is supported by the panel-to-beam connections on the bottom beam only (Figure 7-10a). At that moment, the force in the connections amounts to  $N_{x;c;beam;G} = \frac{1}{2}G_p$ . When the infilled frame is loaded, the panel will be lifted at one side from its connection until it loses contact with this connection. This moment is called the overturning moment. The load distribution of the panel’s dead weight at the overturning moment is shown in Figure 7-10b.

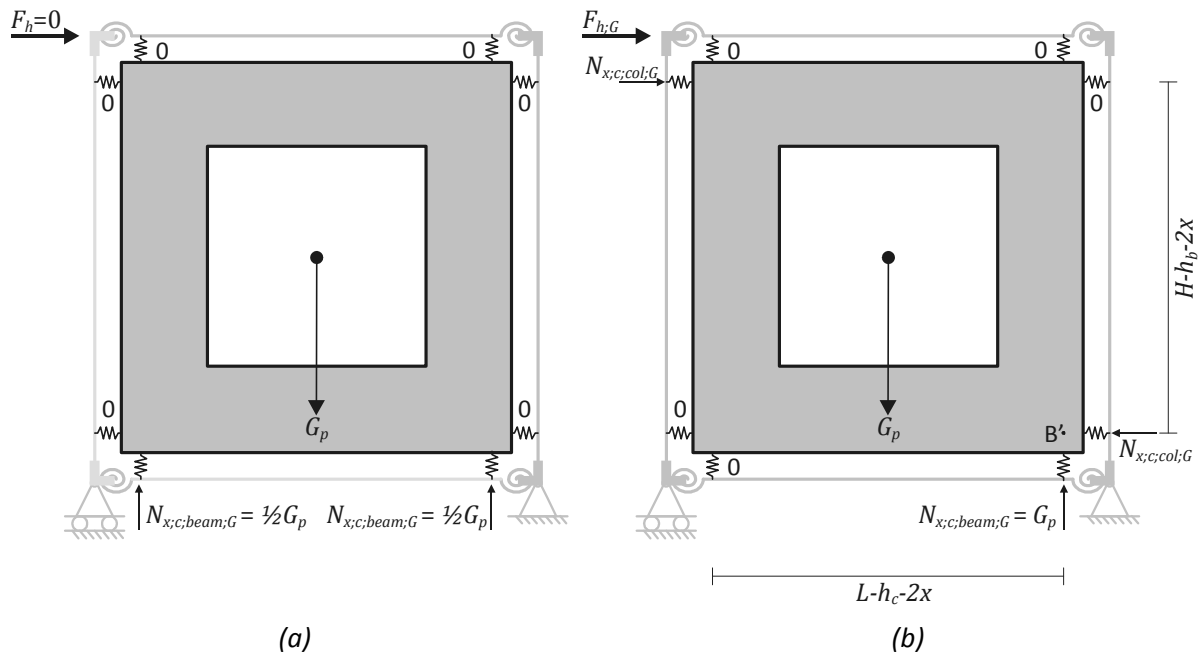


Figure 7-10: Distribution dead weight panel for  $F_h = 0$  (a) and at overturning moment  $F_h = F_{h;G}$  (b)

The axial force in the panel-to-column connections at the overturning moment ( $N_{x;c;col;G}$ ) can be derived by considering the equilibrium of moments with respect to point B’:

$$N_{x;c;col;G} = G_p \frac{\frac{1}{2}(L - h_c - 2x)}{H - h_b - 2x} \quad [7-43]$$

The force in the panel-to-beam connection at the overturning moment ( $N_{x;c;beam;G}$ ) equals:

$$N_{x;c;beam;G} = G_p \quad [7-44]$$

Accordingly, the required lateral load at the overturning moment  $F_{h;G}$  can be derived by substituting the expression for  $N_{x;c;col;G}$  according to equation [7-43] in equation [7-21]. This results in the following equation for  $F_{h;G}$ :

$$F_{h,G} = G_p \frac{1/2(L - h_c - 2x)\beta_f}{H} \quad [7-45]$$

### 7.2.2 Ultimate lateral load models

The results of the parameter study showed that failure can occur by one of two possible modes of failure, depending on the aspect ratio of the infilled frame. These are referred to as panel-to-beam connection failure and panel-to-column connection failure. The equations for calculating the resistance for both failure modes are derived in the following paragraph.

To find the ultimate lateral load, two load cases have to be considered, which are the panel's dead load ( $G_p$ ) and the lateral load ( $F_h$ ). The panel's dead load generates the lateral load carrying capacity ( $F_{h,G}$ ) according to equation [7-45]. Consequently, the corresponding forces in the panel-to-column and panel-to-beam connection given by equations [7-43] and [7-44] respectively have to be subtracted from the connection capacity ( $F_c$ ). The remaining connection capacity can be utilized for loading by strut action. The relation between the force in the panel-to-frame connections and the lateral load for strut action is given by equations [7-21] and [7-22]. Accordingly, this results in the following equations for the resistance for the two failure modes:

#### Mode 1: Panel-to-column connection failure

$$F_{u,if} = \frac{1}{\mu} \left( F_{h,G} + \left( \frac{(H - h_b - 2x)\beta_f}{H} \right) (F_{c,col} - N_{x;c,col,G}) \right) \quad [7-46]$$

Where  $\mu$  accounts for the relative stiffness of the frame ( $k_{h,f}$ ) to the infilled frame ( $k_{if;sec}$ ) according to the following equation:

$$\mu = 1 - \frac{k_{h,f}}{k_{if;sec}} \quad [7-47]$$

The factor  $\mu$  determines what part of the lateral load is supported by the frame and what part by composite action between the infill and the frame (strut action) and thus actually utilizes the connection capacity.

Substitution of the expressions for  $N_{x;c,col,G}$  and  $F_{h,G}$  given by equations [7-43] and [7-45] respectively results in:

$$F_{u,if} = F_{c,col} \frac{(H - h_b - 2x)\beta_f}{\mu H} \quad [7-48]$$

Mode 2: Panel-to-beam connection failure

$$F_{u;if} = \frac{1}{\mu} \left( F_{h;G} + \left( \frac{(H - h_b - 2x)\beta_f}{H \tan \phi_p} \right) (F_{c;beam} - N_{x;c;beam;G}) \right) \quad [7-49]$$

Substitution of the expressions for  $N_{x;c;beam;G}$  and  $F_{h;G}$  given by equations [7-44] and [7-45] respectively results in:

$$F_{u;if} = (F_{c;beam} - \frac{1}{2}G_p) \frac{(L - h_c - 2x)\beta_f}{\mu H} \quad [7-50]$$

Accordingly, the strength of the structure should be taken as the smallest value of the two possible failure modes.

In the following section, the analytical models are validated.

### 7.3 Validation of analytical models

In the previous two sections, analytical models were presented to predict the lateral stiffness and the ultimate lateral load of the semi-integral infilled frame with a window opening. This section presents and validates results from these analytical models with results obtained from finite element analyses performed in the parameter study (chapter 6.2).

First, the bare frame stiffnesses obtained with the analytical model (A-Model) (according to equation [7-39]) are compared with the stiffnesses obtained from finite element analyses performed in the parameter study (FE) in (Table 7-2), where the ratio is A-Model/FE.

Table 7-2: Comparison of FE and analytical results for bare frame stiffness

Frame type	Aspect ratio	FE	A-Model	ratio
Weak	½	2.12E+03	2.12E+03	1.00
Weak	⅔	2.32E+03	2.32E+03	1.00
Weak	1	2.59E+03	2.59E+03	1.00
Weak	1½	2.86E+03	2.86E+03	1.00
Strong	½	5.78E+03	5.79E+03	1.00
Strong	⅔	6.29E+03	6.29E+03	1.00
Strong	1	6.95E+03	6.95E+03	1.00
Strong	1½	7.57E+03	7.57E+03	1.00

Comparison shows that the analytical model provides an exact prediction of the bare frame stiffness.

Next, the results for the infilled frame are compared. Table 7-3 and Table 7-4 present the finite element results (FE) and predictions according to the analytical models (A-Model) for the weak and strong frame respectively. Comparisons are made for the initial stiffness ( $k_{ini}$ ), the secant stiffness ( $k_{sec;2}$ ) and the ultimate load ( $F_u$ ) (Figure 7-11). A comparison is made in the columns 'ratio' where the ratio = A-Model/FE.

For the determination of the secant stiffness ( $k_{sec;2}$ ), the secant diagonal panel stiffness was used, which incorporates the effect of cracked concrete and the amount of reinforcement. For this purpose, the bending stiffness  $(EI)_d$  of the panel's equivalent frame members has been determined using  $M-N-\kappa$ -diagrams. A survey of the  $M-N-\kappa$ -diagrams used and the bending stiffnesses derived is provided in Appendix E.3.

Table 7-3: Comparison between FE and analytical results for weak frame

$\alpha$	Type	$S_{j,ini}$	$k_{ini}$ [N/mm]			$k_{sec;2}$ [N/mm]			$F_u$ [N]		
			FE	A-Model	ratio	FE	A-Model	ratio	FE	A-Model	ratio
$\alpha = \frac{1}{2}$	1	EC3	5.70E+4	6.38E+4	<b>1.12</b>	3.32E+4	3.05E+4	<b>0.92</b>	6.31E+5	6.19E+5	<b>0.98</b>
	1	0	4.50E+4	5.15E+4	<b>1.14</b>	2.68E+4	2.60E+4	<b>0.97</b>	5.78E+5	5.76E+5	<b>1.00</b>
	2	EC3	4.55E+4	4.75E+4	<b>1.04</b>	2.39E+4	2.20E+4	<b>0.92</b>	6.53E+5	6.37E+5	<b>0.98</b>
	3	EC3	3.97E+4	4.07E+4	<b>1.03</b>	2.02E+4	1.88E+4	<b>0.93</b>	6.65E+5	6.49E+5	<b>0.98</b>
	4	EC3	3.30E+4	3.08E+4	<b>0.93</b>	1.62E+4	1.46E+4	<b>0.90</b>	6.80E+5	6.74E+5	<b>0.99</b>
	5	EC3	2.70E+4	2.49E+4	<b>0.92</b>	1.31E+4	1.20E+4	<b>0.91</b>	6.48E+5	7.00E+5	<b>1.08*</b>
	5	0	2.20E+4	2.12E+4	<b>0.97</b>	1.04E+4	9.57E+3	<b>0.92</b>	5.22E+5	5.76E+5	<b>1.10*</b>
$\alpha = \frac{2}{3}$	1	EC3	5.95E+4	6.23E+4	<b>1.05</b>	3.57E+4	3.31E+4	<b>0.93</b>	6.39E+5	6.27E+5	<b>0.98</b>
	1	0	4.85E+4	4.93E+4	<b>1.02</b>	3.00E+4	2.77E+4	<b>0.92</b>	5.85E+5	5.83E+5	<b>1.00</b>
	2	EC3	5.00E+4	4.79E+4	<b>0.96</b>	2.69E+4	2.40E+4	<b>0.89</b>	6.58E+5	6.45E+5	<b>0.98</b>
	3	EC3	4.50E+4	4.32E+4	<b>0.96</b>	2.31E+4	2.14E+4	<b>0.93</b>	6.64E+5	6.54E+5	<b>0.98</b>
	4	EC3	3.75E+4	3.58E+4	<b>0.95</b>	1.88E+4	1.79E+4	<b>0.95</b>	6.88E+5	6.70E+5	<b>0.97</b>
	5	EC3	3.20E+4	2.88E+4	<b>0.90</b>	1.56E+4	1.44E+4	<b>0.92</b>	7.08E+5	6.95E+5	<b>0.98</b>
	5	0	2.65E+4	2.42E+4	<b>0.91</b>	1.22E+4	1.16E+4	<b>0.95</b>	5.80E+5	5.83E+5	<b>1.00</b>
$\alpha = 1$	1	EC3	5.47E+4	5.22E+4	<b>0.95</b>	3.67E+4	3.28E+4	<b>0.89</b>	6.43E+5	6.35E+5	<b>0.99</b>
	1	0	4.55E+4	4.07E+4	<b>0.89</b>	3.08E+4	2.66E+4	<b>0.86</b>	5.85E+5	5.85E+5	<b>1.00</b>
	2	EC3	4.82E+4	4.50E+4	<b>0.93</b>	2.87E+4	2.66E+4	<b>0.93</b>	6.59E+5	6.49E+5	<b>0.99</b>
	3	EC3	4.45E+4	4.13E+4	<b>0.93</b>	2.42E+4	2.37E+4	<b>0.98</b>	6.70E+5	6.58E+5	<b>0.98</b>
	4	EC3	4.05E+4	3.61E+4	<b>0.89</b>	2.05E+4	2.03E+4	<b>0.99</b>	6.87E+5	6.73E+5	<b>0.98</b>
	5	EC3	3.62E+4	3.19E+4	<b>0.88</b>	1.78E+4	1.76E+4	<b>0.99</b>	7.06E+5	6.89E+5	<b>0.98</b>
	5	0	2.97E+4	2.59E+4	<b>0.87</b>	1.35E+4	1.41E+4	<b>1.04</b>	5.88E+5	5.88E+5	<b>1.00</b>
$\alpha = 1 \frac{1}{2}$	1	EC3	3.70E+4	3.59E+4	<b>0.97</b>	2.87E+4	2.63E+4	<b>0.92</b>	4.16E+5	4.16E+5	<b>1.00</b>
	1	0	3.18E+4	2.80E+4	<b>0.88</b>	2.47E+4	2.08E+4	<b>0.84</b>	3.71E+5	3.71E+5	<b>1.00</b>
	2	EC3	3.50E+4	3.35E+4	<b>0.96</b>	2.63E+4	2.34E+4	<b>0.89</b>	4.21E+5	4.23E+5	<b>1.00</b>
	3	EC3	3.39E+4	3.22E+4	<b>0.95</b>	2.55E+4	2.20E+4	<b>0.86</b>	4.21E+5	4.27E+5	<b>1.01</b>
	4	EC3	3.25E+4	3.04E+4	<b>0.93</b>	2.26E+4	2.02E+4	<b>0.89</b>	4.29E+5	4.33E+5	<b>1.01</b>
	5	EC3	3.08E+4	2.86E+4	<b>0.93</b>	2.07E+4	1.86E+4	<b>0.90</b>	4.34E+5	4.39E+5	<b>1.01</b>
	5	0	2.65E+4	2.26E+4	<b>0.85</b>	1.68E+4	1.45E+4	<b>0.86</b>	3.70E+5	3.72E+5	<b>1.00</b>

\* Early panel failure instead of connection failure in simulation

ANALYTICAL MODELING

Table 7-4: Comparison between FE and analytical results for strong frame

$\alpha$	Type	$S_{j,ini}$	$k_{ini}$ [N/mm]			$k_{sec;2}$ [N/mm]			$F_u$ [N]		
			FE	A-Model	ratio	FE	A-Model	ratio	FE	A-Model	ratio
$\alpha = \frac{1}{2}$	1	EC3	6.75E+4	6.79E+4	<b>1.01</b>	3.74E+4	3.43E+4	<b>0.92</b>	6.92E+5	6.93E+5	<b>1.00</b>
	1	0	5.85E+4	5.97E+4	<b>1.02</b>	3.02E+4	2.80E+4	<b>0.93</b>	5.78E+5	5.76E+5	<b>1.00</b>
	2	EC3	5.35E+4	5.14E+4	<b>0.96</b>	2.78E+4	2.57E+4	<b>0.93</b>	7.44E+5	7.43E+5	<b>1.00</b>
	3	EC3	4.65E+4	4.46E+4	<b>0.96</b>	2.39E+4	2.24E+4	<b>0.94</b>	7.77E+5	7.76E+5	<b>1.00</b>
	4	EC3	3.85E+4	3.46E+4	<b>0.90</b>	1.92E+4	1.82E+4	<b>0.95</b>	8.46E+5	8.44E+5	<b>1.00</b>
	5	EC3	3.16E+4	2.87E+4	<b>0.91</b>	1.75E+4	1.57E+4	<b>0.90</b>	8.41E+5	9.13E+5	<b>1.09*</b>
	5	0	2.47E+4	2.25E+4	<b>0.91</b>	1.13E+4	9.82E+3	<b>0.87</b>	5.37E+5	5.76E+5	<b>1.07*</b>
$\alpha = \frac{2}{3}$	1	EC3	6.70E+4	6.42E+4	<b>0.96</b>	4.08E+4	3.65E+4	<b>0.89</b>	7.02E+5	7.04E+5	<b>1.00</b>
	1	0	5.80E+4	5.54E+4	<b>0.95</b>	3.29E+4	2.95E+4	<b>0.90</b>	5.85E+5	5.83E+5	<b>1.00</b>
	2	EC3	5.60E+4	5.06E+4	<b>0.90</b>	3.13E+4	2.76E+4	<b>0.88</b>	7.44E+5	7.54E+5	<b>1.01</b>
	3	EC3	5.05E+4	4.62E+4	<b>0.91</b>	2.72E+4	2.52E+4	<b>0.93</b>	7.75E+5	7.77E+5	<b>1.00</b>
	4	EC3	4.44E+4	3.91E+4	<b>0.88</b>	2.31E+4	2.17E+4	<b>0.94</b>	8.21E+5	8.21E+5	<b>1.00</b>
	5	EC3	3.70E+4	3.24E+4	<b>0.88</b>	1.99E+4	1.83E+4	<b>0.92</b>	8.99E+5	8.89E+5	<b>0.99</b>
	5	0	2.90E+4	2.56E+4	<b>0.88</b>	1.38E+4	1.19E+4	<b>0.86</b>	5.81E+5	5.83E+5	<b>1.00</b>
$\alpha = 1$	1	EC3	5.50E+4	5.03E+4	<b>0.91</b>	3.97E+4	3.47E+4	<b>0.87</b>	7.15E+5	7.31E+5	<b>1.02</b>
	1	0	4.65E+4	4.15E+4	<b>0.89</b>	3.16E+4	2.70E+4	<b>0.85</b>	5.84E+5	5.85E+5	<b>1.00</b>
	2	EC3	4.95E+4	4.46E+4	<b>0.90</b>	3.21E+4	2.94E+4	<b>0.91</b>	7.55E+5	7.68E+5	<b>1.02</b>
	3	EC3	4.65E+4	4.17E+4	<b>0.90</b>	2.81E+4	2.69E+4	<b>0.95</b>	7.88E+5	7.91E+5	<b>1.00</b>
	4	EC3	4.25E+4	3.74E+4	<b>0.88</b>	2.41E+4	2.37E+4	<b>0.99</b>	8.34E+5	8.30E+5	<b>1.00</b>
	5	EC3	3.86E+4	3.39E+4	<b>0.88</b>	2.22E+4	2.13E+4	<b>0.96</b>	8.83E+5	8.72E+5	<b>0.99</b>
	5	0	3.08E+4	2.62E+4	<b>0.85</b>	1.72E+4	1.42E+4	<b>0.82</b>	5.88E+5	5.88E+5	<b>1.00</b>
$\alpha = 1\frac{1}{2}$	1	EC3	3.54E+4	3.32E+4	<b>0.94</b>	2.95E+4	2.70E+4	<b>0.92</b>	5.01E+5	5.15E+5	<b>1.03</b>
	1	0	2.75E+4	2.48E+4	<b>0.90</b>	2.14E+4	1.89E+4	<b>0.89</b>	3.70E+5	3.71E+5	<b>1.00</b>
	2	EC3	3.40E+4	3.17E+4	<b>0.93</b>	2.77E+4	2.50E+4	<b>0.90</b>	5.13E+5	5.32E+5	<b>1.04</b>
	3	EC3	3.30E+4	3.09E+4	<b>0.94</b>	2.67E+4	2.39E+4	<b>0.90</b>	5.20E+5	5.43E+5	<b>1.04</b>
	4	EC3	3.20E+4	2.97E+4	<b>0.93</b>	2.51E+4	2.26E+4	<b>0.90</b>	5.33E+5	5.58E+5	<b>1.05</b>
	5	EC3	3.10E+4	2.86E+4	<b>0.92</b>	2.33E+4	2.14E+4	<b>0.92</b>	5.53E+5	5.76E+5	<b>1.04</b>
	5	0	2.30E+4	2.04E+4	<b>0.89</b>	1.55E+4	1.35E+4	<b>0.87</b>	3.72E+5	3.72E+5	<b>1.00</b>

\* Early panel failure instead of connection failure in simulation

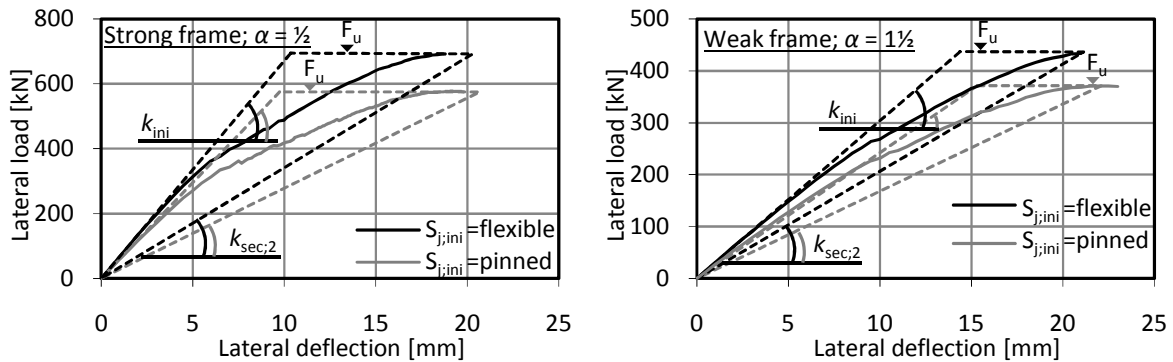


Figure 7-11: Simulated behavior (solid lines) with analytical prediction (dashed lines)

Comparison shows that the analytical model for lateral stiffness and the model for the ultimate lateral load provide an adequate prediction of the actual behavior.

## 7.4 Chapter conclusions

Analytical models have been developed for the lateral stiffness and for the ultimate lateral load of the semi-integral infilled frame with a window opening. The models are based on the concept of the equivalent diagonal strut, considering the structure as an equivalent braced frame system with a compression diagonal replacing the infill.

The load versus deflection response of the equivalent braced frame is represented by a spring system consisting of a spring representing the bare frame stiffness which acts in parallel with three serial springs (bracing system) representing the panel, the discrete interface connections and the frame column. Equations for the four stiffness terms were derived.

The derived equations for the stiffness terms for the bare frame, the discrete interface connections and the frame column result from elementary applied mechanics. To obtain the stiffness term for the diagonal strut, the panel is modeled as an equivalent frame. Accordingly, the stiffness from bending of the equivalent frame members is derived according to applied mechanics. A correction factor was introduced to account for the inconsistency between the panel and its representation as an equivalent frame. Although inaccurate, considering the panel as an equivalent frame provides the opportunity to take the effect of cracked concrete into account by using a reduced Young's modulus. Accordingly, an initial and secant lateral infilled frame stiffness can be found.

Ultimate lateral load models have been developed based on the assumption that the panel-to-frame connections govern the strength of the structure. Two failure modes are recognized, which are panel-to-column connection failure and panel-to-beam connection failure. Strength equations have been derived for both failure modes. Accordingly, the strength of the structure is equal to the smallest value of the two possible failure modes.

The analytical models have been compared with the results obtained from finite element analyses performed in the parameter study. The analytical models showed to provide an accurate prediction of the actual behavior. An example to demonstrate the feasibility of the analytical models in design is treated in the next chapter.

# Chapter 8: DESIGN RECOMMENDATIONS

## *Scope of the chapter*

*In this chapter, a design method for structures consisting of semi-integral infilled frames with window openings is presented (section 8.1). The aim of this method is to get a good prediction of the internal forces and the lateral deflection in the preliminary phase of the design, without the use of advanced computer simulations. Subsequently, an example is treated to demonstrate the application of the design method (section 8.2). Next, recommendations for the development of the structure into a completely integrated tall building system are given in sections 8.3, and a building construction method is proposed for the structure. Finally, at the end of this chapter (section 8.4), the most important findings are summarized.*

## **8.1 Design method**

The design of a high-rise building in the preliminary phase requires a simple design method in order to make decisions with regard to the approximate dimensions of the individual structural elements and subsequently to get a good impression of the lateral deflection (Hoenderkamp, J. C. D. et al., 2000; Hoenderkamp, J. C. D. et al., 2003). For a building structure consisting of semi-integral infilled frames provided with window openings, such a design method is not available yet. However, based on the previous chapters, the following method is proposed:

### Step 1: Obtain the internal design forces

To obtain the internal design forces for the semi-integral infilled frame, the building structure should initially be idealized as a braced frame having compression diagonals only. In this initial phase, all connections in the braced frame are assumed to be hinged. Consequently, the design forces for the beams, columns and struts result from the overall loads on the structure and the geometry, using simple equations based on applied mechanics.

### Step 2: Design the frame members

Having obtained the internal design forces in the structure, the frame members can be designed for stiffness and strength (including stability) according to existing standards.



**Step 3: Design the frame joints**

Having dimensioned the frame members, the frame joints are to be designed. Design methods for the design of joints are given by e.g. Eurocode 3 in EN 1993-1-8. The (initial) rotational stiffness of the joint will additionally be needed to establish the semi-integral infilled frame stiffness in step 6.

**Step 4: Design the panel-to-frame connections**

Having obtained the design forces for the struts, the panel-to-column and panel to-beam connections can be designed as follows:

- a) Design the connection (position of the bolts on the flanges) and select the corresponding strength and stiffness characteristic for web with flanges subject to transverse compression introduced indirectly through the flanges ( $F_{c_{1+2}}, k_{c_{1+2}}$ ) from Tables 6-2, 6-3, 6-5 or 6-6.
- b) Establish the design force for the panel-to-column and panel-to-beam connections, according to equations [7-21] and [7-22] respectively.
- c) Select the bolt size and bolt grade. The bolt-nut assembly should be designed for strength according to Alexander's theory, discussed in section 2.2.2.
- d) Check the flange capacity in order to allow a bolt failure mechanism to govern the strength of the structure. If the flange capacity of the previous selected frame is insufficient, a larger section should be selected. Instead backing plates could be added to increase the flange capacity only locally.
- e) Establish the effective connection spring stiffness ( $k_{c,eff}$ ) according to equation [7-25].

**Step 5: Design the panels**

The required panel reinforcement to fulfill the demanded strength ( $F_p$ ) to allow bolt failure governing the strength of the structure should be determined by using the strut-and-tie method. The strut-and-tie model to be used for an infill panel with panel opening is (schematically) shown in Figure 3-5. Having obtained the required reinforcement, an initial and secant equivalent diagonal panel stiffness ( $k_{p,ini}$  and  $k_{p,sec}$ ) can be derived according to the method described in chapter 7. This method is summarized as follows:

- a) Model the panel as an equivalent frame
- b) Establish the correction factor  $\eta$  according to equation [7-18] by means of linear elastic finite element analysis
- c) Determine the diagonal panel stiffness according to equation [7-20]

Step 6: Determine the stiffness of the single-story, single-bay semi-integral infilled frame

The stiffness of a single-story single-bay semi-integral infilled frame can be determined according to equation [7-38].

Step 7: Check the strength of the single-story, single-bay semi-integral infilled frame

Having obtained the actual stiffness, a check has to be made for the strength according to the equations [7-48] and [7-50].

Step 8: Determine the deflection of the total structure

Finally, the deflection of the entire structure is determined. For this purpose, two stiffnesses have to be taken into account. The first one is the global bending stiffness for bending due to axial strains in the columns. Here, the individual bending stiffness of the columns is ignored. The second stiffness is the lateral (shear) stiffness of the infilled frames. Furthermore, the deflection resulting from rotation of the foundation has to be considered. The deflection for bending added to the deflection for shear and the deflection resulting from rotation of the foundation gives the total deflection of the structure. Finally, a check has to be made for the total deflection of the structure to comply with the serviceability limit state requirements. Generally, the maximum allowable lateral displacement is taken as  $1/500$  times the height of the structure.

## 8.2 Design example

The application of the previously presented design method is demonstrated by means of a design example. The floor plan of a 20-story high-rise structure is presented in Figure 8-1. The story height  $H$  is 3.6 m so the total height of the structure is  $(20 \times 3.6 =) 72.0$  m. The length and width of the building are  $(5 \times 7.2 =) 36$  m and  $(2 \times 7.2 + 5.4 =) 19.8$  m respectively. The lateral load is resisted by semi-integral infilled frames all over the façades. In this design example, only the lateral load resisting structure in the direction of the weak axis of the building is considered. Required is a preliminary design for the ground story columns and infill panels and a prediction of the total deflection of the structure. Second order effects are not considered in this example.

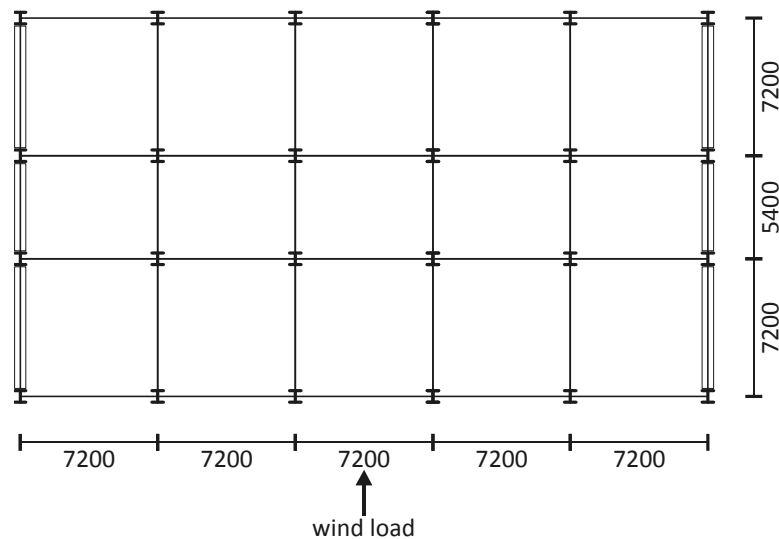


Figure 8-1: Floor plan of 20-story high-rise structure

The following loads act on the structure:

- Dead load: floor:  $4.0 \text{ kN/m}^2$ ; façade:  $15 \text{ kN/m}$ ; the partial load factor  $\gamma_g = 1.2$  for ultimate limit state design (ULS) and 1.0 for serviceability limit state design (SLS)
- Live load:  $3.0 \text{ kN/m}^2$ , the partial load factor  $\gamma_q = 1.5$  for ULS design and 1.0 for SLS design; the load combination factor, accounting for the reduced probability of a number of loads from different sources acting simultaneously,  $\psi = 0.5$
- Wind load An equivalent uniformly distributed wind load over the height of the structure is assumed, equal to  $p_{w;eq} = 1.30 \text{ kN/m}^2$ , the partial load factor  $\gamma_q = 1.5$  (ULS design) and 1.0 (SLS design); the load combination factor  $\psi = 0.0$

The following assumptions are made:

- Precast concrete panels grade C50/60: Young's modulus  $E_c = 3.7E+04 \text{ N/mm}^2$ , characteristic cylinder strength  $f_{ck} = 50 \text{ N/mm}^2$ , density  $\rho = 24 \text{ kN/m}^3$ , the partial material factor  $\gamma_c = 1.5$
- Panel thickness  $t_p = 300 \text{ mm}$
- Panel reinforcement FeB500: Young's modulus  $E_s = 2.0E+05 \text{ N/mm}^2$ , yield strength  $f_y = 500 \text{ N/mm}^2$ ; the partial material factor  $\gamma_s = 1.15$
- Beams HE300B
- Steel structure grade S355: Young's modulus  $E_s = 2.1E+05 \text{ N/mm}^2$ , yield strength  $f_y = 355 \text{ N/mm}^2$
- Gap width  $g = 50 \text{ mm}$
- Dimensions of columns and panels are identical over the height of the structure
- Panels do not carry vertical loads

**Step 1: Obtain the internal design forces**

To obtain the internal design forces, the lateral load resisting structure is idealized as a braced frame as shown in Figure 8-2a. The equivalent wind load on the braced frame  $q_{w,eq}$  equals  $1.30 \text{ kN/m}^2 \times 7.2 \text{ m} \times 2.5 = 23.4 \text{ kN/m}$ .

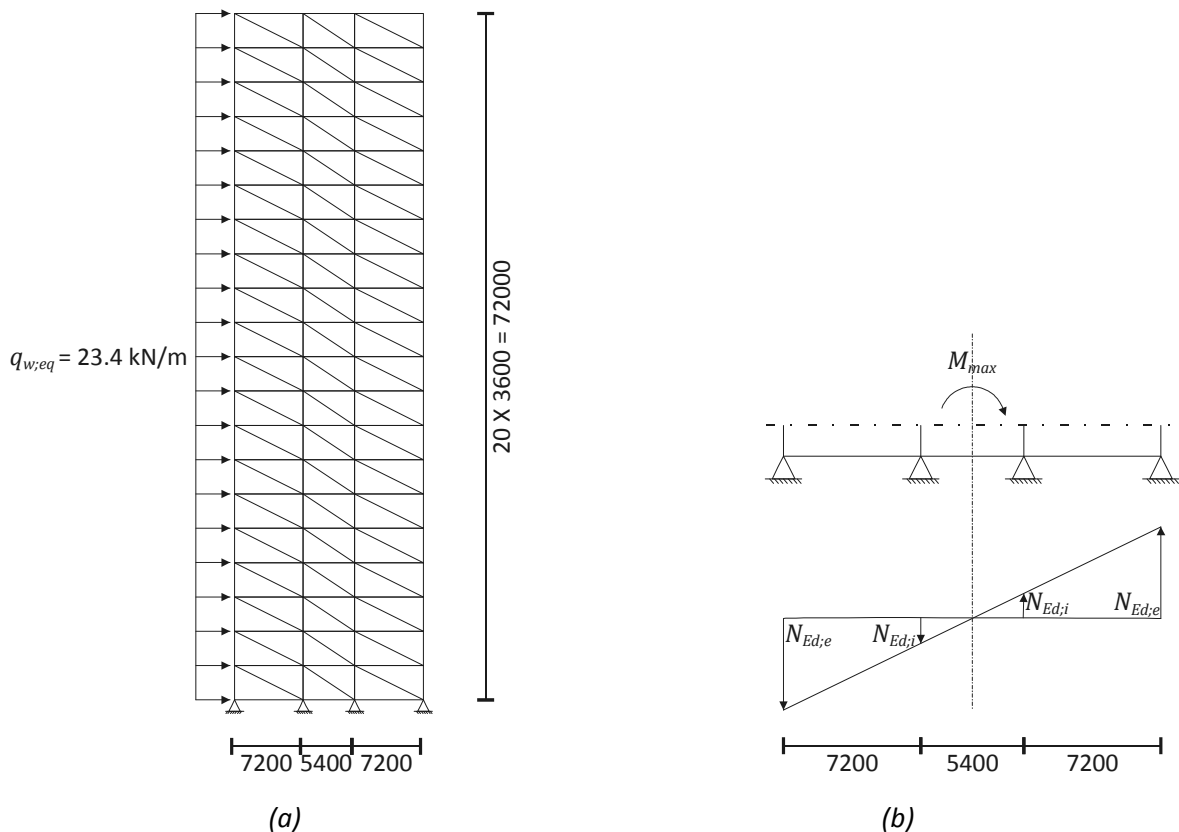


Figure 8-2: Braced frame idealization of structure consisting of semi-integral infilled frames

The axial forces in the columns and diagonals are derived using simple equations based on applied mechanics as follows:

- Ultimate axial forces in the columns

Axial force in the columns due to wind load:

$$M_{max} = \frac{q_{w;eq}\gamma_q H^2}{2} = \frac{23.4 \times 1.5 \times 72^2}{2} = 9.10 \times 10^4 \text{ kNm}$$

This moment is supported by axial forces in the exterior columns ( $N_{Ed,e}$ ) and the interior columns ( $N_{Ed,i}$ ) (Figure 8-2b). The axial forces in the columns are assumed linearly related to the distance to the neutral axis of the braced frame. Consequently, it can be shown that the normal force in the exterior column  $N_{Ed,e}$  equals:

$$N_{Ed,e} = \frac{N_{Ed,i}(2.7 + 7.2)}{2.7} = \frac{11}{3}N_{Ed,i}$$

Accordingly the axial forces in the columns due to the wind load are equal to:

$$N_{Ed,e;wind} = \frac{9.10 \times 10^4}{\left(5.4 \times \frac{3}{11} + 19.8\right)} = 4277 \text{ kN}$$

$$N_{Ed,i;wind} = \frac{3}{11} \times 4277 = 1166 \text{ kN}$$

The axial force in an exterior ground floor (façade) column due to vertical loads equals:

Contributory area:	$3.6 \times 3.6 = 12.96 \text{ m}^2$
Dead load $F_g$ :	$12.96 \times 4.0 + 7.2 \times 15 = 159.8 \text{ kN}$
Live load $F_q$ :	$12.96 \times 3.0 = 38.9 \text{ kN}$

$$N_{Ed,e;vert} = 20(\gamma_g F_g) + 20(\gamma_q \psi F_q)$$

$$N_{Ed,e;vert} = 20(1.2 \times 159.8) + 20(1.5 \times 0.5 \times 38.9) = 4419 \text{ kN}$$

The ultimate axial force in the column including wind load equals:

$$N_{Ed,e;vert+wind} = 4419 + 4277 = 8696 \text{ kN}$$

The axial force in an interior ground floor (façade) column due to the vertical loads equals:

Contributory area:	$3.6 \times 6.3 = 22.68 \text{ m}^2$
Dead load $F_g$ :	$22.68 \times 4.0 + 6.3 \times 15 = 185.2 \text{ kN}$
Live load $F_q$ :	$22.68 \times 3.0 = 68.0 \text{ kN}$

$$N_{Ed;i;vert} = 20(1.2 \times 185.2) + 20(1.5 \times 0.5 \times 68.0) = 5465 \text{ kN}$$

The ultimate axial force in the column including wind load equals:

$$N_{Ed;i;vert+wind} = 5465 + 1166 = 6631 \text{ kN}$$

- Ultimate axial forces in the struts:

To estimate the ultimate axial forces in the struts, the shear force at level one is determined. The actual distribution of the lateral load over the three bays depends on the ratio between the bay stiffnesses, which is currently unknown. Therefore, in this preliminary phase of the design, the lateral load is assumed to be equally divided over the three bays. Accordingly, the shear force acting on one bay equals:

$$V_{Ed} = \frac{n \times q_{w;eq} \gamma_q h}{3} = \frac{19 \times 23.4 \times 1.5 \times 3.6}{3} = 800 \text{ kN}$$

where  $n$  is the number of stories. Accordingly, the axial load in the diagonal equals  $V_{Ed} / \cos \varphi = 895 \text{ kN}$  for the exterior bays and  $961 \text{ kN}$  for the middle bay (where  $\varphi = \tan^{-1}(H/L)$ ).

### Step 2: Design the frame members

The selected column is a HE360M section in steel grade S355, which is classified as a Class 1 cross-section. The column is to be verified against buckling about the weak axis using EN 1993-1-1 section 6.3.1:

$$\frac{N_{Ed}}{N_{b;Rd}} = \frac{N_{Ed}}{\chi A_c f_y} \leq 1.0$$

Where  $N_{Ed}$  and  $N_{b;Rd}$  are the design value of the compressive force and the design buckling resistance of the column respectively. The later is taken as the product of the column area ( $A_c$ ), the yields stress ( $f_y$ ) and a reduction factor ( $\chi$ ).

To determine the value of the reduction factor for flexural buckling about the (weak) z-axis ( $\chi_z$ ), the non-dimensional slenderness  $\bar{\lambda}_z$  is calculated as follows:

$$\bar{\lambda}_z = \frac{L_{cr}}{i_z} \times \frac{1}{\pi \sqrt{\frac{E}{f_y}}} = \frac{3600}{78.3} \times \frac{1}{\pi \sqrt{\frac{2.1 \times 10^5}{355}}} = 0.60 \rightarrow \chi_z = 0.84$$

where  $L_{cr}$  is the buckling length and  $i_z$  the radius of gyration about the z-axis. Accordingly, the value of the reduction factor  $\chi_z$  is obtained from Figure 6.4 of EN 1993-1-1, using

buckling curve b (buckling about the z-axis). Subsequently, the maximum design value of the compression force ( $N_{Ed}$ ) is verified against buckling as follows:

$$\frac{N_{Ed}}{N_{b;Rd}} = \frac{N_{Ed}}{\chi A_c f_y} = \frac{8.70 \times 10^6}{0.84 \times 3.19 \times 10^4 \times 355} = 0.91 \leq 1.0 \rightarrow \text{sufficient}$$

Although not represented by the braced frame representation of the infilled frame, the column is in its strong direction subject to bending with axial compression, where the bending results from the lateral force:  $M_{y;Ed} = V_{Ed} \times (\frac{1}{2}h_b + x)$  (Figure 8-3).

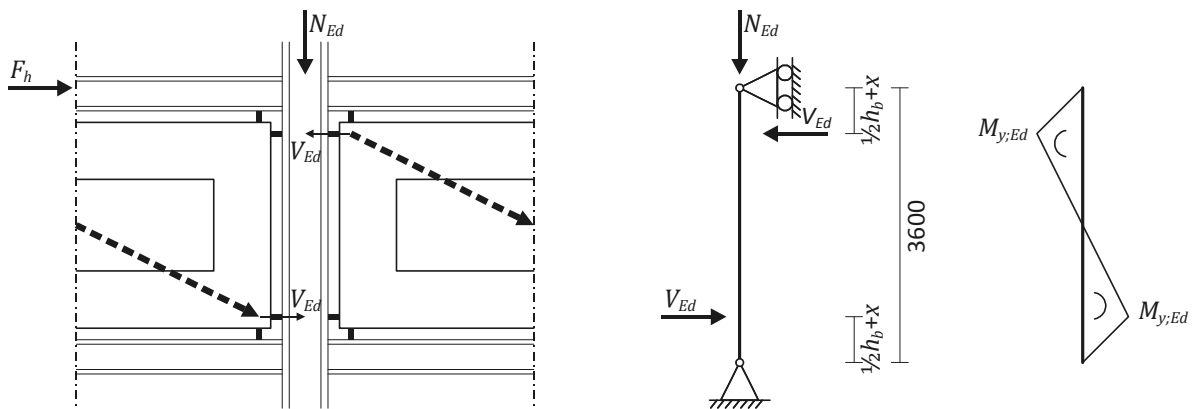


Figure 8-3: Column subject to bending with axial compression

Accordingly, the column is to be verified against bending with axial compression as follows (EN 1993 1-1 section 6.3.3):

$$\frac{N_{Ed}}{\chi_y N_{Rk}} + k_{yy} \frac{M_{y;Ed}}{\chi_{LT} M_{y;Rk}} \leq 1$$

where  $M_{y;Ed}$  and  $M_{y;Rk}$  are the design value of the maximum moments and the design buckling resistance moment of the column respectively. The latter is taken as the product of the yield stress ( $f_y$ ) and the plastic section modulus ( $W_{pl;y}$ ). Reduction factor  $\chi_y$  for flexural buckling about the (strong) y-axis equals:

$$\bar{\lambda}_y = \frac{L_{cr}}{i_y} \times \frac{1}{\pi \sqrt{\frac{E}{f_y}}} = \frac{3600}{163} \times \frac{1}{\pi \sqrt{\frac{2.1 \times 10^5}{355}}} = 0.29 \rightarrow \chi_y = 0.98$$

The interaction factor  $k_{yy}$  is derived from Annex B of EN 1993-1-1:

$$k_{yy} = C_{my} \left( 1 + (\bar{\lambda}_y - 0.2) \frac{N_{Ed}}{\chi_y N_{Rk}} \right) \leq C_{my} \left( 1 + 0.8 \frac{N_{Ed}}{\chi_y N_{Rk}} \right)$$

The equivalent uniform moment factor  $C_{my}$  is derived from Table B.3 of EN 1993-1-1:

$$C_{my} = 0.6 + 0.4\psi \geq 0.4 \text{ where } \psi = -1$$

Accordingly,

$$C_{my} = 0.4$$

$$k_{yy} = 0.4 \left( 1 + (0.29 - 0.2) \frac{8.70 \times 10^6}{0.98 \times 1.13 \times 10^7} \right)$$

$$\leq 0.4 \left( 1 + 0.8 \frac{8.70 \times 10^6}{0.98 \times 1.13 \times 10^7} \right)$$

$$k_{yy} = 0.43$$

Subsequently, the maximum design value of the compression force and bending moment are verified against buckling as follows:

$$\frac{8.70 \times 10^6}{0.98 \times 1.13 \times 10^7} + 0.43 \times \frac{2.10 \times 10^8}{1.0 \times 1.77 \times 10^9} = 0.84 \leq 1.0 \rightarrow \text{sufficient}$$

Having dimensioned the frame members, the panel dimensions result from the frame member heights ( $h_c = 395$  and  $h_b = 300$  mm) and the gap width  $g = 50$  mm. Accordingly, the panel dimensions  $l \times h$  are  $6705 \times 3200$  mm and  $4905 \times 3200$  mm for the exterior and interior bay respectively.

### Step 3: Design the frame joints

A complete frame joint design is not considered in this example. Design rules for frame joints can be found in e.g. Eurocode 3 EN 1993-1-8. For this example, an initial joint stiffness ( $S_{j,ini}$ ) is estimated using design equation [6-3]. A bolted end plate connection is assumed ( $k_x = 11.5$ ), with a lever arm (centre of compression to the bolt row in tension)  $z = 200$  mm. This gives the following initial rotational stiffness for the frame joints:

$$S_{j,ini} = \frac{Ez^2t_f}{k_x} = \frac{2.1 \times 10^5 \times 200^2 \times 40}{11.5} = 29.2 \times 10^3 \text{ kNm/rad}$$

This rotational stiffness will be needed to establish the infilled frame stiffness in step 6.

### Step 4: Design the panel-to-frame connections

a) Design the connection

The position of the bolts on the flanges is taken  $\zeta = x / b = \frac{1}{3}$ . Accordingly the distance  $x$  for the columns and beams ( $b = 300$  mm) equals 112.5 mm. Subsequently, the



characteristics for the HE300B section for  $\zeta = \frac{3}{8}$  are taken from Table 6-3 and shown in Table 8-1. The HE360M characteristics were derived performing a numerical simulation for that section with the finite element discussed in section 5.1.

Table 8-1: Used characteristics for sections subject to transverse compression

Section	$k_{c_{1+2}}$ [kN/m]	$F_{c_{1+2}}$ [kN]
HE300B	7.29E+05	589
HE360M	37.4E+05	1501

b) Estimate the design force for the panel-to-frame connections

Having obtained the maximum lateral load acting on a single-story, single-bay infilled frame ( $V_{Ed}$ ), the load that acts on the panel-to-column and panel-to-beam connection can be derived using equations [7-21] and [7-22]:

- For the exterior bays:

$$\beta_f = \frac{L}{L - h_c} = \frac{7200}{7200 - 395} = 1.06$$

$$N_{x;c;col} = \frac{V_{Ed}H}{(H - h_b - 2x)\beta_f} = \frac{800 \times 3600}{(3600 - 300 - 225)1.06} = 885 \text{ kN}$$

$$N_{x;c;beam} = N_{x;c;col} \tan \varphi_p = 414 \text{ kN}$$

- For the interior bay:

$$\beta_f = \frac{L}{L - h_c} = \frac{5400}{5400 - 395} = 1.08$$

$$N_{x;c;col} = V_{Ed} \frac{H}{(H - h_b - 2x)\beta_f} = 800 \frac{3600}{(3600 - 300 - 225)1.08} = 868 \text{ kN}$$

$$N_{x;c;beam} = N_{x;c;col} \tan \varphi_p = 559 \text{ kN}$$

Thus, the maximum panel-to-column and panel-to-beam connection forces equal 885 kN and 559 kN respectively.

c) Select the bolt size and bolt grade

8.8M30 bolts with grade 8 nuts are selected to construct the connection. For this bolt-nut assembly, the stripping strength is determined according to Alexander's theory (see chapter 2.2). The shear areas of the bolt ( $A_{Sb}$ ) and nut threads ( $A_{Sn}$ ) equal:

$$A_{sb} = \frac{\pi m^* D_1}{p} \left[ \frac{p}{2} + \frac{1}{\sqrt{3}} (d_2 - D_1) \right]$$

$$A_{sb} = \frac{\pi \times 22.5 \times 26.211}{3.5} \times \left[ \frac{3.5}{2} + \frac{1}{\sqrt{3}} (27.727 - 26.211) \right] = 1389.7 \text{ mm}^2$$

$$A_{sn} = \frac{\pi m^* d}{p} \left[ \frac{p}{2} + \frac{1}{\sqrt{3}} (d - D_2) \right]$$

$$A_{sn} = \frac{\pi \times 22.5 \times 30.000}{3.5} \times \left[ \frac{3.5}{2} + \frac{1}{\sqrt{3}} (30.000 - 27.727) \right] = 1855.4 \text{ mm}^2$$

Reduction factors  $C_1$  to  $C_3$ :

$$C_1 = -\left(\frac{S}{D}\right)^2 + 3.8\left(\frac{S}{D}\right) - 2.61 = -\left(\frac{46}{30}\right)^2 + 3.8\left(\frac{46}{30}\right) - 2.61 = 0.87$$

$$R_s = \frac{f_{un} A_{sn}}{f_{ub} A_{sb}} = \frac{800 \times 1855.4}{800 \times 1389.7} = 1.34$$

$$C_2 = 5.594 - 13.682R_s + 14.107R_s^2 - 6.057R_s^3 + 0.9353R_s^4 = 1.03$$

$$C_3 = 0.897$$

Accordingly, the bolt ( $F_{sb}$ ) and nut ( $F_{sn}$ ) thread stripping strengths are:

$$F_{sb} = \frac{f_{yb}}{\sqrt{3}} A_{sb} C_1 C_2 = \frac{640}{\sqrt{3}} \times 1389.7 \times 0.87 \times 1.03 = 460 \text{ kN}$$

$$F_{sn} = \frac{f_{yn}}{\sqrt{3}} A_{sn} C_1 C_3 = \frac{640}{\sqrt{3}} \times 1855.4 \times 0.87 \times 0.897 = 535 \text{ kN}$$

Bolt thread stripping failure governs the strength of the bolt-nut assembly. The strength of two bolts equals  $2F_{sb} = 920 \text{ kN}$  which is larger than the maximum panel-to-column force ( $N_{x;c,col}$ ):

$$\frac{N_{x;c,col}}{2F_{sb}} = \frac{885}{920} = 0.96 \leq 1.0 \rightarrow \text{sufficient}$$

d) Check the flange capacity

To allow bolt failure governing the strength of the structure, the flange capacity (as defined in chapter 6) of the previous selected column ( $F_{c,col}$ ) must be larger than the capacity of the two bolts:

$$\frac{F_{c;col}}{2F_{sb}} = \frac{1501}{920} = 1.63 \geq 1.0 \rightarrow \text{sufficient}$$

Finally, the flange capacity of the beam ( $F_{c;beam}$ ) is checked against the maximum panel-to-beam connection force ( $N_{x;c;beam}$ ) as follows:

$$\frac{N_{x;c;beam}}{F_{c;beam}} = \frac{559}{589} = 0.95 \leq 1.0 \rightarrow \text{sufficient}$$

Because the margin on the panel-to-beam connection is larger than the margin on the panel-to-column connection (0.95 and 0.96 respectively), bolt failure of the panel-to-column connection will govern the strength of the structure, although the difference is only marginal. Backing plates should be applied to increase the beam flange capacity, in order to guarantee the bolts of the panel-to-column connection to govern the strength.

e) Determine the effective connection stiffness

Subsequently, the effective panel-to-frame connection stiffness ( $k_{c,eff}$ ) according to equation [7-25] is calculated, which includes, in addition to the initial spring stiffness ( $k_{c;ini}$ ), stiffness coefficients for shear ( $k_{c;V}$ ) and bending deformation ( $k_{c;M}$ ).

The initial connection stiffness consists of two components which are the flange with web stiffness ( $k_{c_{1+2}}$ ) and the bolt with cap stiffness ( $k_{c_{3+4}}$ ). The flange with web stiffness is given in Table 8-1. The bolt with cap stiffness is predicted using the experimentally determined stiffness for a M24 bolt with cap as follows:

$$(k_{c_{3+4}})_{M30} = \frac{A_{s;M30}}{A_{s;M24}} \times (k_{c_{3+4}})_{M24} = \frac{561}{353} \times 6.0 \times 10^5 = 9.5 \times 10^5 \text{ kN/m}$$

Accordingly, the initial panel-to-beam connection stiffness equals (using equation [7-26]):

$$k_{c;ini;beam} = \left[ \frac{1}{k_{c_{1+2}}} + \frac{1}{2k_{c_{3+4}}} \right]^{-1} = \left[ \frac{1}{7.29 \times 10^5} + \frac{1}{2 \times 9.5 \times 10^5} \right]^{-1} \\ = 5.27 \times 10^5 \text{ kN/m}$$

and the initial panel-to-column connection spring stiffness:

$$k_{c;ini;col} = \left[ \frac{1}{37.4 \times 10^5} + \frac{1}{2 \times 9.5 \times 10^5} \right]^{-1} = 1.26 \times 10^6 \text{ kN/m}$$

The stiffness coefficient resulting from shear deformation for the panel-to-beam connection given by equation [7-27]:

$$k_{c;V;beam} = \frac{GA_{v;b}(L - h_c)}{(L - h_c - x)x} = \frac{8.08 \times 10^4 \times 4743 \times (7200 - 395)}{(7200 - 395 - 112.5)112.5} = 3.46 \times 10^6 \text{ kN/m}$$

The stiffness coefficient resulting from shear deformation for the panel-to-column connection is given by equation [7-28]:

$$k_{c;V;col} = \frac{GA_{v;c}(H - h_b)}{(H - h_b - x)x} = \frac{8.08 \times 10^4 \times 10240 \times (3600 - 300)}{(3600 - 300 - 112.5)112.5} = 3.92 \times 10^6 \text{ kN/m}$$

The stiffness coefficient resulting from bending deformation is considered negligible ( $S_j \neq 0$ ). Accordingly, the effective panel-to-column and panel-to-frame connection stiffness is:

$$k_{c,eff;beam} = \frac{1}{k_{c;ini;beam}} + \frac{1}{k_{c;V;beam}} = \left[ \frac{1}{5.27 \times 10^5} + \frac{1}{3.46 \times 10^6} \right]^{-1} = 4.57 \times 10^5 \text{ kN/m}$$

$$k_{c,eff;col} = \frac{1}{k_{c;ini;col}} + \frac{1}{k_{c;V;col}} = \left[ \frac{1}{1.26 \times 10^6} + \frac{1}{3.92 \times 10^6} \right]^{-1} = 9.53 \times 10^5 \text{ kN/m}$$

Step 5: Design the panels

The required amount of reinforcement to provide the demanded strength such that bolt failure governs the strength ( $F_p > 920 \text{ kN}$ ) is determined with the strut-and-tie method. Figure 8-4 shows the panels with the strut-and-tie models (struts 1 to 10, ties 11 to 18 and nodes A to J) for the middle and exterior bays. The distance from the nodes to panel edges is taken 75 mm. The strut-and-tie models are analyzed elastically to find the internal forces in the individual members. Subsequently, the material properties of the struts, nodes and ties are determined and the dimensions of the struts and nodes are evaluated.

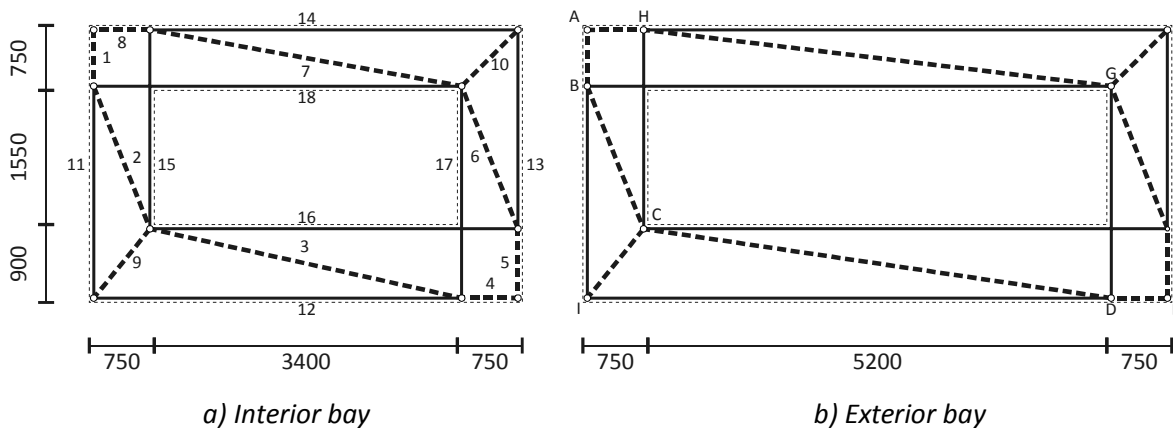


Figure 8-4: Infill panels with strut-and-tie models

## DESIGN RECOMMENDATIONS

Table 8-2 gives the maximum axial tensile forces in the ties ( $N_{x,max}$ ) which have to be supported by the reinforcement. The required steel area ( $A_{s,min}$ ) is given which can be derived by dividing the tie force by the design yield strength of the reinforcing steel. The design yield strength for the steel reinforcement equals:

$$f_{syd} = \frac{f_{sy}}{\gamma_s} = \frac{500}{1.15} = 435 \text{ N/mm}^2$$

In the last column, the selected reinforcement is shown ( $A_s$ ).

Table 8-2: Maximum tensile force in reinforcement

Members	$N_{x,max}$ [kN]	$N_{x,max}$ [kN]	$A_{s,min}$ [mm <sup>2</sup> ]	$A_{s,min}$ [mm <sup>2</sup> ]	$A_s$ [mm <sup>2</sup> ]
	(Int. bay)	(Ext. bay)	(Int. bay)	(Ext. bay)	
<b>11, 12, 13, 14</b>	810 (tie 11)	1014 (tie 11)	1862	2331	3Ø32 = 2413
<b>15, 16, 17, 18</b>	494 (tie 18)	509 (tie 11)	1136	1170	2Ø32 = 1608

Table 8-3 gives the compressive axial force, the stress limit and the minimal height of each strut for the interior and exterior bay. The strut height is derived by dividing the axial strut force by the stress limit for the strut and the panel thickness ( $t_p = 300$  mm). The design strength of the concrete ( $f_{cd}$ ) is related to the characteristic cylinder strength ( $f_{ck}$ ) as follows, using equation [2-15]:

$$f_{cd} = \frac{f_{ck}}{\gamma_c} = \frac{50}{1.5} = 33.3 \text{ N/mm}^2$$

Accordingly, the stress limit  $f_{cu}$  for the struts equals (using equation [2-14]):

$$f_{cu} = k_s f_{cd}$$

Table 8-3: Strut properties

Strut	$k_s$ [-]	$f_{cu}$ [N/mm <sup>2</sup> ]	$N_{x,strut}$	$N_{x,strut}$	$h_{strut,min}$	$h_{strut,min}$
			[kN] (Int. bay)	[kN] (Ext. bay)	[mm] (Int. bay)	[mm] (Ext. bay)
<b>1</b>	1.0	33.3	-591	-428	59	43
<b>2</b>	1.0	33.3	-1485	-1529	149	153
<b>3</b>	1.0	33.3	-1603	-1748	160	175
<b>4</b>	1.0	33.3	-920	-920	92	92
<b>5</b>	1.0	33.3	-591	-428	59	43
<b>6</b>	1.0	33.3	-1279	-1235	128	124
<b>7</b>	1.0	33.3	-1557	-1667	156	167
<b>8</b>	1.0	33.3	-920	-920	92	92
<b>9</b>	0.48	16.0	-1037	-1298	216	270
<b>10</b>	0.48	16.0	-870	-1041	181	217

DESIGN RECOMMENDATIONS

Table 8-4 gives the node properties and the minimal strut height of the adjacent strut. The concrete compressive stresses ( $f_{cu}$ ) in the nodal zone boundaries are limited as follows, using equation [2-16]:

$$f_{cu} = k_n \left( 1 - \frac{f_{ck}}{250} \right) f_{cd}$$

Table 8-4: Node properties

Node	Type	$k_n$ [-]	$f_{cu}$ [N/mm <sup>2</sup> ]	Strut	$N_{x,max}$ [kN] (Int. bay)	$N_{x,max}$ [kN] (Ext. bay)	$h_{strut,min}$ [mm] (Int. bay)	$h_{strut,min}$ [mm] (Ext. bay)
A	CCC	1.00	27	8	-920	-920	114	114
B	CCT	0.85	23	2	-1485	-1529	215	222
C	CCC	1.00	27	3	-1603	-1748	198	216
D	CCT	0.85	23	3	-1603	-1748	232	253
E	CCC	1.00	27	4	-920	-920	114	114
F	CCT	0.85	23	6	-1279	-1235	185	179
G	CCC	1.00	27	7	-1557	-1667	192	206
H	CCT	0.85	23	7	-1557	-1667	226	242
I	CTT	0.75	20	9	-1037	-1298	173	216
J	CTT	0.75	20	10	-870	-1041	145	174

Finally, it has been checked if the size of the struts and nodes is compatible with the actual size of the structure to guarantee the development of the strut-and-tie model in the panels.

Having dimensioned the panel reinforcement, the diagonal panel stiffness is derived. To find the diagonal panel stiffness ( $k_p$ ) the panels are modeled as equivalent frames having dimensions  $h' \times l'$  of 4150 x 2375 mm and 5950 x 2375 mm respectively (Figure 8-5).

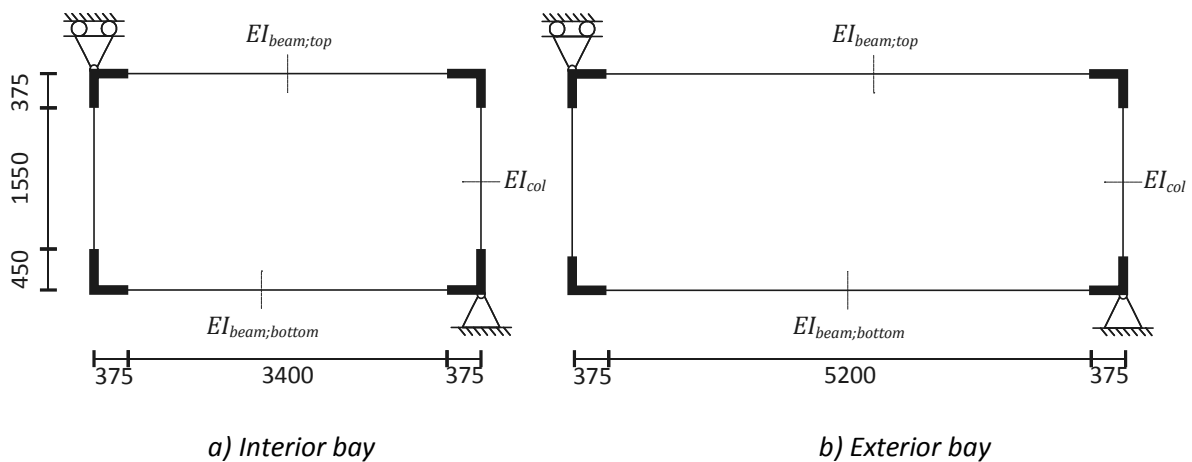


Figure 8-5: Equivalent frame representation of infill panels

DESIGN RECOMMENDATIONS

Subsequently, the stiffness resulting from bending of the frame members is calculated. Table 8-5 gives the applied bending stiffness ( $EI$ ) of the equivalent frame members. The bending stiffness of cracked concrete has been determined using  $M-N-\kappa$ -diagrams.

Using equation [7-20] for the diagonal panel stiffness ( $k_p$ ) in combination with the properties given in Table 8-5 and Table 8-6 gives an initial and secant diagonal panel stiffness, shown in Table 8-7.

Table 8-5: Properties used for equivalent frame

	Interior bay		Exterior bay	
	Initial	Cracked	Initial	Cracked
$EI_{b,top}$ [kNm <sup>2</sup> ]	3.90E+05	1.29E+05	3.90E+05	1.29E+05
$EI_{b,bottom}$ [kNm <sup>2</sup> ]	6.74E+05	1.96E+05	6.74E+05	1.96E+05
$EI_{col}$ [kNm <sup>2</sup> ]	3.90E+05	1.22E+05	3.90E+05	1.22E+05

Table 8-6: Properties used for calculation of the diagonal panel stiffness

	Interior bay	Exterior bay
$\eta$ [-]	1.89	2.24
$\varphi_p = \tan^{-1}(h'/l')$	0.57	0.44
$\beta_p = l'/a$ [-]	1.22	1.14
$\gamma_p = h'/b$ [-]	1.53	1.53

$$k_p = \frac{48\beta_p^3 EI_{b,top} \beta_p^3 EI_{b,bottom} \gamma_p^3 EI_{col}}{h'^2 (\gamma_p^3 EI_{col} \beta_p^3 EI_{b,bottom} l' + \gamma_p^3 EI_{col} \beta_p^3 EI_{b,top} l' + 2\beta_p^3 EI_{b,bottom} \beta_p^3 EI_{b,top} h')} \eta \cos^2 \varphi_p$$

Table 8-7: Diagonal panel stiffness

	Interior bay	Exterior bay
$k_{p,ini}$	5.05E+05	2.38E+05
$k_{p,sec}$	1.59E+05	7.50E+04

The diagonal panel stiffnesses will be used to establish the lateral infilled frame stiffness in step 6.

Step 6: Determine the lateral stiffness of the single-story single-bay infilled frames

The lateral stiffness of the single-story single-bay infilled frames is determined using equations [7-38] to [7-42].

- Interior bay:

Frame:  $L = 5400$  mm;  $H = 3600$  mm;  $\tan \varphi_f = H/L = 0.59$ ;  $L_{strut} = L / \cos \varphi_f = 6490$  mm

Panel:  $l = 4900$  mm;  $h = 3200$  mm;  $\tan \varphi_p = h/l = 0.57$ ;  $l_{strut} = L / \cos \varphi_p = 5679$  mm

Beams HE300B:  $I_b = 2.52E+08$  mm<sup>4</sup>;  $h_b = 300$  mm;  $A_b = 1.49E+04$  mm<sup>2</sup>;  
 $A_{v;b} = 4.74E+03$  mm<sup>2</sup>

Columns HE360M:  $I_c = 8.49E+08$  mm<sup>4</sup>;  $h_c = 395$  mm;  $A_c = 3.19E+04$  mm<sup>2</sup>;  
 $A_{v;c} = 1.02E+04$  mm<sup>2</sup>

$S_j = 29.2E+10^9$  Nmm/rad

$x = 112.5$  mm

$\beta_f = L/(L - h_c) = 1.08$

$\gamma_f = H/(H - h_b) = 1.09$

$$k_{h,f} = \left[ \frac{LH^2}{24E\beta_f^3 I_b} + \frac{H^3}{24E\gamma_f^3 I_c} + \frac{H^2}{4\beta_f^2 S_j} + \frac{L}{2E\beta_f A_b} + \frac{H \tan^2 \varphi_f}{2E\gamma_f A_c} + \frac{H}{2G\gamma_f A_{v;c}} + \frac{H \tan \varphi_f}{2G\beta_f A_{v;b}} \right]^{-1} = 6.45 \times 10^3 \text{ kN/m}$$

$$k_{h,p;ini} = \frac{k_{p;ini} \cos \varphi_f \cos \varphi_p l_{strut} (H - h_b - 2x) \beta_f}{HL_{strut}} = 2.85 \times 10^5 \text{ kN/m}$$

$$k_{h,p;sec} = \frac{k_{p;sec} \cos \varphi_f \cos \varphi_p l_{strut} (H - h_b - 2x) \beta_f}{HL_{strut}} = 8.95 \times 10^4 \text{ kN/m}$$

$$k_{h,\Sigma con} = \frac{k_{c;eff;beam} k_{c;eff;col} l_{strut} (H - h_b - 2x) \beta_f}{2HL_{strut} (k_{c;eff;beam} + k_{c;eff;col} \tan \varphi_p \tan \varphi_f)} = 2.03 \times 10^5 \text{ kN/m}$$

$$k_{h,col} = \frac{EA_c (L - h_c) (H - h_b - 2x) \beta_f}{H^2 \tan \varphi_p \tan \varphi_f (L - h_c - x)} = 4.08 \times 10^6 \text{ kN/m}$$

$$k_{if} = k_{h,f} + \left[ \frac{1}{k_{h;p}} + \frac{1}{k_{h,\Sigma con}} + \frac{1}{k_{h,col}} \right]^{-1}$$

$$\mathbf{k_{if;ini} = 6.45 \times 10^3 + \left[ \frac{1}{2.85 \times 10^5} + \frac{1}{2.03 \times 10^5} + \frac{1}{4.08 \times 10^6} \right]^{-1} = 1.22 \times 10^5 \text{ kN/m}}$$

$$\mathbf{k_{if;sec} = 6.45 \times 10^3 + \left[ \frac{1}{8.95 \times 10^4} + \frac{1}{2.03 \times 10^5} + \frac{1}{4.08 \times 10^6} \right]^{-1} = 6.76 \times 10^4 \text{ kN/m}}$$



▪ Exterior bays:

Frame:  $L = 7200$  mm;  $H = 3600$  mm;  $\tan \varphi_f = H/L = 0.46$ ;  $L_{strut} = L / \cos \varphi_f = 8050$  mm

Panel:  $l = 6700$  mm;  $h = 3200$  mm;  $\tan \varphi_p = h/l = 0.44$ ;  $l_{strut} = L / \cos \varphi_p = 7259$  mm

Beams HE300B:  $I_b = 2.52E+08$  mm<sup>4</sup>;  $h_b = 300$  mm;  $A_b = 1.49E+04$  mm<sup>2</sup>;  
 $A_{v;b} = 4.74E+03$  mm<sup>2</sup>

Columns HE360M:  $I_c = 8.49E+08$  mm<sup>4</sup>;  $h_c = 395$  mm;  $A_c = 3.19E+04$  mm<sup>2</sup>;  
 $A_{v;c} = 1.02E+04$  mm<sup>2</sup>

$S_j = 29.2E+10^9$  Nmm/rad

$x = 112.5$  mm

$\beta_f = L/(L - h_c) = 1.06$

$\gamma_f = H/(H - h_b) = 1.09$

$$k_{h,f} = \left[ \frac{LH^2}{24E\beta_f^3 I_b} + \frac{H^3}{24E\gamma_f^3 I_c} + \frac{H^2}{4\beta_f^2 S_j} + \frac{L}{2E\beta_f A_b} + \frac{H \tan^2 \varphi_f}{2E\gamma_f A_c} + \frac{H}{2G\gamma_f A_{v;c}} + \frac{H \tan \varphi_f}{2G\beta_f A_{v;b}} \right]^{-1} = 5.66 \times 10^3 \text{ kN/m}$$

$$k_{h,p;ini} = \frac{k_{p;ini} \cos \varphi_f \cos \varphi_p l_{strut} (H - h_b - 2x) \beta_f}{HL_{strut}} = 1.57 \times 10^5 \text{ kN/m}$$

$$k_{h,p;sec} = \frac{k_{p;sec} \cos \varphi_f \cos \varphi_p l_{strut} (H - h_b - 2x) \beta_f}{HL_{strut}} = 4.95 \times 10^4 \text{ kN/m}$$

$$k_{h,\Sigma con} = \frac{k_{c;eff;beam} k_{c;eff;col} l_{strut} (H - h_b - 2x) \beta_f}{2HL_{strut} (k_{c;eff;beam} + k_{c;eff;col} \tan \varphi_p \tan \varphi_f)} = 2.61 \times 10^5 \text{ kN/m}$$

$$k_{h,col} = \frac{EA_c (L - h_c) (H - h_b - 2x) \beta_f}{H^2 \tan \varphi_p \tan \varphi_f (L - h_c - x)} = 7.31 \times 10^6 \text{ kN/m}$$

$$k_{if} = k_{h,f} + \left[ \frac{1}{k_{h;p}} + \frac{1}{k_{h,\Sigma con}} + \frac{1}{k_{h,col}} \right]^{-1}$$

$$\mathbf{k_{if;ini} = 5.66 \times 10^3 + \left[ \frac{1}{1.57 \times 10^5} + \frac{1}{2.61 \times 10^5} + \frac{1}{7.31 \times 10^6} \right]^{-1} = 1.02 \times 10^5 \text{ kN/m}}$$

$$\mathbf{k_{if;sec} = 5.66 \times 10^3 + \left[ \frac{1}{4.95 \times 10^4} + \frac{1}{2.61 \times 10^5} + \frac{1}{7.31 \times 10^6} \right]^{-1} = 4.70 \times 10^4 \text{ kN/m}}$$

Step 7: Check the strength of the infilled frames

- interior bay:

$$G_p = (4.9 \times 3.2 - 3.4 \times 1.55) \times 0.3 \times 24 = 75 \text{ kN}$$

$$\mu = 1 - \frac{k_{h,f}}{k_{if;sec}} = 1 - \frac{6.45 \times 10^3}{6.76 \times 10^4} = 0.90$$

Mode 1: Panel-to-column connection failure (according to equation [7-48]):

$$F_{u;if} = F_{u;c,col} \frac{(H - h_b - 2x)\beta_f}{\mu H} = 920 \frac{(3600 - 300 - 225)1.08}{0.90 \times 3600} = \mathbf{937 \text{ kN}}$$

Mode 2: Panel-to-beam connection failure (according to equation [7-50]):

$$\begin{aligned} F_{u;if} &= (F_{u;c,beam} - \frac{1}{2}G_p) \frac{(L - h_c - 2x)\beta_f}{\mu H} \\ &= (589 - \frac{1}{2} \times 75) \frac{(5400 - 395 - 225)1.08}{0.90 \times 3600} = \mathbf{873 \text{ kN}} \end{aligned}$$

Thus, the ultimate strength of the single-story single-bay (interior) infilled frame equals 873 kN and is governed by panel-to-beam connection failure.

- Exterior bays:

$$G_p = (6.7 \times 3.2 - 5.2 \times 1.55) \times 0.3 \times 24 = 96 \text{ kN}$$

$$\mu = 1 - \frac{k_{h,f}}{k_{if;sec}} = 1 - \frac{5.66 \times 10^3}{4.70 \times 10^4} = 0.88$$

Mode 1: Panel-to-column connection failure (according to equation [7-48]):

$$F_{u;if} = F_{u;c,col} \frac{(H - h_b - 2x)\beta_f}{\mu H} = 920 \frac{(3600 - 300 - 225)1.06}{0.88 \times 3600} = \mathbf{945 \text{ kN}}$$

Mode 2: Panel-to-beam connection failure (according to equation [7-50]):

$$\begin{aligned} F_{u;if} &= (F_{u;c,beam} - \frac{1}{2}G_p) \frac{(L - h_c - 2x)\beta_f}{\mu H} \\ &= (589 - \frac{1}{2} \times 96) \frac{(7200 - 400 - 225)1.06}{0.88 \times 3600} = \mathbf{1189 \text{ kN}} \end{aligned}$$

Thus, the ultimate strength of the single-story single-bay (exterior) infilled frame equals 945 kN and is governed by panel-to-column connection failure.

Finally, a check is made for ultimate strength of the structure. Therefore, the design value of the lateral load  $V_{Ed}$  (obtained in step 1) is compared with the minimum lateral resistance of the structure as follows:

$$\frac{V_{Ed}}{F_{u;lf}} = \frac{800}{873} = 0.92 \leq 1.0 \rightarrow \text{sufficient}$$

**Step 8: Determine the horizontal deflection of the building**

The horizontal deflection of the building consists of two components: flexure due to axial forces in the columns, and shear due to panel deformations. Rotation of the foundation due to axial forces in the piles is not considered in this design example.

The total axial bending stiffness of the braced frame equals:

$$EAc^2 = \sum EA_i \times c_i^2 = 2 \times (210 \times 3.19 \times 10^4 \times (2.7^2 + 9.9^2)) = 1.41 \times 10^9 \text{ kNm}^2$$

where  $A_i$  is the column area and  $c_i$  is the distance to the neutral axis of the braced frame. Accordingly, the deflection at the top due to bending ( $\delta_b$ ) equals:

$$\delta_b = \frac{1}{8} \frac{q_{eq} \gamma_q H^4}{(EAc^2)} = \frac{23.4 \times 1.0 \times 72^4}{8 \times 1.41 \times 10^9} = 0.056 \text{ m}$$

The shear stiffness of one story is assumed to be equal to the sum of the three previously obtained single bay stiffnesses. As a consequence, the contribution of the frame is slightly overestimated as the bending stiffness of 2 columns and 3 beams are twice taken into account. However, due to the nature of the semi-integral infilled frame, major part of the load is transferred through the panels while the contribution of the frame is only marginal. Therefore, this assumption is acceptable for preliminary design considerations. Accordingly, the shear stiffness for one story ( $k_{lf;storey}$ ) equals:

$$k_{lf;storey} = 2k_{lf;sec;ext} + k_{lf;sec;int} = 2 \times 4.70 \times 10^4 + 6.76 \times 10^4 = 1.62 \times 10^5 \text{ kN/m}$$

The deflection of a single story due to shear force equals:

$$\delta_i = \frac{V_i}{k_{lf;storey}}$$

Accordingly the deflection at the top of the structure due to shear ( $\delta_s$ ) is the sum of the story deflections (see Table 8-8) and equals:

$$\delta_s = \sum_{i=1}^n \delta_i = 0.104 \text{ m}$$

Table 8-8: Story deflections due to shear force

Story no.	$q_{eq}h$ [kN]	$V_i$ [kN]	$k_{if;storey}$ [kN/m]	$\delta_i$ [m]	$\sum\delta_i$ [m]
20	42	42	1.62E+05	2.60E-04	1.04E-01
19	84	126	1.62E+05	7.79E-04	1.03E-01
18	84	210	1.62E+05	1.30E-03	1.03E-01
17	84	294	1.62E+05	1.82E-03	1.01E-01
16	84	378	1.62E+05	2.34E-03	9.95E-02
15	84	462	1.62E+05	2.86E-03	9.72E-02
14	84	546	1.62E+05	3.38E-03	9.43E-02
13	84	630	1.62E+05	3.90E-03	9.09E-02
12	84	714	1.62E+05	4.42E-03	8.70E-02
11	84	798	1.62E+05	4.94E-03	8.26E-02
10	84	882	1.62E+05	5.46E-03	7.77E-02
9	84	966	1.62E+05	5.97E-03	7.22E-02
8	84	1050	1.62E+05	6.49E-03	6.62E-02
7	84	1134	1.62E+05	7.01E-03	5.97E-02
6	84	1218	1.62E+05	7.53E-03	5.27E-02
5	84	1302	1.62E+05	8.05E-03	4.52E-02
4	84	1386	1.62E+05	8.57E-03	3.71E-02
3	84	1470	1.62E+05	9.09E-03	2.86E-02
2	84	1554	1.62E+05	9.61E-03	1.95E-02
1	42	1596	1.62E+05	9.87E-03	9.87E-03

For the total deflection of the structure, the deflections for bending are added to the deflections for shear. This gives the following result:

$$\delta_{total} = \delta_b + \delta_s = 0.056 + 0.104 = 0.160 \text{ m}$$

$$\frac{\delta_{total}}{H} = \frac{0.160}{72} = 1/450H > 1/500H$$

The actual deflection of the structure is too large by 10%, but is acceptable in this preliminary phase of the design.

### 8.3 Towards a completely integrated tall building system

Finally, some suggestions are made for the development of the semi-integral infilled frame into a completely integrated tall building system. An investigation into building concepts using semi-integral infilled frames, and possible construction methods can be found in the Master's thesis of Kansen (2009). In this work, a construction method has been developed for a high-rise building structure consisting of semi-integral infilled frames, aiming at a high level of prefabrication and a decrease of the construction time. The construction method resulting from this investigation is presented stepwise in Figure 8-6 to Figure 8-8. For a comprehensive description of the original research, one is referred to the publication.

Construction method

The proposed method of construction for a semi-integral infilled frame building structure consists of the following 6 steps:

Step 1: The steel columns and beams for the first story have been assembled and the floor elements for the first story floor have been installed. The bolts of the discrete panel-to-frame connection on the columns and beams are used to set the exact position for the prefabricated elements to be installed (Figure 8-6a).

Step 2: The prefabricated elements for the first story are installed, supplied with insulation (indicated yellow), windows, an outer skin of cladding (indicated light gray) and preinstalled installations for vertical transport within the building. These elements arrive ready for installation on-site, and are lifted directly from a truck into place. With a minimum of manpower, the prefabricated elements are immediately fixed to the steel structure by tightening the bolts on the columns (Figure 8-6b).

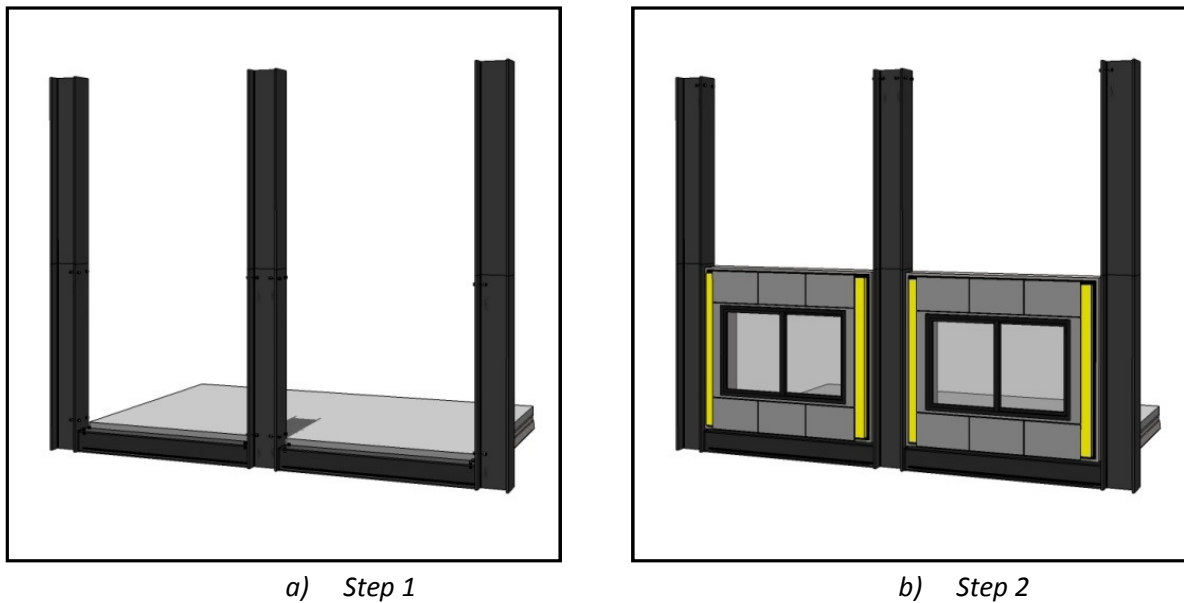
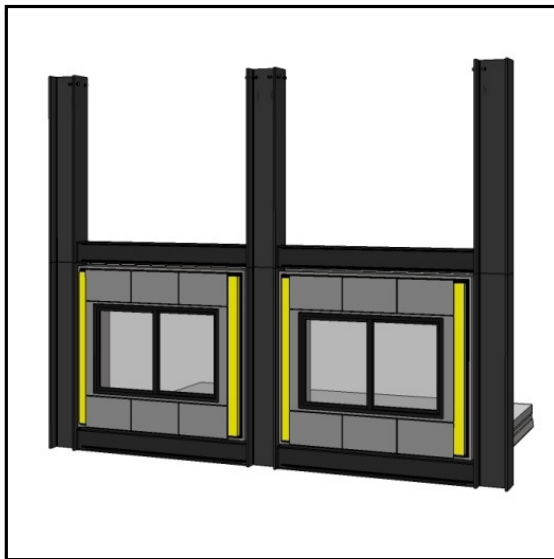


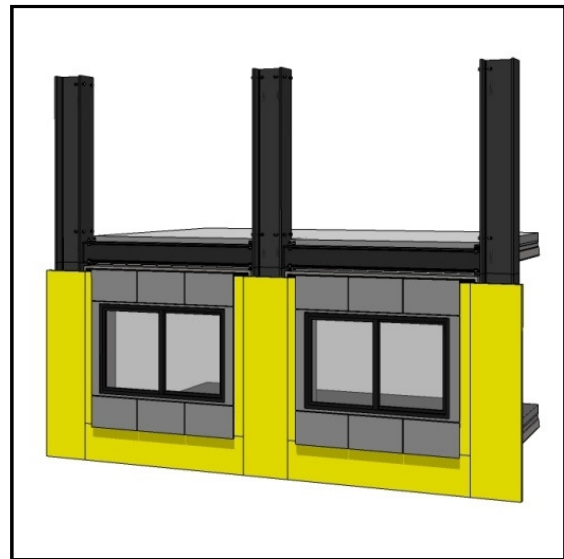
Figure 8-6: Step 1 and 2 of construction process for semi-integral infilled frame building structure

Step 3: The beams for the following story floor are assembled to the columns. Subsequently the prefabricated elements are fixed in vertical direction by tightening the bolts on the top beams. At that moment, stability of the story against lateral loads is provided (Figure 8-7a).

Step 4: The floor elements for the following floor are installed and absent insulation between the prefabricated elements is fixed. Consequently, a thermal, wind and waterproof story is provided and does not require protection from weather. The bolts on the columns and beams are used to set the exact position for the prefabricated elements to be installed on the next story (Figure 8-7b).



a) Step 3

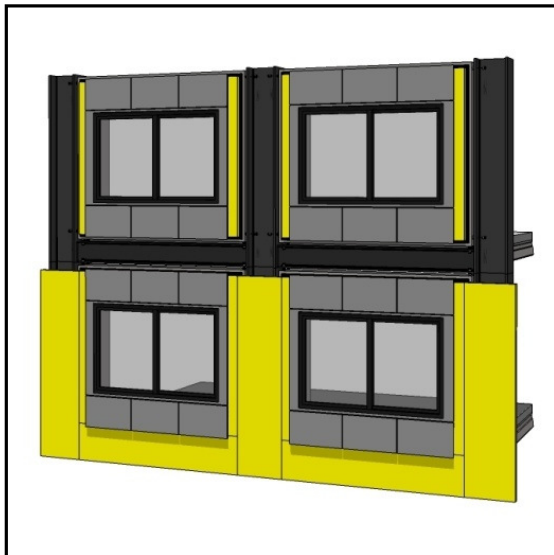


b) Step 4

Figure 8-7: Step 3 and 4 of construction process for semi-integral infilled frame building structure

Step 5: The prefabricated elements for the next story are installed and fixed by tightening the bolts on the columns (Figure 8-8a).

Step 6: The beams for the following story floor are fixed to the structure, and the prefabricated elements are fixed in vertical direction by tightening the bolts on the top beam. Absent cladding is installed between the prefabricated elements on the story underneath. If required, columns are installed for a next story (Figure 8-8b).



a) Step 5



b) Step 6

Figure 8-8: Step 5 and 6 of construction process for semi-integral infilled frame building structure

Hereafter, the construction process is repeated for each new story from step 4 to step 6 until the top of the building has been reached.

In the Master's thesis of Kansen, a high-rise building structure consisting of a combination of semi-integral infilled frames and a central core has successfully been designed. This has resulted in the building shown in Figure 8-9. The work demonstrates the significant contribution of semi-integral infilled frames to the overall lateral building stiffness.

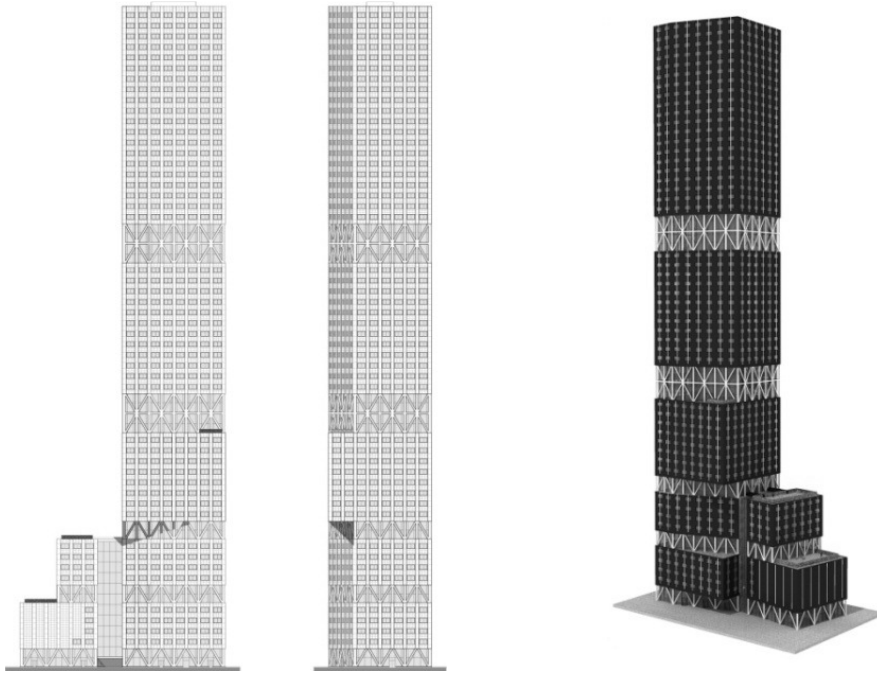


Figure 8-9: High-rise building with semi-integral infilled frames and core structure (Kansen, 2009)

#### 8.4 Chapter conclusions

A design method, incorporating the in the previous chapter developed analytical models for the evaluation of stiffness and strength, was presented for the design of building structures consisting of semi-integral infilled frames with window openings. Subsequently, a design example demonstrated the application of the design method.

The design example showed that the analytical models are useful for the evaluation of the stiffness and strength in the preliminary phase of the design, in order to make decisions with regard to the approximate dimensions of the individual structural elements, without the use of advanced computer simulations.

The design method provides a useful guideline that a structural engineer can easily follow, resulting in a ductile structure, possessing both adequate strength and stiffness.

A building construction method was proposed for the semi-integral infilled frame. The method provides an alternative construction method for tall buildings, resulting in a high level of prefabrication thus in high quality buildings and a considerable decrease of the on-site construction time.

# Chapter 9: CONCLUSIONS & RECOMMENDATIONS

## *Scope of the chapter*

*This concluding chapter presents the overall conclusions of the research described in this thesis (section 9.1). Recommendations for future research are given (section 9.2).*

## **9.1 Conclusions**

An infilled frame is a type of structure that has shown to be effective and efficient in bracing low-rise and medium-rise building structures to resist in-plane lateral loads. Gravity loads acting on the building structure are supported by the frame structure only, while lateral loads are resisted by composite action between the infill and its confining frame. The interaction between the infill and the frame is generally achieved by contact pressure or continuous bonding.

The application of discrete connections between precast concrete infill panels and steel frame structures represents a new area of research in infilled frames. The main objective of this investigation was to develop practical universally applicable design models for this type of structure. Based on the research described in this thesis, the following conclusions can be drawn.

### Experiments

Discretely connected precast concrete panels with openings can be successfully used to provide lateral stability to steel frames. Applying discrete panel-to-frame connections consisting of structural bolts on the column and beam in every corner of the steel frame, acting under compression only, the overall behavior of this structure is comparable to that of a braced frame with a compression diagonal only. Designed for a panel-to-frame connection failure by a bolt failure mechanism, the connection fails by shearing of the bolts through the nuts by stripping of the threads, providing a safe failure mechanism for the structure as failure of the bolts does not result in collapse of the structure. Accordingly, good ductility is achieved. Alexander's theory can be applied for an accurate strength prediction of the bolt-nut assembly in the discrete panel-to-frame connection.

### Finite element modeling

A three dimensional finite element model consisting of solid elements is most suited to accurately simulate the local behavior of H-sections subject to transverse compression introduced indirectly through the flange. Using such a model, the structural characteristics of European rolled HEA- and HEB-sections related to the position of the load on the flange have successfully been determined.



---

**CONCLUSIONS & RECOMMENDATIONS**

A two-dimensional finite element model developed for simulating the full-scale experiments is able to predict the lateral load versus deflection relationship and the ultimate lateral load with good accuracy. The finite element model simulates connection failure as well as panel failure. The non-linear material model used for concrete, combining the Drucker-Prager plasticity model for the compressive regime with a smeared cracking model for the tensile regime, is well suited to accurately model the behavior of the infill panel.

The complex composite behavior of the structure is endorsed by the observation that parameters that affect the relative stiffness between the infill panel and frame influence the ultimate lateral load of the structure as well.

*Analytical modeling*

Analytical models based on the concept of the equivalent diagonal strut, considering the structure as an equivalent braced frame system with a compression diagonal replacing the infill, provide an accurate prediction of the behavior of steel frames with discretely connected precast concrete infill panels. The models are useful for the evaluation of the stiffness and strength of the structure in the preliminary phase of the design. The practical design method incorporating the analytical models provides a useful guideline for structural engineers in order to design building structures consisting of semi-integral infilled frames.

*Construction technology*

The semi-integral infilled frame offers an alternative construction method for tall buildings, enabling the assembly of tall buildings with entirely prefabricated elements directly from a truck. A considerable decrease of the on-site construction time is achieved as building activities are mainly restricted to assembly works, while high quality buildings can be realized as the building elements are manufactured in favorable environments under strictly controlled conditions.

## 9.2 Recommendations for future research

Based on the research presented in this thesis, the following recommendations for future research into semi-integral infilled frames are given:

- Due to the extent of the full-scale tests, only a limited number of tests has been carried out, considering square infilled-frames only (aspect ratio 1). Although other aspect ratios have been numerically investigated, it is recommended to extend the experimental research to other aspect ratios, to investigate other possible failure mechanisms such as out-of-plane failure of the infill panel.
- In practice, the semi-integral infilled frame will, in addition to in-plane loading, be loaded out of the plane of the structure as a result of wind pressure on the façade. Besides the possible out-of-plane failure of the infill panel as mentioned in the previous point, the failure mechanism and ultimate load of the bolts might substantially be influenced when loaded by a combination of compression and shear. Therefore, it is recommended to investigate the behavior of the structure under a combination of in-plane and out-of-plane loading.
- In the current thesis, the behavior of semi-integral infilled frames under in-plane monotonic loading has been studied. However, in practice building structures are subject to reversed and cyclic loading because of the nature of lateral loads. Therefore, it is recommended to investigate the cyclic behavior of the structure.
- Infilled frame systems are often applied in seismic zones. Therefore, it is recommended to evaluate the earthquake response of the semi-integral infilled frame and to develop design rules to allow application of the structure in seismic areas as well.



## REFERENCES

- Afefy, H. M., Taher, S. E. F., Khalil, A. H. A., and Issa, M. E. (2002), Statistically equivalent nonlinear finite element model for infilled RC framed systems, *Engineering Computations*, Vol 19(2), pp 190-205
- Alexander, E. M. (1977), Analysis and design of threaded assemblies, SAE Papers (No. 770420), pp 1-15
- ANSYS Inc. (2007), *ANSYS V11.0 User Manual*, Canonsburg, PA, USA
- ASCE Task Committee on Concrete and Masonry Structure (1982), *State-of-the-art report on finite element analysis of reinforced concrete*, ASCE, New York, 553 p
- ASCE-ACI Committee 445 (1998), Recent approaches to shear design of structural concrete, *Journal of Structural Engineering - ASCE*, Vol 124(12), pp 1375-1471
- Asteris, P. G. (2003), Lateral stiffness of brick masonry infilled plane frames, *Journal of the Structural Division - ASCE*, Vol 129(8), pp 1071-1079
- Asteris, P. G. (2008), Finite element micro-modelling of infilled frames, *Electronic Journal of Structural Engineering*, Vol 8, pp 1-11
- Barua, H. K and Mallick, S. K. (1977), Behaviour of mortar infilled steel frames under lateral load, *Building and Environment*, Vol 12, pp 263-272
- Benjamin, J. R. and Williams, H. A. (1958), The behaviour of one-storey brick shear walls, *Journal of the Structural Division - ASCE*, Vol 84(4), pp 1723/1-1723/30
- Comité Euro-International du Béton (1993), *CEB-FIP Model Code 1990*, Thomas Telford, London, 437 p
- Crisafulli, F. J., Carr, A. J., and Park, R. (2000), Analytical modelling of infilled frame structures - a general review, *Bulletin of the New Zealand Society for Earthquake Engineering*, Vol 33(1), pp 30-47
- Dawe, J. L. and Seah, C. K. (1989), Behaviour of masonry infilled steel frames, *Canadian Journal of Civil Engineering*, Vol 16(6), pp 865-876
- Dawe, J. L., Seah, C. K., and Liu, Y. (2001), A computer model for predicting infilled frame behaviour, *Canadian Journal of Civil Engineering*, Vol 28(1), pp 133-148
- de Borst, R. (2002), Fracture in quasi-brittle materials: a review of continuum damage-based approaches, *Engineering Fracture Mechanics*, Vol 69(2), pp 95-112

- DIANA (2007), *DIANA users manual - release 9.2*, TNO Diana B.V., Delft, The Netherlands
- Drucker, D. C. (1961), On structural concrete and the theorems of limit analysis, *International Association for Bridge and Structural Engineering*, IABSE-Reports 21, pp 45-59
- EN 1992-1-1 (2004), *Eurocode 2: Design of concrete structures - Part 1-1: General rules and rules for buildings*, CEN, Brussels
- EN 1993-1-1 (2005), *Eurocode 3: Design of steel structures - Part 1-1: General rules and rules for buildings*, CEN, Brussels
- EN 1993-1-5 (2006), *Eurocode 3: Design of steel structures - Part 1-5: General rules - Plated structural elements*, CEN, Brussels
- EN 1993-1-8 (2005), *Eurocode 3: Design of steel structures - Part 1-8: Design of joints*, CEN, Brussels
- ENV 1993-1-1 (1992), *Eurocode 3: Design of steel structures - Part 1-1: General rules and rules for buildings*, CEN, Brussels
- FEMA 356 (2000), *Prestandard and commentary for the seismic rehabilitation of buildings*, Federal Emergency Management Agency, Washington
- FIP Commission 3 on Practical Design (1999), *Practical design of structural concrete*, Fédération Internationale de la Précontrainte, London, 113 p
- Frosch, R. J. (1996), *Seismic rehabilitation using precast infill walls*, Ph.D. Dissertation, University of Texas at Austin, 224 p
- Frosch, R. J. (1999a), Panel connections for precast concrete infill walls, *ACI Structural Journal*, Vol 96(4), pp 467-472
- Frosch, R. J. (1999b), Shear transfer between concrete elements using steel pipe connection, *ACI Structural Journal*, Vol 96(6), pp 1003-1008
- Ghosh, A. K. and Amde, A. M. (2002), Finite element analysis of infilled frames, *Journal of the Structural Division - ASCE*, Vol 128(7), pp 881-889
- Hendry, A. W. (1981), *Structural brickwork*, MacMillan, London, 209 p
- Hoenderkamp, J. C. D., Hofmeyer, H., and Snijder, H. H. (2005), Composite behaviour of steel frames with precast concrete infill panels, *Proceedings of the 4th European conference on steel, space & composite structures* (Vol B), Druck und Verlagshaus Mainz GmbH, Aachen, pp 31-40

## References

---

- Hoenderkamp, J. C. D., Hofmeyer, H., and Snijder, H. H. (2007), Experimental investigations into in-plane stiffness and strength of steel frames with precast concrete infill panels, *Proceedings of the 5th international conference on advances in steel structures* (Vol. 3), Research Publishing Services, Singapore/Chennai, pp 826-832
- Hoenderkamp, J. C. D. and Snijder, H. H. (2000), Approximate analysis of high-rise frames with flexible connections, *The Structural Design of Tall Buildings*, Vol 9(3), pp 233-250
- Hoenderkamp, J. C. D. and Snijder, H. H. (2003), Preliminary analysis of high-rise braced-frames with facade riggers, *Journal of Structural Engineering - ASCE*, Vol 129(5), pp 640-647
- Holmes, M. (1961), Steel frames with brickwork and concrete infilling, *Proceedings of the Institution of Civil Engineers - Structures and Buildings*, Vol 19, pp 473-478
- ISO/DIS 1920-10 (2009), *Testing of concrete - Part 10: Determination of static modulus of elasticity in compression*
- Kansen, J. P. S. (2009), *Hybrid Verticality*, Report number A-2009.3, Eindhoven University of Technology, 190 p (in Dutch)
- King, G. J. W. and Pandey, P. C. (1978), The analysis of infilled frames using finite elements, *Proceedings of the Institution of Civil Engineers*, Vol 65(4), pp 749-760
- Kwan, K. H. and Liauw, T. C. (1984), Nonlinear analysis of integral infilled frames, *Engineering Structures*, Vol 6(3), pp 223-231
- Kwan, K. H., Lo, C. G., and Liauw, T. C. (1990), Large-scale model tests and plastic analysis of multibay infilled frames, *Proceedings of the Institution of Civil Engineers*, Vol 89(Part 2), pp 261-277
- la Poutré, D. B. (2005), *Inelastic spatial stability of circular wide flange steel arches*, Ph.D. Dissertation, Eindhoven University of Technology, XII + 188 p
- Leu, L. J., Huang, C. W., Chen, C. S., and Liao, Y. P. (2006), Strut-and-tie design methodology for three-dimensional reinforced concrete structures, *Journal of Structural Engineering - ASCE*, Vol 132(6), pp 929-938
- Liang, Q. Q., Uy, B., and Steven, G. P. (2002), Performance-based optimization for strut-tie modeling of structural concrete, *Journal of Structural Engineering - ASCE*, Vol 128(6), pp 815-823
- Liauw, T. C. (1972), An approximate method of analysis for infilled frames with or without opening, *Building Science*, Vol 7(4), pp 233-238

## References

---

- Liau, T. C. and Kwan, K. H. (1982), Non-linear analysis of multistorey infilled frames, *Proceedings of the Institution of Civil Engineers*, Vol 73(2), pp 441-454
- Liau, T. C. and Kwan, K. H. (1983), Plastic theory of non-integral infilled frames, *Proceedings of the Institution of Civil Engineers*, Vol 75, pp 379-396
- Liau, T. C. and Kwan, K. H. (1984a), Nonlinear behaviour of non-integral infilled frames, *Computers & Structures*, Vol 18(3), pp 551-560
- Liau, T. C. and Kwan, K. H. (1984b), Plastic design of infilled frames, *Proceedings of the Institution of Civil Engineers*, Vol 77, pp 367-377
- Liau, T. C. and Lee, S. W. (1977), On the behaviour and the analysis of multi-storey infilled frames subject to lateral loading, *Proceedings of the Institution of Civil Engineers*, Vol 63(PART 2), pp 641-656
- Liau, T. C. and Lo, C. G. (1988), Multibay infilled frames without shear connectors, *ACI Structural Journal*, Vol 85(4), pp 423-428
- Mainstone, R. J. (1971), On the stiffnesses and strengths of infilled frames, *Proceedings of the Institution of Civil Engineers*, Supplement IV, pp 57-90
- Mallick, D. V. and Garg, R. P. (1971), Effect of openings on the lateral stiffness of infilled frames, *Proceedings of the Institution of Civil Engineers - Structures and Buildings*, Vol 49, pp 193-209
- Mallick, D. V. and Severn, R. T. (1967), The behavior of infilled frames under static loading, *Proceedings of the Institution of Civil Engineers*, Vol 38, pp 639-656
- Moghaddam, H. A., Mohammadi, M. G., and Ghaemian, M. (2006), Experimental and analytical investigation into crack strength determination of infilled steel frames, *Journal of Constructional Steel Research*, Vol 62(12), pp 1341-1352
- Mohebkah, A, Tasnimi, A. A., and Moghadam, H. A. (2008), Nonlinear analysis of masonry-infilled steel frames with openings using discrete element method, *Journal of Constructional Steel Research*, Vol 64(12), pp 1463-1472
- Mondal, G. and Jain, S. K. (2008), Lateral stiffness of masonry infilled reinforced concrete (RC) frames with central opening, *Earthquake Spectra*, Vol 24(3), pp 701-723
- Mörsch, E. (1908), *Der Eisenbetonbau, seine Theorie und Anwendung*, Wittwer, Stuttgart
- Muttoni, A., Schwartz, J., and Thürlimann, B. (1997), *Design of concrete structures with stress fields*, Birkhäuser, Basel, 143 p

- NEN-EN 12390-3 (en) (2009), *Testing hardened concrete - Part 3: Compressive strength of test specimens*, Nederlands Normalisatie-instituut, Delft
- NEN-EN 12390-6 (en) (2000), *Testing hardened concrete - Part 6: Tensile splitting strength of test specimens*, Nederlands Normalisatie-instituut, Delft
- Ng'andu, B. M. (2006), *Bracing steel frames with calcium silicate element walls*, Ph.D. Dissertation, Eindhoven University of Technology, XII + 187 p
- Paulay, T. and Priestley, M. J. N. (1992), *Seismic design of reinforced concrete and masonry buildings*, John Wiley & Sons, Chichester, 744 p
- Polyakov, S. V. (1956), On the interaction between masonry filler walls and enclosing frame when loaded in the plane of the wall, Translation in *Earthquake Engineering*, Earthquake Engineering Research Institute, San Francisco, pp 36-42
- Puglisi, M., Uzcategui, M., and Florez-Lopez, J. (2009), Modeling of masonry of infilled frames, Part II: Cracking and damage, *Engineering Structures*, Vol 31(1), pp 119-124
- Riddington, J. R. and Stafford Smith, B. (1977), Analysis of infilled frames subject to racking with design recommendations, *Structural Engineer*, Vol 55(6), pp 263-268
- Ritter, W. (1899), Die Bauweise Hennebique, *Schweizerische Bauzeitung*, Vol Bd. XXXIII(7), pp 59-61
- Saneinejad, A. and Hobbs, B. (1995), Inelastic design of infilled frames, *Journal of the Structural Division - ASCE*, Vol 121(4), pp 634-650
- Schlaich, J. and Schäfer, K. (1991), Design and detailing of structural concrete using strut-and-tie models, *Structural Engineer*, Vol 69(6), pp 113-125
- Schlaich, J., Schäfer, K., and Jennewein, M. (1987), Toward a consistent design of structural concrete, *Journal of the prestressed concrete institute*, Vol 32(3), pp 74-150
- Sharpe, W. N. J. (2008), *Springer handbook of experimental solid mechanics*, Springer, New York, 1098 p
- Stafford Smith, B. (1962), Lateral stiffness of infilled frames, *Journal of the Structural Division - ASCE*, Vol 88(6), pp 183-199
- Stafford Smith, B. (1966), Behaviour of square infilled frames, *Journal of the Structural Division - ASCE*, Vol 92(1), pp 381-403
- Stafford Smith, B. (1967a), Methods for predicting the lateral stiffness and strength of multi-storey infilled frames, *Building Science*, Vol 2(3), pp 247-257



## References

---

- Stafford Smith, B. (1967b), The composite behaviour of infilled frames, *Tall buildings: Proceedings of a Symposium on Tall Buildings*, Pergamon Press, London, pp 481-495
- Stafford Smith, B. and Carter, C. (1969), A method of analysis for infilled frames, *Proceedings of the Institution of Civil Engineers*, Vol 44, pp 31-48
- Stafford Smith, B. and Coull, A. (1991), *Tall building structures - analysis and design*, John Wiley and Sons Inc., New York, 537 p
- Stafford Smith, B. and Riddington, J. R. (1978), The design of masonry infilled steel frames for bracing structures, *Structural Engineer*, Vol 56(1), pp 1-7
- Stark, J. W. B. and Bijlaard, F. S. K. (1988), Design rules for beam-to-column connections in Europe, *Journal of Constructional Steel Research*, Vol 10, pp 415-462
- Steenhuis, C. M., Gresnigt, N., and Weynand, K. (1994), Pre-design of semi-rigid joints in steel frames, *Proceedings of the Second State of the Art Workshop Prague*, pp 131-140
- Steenhuis, C. M., Vrouwenvelder, A. C. W. M., van Herwijnen, F., and Snijder, H. H. (2002), Definitions of resistance and deformation capacity for non-sway steel and composite structures, *Heron*, Vol 47(1), pp 3-27
- Swanson, J. A. and Leon, R. T. (2001), Stiffness modelling of bolted T-stub connections, *Journal of Structural Engineering*, Vol 127(5), pp 498-505
- Tang, R. B., Hoenderkamp, J. C. D., and Snijder, H. H. (2003), Preliminary numerical research on steel frames with precast reinforced concrete infill panels, *Proceedings of the 1st conference on structural stability and dynamics*, Taipei, pp 575-580
- Teeuwen, P. A., Kleinman, C. S., and Snijder, H. H. (2006), The effect of window openings on the composite behaviour of infilled steel frames with precast concrete infill panels, *Proceedings of the 8th international conference on steel, space & composite structures*, CI-Premier Pte Ltd, Singapore, pp 185-192
- Timoshenko, S. P. and Goodier, J. N. (1970), *Theory of elasticity*, 3rd ed., McGraw-Hill, New York, 567 p
- Witteveen, J., Stark, J. W. B., Bijlaard, F. S. K., and Zoetemeijer, P. (1982), Welded and bolted beam-to-column connections, *Journal of the Structural Division - ASCE*, Vol 108(2), pp 433-455
- Wood, R. H. (1978), Plasticity, composite action and collapse design of unreinforced shear wall panels in frames, *Proceedings of the Institution of Civil Engineers - Structures and Buildings*, Vol 65(JUNE), pp 381-411

## References

---

- Yun, Y. M. (2000), A refined strut-tie model approach and its application tool, *Proceedings of the Institution of Civil Engineers - Structures and Buildings*, Vol 140(1), pp 13-24
- Yun, Y. M. (2006), Strength of two-dimensional nodal zones in strut-tie models, *Journal of Structural Engineering - ASCE*, Vol 132(11), pp 1764-1783
- Yun, Y. M. and Ramirez, J. A. (1996), Strength of struts and nodes in strut-tie model, *Journal of Structural Engineering - ASCE*, Vol 122(1), pp 20-29
- Zoetemeijer, P. (1974), A design method for the tension side of statically loaded, bolted beam-to-column connections, *Heron*, Vol 20(1), pp 1-59
- Zoetemeijer, P. (1975), Influence of normal, bending and shear stresses in the web of European rolled sections, Report no. 6-75-18, Stevin Laboratory, Delft University of Technology



# APPENDIX A

## A.1 Resistance of H-section subject to transverse compression

The resistance of an H-section subject to transverse compression applied indirectly via the flanges is governed by one of the following modes of failure:

- Yielding of the flanges
- Yielding of the web close to the flange
- Crippling of the web in the form of localized buckling
- Buckling of the web over most of the depth of the section

However, when the load is resisted by shear force in the web and not transferred directly to the other flange through the web, buckling failure does not occur.

A calculation is made to demonstrate that yielding of the flanges is the governing failure mode for HEA- and HEB-sections subject to compression applied indirectly via the flanges. The equations applied are derived from Eurocode 3, EN 1993. In these equations, the length of stiff bearing ( $s_s$ ) is included. This length depends, in the case of loading indirectly via the flanges, on the dispersion of the load over the width of the flange at an angle  $\varphi$  (Figure A-1). Although the value of  $\varphi$  is not exactly known, adopting a conservative value will demonstrate that the web failure mechanisms are not likely to occur, and that consequently flange yielding governs the strength.

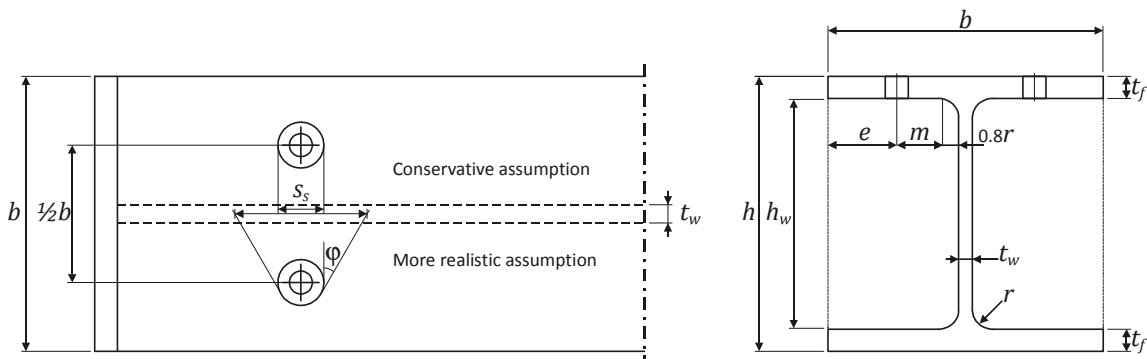


Figure A-1: Definition of geometrical parameters

In the following calculations, no dispersions of the load over the width of the flange is assumed ( $\varphi = 0$ ). Accordingly, the length of stiff bearing ( $s_s$ ) is taken equal to the diameter of the washer, which equals 44 mm for M24.

The following equations from Eurocode 3 EN 1993, are applied to find the resistance of the web in compression (EN 1993-1-5) and the flange in bending (EN 1993-1-8):

Transverse loading resistance web

The transverse loading resistance ( $F_{Rd}$ ) of the web of rolled beams is given by the following equation (equation 6.1 of EN 1993-1-5):

$$F_{Rd} = \frac{t_w L_{eff} f_{yw}}{\gamma_{M1}}$$

Where:

$t_w$  = thickness of the web [mm]

$f_{yw}$  = yield strength of the web [N/mm<sup>2</sup>]

$\gamma_{M1}$  = partial factor for resistance of members to instability assessed by member checks [-]

$L_{eff}$  is the effective length for resistance to transverse forces [mm], which should be determined from:

$$L_{eff} = \chi_F l_y$$

Where:

$\chi_F$  = the reduction factor due to local buckling [-]

$l_y$  = the effective loaded length, appropriate to the length of stiff bearing [mm]

The reduction factor  $\chi_F$  is to be determined from:

$$\chi_F = \frac{0.5}{\bar{\lambda}_F} \leq 1.0$$

Where:

$$\bar{\lambda}_F = \sqrt{\frac{l_y t_w f_{yw}}{F_{cr}}}$$

$$F_{cr} = 0.9 k_F E \frac{t_w^3}{h_w}$$

$$k_F = 6 + 2 \left( \frac{h_w}{a} \right)^2$$

Where:

$h_w$  = distance between the flanges as indicated in Figure A-1 [mm]

$a$  = length of the unstiffened web [mm]

The effective loaded length ( $l_y$ ) is calculated as follows:

$$l_y = s_s + 2t_f(1 + \sqrt{m_1 + m_2})$$

Where:

$s_s$  = length of stiff bearing as indicated in Figure A-1 [mm]

$m_1$  and  $m_2$  are two dimensionless parameters, to be obtained from:

$$m_1 = \frac{f_{yf} b_f}{f_{yw} t_w}$$

$$m_2 = 0.02 \left( \frac{h_w}{t_f} \right)^2 \text{ if } \bar{\lambda}_F > 0.5$$

$$m_2 = 0 \text{ if } \bar{\lambda}_F < 0.5$$

#### Bending resistance flange

The bending resistance of the flange in bending is determined using an equivalent T-stub in tension. Accordingly, the tension resistance of the T-stub flange ( $F_{T,Rd}$ ) is obtained from (Table 6.2 of EN 1993-1-8):

$$F_{T,Rd} = \frac{4M_{pl}}{m} \text{ (Mode 1: complete yielding of the flange)}$$

Where  $M_{pl}$  is given by:

$$M_{pl} = \frac{0.25 l_{eff} t_f^2 f_{yf}}{\gamma_{M0}}$$

Where:

$t_f$  = thickness of the flange [mm]

$f_{yf}$  = yield strength of the flange [N/mm<sup>2</sup>]

$l_{eff}$  = the smaller of  $4m + 1.25e$  and  $2\pi m$

$e$  = edge distance to the bolt as indicated in Figure A-1 [mm]

$m$  = distance as indicated in Figure A-1 [mm]

$\gamma_{M1}$  = partial factor for resistance of cross-sections whatever the class is [-]

Results

Using the preceding equations, the web and flange resistance of HEA and HEB-sections in steel grade S235 is determined. A survey of the results is given in Table A-1 and Table A-2 respectively.

*Table A-1: Resistance of HEA-sections subject to transverse compression*

Section type	Flange resistance [kN]	Web resistance [kN]
HE200A	1.39E+05	2.67E+05
HE220A	1.66E+05	3.11E+05
HE240A	2.00E+05	3.59E+05
HE260A	2.18E+05	3.81E+05
HE280A	2.33E+05	4.21E+05
HE300A	2.72E+05	4.76E+05
HE320A	3.34E+05	5.37E+05
HE340A	3.79E+05	5.86E+05
HE360A	4.27E+05	6.36E+05
HE400A	5.05E+05	7.25E+05
HE450A	6.18E+05	8.12E+05
HE500A	7.43E+05	9.02E+05
HE550A	8.11E+05	9.61E+05
HE600A	8.81E+05	1.02E+06

*Table A-2: Resistance of HEB-sections subject to transverse compression*

Section type	Flange resistance [kN]	Web resistance [kN]
HE200B	3.18E+05	4.56E+05
HE220B	3.56E+05	5.13E+05
HE240B	4.05E+05	5.75E+05
HE260B	4.31E+05	6.05E+05
HE280B	4.51E+05	6.56E+05
HE300B	5.05E+05	7.25E+05
HE320B	5.89E+05	7.96E+05
HE340B	6.49E+05	8.52E+05
HE360B	7.12E+05	9.09E+05
HE400B	8.13E+05	1.01E+06
HE450B	9.56E+05	1.11E+06
HE500B	1.11E+06	1.21E+06
HE550B	1.19E+06	1.27E+06
HE600B	1.28E+06	1.34E+06

The tables show that the resistance of the flanges to transverse loading is lower than that of the webs, assuming no dispersions of the load over the width of the flange which is a conservative assumption. Consequently, web failure can be excluded as being a possible failure mode for HEA and HEB-sections subject to transverse compression applied indirectly via the flanges.

# APPENDIX B

## B.1 Test specimens

### Steel frame

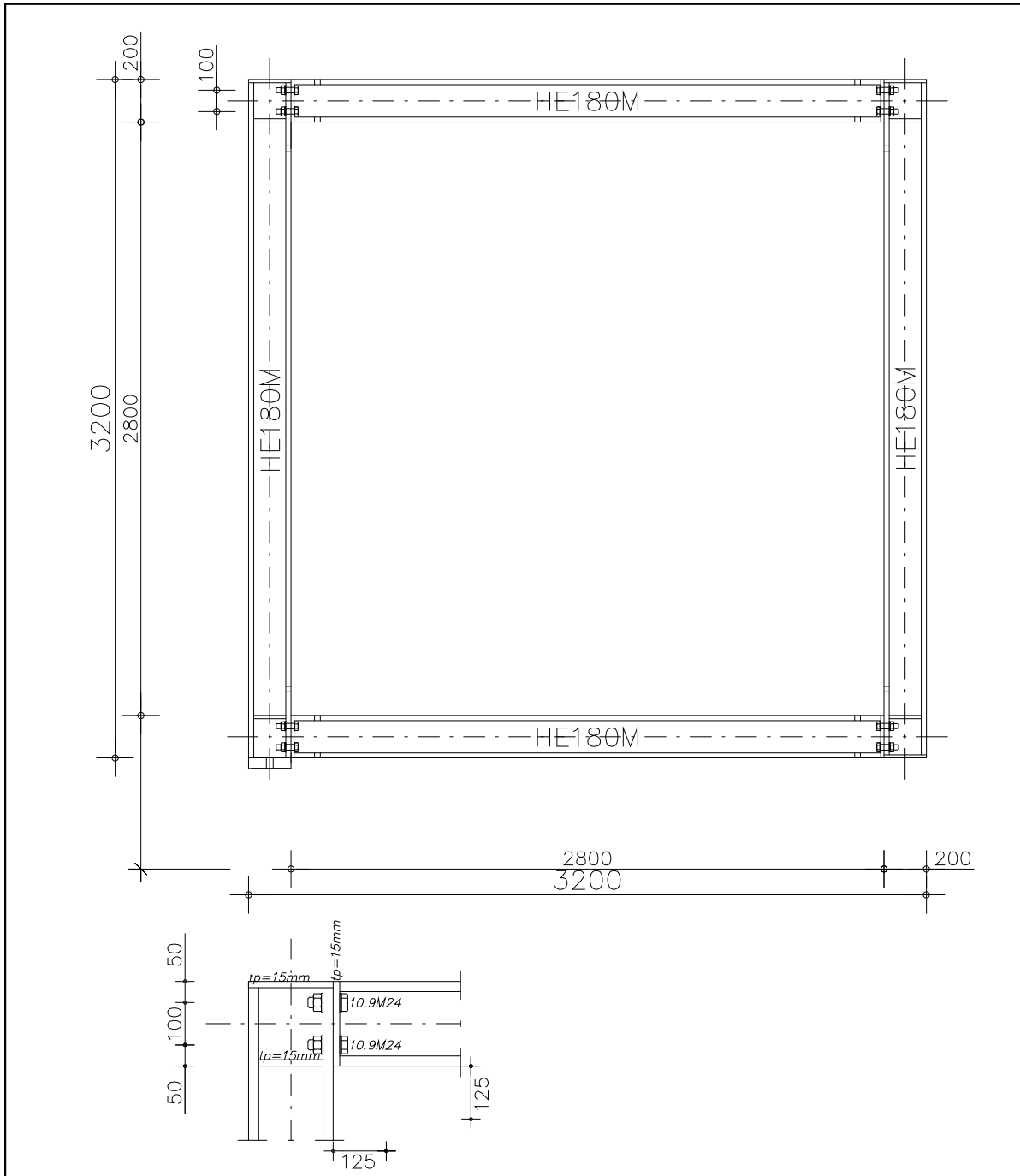


Figure B-1: Steel frame with beam-to-column connection



Panel type 1

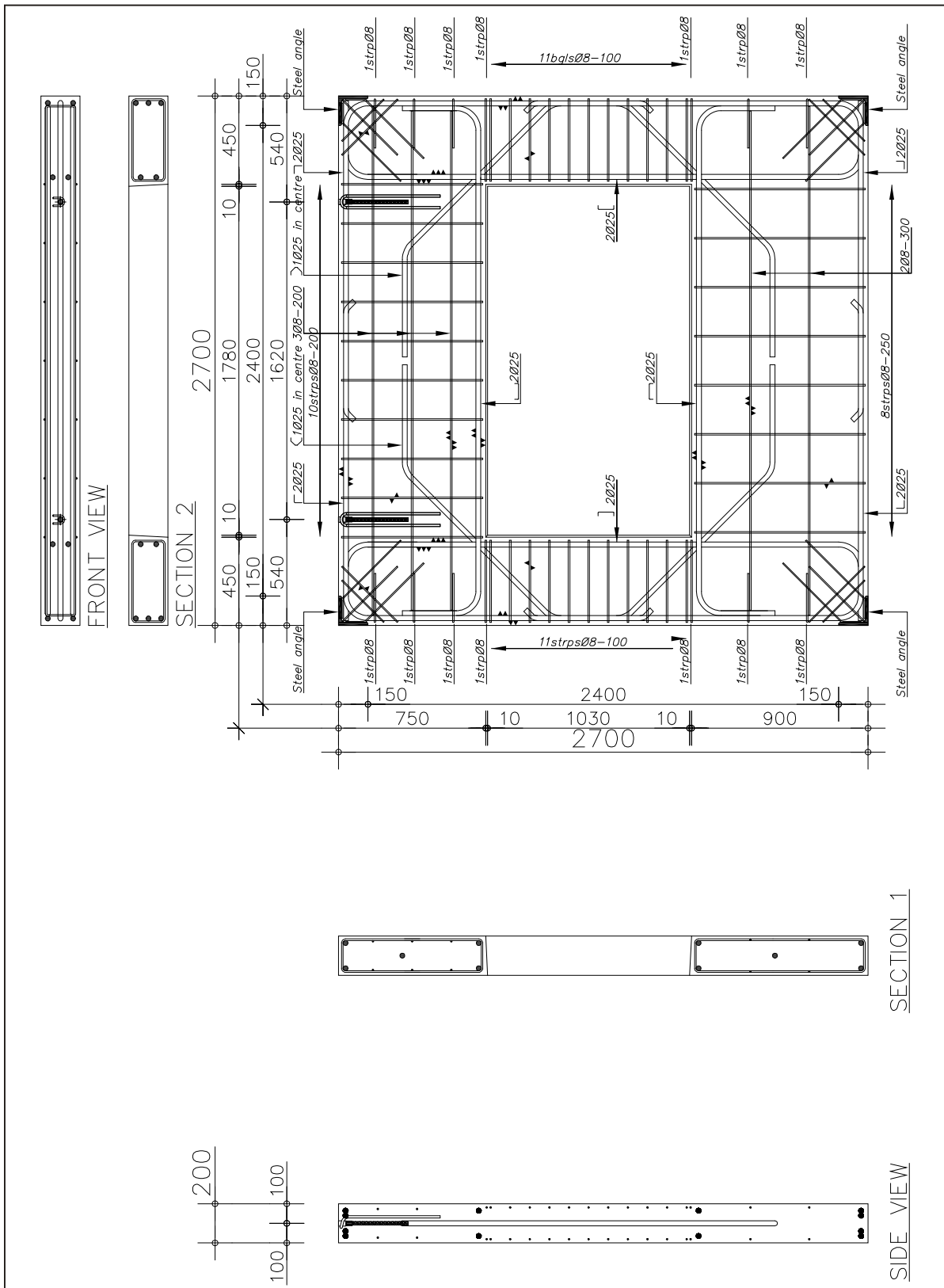


Figure B-2: Reinforcement configuration of panel type 1

Panel type 2

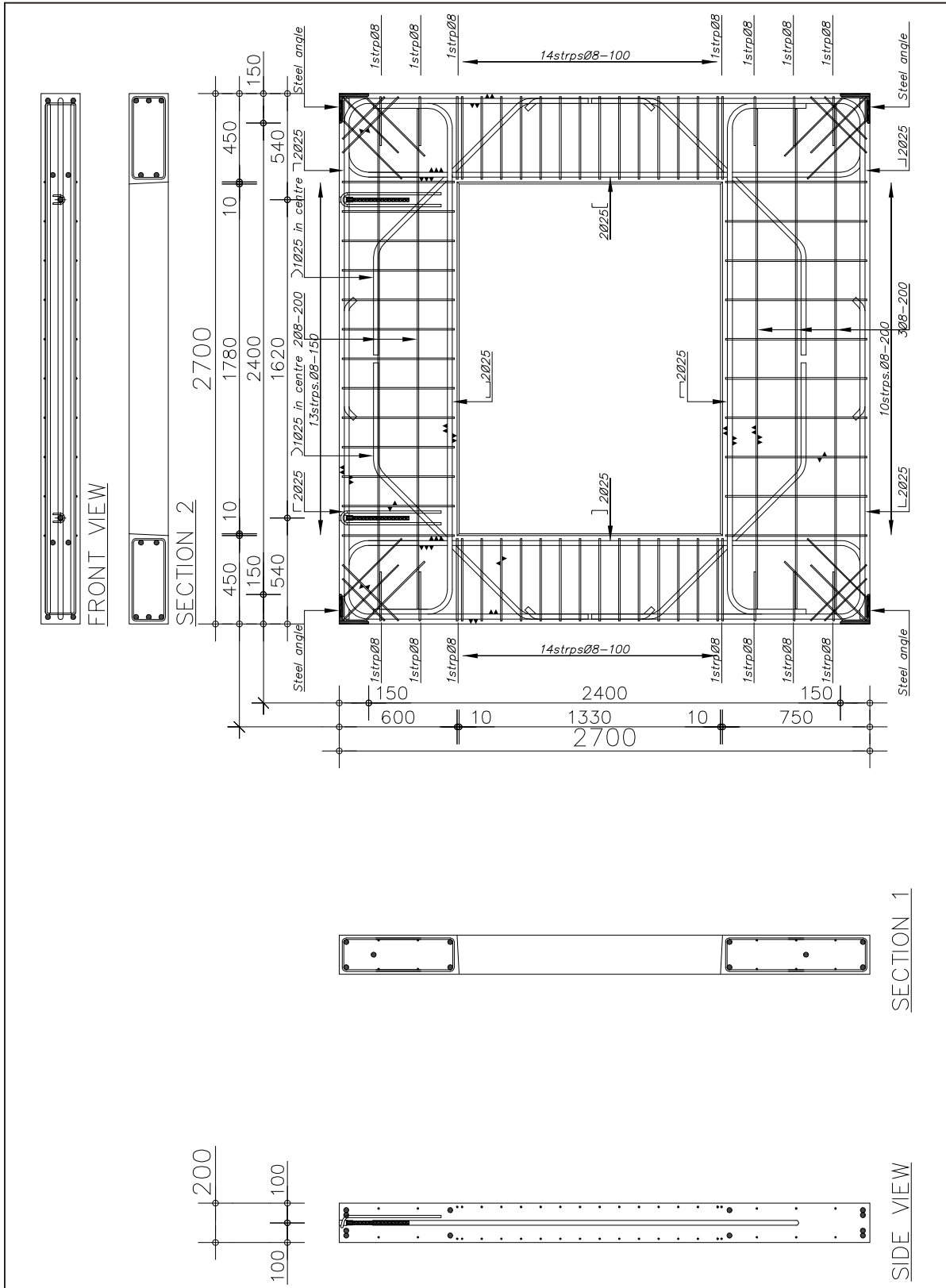


Figure B-3: Reinforcement configuration of panel type 2



Panel type 4

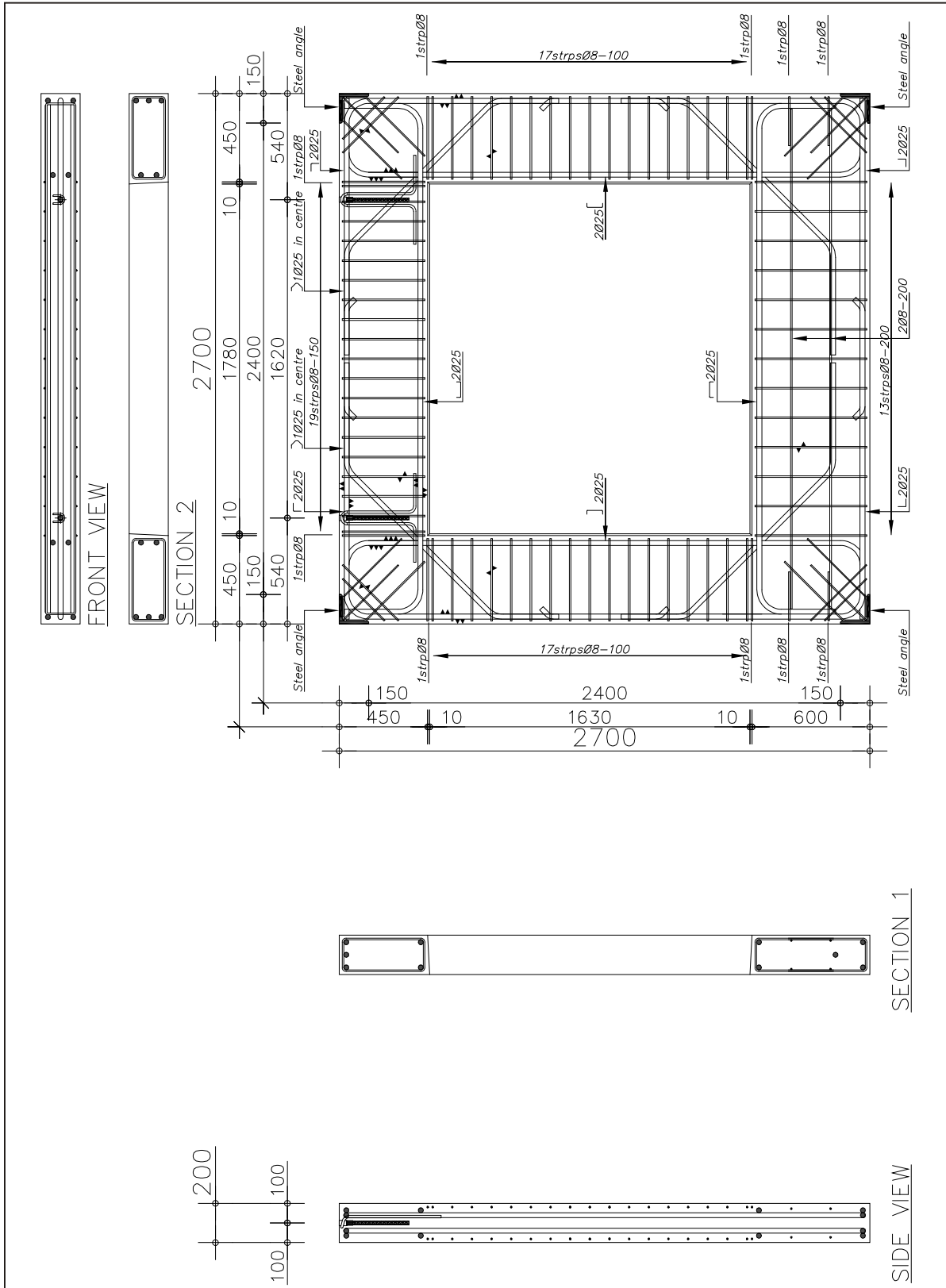


Figure B-5: Reinforcement configuration of panel type 4

Panel type 5

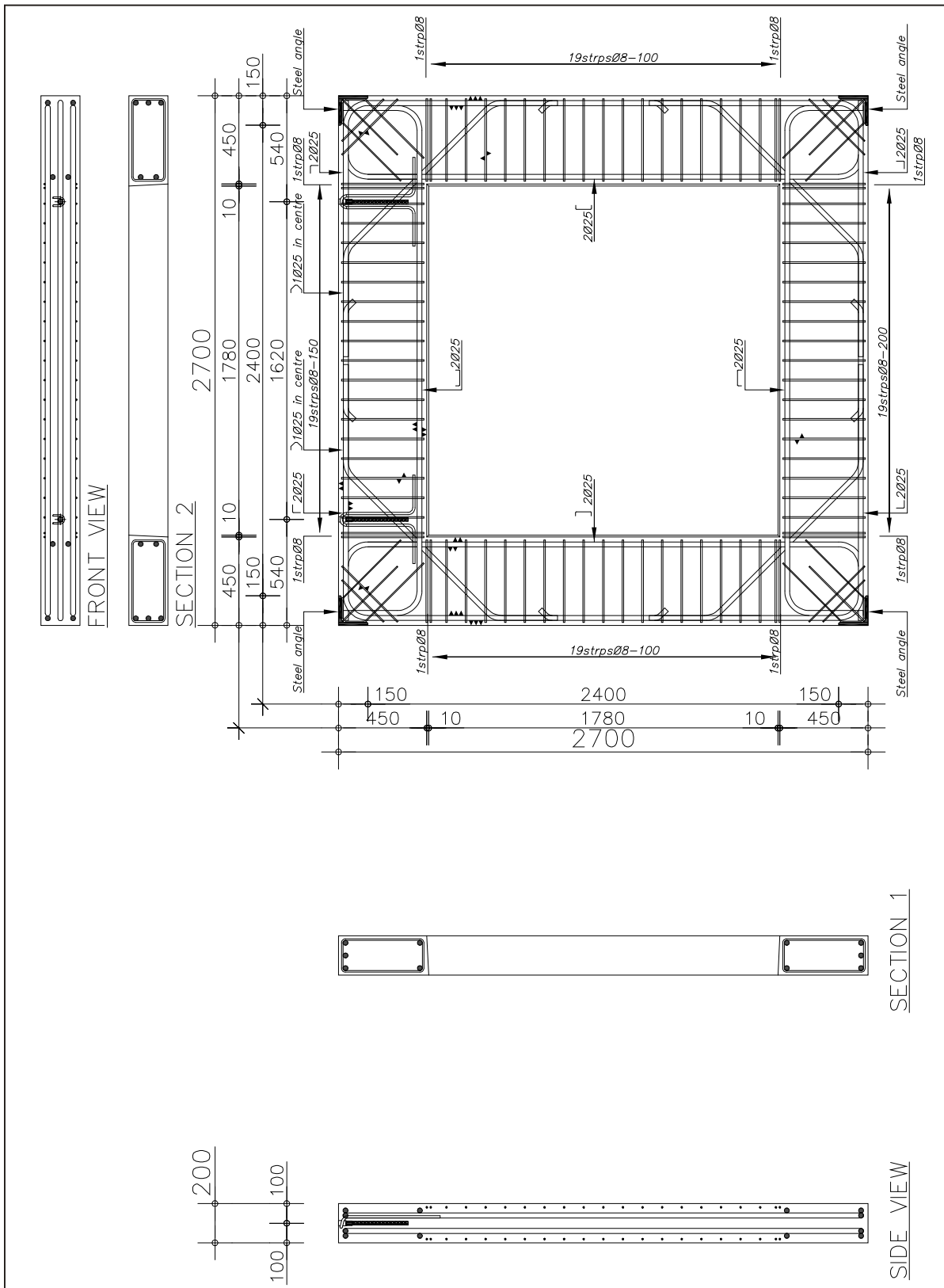
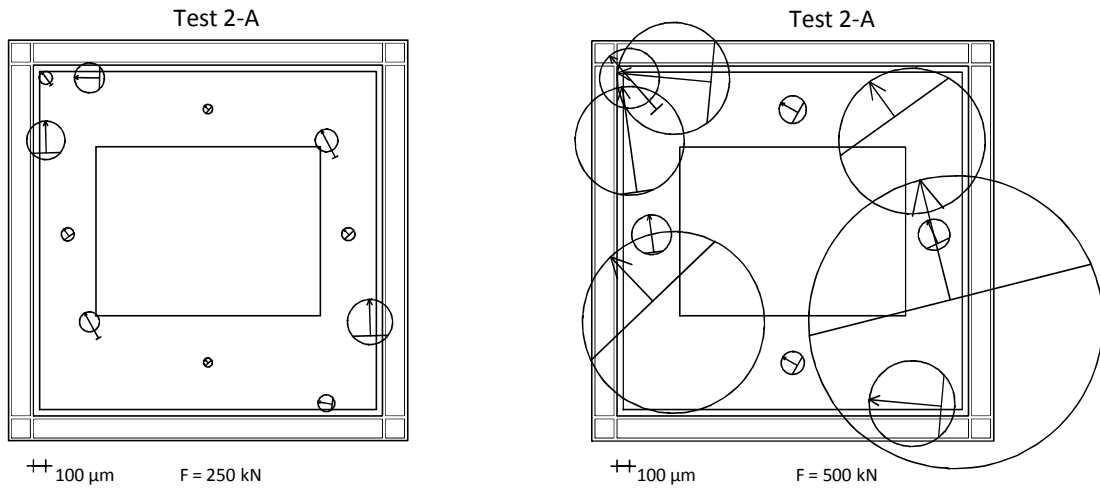
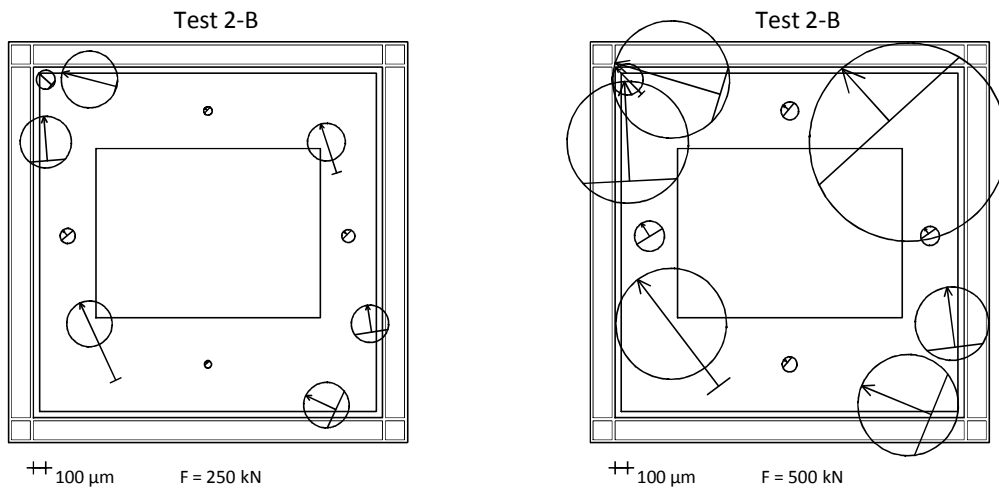


Figure B-6: Reinforcement configuration of panel type 5

**B.2 Measurement results**



*Figure B-7: Principal strain distribution represented as Mohr's circles for test 2A*



*Figure B-8: Principal strain distribution represented as Mohr's circles for test 2B*

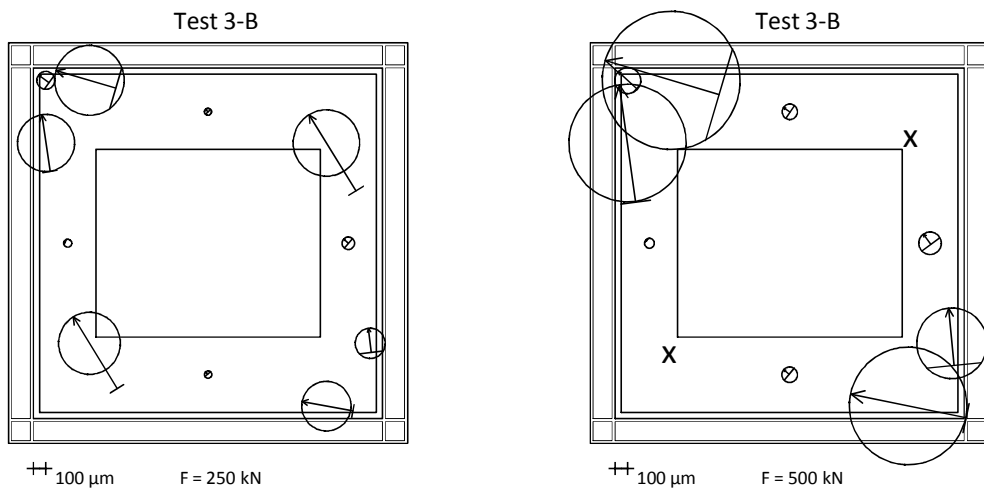


*Figure B-9: Principal strain distribution represented as Mohr's circles for test 3B*

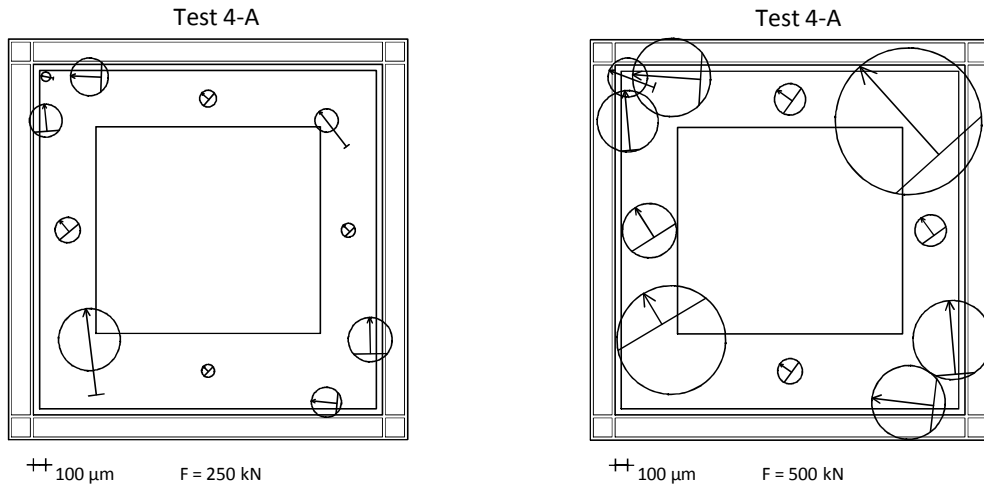


Figure B-10: Principal strain distribution represented as Mohr's circles for test 4A

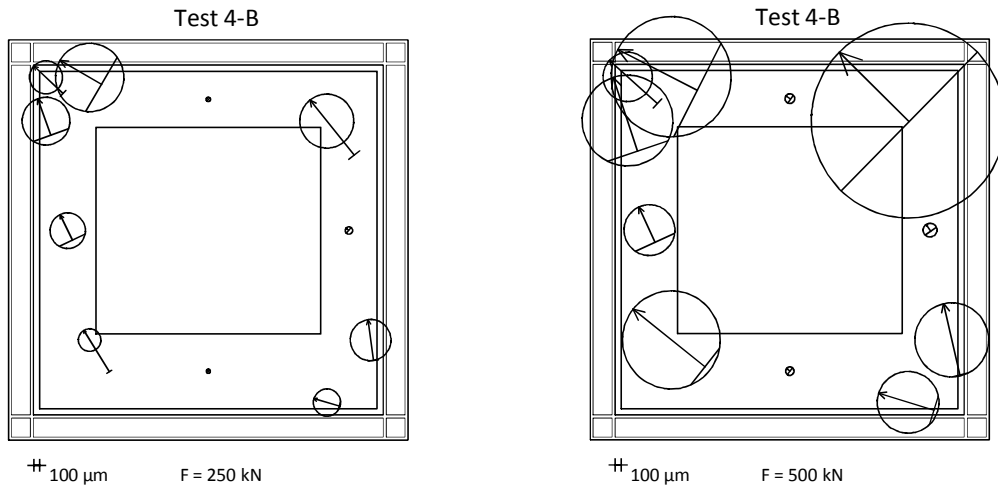


Figure B-11: Principal strain distribution represented as Mohr's circles for test 4B

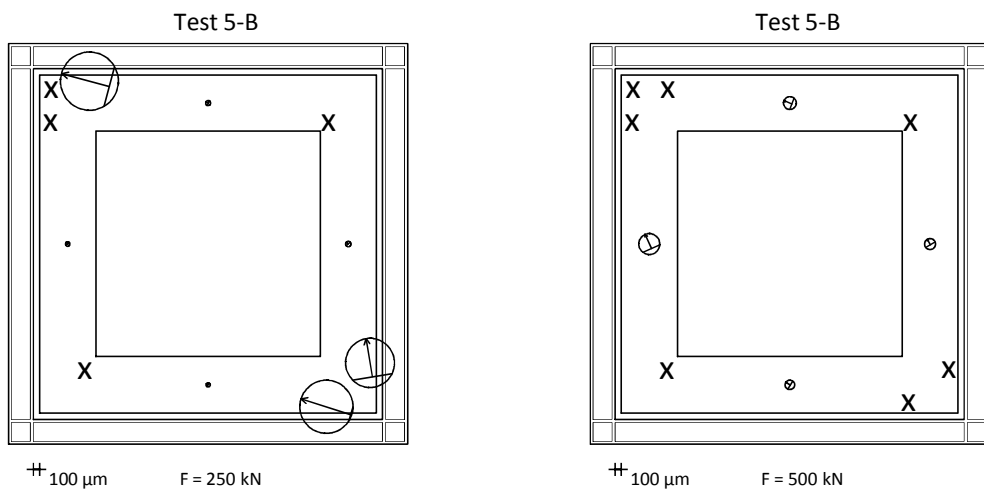


Figure B-12: Principal strain distribution represented as Mohr's circles for test 5B

# APPENDIX C

## C.1 Moment-rotation curves for rotational springs used in FE-analyses

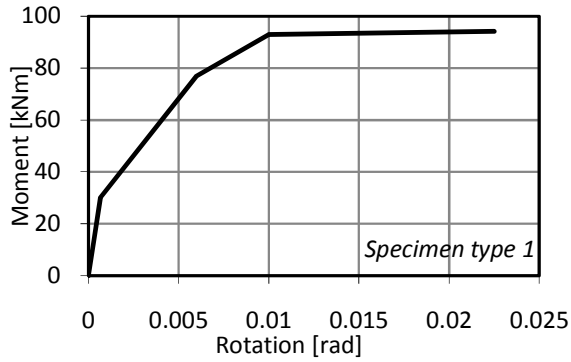


Figure C-1: Moment-rotation response of rotational springs for specimen type 1

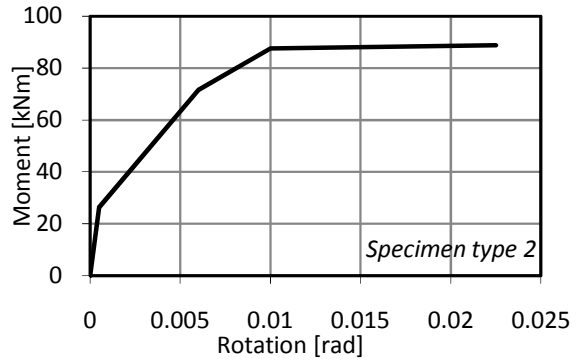


Figure C-2: Moment-rotation response of rotational springs for specimen type 2

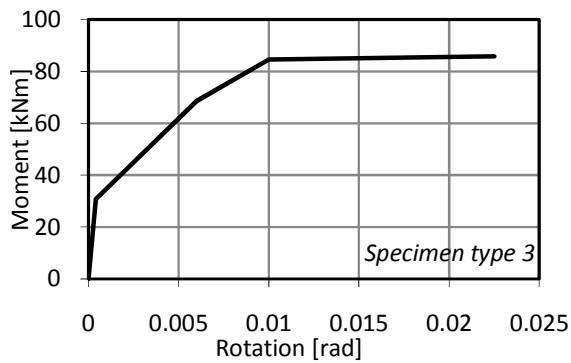


Figure C-3: Moment-rotation response of rotational springs for specimen type 3

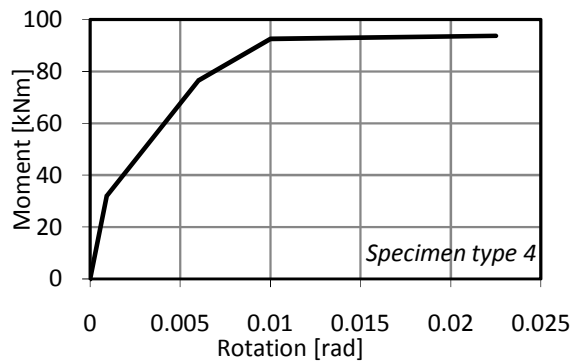


Figure C-4: Moment-rotation response of rotational springs for specimen type 4

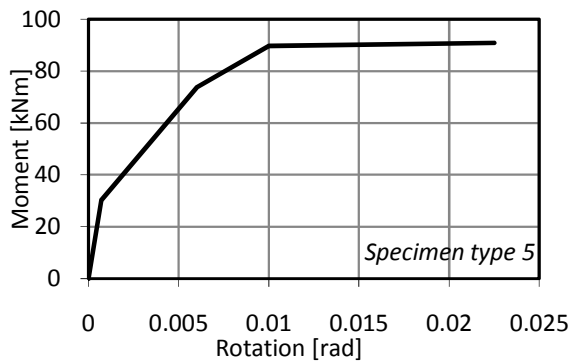


Figure C-5: Moment-rotation response of rotational springs for specimen type 5



## C.2 Comparison of FE- and experimental results

### C.2.1 Measured and simulated strains

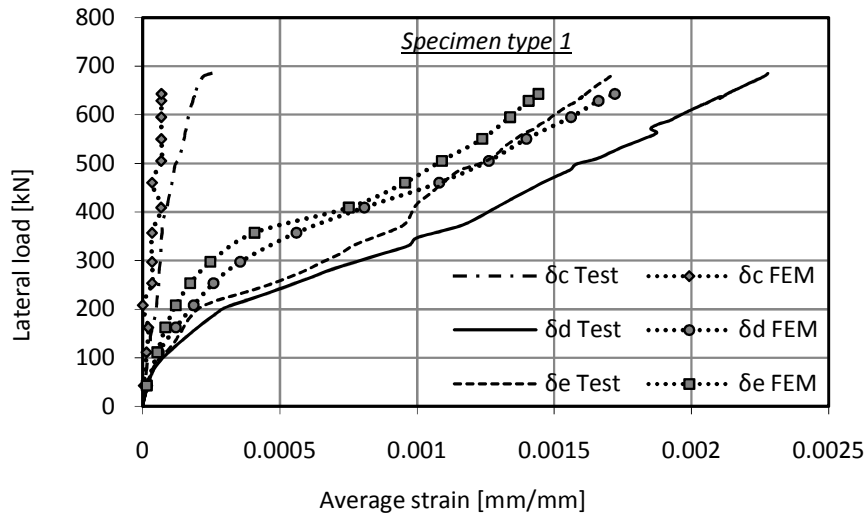


Figure C-6: Measured and simulated strains for specimen type 1

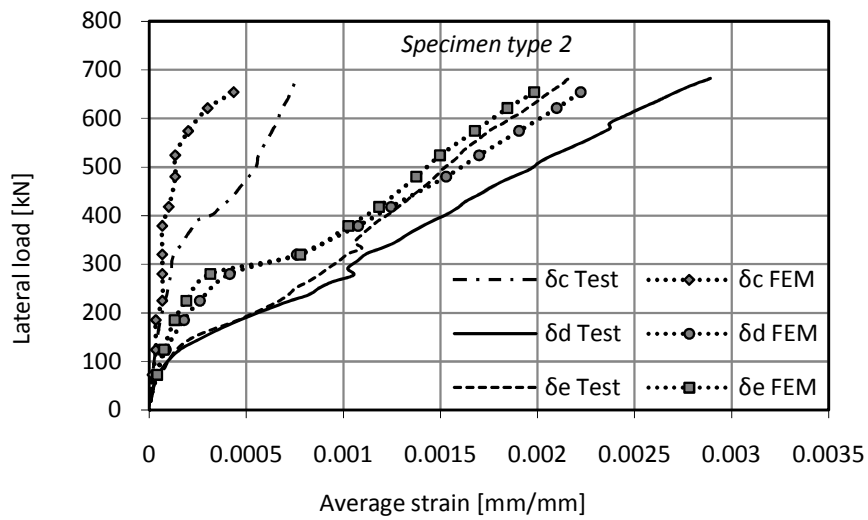


Figure C-7: Measured and simulated strains for specimen type 2

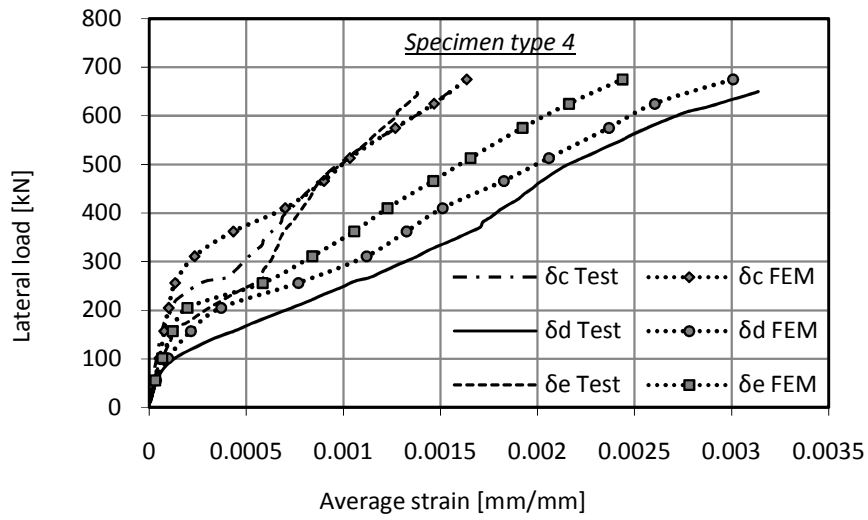


Figure C-8: Measured and simulated strains for specimen type 4

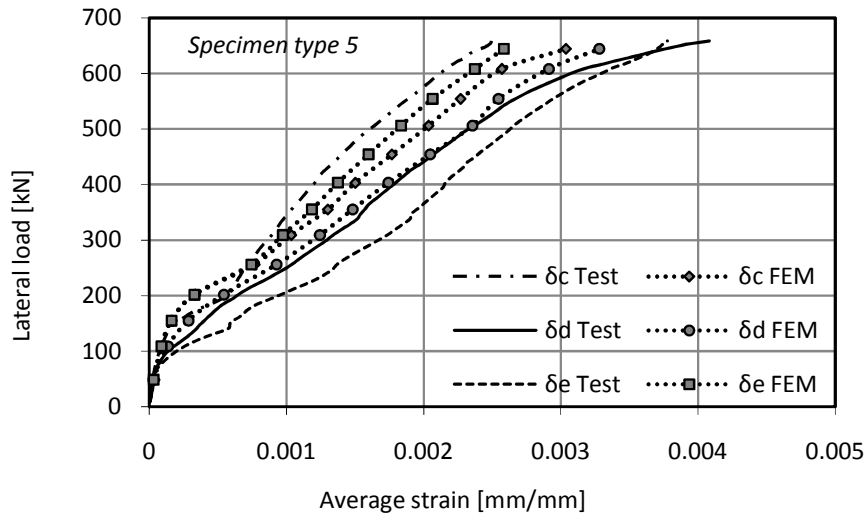


Figure C-9: Measured and simulated strains for specimen type 5

**C.2.2 Experimental and simulated crack patterns**

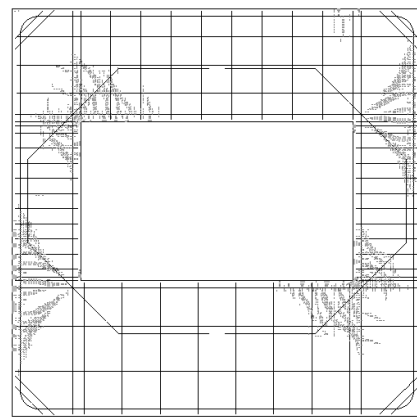
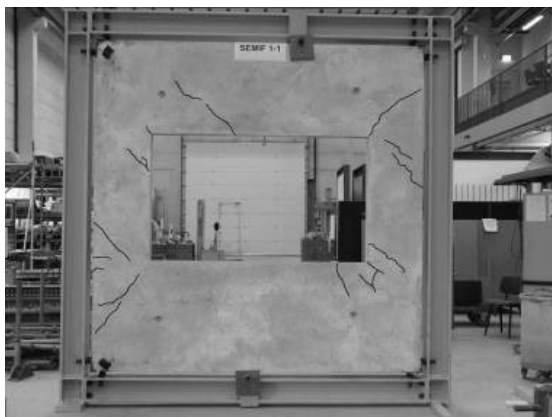


Figure C-10: Experimental and simulated final crack patterns for specimen type 1

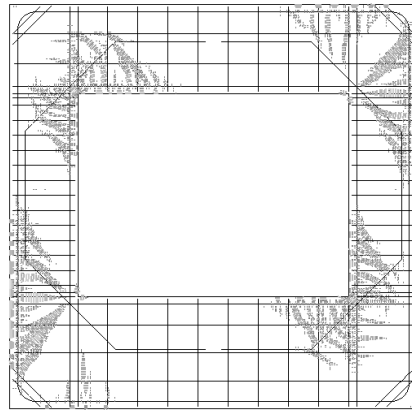


Figure C-11: Experimental and simulated final crack patterns for specimen type 2

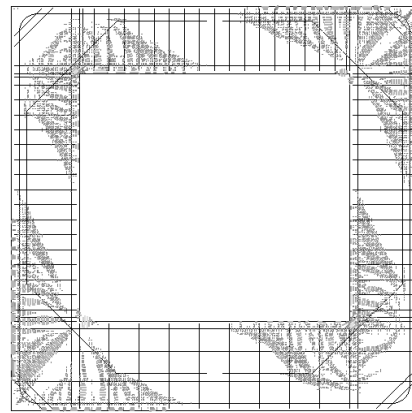


Figure C-12: Experimental and simulated final crack patterns for specimen type 4

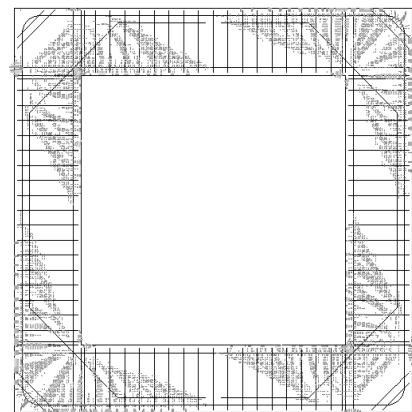


Figure C-13: Experimental and simulated final crack patterns for specimen type 5

# APPENDIX D

## D.1 Results parameter study on component

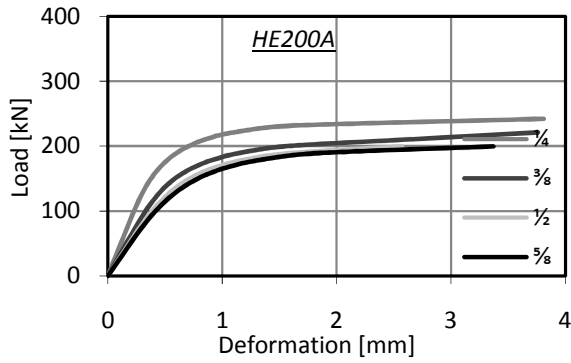


Figure D-1: Load-deformation curves for HE200A section in S355

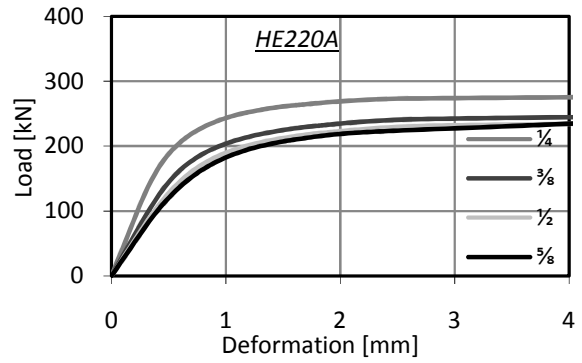


Figure D-2: Load-deformation curves for HE220A section in S355

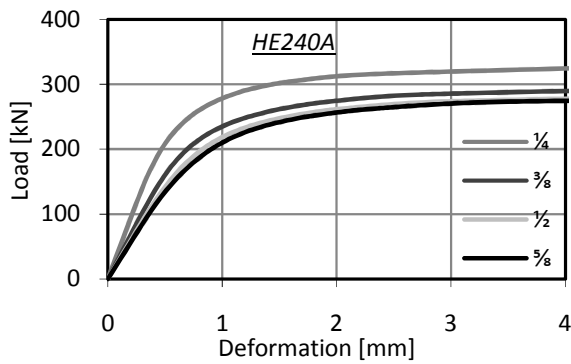


Figure D-3: Load-deformation curves for HE240A section in S355

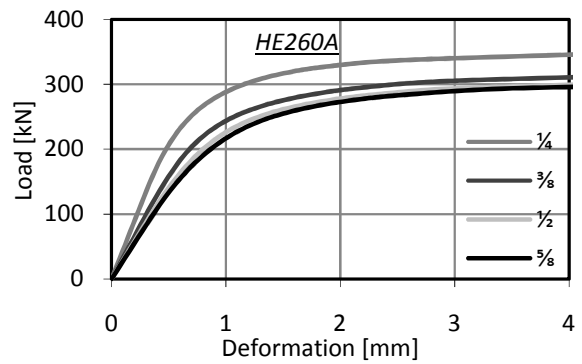


Figure D-4: Load-deformation curves for HE260A section in S355

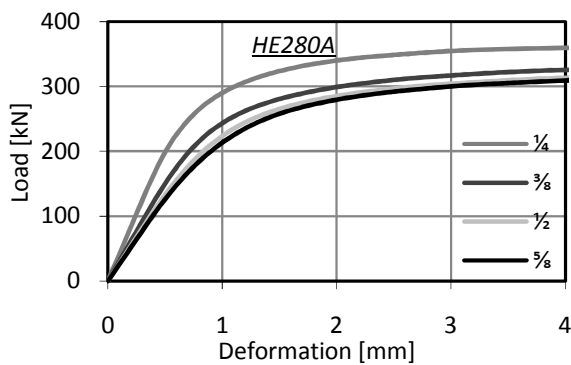


Figure D-5: Load-deformation curves for HE280A section in S355

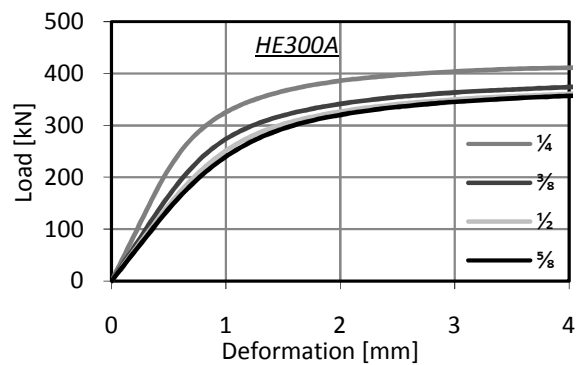


Figure D-6: Load-deformation curves for HE300A section in S355

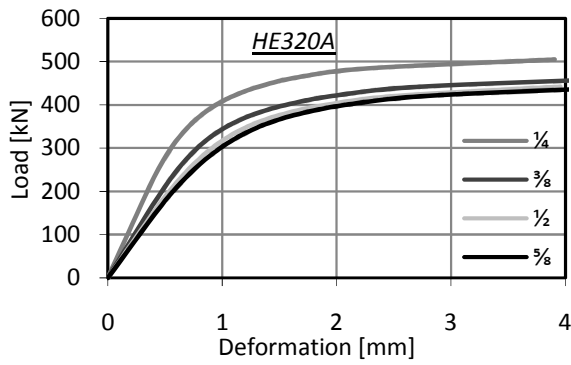


Figure D-7: Load-deformation curves for HE320A section in S355

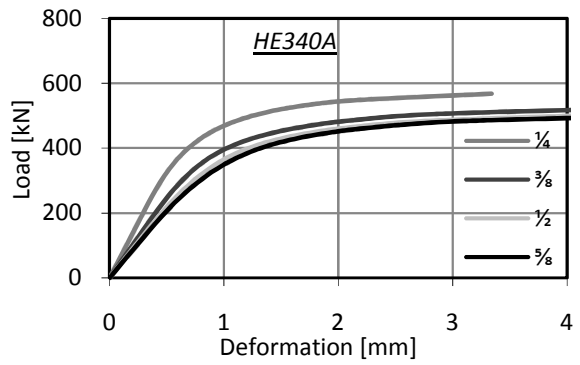


Figure D-8: Load-deformation curves for HE340A section in S355

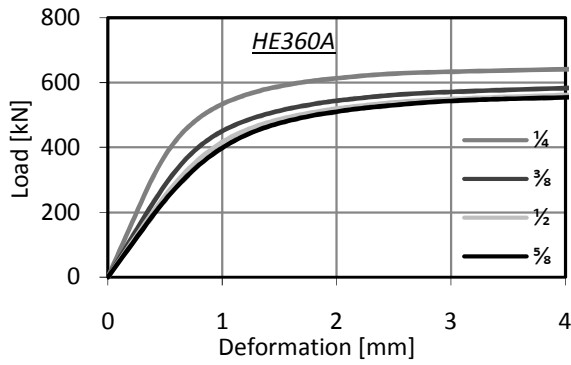


Figure D-9: Load-deformation curves for HE360A section in S355

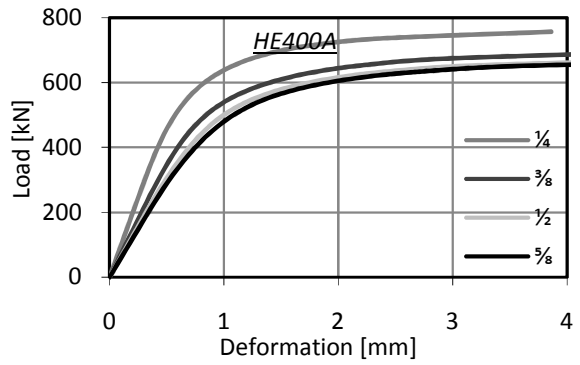


Figure D-10: Load-deformation curves for HE400A section in S355

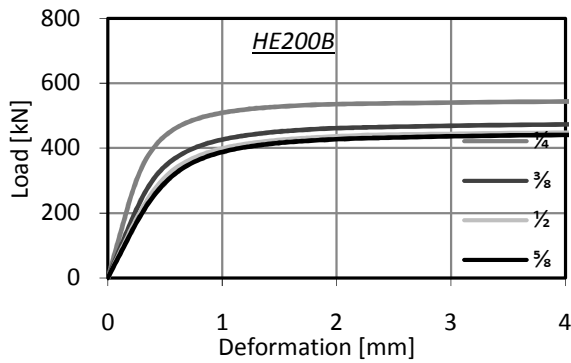


Figure D-11: Load-deformation curves for HE200B section in S355

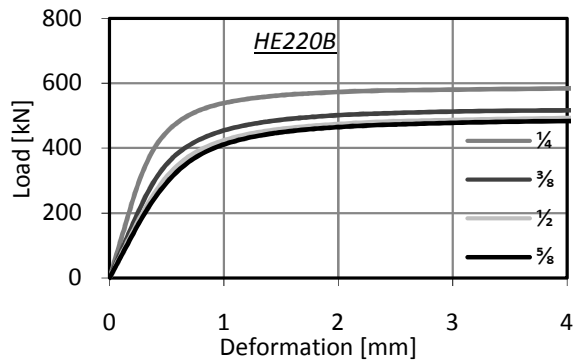


Figure D-12: Load-deformation curves for HE220B section in S355

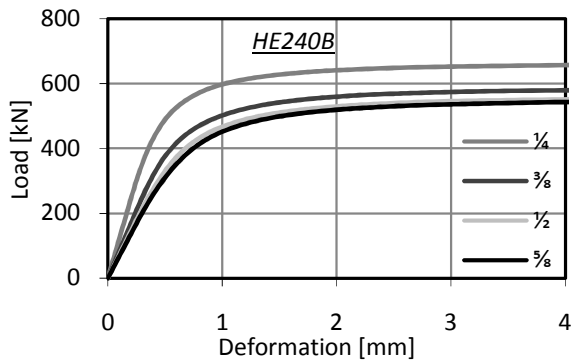


Figure D-13: Load-deformation curves for HE240B section in S355

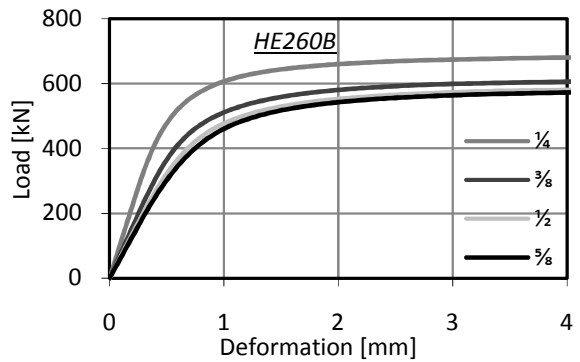


Figure D-14: Load-deformation curves for HE2600B section in S355

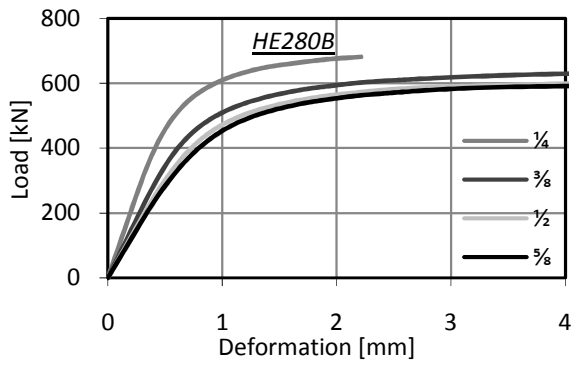


Figure D-15: Load-deformation curves for HE280B section in S355

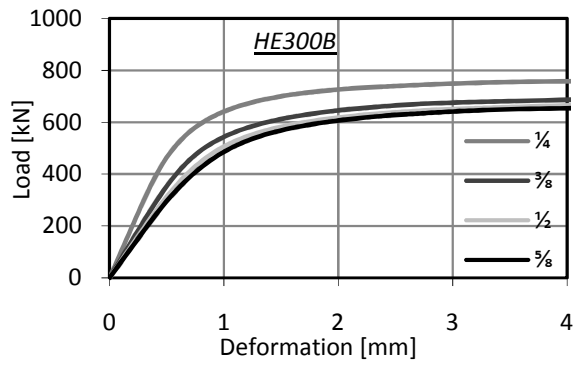


Figure D-16: Load-deformation curves for HE300B section in S355

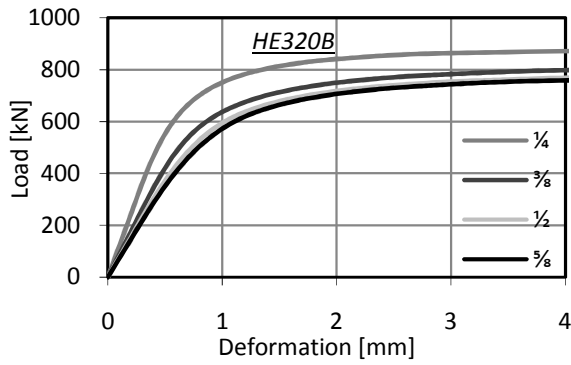


Figure D-17: Load-deformation curves for HE320B section in S355

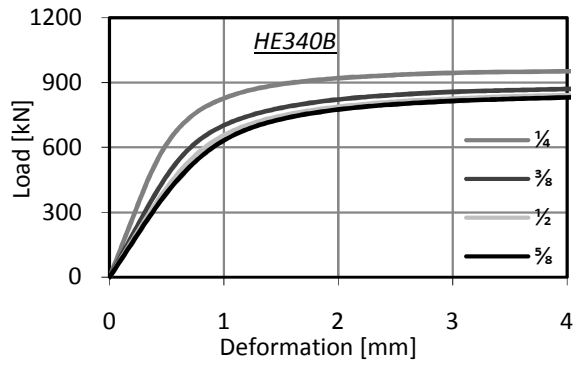


Figure D-18: Load-deformation curves for HE340B section in S355

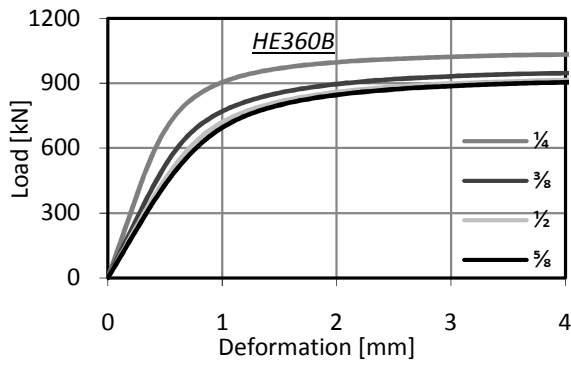


Figure D-19: Load-deformation curves for HE360B section in S355

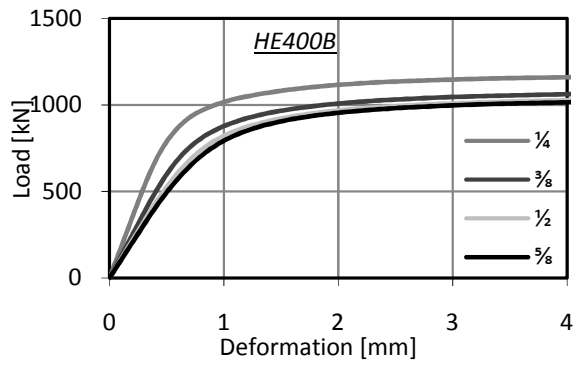


Figure D-20: Load-deformation curves for HE400B section in S355

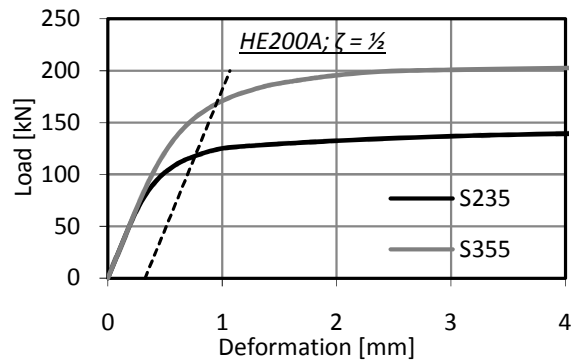


Figure D-21: Load-deformation curve for HE200A section in S235

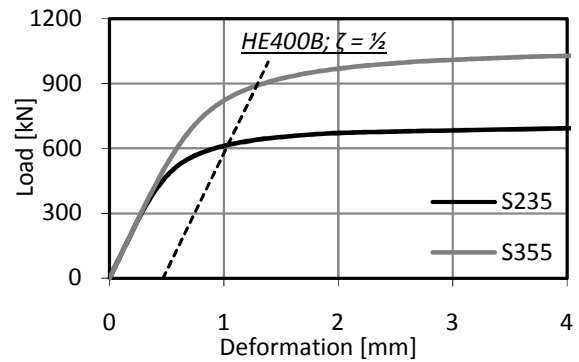


Figure D-22: Load-deformation curve for HE400B section in S235

## D.2 Reinforcement configuration for panels used in parameter study

### Panel type 1

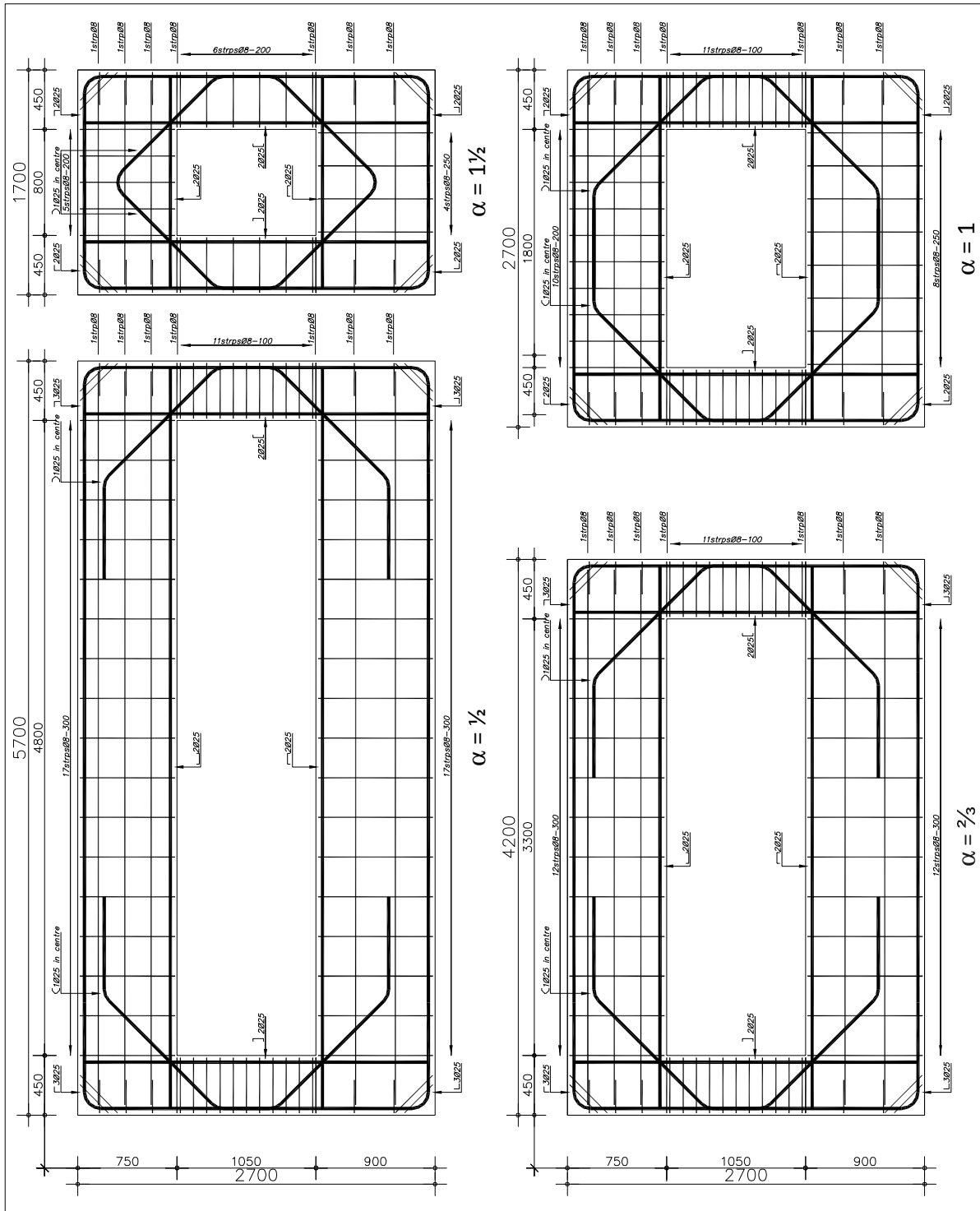


Figure D-23: Reinforcement configurations for panels of type 1 for  $\alpha = 1/2, 2/3, 1$  and  $1 1/2$

Panel type 2

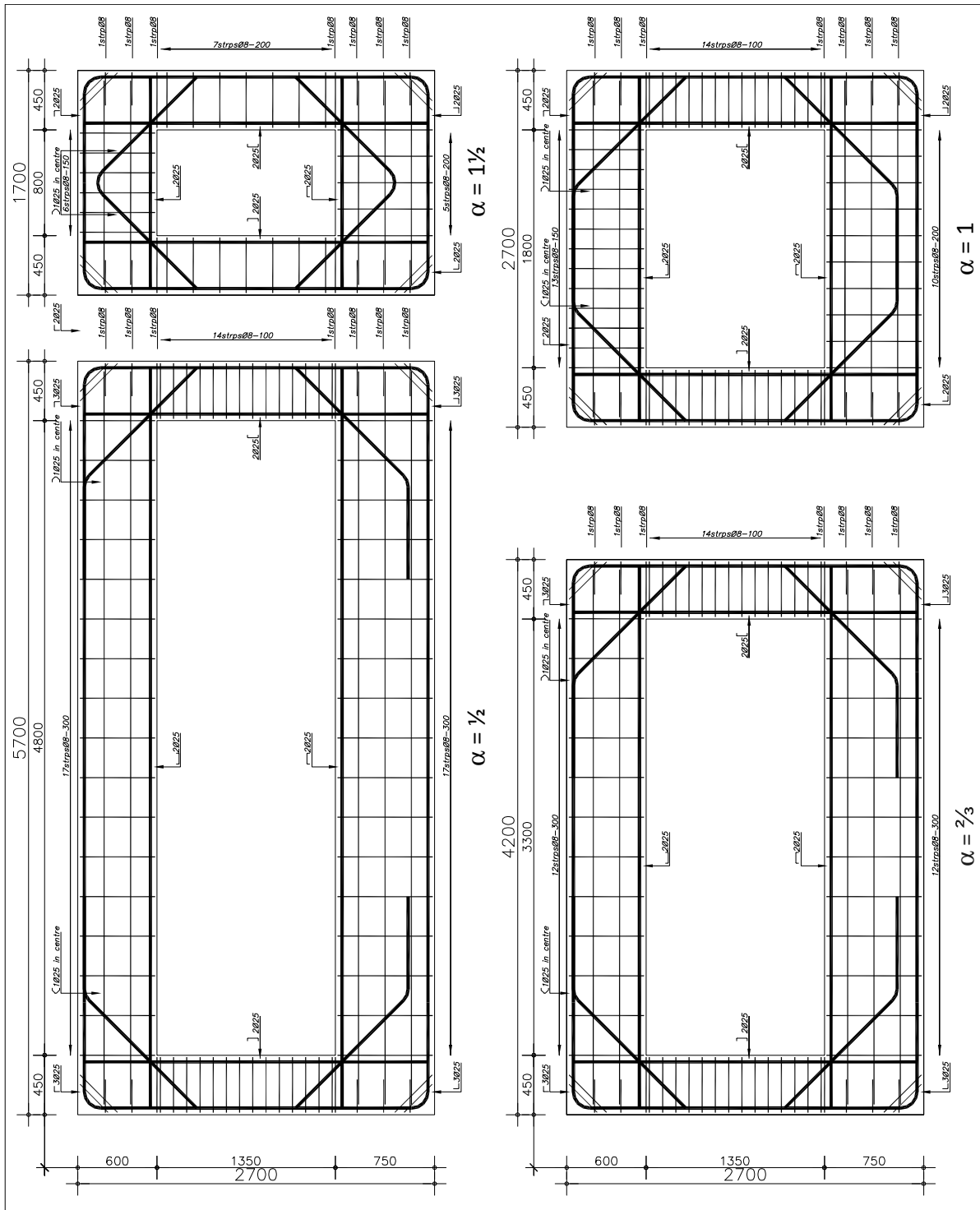


Figure D-24: Reinforcement configurations for panels of type 2 for  $\alpha = 1/2, 2/3, 1$  and  $1 1/2$



Panel type 3

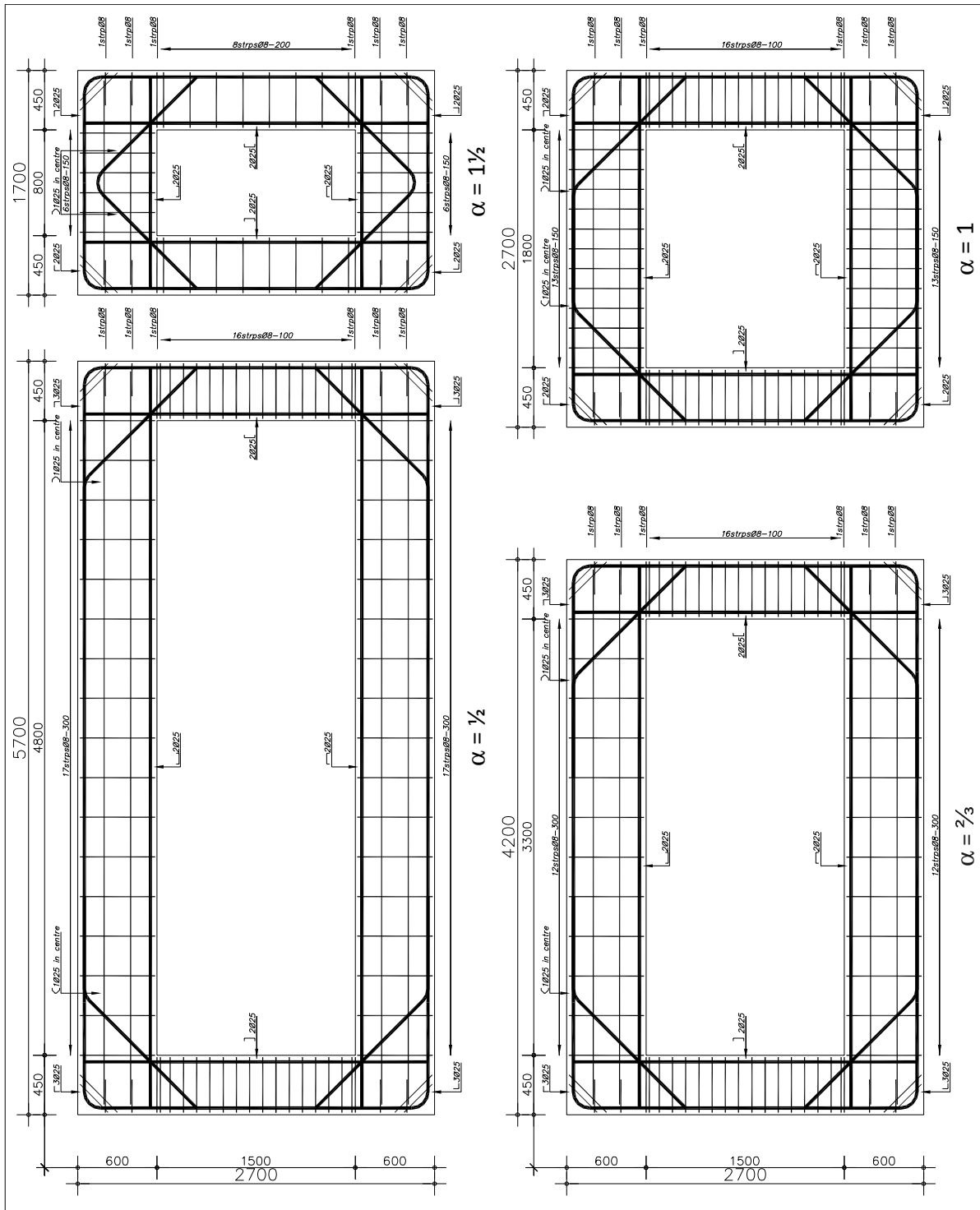


Figure D-25: Reinforcement configurations for panels of type 3 for  $\alpha = 1/2, 2/3, 1$  and  $1 1/2$

Panel type 4

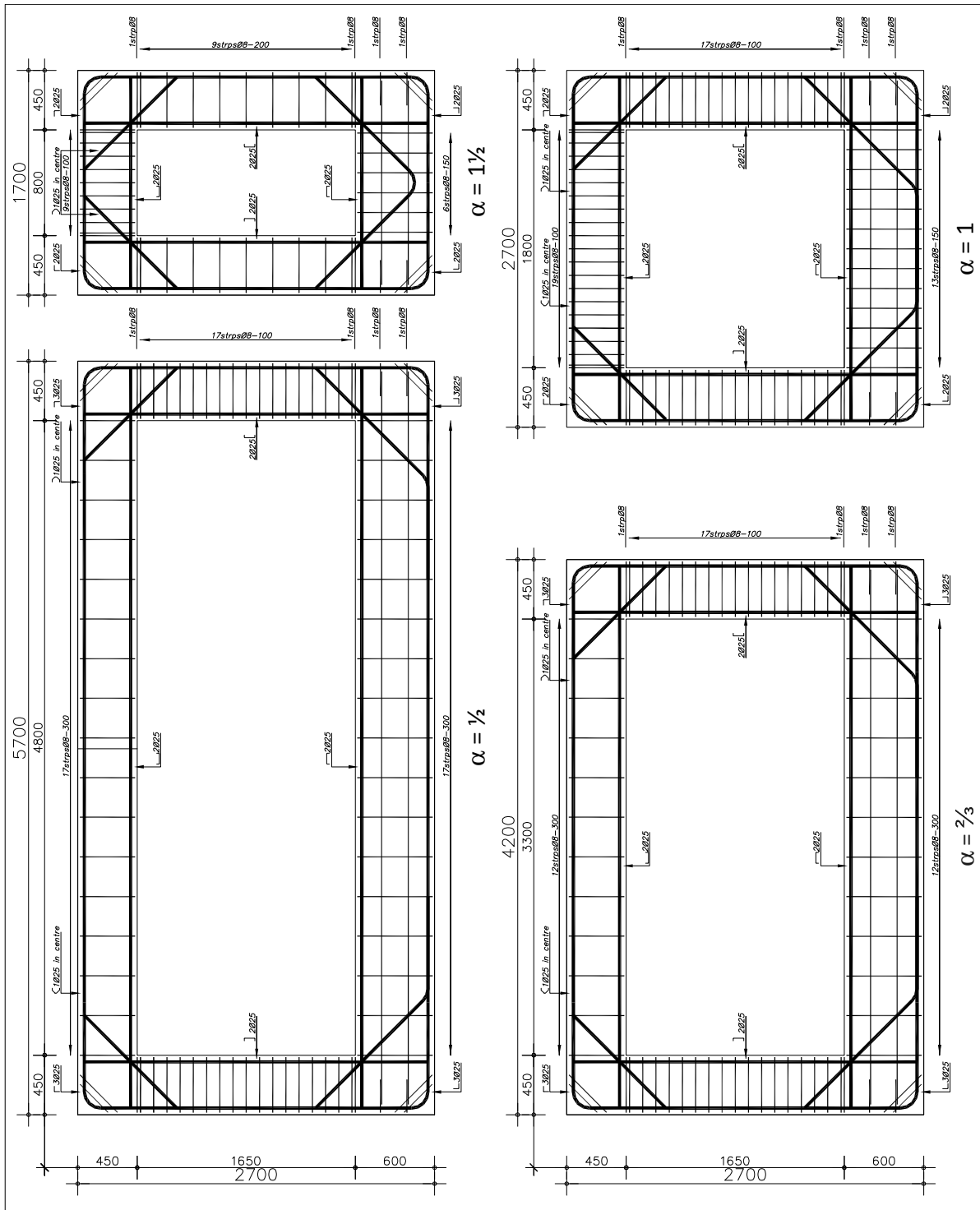


Figure D-26: Reinforcement configurations for panels of type 4 for  $\alpha = 1/2, 2/3, 1$  and  $1 1/2$

Panel type 5

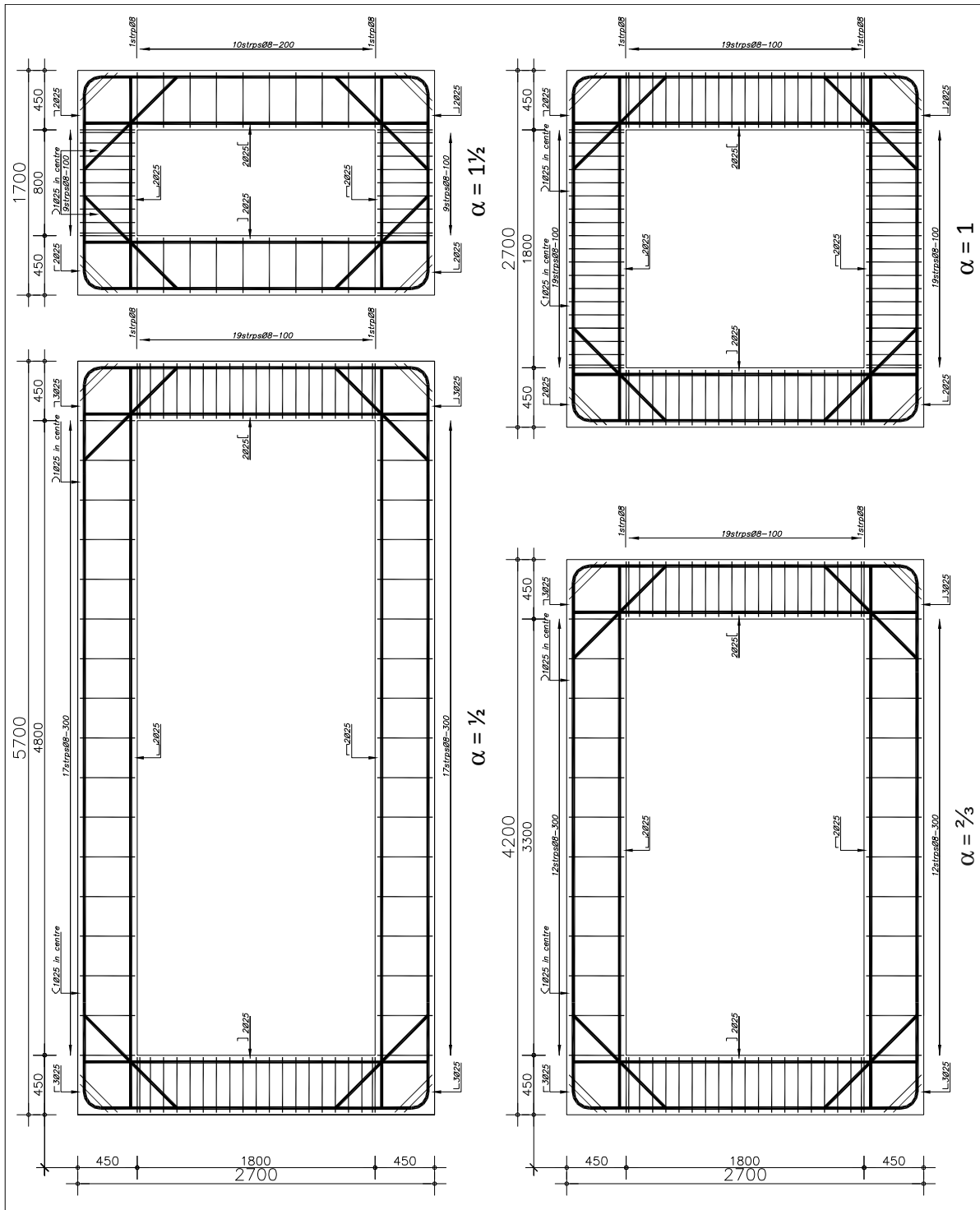


Figure D-27: Reinforcement configurations for panels of type 5 for  $\alpha = 1/2, 2/3, 1$  and  $1 1/2$

### D.3 Results parameter study on infilled frame

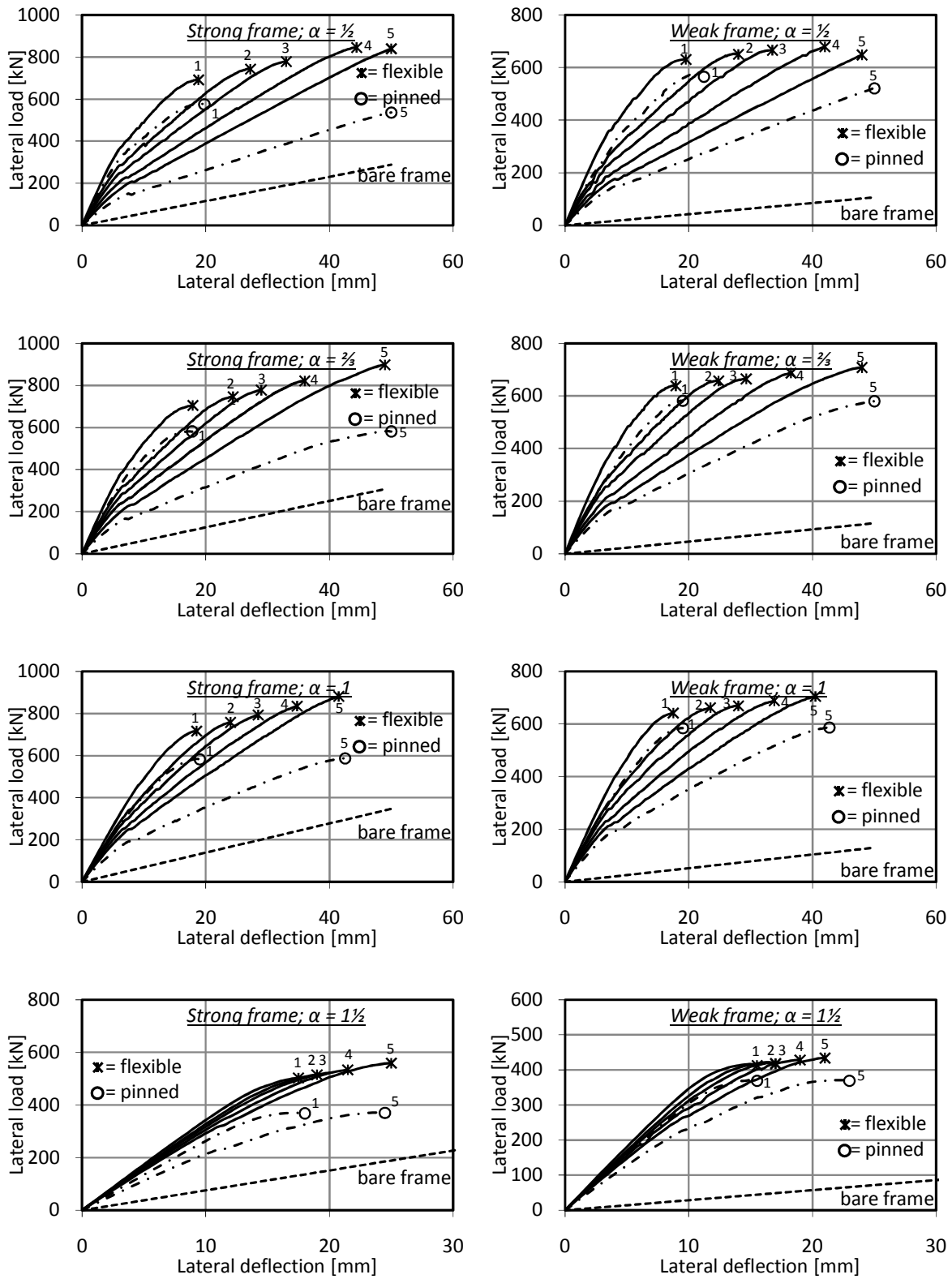


Figure D-28: Simulated load-deflection response of all infilled frames considered in parameter study

Table D-1: Results parameter study for weak frame

$\alpha$	Panel type	$S_{j,ini}$	$F_u$ [N]	Failure location*	$k_{ini}$ [N/mm]	$k_{sec;2}$ [N/mm]
$\alpha = \frac{1}{2}$	1	EC3	6.31E+05	C1-B	5.70E+04	3.32E+04
	1	0	5.78E+05	C1-B	4.50E+04	2.68E+04
	2	EC3	6.53E+05	C1-B	4.55E+04	2.39E+04
	3	EC3	6.65E+05	C1-B	3.97E+04	2.02E+04
	4	EC3	6.80E+05	C1-B	3.30E+04	1.62E+04
	5	EC3	6.48E+05	panel	2.70E+04	1.35E+04
	5	0	5.22E+05	Panel	2.20E+04	1.04E+04
	$\alpha = \frac{2}{3}$	1	EC3	6.39E+05	C1-B	5.95E+04
1		0	5.85E+05	C1-B	4.85E+04	3.00E+04
2		EC3	6.58E+05	C1-B	5.00E+04	2.69E+04
3		EC3	6.64E+05	C1-B	4.50E+04	2.31E+04
4		EC3	6.88E+05	C1-B	3.75E+04	1.88E+04
5		EC3	7.08E+05	C1-B	3.20E+04	1.48E+04
5		0	5.80E+05	C1-B	2.65E+04	1.16E+04
$\alpha = 1$		1	EC3	6.43E+05	C2-B	5.47E+04
	1	0	5.85E+05	C2-B	4.55E+04	3.08E+04
	2	EC3	6.59E+05	C2-B	4.82E+04	2.87E+04
	3	EC3	6.70E+05	C2-B	4.45E+04	2.42E+04
	4	EC3	6.87E+05	C2-B	4.05E+04	2.05E+04
	5	EC3	7.06E+05	C2-B	3.62E+04	1.74E+04
	5	0	5.88E+05	C2-B	2.97E+04	1.38E+04
	$\alpha = 1 \frac{1}{2}$	1	EC3	4.16E+05	C2-B	3.70E+04
1		0	3.71E+05	C2-B	3.18E+04	2.47E+04
2		EC3	4.21E+05	C2-B	3.50E+04	2.63E+04
3		EC3	4.21E+05	C2-B	3.39E+04	2.55E+04
4		EC3	4.29E+05	C2-B	3.25E+04	2.26E+04
5		EC3	4.34E+05	C2-B	3.08E+04	2.07E+04
5		0	3.70E+05	C2-B	2.65E+04	1.68E+04

\* For locations, see Figure 5-13

Table D-2: Results parameter study for strong frame

$\alpha$	Panel type	$S_{j,ini}$	$F_u$ [N]	Failure location*	$k_{ini}$ [N/mm]	$k_{sec;2}$ [N/mm]
$\alpha = \frac{1}{2}$	1	EC3	6.92E+05	C1-B	6.75E+04	3.74E+04
	1	0	5.78E+05	C1-B	5.85E+04	3.02E+04
	2	EC3	7.44E+05	C1-B	5.35E+04	2.78E+04
	3	EC3	7.77E+05	C1-B	4.65E+04	2.39E+04
	4	EC3	8.46E+05	C1-B	3.85E+04	1.92E+04
	5	EC3	8.41E+05	panel	3.16E+04	1.68E+04
	5	0	5.37E+05	Panel	2.47E+04	1.07E+04
	$\alpha = \frac{2}{3}$	1	EC3	7.02E+05	C1-B	6.70E+04
1		0	5.85E+05	C1-B	5.80E+04	3.29E+04
2		EC3	7.44E+05	C1-B	5.60E+04	3.13E+04
3		EC3	7.75E+05	C1-B	5.05E+04	2.72E+04
4		EC3	8.21E+05	C1-B	4.44E+04	2.31E+04
5		EC3	8.99E+05	C1-B	3.70E+04	1.83E+04
5		0	5.81E+05	C1-B	2.90E+04	1.16E+04
$\alpha = 1$		1	EC3	7.15E+05	C2-B	5.50E+04
	1	0	5.84E+05	C2-B	4.65E+04	3.16E+04
	2	EC3	7.55E+05	C2-B	4.95E+04	3.21E+04
	3	EC3	7.88E+05	C2-B	4.65E+04	2.81E+04
	4	EC3	8.34E+05	C2-B	4.25E+04	2.41E+04
	5	EC3	8.83E+05	C2-B	3.86E+04	2.13E+04
	5	0	5.88E+05	C2-B	3.08E+04	1.38E+04
	$\alpha = 1 \frac{1}{2}$	1	EC3	5.01E+05	C2-B	3.54E+04
1		0	3.70E+05	C2-B	2.75E+04	2.14E+04
2		EC3	5.13E+05	C2-B	3.40E+04	2.77E+04
3		EC3	5.20E+05	C2-B	3.30E+04	2.67E+04
4		EC3	5.33E+05	C2-B	3.20E+04	2.51E+04
5		EC3	5.53E+05	C2-B	3.10E+04	2.33E+04
5		0	3.72E+05	C2-B	2.30E+04	1.55E+04

\* For locations, see Figure 5-13



## APPENDIX E

### E.1 Derivation of equations [7-21] to [7-24]

The mechanical model for the semi-integral infilled frame presented in Figure E-1 is considered. The frame joints are represented by rigid offsets to take the depth of the columns and beams into account. The beams are connected pinned to the columns, thus  $S_j = 0$ .

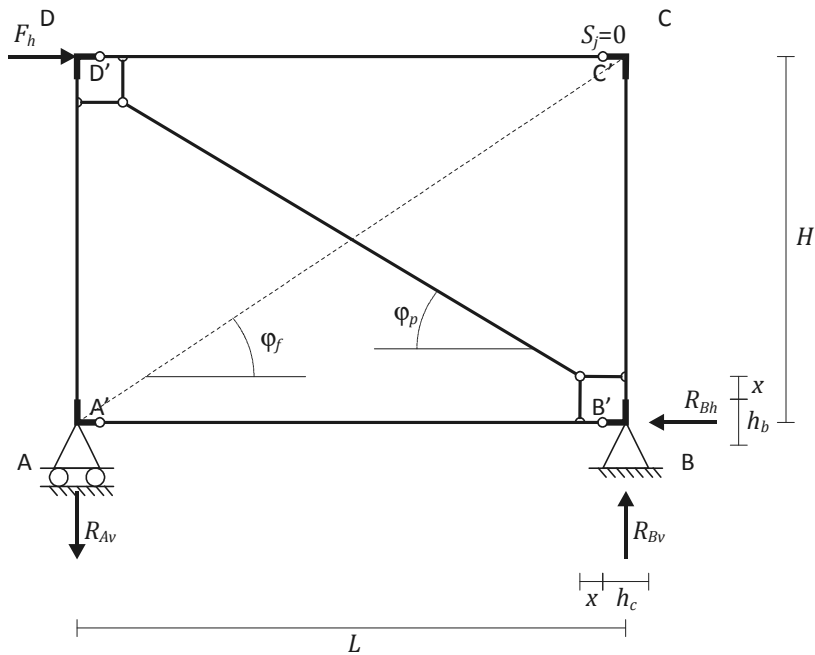


*Figure E-1: Mechanical model for semi-integral infilled frame*

Considering the equilibrium in horizontal direction ( $\Sigma H$ ), gives the horizontal reaction at support B ( $R_{Bh}$ ):

$$\Sigma H = 0 \rightarrow R_{Bh} = F_h$$

Taking the moment about A gives the vertical reaction at support B ( $R_{Bv}$ ):

$$\Sigma M_{\text{about } A} = 0 \rightarrow F_h H - R_{Bv} L = 0$$

$$R_{Bv} = \frac{F_h H}{L} = F_h \tan \varphi_f$$

Finally, the sum of the vertical forces  $\Sigma V$  gives the horizontal reaction at support A ( $R_{Av}$ ):

$$\Sigma V = 0 \rightarrow R_{Av} = F_h \tan \varphi_f$$



Subsequently, the strut is taken out of the structure. An axial force in the strut is assumed equal to  $N_{x;strut} = N_x$ . Accordingly, the axial forces in the strut-to-column and strut-to-beam connection equal  $N_{x;c;col} = N_x \cos \varphi_p$  and  $N_{x;c;beam} = N_x \sin \varphi_p$ . These internal forces are placed on the frame structure (Figure E-3).

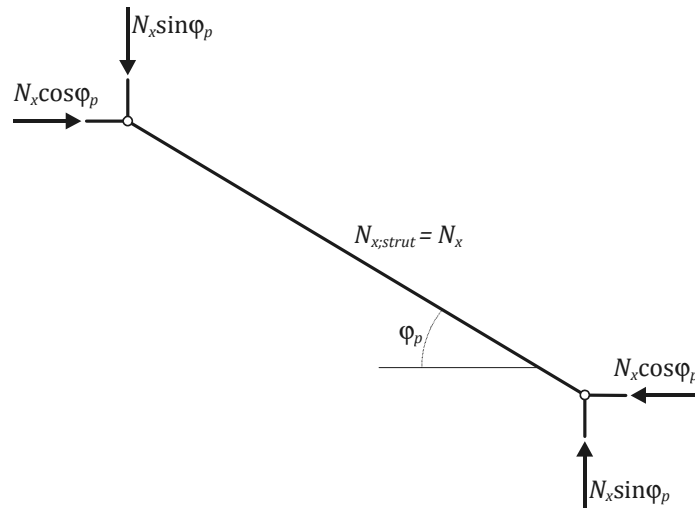


Figure E-2: Free body diagram of strut

Next, the encircled part (Figure E-3) is isolated from the structure.

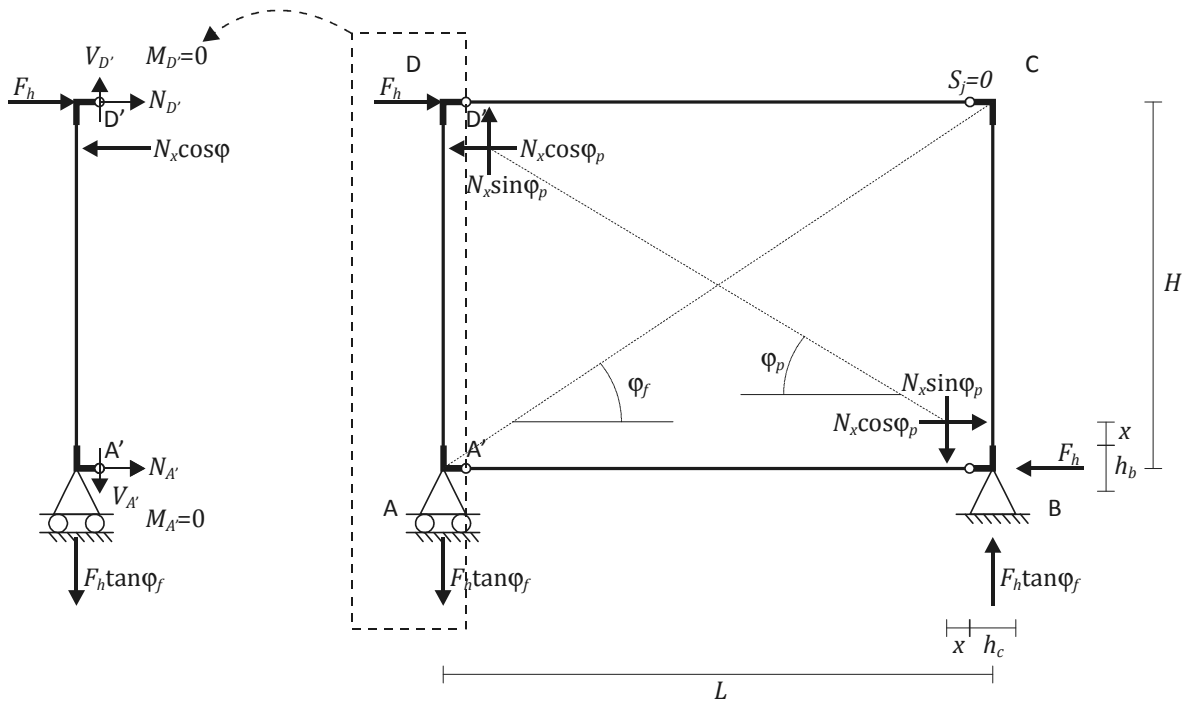


Figure E-3: Mechanical model with internal strut forces

Accordingly, the equilibrium of moments is considered for the isolated part of the structure with respect to point D':

$$\Sigma M_{about D'} = 0$$

$$\Sigma M_{about D'} = N_x \cos \varphi_p \left( \frac{h_b}{2} + x \right) - F_h \tan \varphi_f \left( \frac{h_c}{2} \right) - N_{A'} H = 0$$

Considering the equilibrium in horizontal direction ( $\Sigma H$ ) gives:

$$\Sigma H = 0 \rightarrow N_x \cos \varphi_p - F_h - N_{A'} - N_{D'}$$

$$N_{D'} + N_{A'} = N_x \cos \varphi_p - F_h$$

From symmetry conditions it follows that:

$$N_{D'} = N_{A'}$$

Accordingly:

$$N_{D'} = N_{A'} = \frac{N_x \cos \varphi_p - F_h}{2}$$

Substituting  $N_{A'}$  gives:

$$N_x \cos \varphi_p \left( \frac{h_b}{2} + x \right) - F_h \tan \varphi_f \left( \frac{h_c}{2} \right) - H \left( \frac{N_x \cos \varphi_p - F_h}{2} \right) = 0$$

Accordingly:

$$N_x = \frac{F_h (\tan \varphi_f h_c - H)}{\cos \varphi_p (h_b + 2x - H)} = \frac{F_h \tan \varphi_f h_c - H}{\cos \varphi_p h_b + 2x - H}$$

Substituting:

$$H = \tan \varphi_f L$$

Gives:

$$N_x = \frac{F_h}{\cos \varphi_p} \left( \frac{\tan \varphi_f h_c - \tan \varphi_f L}{h_b + 2x - H} \right) = \frac{F_h}{\cos \varphi_p} \left( \frac{\tan \varphi_f (h_c - L)}{h_b + 2x - H} \right)$$

Substituting:

$$\tan \varphi_f = \frac{H}{L}$$

Gives:

$$N_x = \frac{F_h}{\cos \varphi_p} \left( \frac{H(h_c - L)}{(h_b + 2x - H)L} \right)$$

Using equation 7-2:

$$\beta_f = \frac{L}{L - h_c} \quad [7-2]$$

Accordingly:

$$\frac{h_c - L}{L} = \frac{1}{-\beta_f}$$

Substitution gives:

$$N_x = \frac{F_h H}{(H - h_b - 2x)\beta_f \cos \varphi_p} \quad [7-23]$$

Accordingly, the axial force in the panel-to-column connection ( $N_{x;c,col}$ ) equals:

$$N_{x;c,col} = N_x \cos \varphi_p = \frac{F_h H}{(H - h_b - 2x)\beta_f} \quad [7-21]$$

The axial force in the panel-to-beam connection ( $N_{x;c,beam}$ ):

$$N_{x;c,beam} = N_x \sin \varphi_p = \frac{F_h H \tan \varphi_p}{(H - h_b - 2x)\beta_f} \quad [7-22]$$

The top beam is isolated from the structure. The axial force in the loaded column ( $N_{x,col;1}$ ) is equal to the shear force  $V_{D'}$  (Figure E-4).

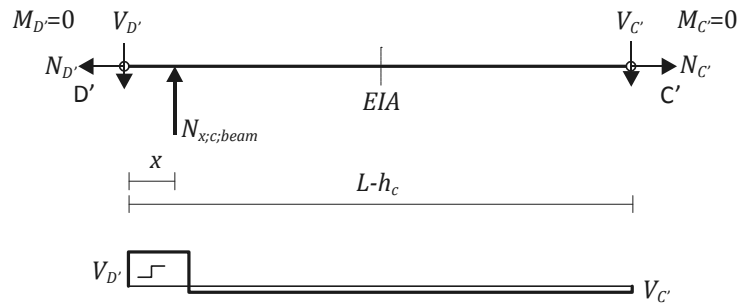


Figure E-4: Free body diagram of top beam

Taking the moment about C' gives shear force ( $V_{D'}$ ), and thus the axial force in the column:

$$\Sigma M_{about C'} = 0 \rightarrow N_{x;c;beam}(L - h_c - x) - V_{D'}(L - h_c) = 0$$

$$R_{D'v} = \frac{N_{x;c;beam}(L - h_c - x)}{(L - h_c)}$$

Substitution of equation 7-22 for  $N_{x;c;beam}$  gives the following equation for the axial force in the loaded column ( $N_{x;col;1}$ )

$$N_{x;col;1} = \frac{(L - h_c - x)F_h H \tan \phi_p}{(L - h_c)(H - h_b - 2x)\beta_f} \quad [7-24]$$

## E.2 Derivation of equations [7-27] to [7-31]

The bottom frame beam is considered. Assuming it to be connected pinned to the columns, it can be considered as a simply supported beam as shown in figure E-5. The length of the beam equals  $(L - h_c)$ . The beam is loaded by a point load  $F$  at a distance  $x$  from support B:

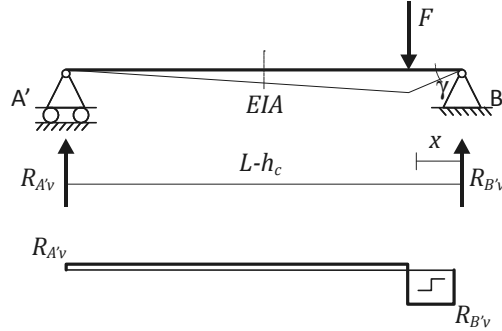


Figure E-5: Bottom frame beam isolated from the structure

Considering the equilibrium of moments about point  $A'$  gives the vertical reaction at support  $B'$  ( $R_{B'v}$ ):

$$\Sigma M_{\text{about } A'} = 0 \rightarrow R_{B'v} = \frac{F(L - h_c - x)}{L - h_c}$$

Subsequently, the sum of the vertical forces  $\Sigma V$  gives the vertical reaction at support A ( $R_{A'v}$ ):

$$\Sigma V = 0 \rightarrow R_{A'v} = F \frac{x}{L - h_c}$$

The vertical deformation at the point load due to shear ( $\delta_v$ ) can be expressed by the following equation:

$$\delta_v = \gamma x$$

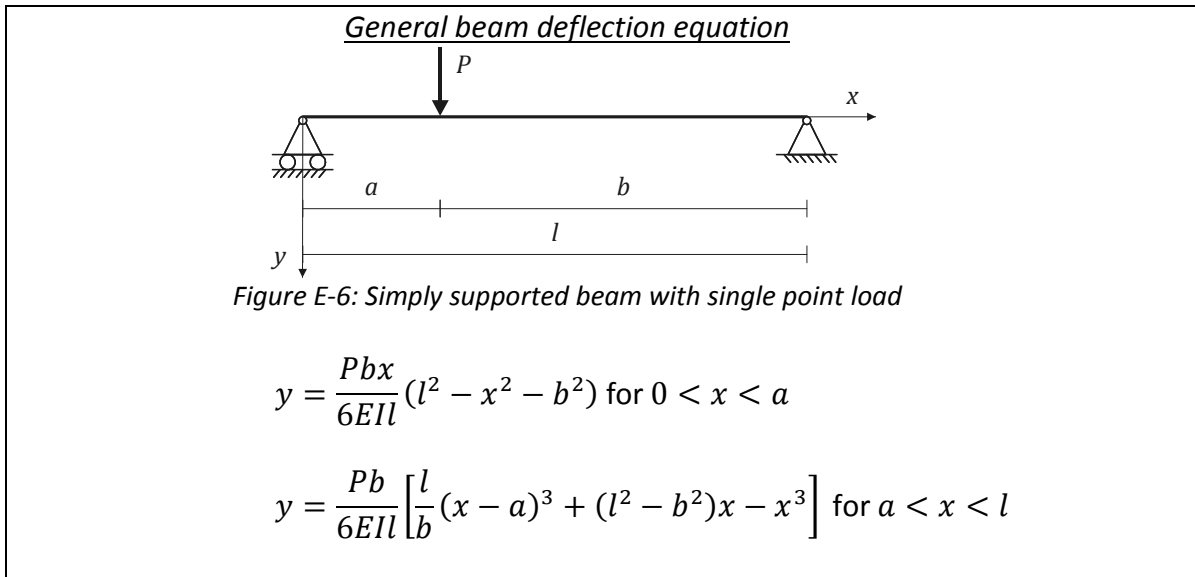
Where:

$$\gamma = \frac{R_{B'v}}{GA_{v,b}}$$

Consequently, the stiffness resulting from shear deformation is given by:

$$k_v = \frac{F}{\delta_v} = \frac{FGA_{v,b}}{R_{B'v}x} = \frac{FGA_{v,b}}{\left(\frac{F(L - h_c - x)}{L - h_c}\right)x} = \frac{GA_{v,b}(L - h_c)}{(L - h_c - x)x} \quad [7-27]$$

The general beam deflection equation for bending of a simply supported beam of length  $l$  with a single point load  $P$  at any point (Figure E-6) is given below.



Substituting  $a = x$  and  $l = L - h_c$  in one of the general equations above gives the following equation for the deflection at the point load due to bending:

$$\delta_M = \frac{F(L - h_c - x)^2 x^2}{3EI(L - h_c)}$$

Accordingly, the stiffness resulting from bending is given by:

$$k_M = \frac{F}{\delta_M} = \frac{3EI(L - h_c)}{F(L - h_c - x)^2 x^2} \quad [7-29]$$

Next, the loaded column is considered. The column is supposed to be pin-connected to its rigid offset. This results in slightly conservative stiffnesses for bending and shear.

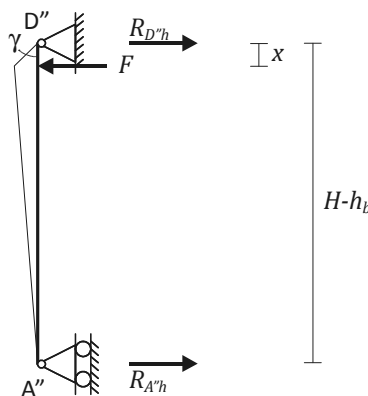


Figure E-7: Loaded column isolated from the structure

Considering the equilibrium of moments about point A'' gives the horizontal reaction at support D'' ( $R_{D''h}$ ):

$$\Sigma M_{about A''} = 0 \rightarrow R_{D''h} = \frac{F(H - h_b - x)}{H - h_b}$$

Subsequently, the sum of the horizontal forces ( $\Sigma H$ ) gives the horizontal reaction at support A'' ( $R_{A''h}$ ):

$$\Sigma H = 0 \rightarrow R_{A''h} = F \frac{x}{H - h_b}$$

The vertical deformation at the point load due to shear ( $\delta_V$ ) can be expressed by the following equation:

$$\delta_V = \gamma x$$

Where:

$$\gamma = \frac{R_{D''h}}{GA_{v;c}}$$

Accordingly, the stiffness resulting from shear deformation is given by:

$$k_V = \frac{F}{\delta_V} = \frac{FGA_{v;c}}{R_{D''h}x} = \frac{FGA_{v;c}}{\left(\frac{F(H - h_b - x)}{H - h_b}\right)x} = \frac{GA_{v;c}(H - h_b)}{(H - h_b - x)x} \quad [7-28]$$

The vertical deformation at the point load due to bending is given by the following equation (specific beam loading case):

$$\delta_M = \frac{F(H - h_b - x)^2 x^2}{3EI(H - h_b)}$$

Consequently, the stiffness resulting from bending is given by:

$$k_M = \frac{F}{\delta_M} = \frac{3EI(H - h_b)}{(H - h_b - x)^2 x^2} \quad [7-29]$$

### E.3 $M-N-\kappa$ -diagrams used for equivalent frame members

The following stress-strain relationships were used for concrete and reinforcement steel to create the  $M-N-\kappa$ -diagrams (Figure E-8)

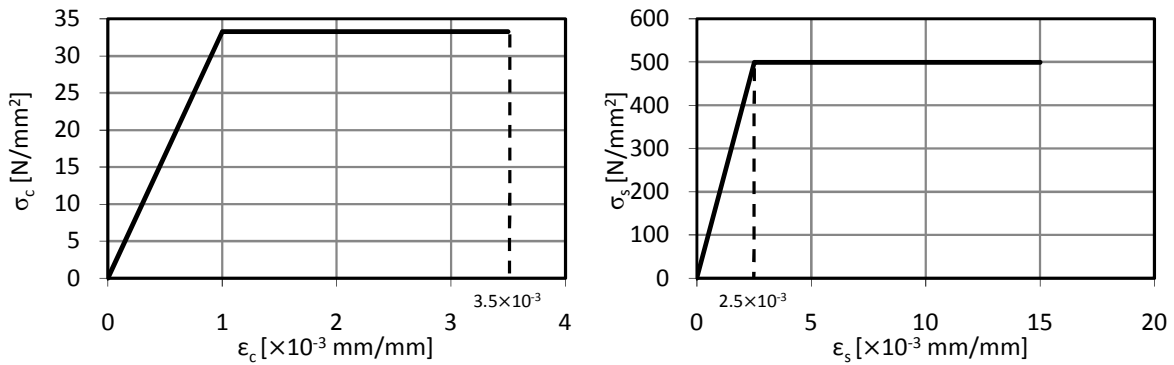


Figure E-8: Stress-strain curves for concrete (left) and reinforcement steel (left)

The concrete cover ( $c$ ) on the longitudinal reinforcement ( $\varnothing 25$ ) equals 23 mm.

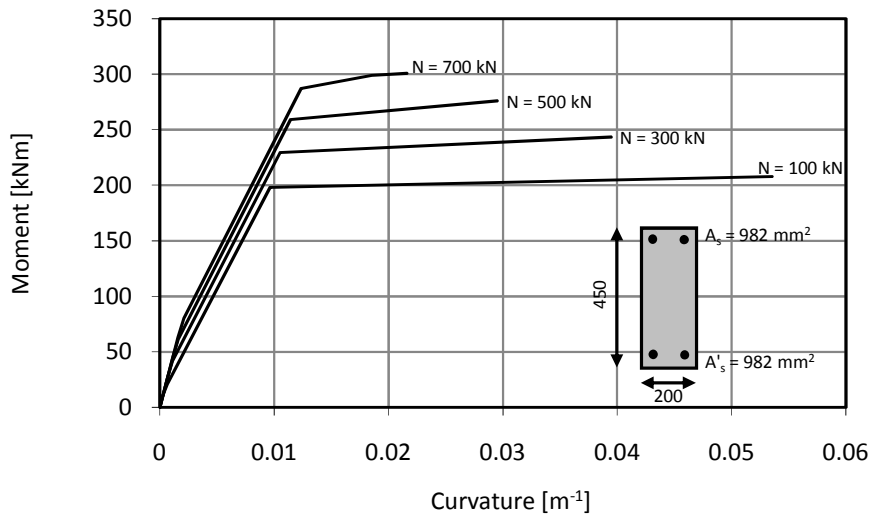


Figure E-9:  $M-N-\kappa$ -diagram for cross-section 200 x 450 mm



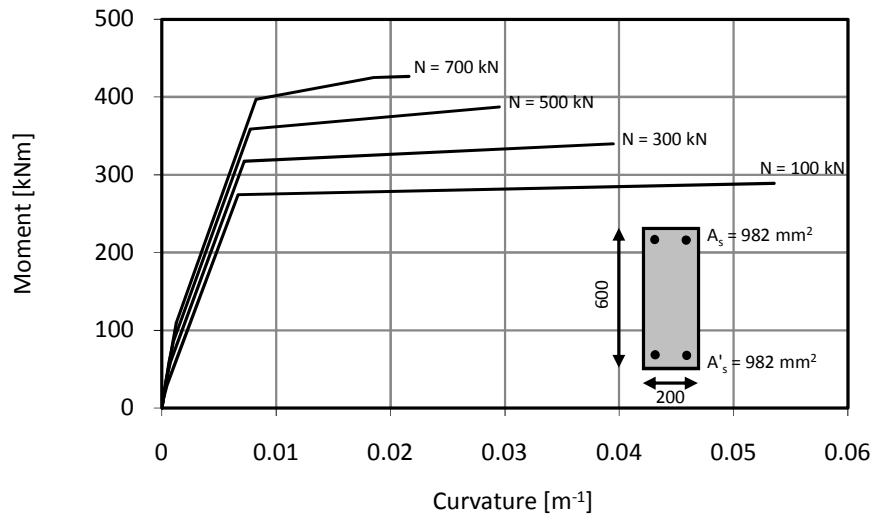


Figure E-10:  $M-N-\kappa$ -diagram for cross-section 200 x 600 mm

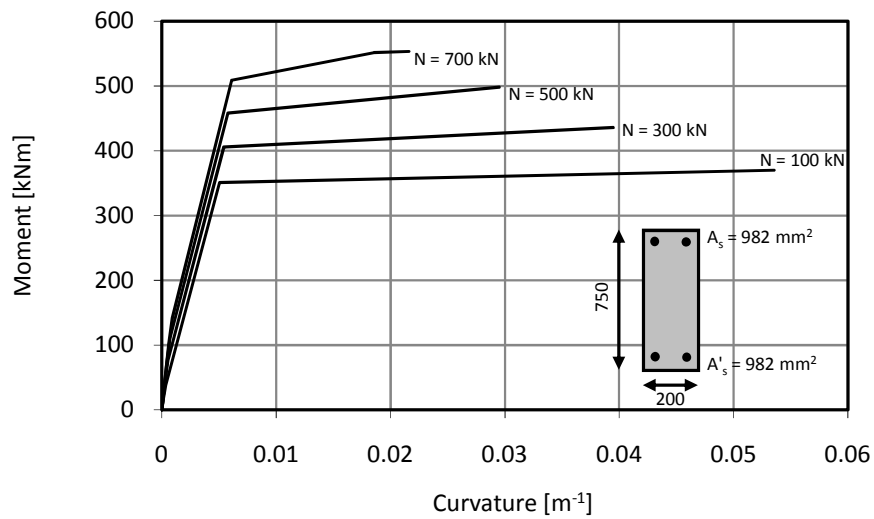


Figure E-11:  $M-N-\kappa$ -diagram for cross-section 200 x 750 mm

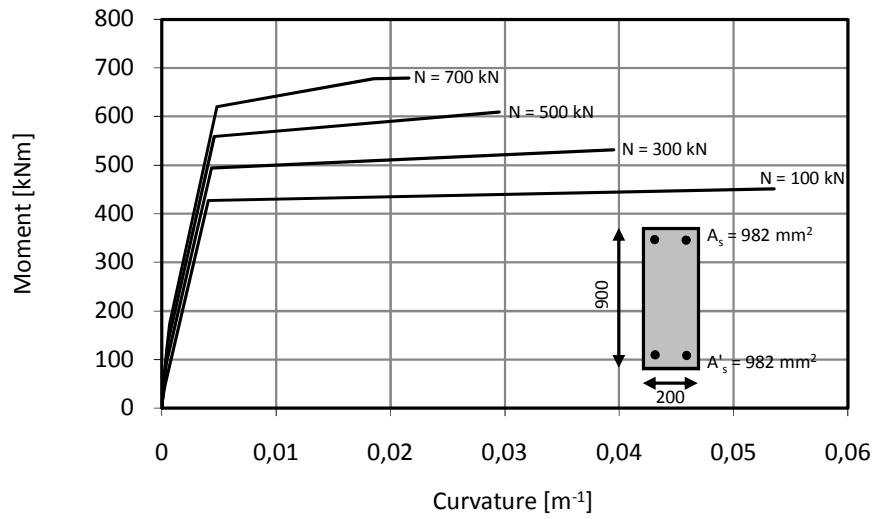


Figure E-12:  $M-N-\kappa$ -diagram for cross-section 200 x 900 mm

Table E-1 gives the derived bending stiffnesses:

Table E-1: Bending stiffnesses [ $Nmm^2$ ] derived from  $M-N-\kappa$ -diagrams

$\alpha$	Panel type	Column		Top beam		Bottom beam	
		$(EI)_{ini}$	$(EI)_d$	$(EI)_{ini}$	$(EI)_d$	$(EI)_{ini}$	$(EI)_d$
$\alpha = \frac{1}{2}$	1	5.62E+13	2.09E+13	2.60E+14	7.48E+13	4.50E+14	1.14E+14
	2	5.62E+13	2.09E+13	1.33E+14	4.40E+13	2.60E+14	7.48E+13
	3	5.62E+13	2.09E+13	1.33E+14	4.40E+13	1.33E+14	4.40E+13
	4	5.62E+13	2.09E+13	5.62E+13	2.18E+13	1.33E+14	4.40E+13
	5	5.62E+13	2.09E+13	5.62E+13	2.18E+13	5.62E+13	2.18E+13
$\alpha = \frac{2}{3}$	1	5.62E+13	2.12E+13	2.60E+14	7.48E+13	4.50E+14	1.14E+14
	2	5.62E+13	2.12E+13	1.33E+14	4.40E+13	2.60E+14	7.48E+13
	3	5.62E+13	2.12E+13	1.33E+14	4.40E+13	1.33E+14	4.40E+13
	4	5.62E+13	2.12E+13	5.62E+13	2.18E+13	1.33E+14	4.40E+13
	5	5.62E+13	2.12E+13	5.62E+13	2.18E+13	5.62E+13	2.18E+13
$\alpha = 1$	1	5.62E+13	2.18E+13	2.60E+14	7.48E+13	4.50E+14	1.14E+14
	2	5.62E+13	2.18E+13	1.33E+14	4.40E+13	2.60E+14	7.48E+13
	3	5.62E+13	2.18E+13	1.33E+14	4.40E+13	1.33E+14	4.40E+13
	4	5.62E+13	2.18E+13	5.62E+13	2.18E+13	1.33E+14	4.40E+13
	5	5.62E+13	2.18E+13	5.62E+13	2.18E+13	5.62E+13	2.18E+13
$\alpha = 1 \frac{1}{2}$	1	5.62E+13	2.18E+13	2.60E+14	7.48E+13	4.50E+14	1.14E+14
	2	5.62E+13	2.18E+13	1.33E+14	4.40E+13	2.60E+14	7.48E+13
	3	5.62E+13	2.18E+13	1.33E+14	4.40E+13	1.33E+14	4.40E+13
	4	5.62E+13	2.18E+13	5.62E+13	2.18E+13	1.33E+14	4.40E+13
	5	5.62E+13	2.18E+13	5.62E+13	2.18E+13	5.62E+13	2.18E+13



# CURRICULUM VITAE

## Personal data

Name: Paul Teeuwen  
Date of birth: November 10<sup>th</sup>, 1980  
Place of birth: Geldrop, The Netherlands  
Current address: Pieter Pauluslaan 23  
5652 VD Eindhoven  
The Netherlands  
E-mail: p.a.teeuwen@upcmail.nl



## Education

1999 - 2005 Eindhoven University of Technology  
Faculty of Architecture, Building and Planning  
Department of Structural Design  
Master thesis "The effect of window openings in precast reinforced concrete infills on the structural behavior of semi-integral infilled frames"  
1993 - 1999 Varendonck College Asten  
Atheneum

## PhD research

2005 - 2009 Eindhoven University of Technology  
Faculty of Architecture, Building and Planning  
Department of Structural Design